



University of Pennsylvania
ScholarlyCommons


Publicly Accessible Penn Dissertations

2018

Cross-Talk Between Protein Degradation And Mrna Decay In Diffuse Large B-Cell Lymphoma

Jaewoo Choi
University of Pennsylvania, cjwoo8686@gmail.com

Follow this and additional works at: <https://repository.upenn.edu/edissertations>

 Part of the [Biochemistry Commons](#), [Molecular Biology Commons](#), and the [Oncology Commons](#)

Recommended Citation

Choi, Jaewoo, "Cross-Talk Between Protein Degradation And Mrna Decay In Diffuse Large B-Cell Lymphoma" (2018). *Publicly Accessible Penn Dissertations*. 2754.
<https://repository.upenn.edu/edissertations/2754>

This paper is posted at ScholarlyCommons. <https://repository.upenn.edu/edissertations/2754>
For more information, please contact repository@pobox.upenn.edu.

Cross-Talk Between Protein Degradation And Mrna Decay In Diffuse Large B-Cell Lymphoma

Abstract

The ubiquitin-proteasome system (UPS) plays a critical role in the maintenance of cellular homeostasis as it mediates the precise and temporal degradation of intracellular proteins and affects a variety of cellular processes. The misregulation of the ubiquitin-proteasome system (UPS) can result in the pathogenesis of human diseases including cancer. A proteasome inhibitor has been proven an effective treatment for lymphoid malignancies, rendering the UPS appealing as a new therapeutic target for cancer. Despite the significant progress, much more remains to be explored in the field of ubiquitin and molecular mechanisms of tumorigenesis. KLHL6 is a frequently mutated in mature B-cell cancers, but the relevance of these mutations and molecular function of KLHL6 are currently not known. Here, we show that KLHL6 is a novel E3 ubiquitin ligase and cancer-associated somatic mutations disrupt its catalytic activity. Via proteomic analysis and mutagenesis screening approaches, we have further identified and validated Roquin2, a mRNA decay factor, as a substrate of KLHL6. The interaction between KLHL6 and Roquin2 requires a tyrosine in position 691 of Roquin2 and can be inhibited when tyrosine 691 is phosphorylated. Furthermore, using in vitro cell proliferation assays and xenograft mouse models, we show that KLHL6 has tumor suppressive effects that are dependent on Roquin2 stabilization in diffuse large B-cell lymphoma (DLBCL). RNA sequencing analysis has revealed that Roquin2 regulated genes are implicated in the NF- κ B pathway and as lymphoid tumor suppressors, correlating with B-cell lymphoma proliferation and survival. Taken together, the work described here highlights a previously uncharacterized molecular mechanism whereby the novel E3 ligase modulates mRNA decay through its substrate degradation and plays role in the pathogenesis of mature B-cell cancers.

Degree Type

Dissertation

Degree Name

Doctor of Philosophy (PhD)

Graduate Group

Cell & Molecular Biology

First Advisor

Luca Busino

Keywords

Cancer, Lymphoma, mRNA decay, Protein degradation, Tumor suppressor, Ubiquitin

Subject Categories

Biochemistry | Molecular Biology | Oncology

This dissertation is available at ScholarlyCommons: <https://repository.upenn.edu/edissertations/2754>

CROSS-TALK BETWEEN PROTEIN DEGRADATION AND MRNA DECAY IN
DIFFUSE LARGE B-CELL LYMPHOMA

Jaewoo Choi

A DISSERTATION

in

Cell and Molecular Biology

Presented to the Faculties of the University of Pennsylvania

in

Partial Fulfillment of the Requirements for the
Degree of Doctor of Philosophy

2018

Supervisor of Dissertation

Graduate Group Chairperson

Luca Busino, Ph.D.,

Daniel S. Kessler, Ph.D.,

Assistant Professor of

Associate Professor of

Cancer Biology

Cell and Developmental Biology

Dissertation Committee

Roger A. Greenberg, M.D., Ph.D., Professor of Cancer Biology

Craig H. Bassing, Ph.D., Associate Professor of Pathology and Laboratory Medicine

Paula M. Oliver, Ph.D., Associate Professor of Pathology and Laboratory Medicine

David M. Feldser, Ph.D., Assistant Professor of Cancer Biology

ACKNOWLEDGMENTS

I am very thankful to Dr. Luca Busino for his mentorship throughout my Ph.D program at Upenn. He has always supported me with constant encouragement whenever I was frustrated with experimental results and faced with obstacles. He gave me the freedom to work independently, but, at the same time, he was always there to provide advice and help when asked. Although there were many ups and downs and times where we did not agree on something, now I realize that all those experiences had beneficial effects on me. I really learned how to be a rigorous biochemist and I felt like I became a much more mature scientist from coming out of his laboratory. He has profoundly influenced me in many ways and I will be grateful forever for his time and support.

I thank you very much to my parents, Yongho Choi and Soonja Seok, and my sister, Eunseon Choi, for all of their unconditional support and encouragement. Whenever I had to make a decision on anything, they were always on my side and proud of me. I could not have come to this stage without their support, and their unconditional love always made me feel happy and pushed me to try and work harder. One day, I would like to go back to South Korea and give back what I have gotten and make them feel happy.

Also, I am very lucky to have wonderful lab mates and colleagues who created an enjoyable and wonderful lab environment to do science over the years. I will always remember the times that we went out dinner regularly and were always so full after having the “hot-pot” in china town. Thank you for all the good memories.

In addition, I would like to thank the following people:

Busino lab, past and present: David Kyutae Lee, Rizwan Saffie, Dahmane Ouazia, Nan Zhou, Grant Grothusen, Ashley Hughes, Alvaro Gutierrez-Uzquiza, Daniela Ricci

Thesis Committee: Roger Greenberg, Craig Bassing, Paula Oliver, David Feldser

Rotation labs: Alan Diehl, Andrei Thomas-Tikhonenko

Collaborators: Roberto Bonasio (Upenn), Kristin Ingvarsdottir (Upenn), Anita Saraf (Stowers Institute), Laurence Florens (Stowers Institute), Michael Washburn (Stowers Institute), Saber Tadros (MD Anderson), Michael R. Green (MD Anderson)

AFCRI 7th floor labs: Ryeom Lab (Bang-Jin Kim), Feldser Lab, Witze Lab, Alwine Lab

ABSTRACT

CROSS-TALK BETWEEN PROTEIN DEGRADATION AND MRNA DECAY IN DIFFUSE LARGE B-CELL LYMPHOMA

Jaewoo Choi

Luca Busino

The ubiquitin-proteasome system (UPS) plays a critical role in the maintenance of cellular homeostasis as it mediates the precise and temporal degradation of intracellular proteins and affects a variety of cellular processes. The misregulation of the ubiquitin-proteasome system (UPS) can result in the pathogenesis of human diseases including cancer. A proteasome inhibitor has been proven an effective treatment for lymphoid malignancies, rendering the UPS appealing as a new therapeutic target for cancer. Despite the significant progress, much more remains to be explored in the field of ubiquitin and molecular mechanisms of tumorigenesis. KLHL6 is a frequently mutated in mature B-cell cancers, but the relevance of these mutations and molecular function of KLHL6 are currently not known. Here, we show that KLHL6 is a novel E3 ubiquitin ligase and cancer-associated somatic mutations disrupt its catalytic activity. Via proteomic analysis and mutagenesis screening approaches, we have further identified and validated Roquin2, a mRNA decay factor, as a substrate of KLHL6. The interaction between KLHL6 and Roquin2 requires a tyrosine in position 691 of Roquin2 and can be inhibited when tyrosine 691 is phosphorylated. Furthermore, using *in vitro* cell proliferation assays and xenograft mouse models, we show that KLHL6 has tumor

suppressing effects that are dependent on Roquin2 stabilization in diffuse large B-cell lymphoma (DLBCL). RNA sequencing analysis has revealed that Roquin2 regulated genes are implicated in the NF- κ B pathway and as lymphoid tumor suppressors, correlating with B-cell lymphoma proliferation and survival. Taken together, the work described here highlights a previously uncharacterized molecular mechanism whereby the novel E3 ligase modulates mRNA decay through its substrate degradation and plays a role in the pathogenesis of mature B-cell cancers.

TABLE OF CONTENTS

ACKNOWLEDGMENTS.....	ii
ABSTRACT	iv
LIST OF TABLES.....	x
LIST OF FIGURES.....	xi
PREFACE	xiii
CHAPTER 1 : INTRODUCTION	1
CULLIN-RING ubiquitin ligases	2
CULLIN3-RING ubiquitin ligases.....	3
CULLIN3-RING ubiquitin ligases in cancer	6
Protein ubiquitylation and de-ubiquitylation in lymphoid malignancies.....	11
Protein ubiquitination in the oncogenic signaling pathway of ABC-DLBCLs.....	12
TNFAIP3/A20 in ABC-DLBCLs	16
Pharmacological inhibitions in lymphoid malignancies	18
CHAPTER 2 : EXPERIMENTAL METHODS	24
Cell lines, antibodies, drugs, and other reagents	24
Immunoblotting and immunoprecipitation	26
Nuclear extraction	26
λ -Phosphatase treatment.....	27
Chromatin immunoprecipitation	27
Xenograft experiments	28

KLHL6 complexes purification for mass spectrometry	29
In vitro binding assays	29
In vitro and in vivo ubiquitylation assay	30
Transient transfections, generation of viruses for infection, and electroporation	31
Generation clonal KLHL6 ^{-/-} cell lines	31
Plasmids, cloning, shRNA, gRNA, and siRNA sequences	31
mRNA Analysis and q-PCR primers	35
Normalization and quantification of protein levels	37
Cell proliferation assay	38
Flow cytometry	38
MudPIT analysis	39
Analysis of KLHL6 expression in DLBCL patients	40
RNA sequencing	41
CHIP sequencing	42
Statistics and reproducibility	42

CHAPTER 3 : BIOCHEMICAL ANALYSIS OF KLHL6 AND ROQUIN2 AS AN	
E3 LIGASE-SUBSTRATE PAIR	44
Chapter Summary	44
Introduction.....	45
Results	47
Cancer-associated mutations of KLHL6 in B-cell malignancies	47
KLHL6 assembles a CULLIN3-based E3 ligase	48

BTB-domain mutations of KLHL6 abolishes its ligase activity	50
KLHL6 specifically interacts with Roquin2	51
KLHL6 promotes ubiquitylation and degradation of Roquin2.	52
BTB-mutations of KLHL6 are not dominant-negative	54
Interaction between KLHL6 and Roquin2 requires a functional tyrosine residue	
Y691 in Roquin2	55
KLHL6 promotes Roquin2 degradation upon BCR stimulation.....	56
Discussion	58
 CHAPTER 4 : THE BIOLOGICAL FUNCTION OF KLHL6-ROQUIN2 AXIS IN	
ABC-DLBCLS	90
Chapter summary	90
Introduction.....	91
Results	94
KLHL6 is a tumor suppressor in ABC-DLBCL subtype.....	94
Roquin2 stabilization promotes ABC-DLBCL growth and survival	97
Stabilization of Roquin2 down-regulate BCR responsive genes	98
KLHL6-Roquin2 axis controls NF- κ B activation via TNFAIP3	101
KLHL6 BTB-domain mutations and TNFAIP3 mutations are mutually exclusive in	
DLBCL patients	103
Discussion	104
 CHAPTER 5 : TYROSINE PHOSPHATASE PTPN14 REGULATES ROQUIN2	
PROTEIN STABILITY	139

Chapter summary	139
Introduction.....	140
Results	142
Tyrosine 691 in Roquin2 is phosphorylated in vivo	142
Tyrosine 691 phosphorylation in Roquin2 is inhibitory for KLHL6 interaction.....	144
PTPN14 specifically interacts with Roquin2	144
PTPN14 binds the C-terminal region of the Roquin2 protein through its phosphatase domain.....	146
PTPN14 enhances interaction between KLHL6 and Roquin2.....	147
PTPN14 regulates Roquin2 protein stability.....	148
Discussion	149
CHAPTER 6 : CONCLUSIONS AND FUTURE DIRECTIONS	164
KLHL6 as a tumor suppressor in DLBCL	164
Roquin2 as an oncogene in DLBCL	166
PTPN14 as a tumor suppressor in DLBCL	169
Concluding remarks	171
CHAPTER 7 : REFERENCES	172

LIST OF TABLES

Table 3.1.....	86
Table 3.2.....	89
Table 4.1.....	131
Table 4.2.....	132
Table 4.3.....	134
Table 5.1.....	163

LIST OF FIGURES

Figure 3.1A-E.....	63
Figure 3.2A-C.....	65
Figure 3.3A-D.....	67
Figure 3.4A-E.....	69
Figure 3.5A-H.....	72
Figure 3.6A-E.....	76
Figure 3.7A-K.....	78
Figure 3.8A-H.....	82
Figure 4.1A-L.....	107
Figure 4.2A-E.....	114
Figure 4.3A-I.....	117
Figure 4.4A-M.....	122
Figure 4.5A-F.....	127
Figure 5.1A-C.....	152
Figure 5.2A-B.....	154
Figure 5.3A-C.....	156

Figure 5.4A-B.....	158
Figure 5.5A-B.....	161
Figure 5.6A-B.....	162

PREFACE

This thesis consist of a series of chapters based on the manuscript that is recently accepted in Nature Cell Biology, as well as unpublished data that I am planning to submit for publication in a small journal and some of ongoing studies in our laboratory. Chapter 1 contains general background and introduction for all, and each chapter contains an introduction, result, and discussion. Chapter 2 contains experimental methods and Chapter 6 contains conclusions and future directions for chapter 3, 4, and 5.

CHAPTER 1 : INTRODUCTION

The ubiquitin proteasome system (UPS) plays a critical role in the regulation of cell growth and survival and in maintaining cellular homeostasis. UPS mediates the precise and temporal degradation of 80% of intracellular proteins, and the failure to terminate such signals effectively results in numerous diseases, including hematological malignancies and cancer (Silverman et al., 2012; Skaar et al., 2013). The ubiquitin–proteasome system is catalyzed in a stepwise manner through an enzymatic cascade in which ubiquitin is activated by an E1 enzyme, transferred to an E2 ubiquitin-conjugating enzyme, and finally transferred to a substrate selected by an E3 ubiquitin ligase. The E3 ubiquitin ligase determines the substrate specificity for the ubiquitination of critical regulators. These enzymes act together in a precise and specific manner to target and regulate the degradation of the proteins in the proteasome complex. The proteasome consists of regulatory 19S cap complexes that unfold the substrates in an ATP-dependent manner and catalytic 20S core complexes that have proteolytic activities. (Hershko and Ciechanover, 1998) Proteins that are tagged by the ubiquitin chains are recognized, deubiquitylated, and unfolded by the 19S complex and then fed through inner components of the 20S proteasome chamber (Braun et al., 1999). The success of a proteasome inhibitor (bortezomib) in multiple myeloma and mantle cell lymphoma has inspired to develop novel therapeutic approaches in investigating the biological significance of protein ubiquitylation and degradation in B-cell cancers (Yang and Staudt, 2015). However, bortezomib affects thousands of intra-cellular proteins and results in toxic side effects, which require substrate specificity. Thus, understanding how

ubiquitylation of protein is achieved and the downstream consequences of molecular and signaling events becomes essential in developing therapeutic targets and studying their efficacy.

CULLIN-RING ubiquitin ligases

Among more than 800 E3 ubiquitin ligases in the human genome, the CULLIN-RING ligases (CRLs) are the largest family of E3 ubiquitin ligases. They consist of a CULLIN scaffold protein (CULLIN 1, 2, 3, 4A, 4B, 5, 7), a substrate receptor protein, an adaptor protein, and a RING protein for recruitment of the E2 enzyme (Cardozo and Pagano, 2004; Petroski and Deshaies, 2005c). The properties and biological function of CULLINs are very different and they are involved in variety of cellular processes such as cell growth, signal transduction, DNA replication, cell cycle, cell redox homeostasis, and others (Petroski and Deshaies, 2005a). In terms of a structural module, a large body of evidence suggests that CRLs share a similar architecture as substrates are recruited to the N-terminal regions of CULLINs that comprises a substrate receptor and adaptor. For the well-characterized example of CULLIN1, an adaptor protein SKP1 recruits numerous substrate receptors, F-box proteins. SKP1 can interact with both CULLIN1 and CULLIN7 (Dias et al., 2002). CULLIN2 and CULLIN5 utilize an elongin B/C adaptor protein and recruits substrates through suppressor of cytokine signaling/elongin BC (SOCS/BC)-box-protein, a substrate receptor. CULLIN3 utilizes BTB-domain-containing proteins where it can function both as an adaptor and substrate receptor. CULLIN4A uses an adaptor protein, DNA-damage-binding protein-1 (DDB1) (Petroski and Deshaies,

2005a). The activity of these CULLIN ligases is regulated by reversible conjugation of a small-ubiquitin like protein; Neural precursor cell expressed developmentally down-regulated protein 8 (Nedd8) (Wu et al., 2005). Nedd8 can be covalently attached to CULLINs at a conserved lysine residue and follows a similar enzymatic cascade like ubiquitination: E1 activating enzyme (Uba/APP-BP1) and E2 (Ubc12) conjugating enzyme (Osaka et al., 2000; Read et al., 2000). Neddylation is critical for the function of CULLINs and it can also increase CULLIN1-dependent ligase activity, which can support the recruitment of E2s loaded with ubiquitin (Kawakami et al., 2001; Read et al., 2000). In addition, Defective in CULLIN neddylation 1 (DCN1) works together with RBX1 RING finger subunit within CULLINs to stimulate NEDD8 conjugation, suggesting an E3-like activity for neddylation reaction (Scott et al., 2011). The Cop9 Signalosome (CSN) with a metalloprotease JAMM motif in CSN5 subunit deneddylates NEDD8-CULLINs (Ambroggio et al., 2004; Cope et al., 2002). The cycling of neddylation and deneddylation stimulates conformational changes and allows to CULLINs and RING to be in a dynamic form that facilitates the transfer of ubiquitin to the substrates.

CULLIN3-RING ubiquitin ligases

CULLIN3 is a highly conserved in the genomes of eukaryotes and the function of CULLIN3 has been characterized in many different species. For example, loss of CULLIN3 in *C. elegans* leads to defects in chromosome segregation and cytokinesis

defects during the embryogenesis probably due to katanin Mei1 accumulation (Kurz et al., 2002). The genetic knockout of CULLIN3 in mice causes an embryonic lethal phenotype with disorganization of embryonic tissues. The CULLIN3 knockout embryos accumulate excess of cyclin E leading to misregulation of S phase in cell cycle (Singer et al., 1999). Depletion of CULLIN3 homolog in fission yeast shows a retarded growth and elongation phenotype with increased sensitivity for hydroxyurea although no obvious phenotype is observed in budding yeast (Kominami and Toda, 1997; Michel et al., 2003).

The CULLIN3 family of ubiquitin ligases is different from other CULLIN-based complexes in that it only requires a protein that contains a-brac/tramtrack/broad-complex (BTB) that can function both as an adaptor and substrate recognizer. The human genome encodes about 200 BTB domain proteins and the structural analysis has shown that BTB domain forms a five α -helical fold that resembles other adaptors similar to SKP1 and ElonginC (Stogios et al., 2005). Furthermore, sequence analyses of the BTB-domain proteins have identified some of associated domains that can be sub-classified such as Meprin and TRAF homology (MATH), Kelch, BTB-non-phototropic hypocotyl 3 (NPH3), Zinc Finger, and PAM domain. Notably, these analyses also show that not all BTB domain proteins can serve as a adaptor for CULLIN3 (Stogios et al., 2005) as BTBD12 and KLHL39 that lack the 3-box motif critical for CULLIN3 binding fail to interact with CULLIN3 (Chen et al., 2015; Zhuang et al., 2009). In fact, many of these identified BTB protein family function is related to cell cycle regulation as shown by regulation of cyclin E degradation by CULLIN3. The maternal lethal effect-26 protein (MEL26), a MATH-BTB family member, degrades the complex meiosis inhibitor protein

(MEI-1) after meiosis to assemble a functional spindle and activate cytokinesis in the right time and place (Luke-Glaser et al., 2005). In addition, KLHL18-CULLIN3 complex promotes ubiquitylation and proteasomal degradation of Aurora-A kinase, an essential protein for mitotic entry. Depletion of KLHL18 results in a delay in both centrosomal activation of Aurora-A and timely entry into mitotic process (Moghe et al., 2012). Similarly, KLHL21 directly binds and ubiquitylates Aurora-B kinase, a member of the chromosomal passenger complex (CPC) that regulates chromosome alignment and separation, in the middle region of microtubules during anaphase process (Maerki et al., 2009). KLHL22-CULLIN3 complex regulates kinetochore localization of polo-like kinase 1 (PLK1) that regulates mitotic division by controlling spindle assembly and chromosome alignment (Beck et al., 2013; Elowe et al., 2007). Although KLHL22 does not regulate PLK1 stability, loss of KLHL22 results in accumulation of PLK1 on kinetochores and sustained activation of the spindle assembly checkpoint, leading to unstable kinetochore-microtubule interaction.

The other unique property of BTB-domain containing protein is that they can dimerize and form two CULLIN3 complexes within one E3 ligase complex, a feature that can increase the affinity for substrates (Zhuang et al., 2009). The best example for dimerization in substrate recognition is human Keap1 dimer that binds single Nrf2 molecule with two distinct binding sites (McMahon et al., 2006) important for optimal orientation of ubiquitylation. The CULLIN3-SPOP complex and CULLIN3-HIB complex also are shown to assemble dimers to recognize a single substrate (Zhang et al., 2009). Furthermore, SPOP-mediated CULLIN3 dimerization can enhance a rate of

polyubiquitylation by increasing associated E2 enzymes. Furthermore, there are cases where CULLIN3 complexes such as KCTD11 and SPOP form high orders of oligomerization that increase E3 ligase activity similar to dimerization (Correale et al., 2011; Errington et al., 2012).

CULLIN3-RING ubiquitin ligases in cancer

Following, I will provide descriptions for some of CULLIN3-based E3 ligases implicated in cancer biology.

KEAP1: One of the well-characterized CULLIN3 adaptor proteins is the BTB-Kelch-like ECH-associated protein (Keap1 or KLHL19) (Motohashi and Yamamoto, 2004). Keap1 was first identified as a critical inhibitor of the transcription factor Nf-E2-related factor 2 (Nrf2) by targeting it for proteasomal degradation at a steady state (Cullinan et al., 2004; Itoh et al., 1999; Kobayashi et al., 2004). Upon the oxidative or electrophilic stress, cysteine residues in Keap1 can be modified and this leads to a conformational change inhibiting activity of CULLIN3-Keap1 ubiquitin ligase complex. Accordingly, Nrf2 is stabilized and is now free to translocate into the nucleus to bind anti-oxidant responsive elements (ARE) of its target genes encoding many cytoprotective enzymes (Cullinan et al., 2004). Thus, the Keap1-Nrf2 pathway is a critical factor in the stress response and cell protective mechanism. As the oxidative stress is implicated in cancer, it is conceivable that cancer cells might hijack this pathway for their growth and survival under the stress conditions. For instance, increased Nrf2 expression provides

chemo-resistant phenotype in cancer cells while knocking down Nrf2 increases their sensitivity to chemotherapy. Moreover, overexpression of Nrf2 is shown to inhibit p53-dependent apoptosis, suppress reactive oxygen species (ROS) production in response to oncoproteins and promote proliferation of tumor cells (DeNicola et al., 2011; Faraonio et al., 2006).

Accumulating evidence suggests that the components of the Keap1-Nrf2 pathway are mutated in a variety of cancer types including ovarian, liver, lung and gallbladder cancers (Konstantinopoulos et al., 2011; Shibata et al., 2008; Yoo et al., 2012). The somatic mutations of the substrate-binding domain of Keap1 have been first found in lung cancer leading to its loss of function (Ohta et al., 2008; Singh et al., 2006). In addition, the BACK domain of Keap1 has been also altered and mutated, resulting into disruption of CULLIN3 binding and subsequent repression of ligase activity. In some cases, the mutations of Keap1 have a dominant negative effect that can disrupt the function of wild-type Keap1 and consequently activation of Nrf2. The gain of function mutation of Nrf2 has also been observed in several cancers and these mutations directly disrupt the DLG or ETGE motif where Keap1 binds (Ohta et al., 2008; Shibata et al., 2011). Nrf2 can also indirectly activate the transcription of the multidrug resistance-associated protein-1 (MRP1). MRP1 has been considered as a critical regulator of chemo-resistance and is constitutively expressed in the presence of Nrf2 (Ji et al., 2013). Other additional mechanisms such as hyper-methylation or mi-RNA silencing also deregulate the Keap1-Nrf2 pathway to repress Keap1 promoter or target Nrf2 levels, respectively (Eades et al., 2011; Guo et al., 2012; Wang et al., 2008).

SPOP: Emerging evidences have shown that Speckle-type POZ (pox virus and zinc finger protein) protein (SPOP) is involved in prostate and endometrial cancers (Kan et al., 2010). SPOP contains a MATH domain, BTB/POZ domain, and nuclear localization sequence in the C-terminus (Mani, 2014). The MATH domain is utilized for substrate binding while the BTB/POZ domain binds CULLIN3 to form an active E3 ligase complex. To date, all SPOP mutations identified in prostate and endometrial cancers are clustered in the MATH domain, supposedly disrupting the substrate binding. Interestingly, SPOP has a tumor suppressor role in these cancers while it has oncogenic role in kidney cancers where no mutations have been reported (Li et al., 2014). In fact, SPOP is another transcriptional target of HIFs and SPOP accumulation promotes tumorigenesis under the hypoxia condition. In clear cell renal cell carcinoma, SPOP is shown to degrade tumor suppressors such as PTEN, ERK phosphatases (DUSP6 and DUSP7) and pro-apoptotic DAXX protein, suggesting that it acts as a key modulator of proliferation pathway. On the other hand, SPOP directly targets oncoproteins such as androgen receptor (AR) and steroid receptor co-activator (SRC)-3 in the context of prostate cancers. AR signaling is essential for tumor initiation and progression. Importantly, SPOP cancer-associated mutations fail to bind AR, inhibiting AR proteolysis by the proteasome. Moreover, AR splicing mutations have been observed where it loses SPOP-binding hinge domain and are insensitive to SPOP-dependent degradation (An et al., 2014). Similar mechanisms apply for SRC-3 mutations to enhance AR functions and AR signaling pathways and promote prostate cancer development. This dual tumor-promoting or tumor-suppressing function of SPOP is partially explained by

its different substrates in different cancer types, suggesting that SPOP function is cell-context and substrate-dependent.

KLHL25: Recently, KLHL25-CULLIN3 complex has been shown to target ATP-citrate lyase (ACLY), a key regulator of de novo lipid synthesis (Zhang et al., 2016). ACLY is an enzyme that converts citrate to acetyl-CoA in the cytosol, and this acetyl-CoA is utilized to create fatty acids, cholesterol, and isoprenoids (Menendez and Lupu, 2007). ACLY is frequently elevated in several cancers including lung cancer and suppression of ACLY by a small molecular inhibitor has shown an efficacy in slowing down the tumor proliferation (Hatzivassiliou et al., 2005; Milgraum et al., 1997). In lung cancers, CULLIN3 expression is often down-regulated and subsequently ACLY is overexpressed, which is critical for lipid synthesis and proliferation of cancer cells. This novel tumor suppressing mechanism of CULLIN3 could be a potential therapeutic target with lung cancer with lower CULLIN3 expression.

KLHL20: Kelch-like family member 20 (KLHL20) is another adaptor protein that can bind to CULLIN3 and acts as CULLIN3-RING ubiquitin ligase complex. This protein has also been implicated in cancers, as it is first uncovered as a binding partner of death-associated protein kinase (DAPK), a tumor suppressor promoting cell death (Lee et al., 2010). By directly ubiquitylating and degrading DAPK, KLHL20-CULLIN3 complex can antagonize the cellular apoptosis, autophagic death, and necrosis. In addition to cellular death mechanisms, DAPK can also suppress cell migration and motility by regulating cytoskeletal proteins, thereby promoting anti-metastatic effects (Chen et al., 2014). Interferon (IFN) signaling regulates the KLHL20-DAPK pathway as IFN- α and

IFN- γ can sequester KLHL20 into the PML-nuclear body. Induction of PML by interferon promotes INF-induced cell death since PML competes with DAPK for KLHL20 binding, resulting in stabilization of DAPK. This establishes the basis for IFN-based cancer treatment. The fact that PML interacts with KLHL20 suggests that PML serves as a substrate of KLHL20. Previous studies have shown that PML, similar to DAPK, also exerts tumor suppressive effects as it can induce apoptosis and inhibit proliferation, metastasis and neo-angiogenesis (Bernardi et al., 2006; Reineke et al., 2010). Consistent with antitumor effects of PML, this gene is frequently mutated or deleted in a variety of cancer types. One of the main mechanisms to down-regulate PML protein levels in tumors is through hypoxia-inducible factor-1 (HIF-1) (Yuan et al., 2011). HIF-1 and HIF-2 can mediate the transcriptional programs of genes that contain hypoxia responsive element (HRE) and influence many different aspects including metastasis, metabolic reprogramming, tumor initiation and maintenance, angiogenesis, chemotherapy resistance, and others (Semenza, 2012). Since KLHL20 contains HREs in its promoter, its expression is induced under hypoxia condition and potentiates PML ubiquitylation and degradation by proteasome. Accordingly, KLHL20 expression is up-regulated and PML is down-regulated in tumors as HIF-1 α is frequently elevated through hypoxia-regulated mechanism. Specifically, the KLHL20-PML pathway is dysregulated in prostate cancers and KLHL20, HIF-1 α , and PML expression pattern nicely correlates with survival and disease progression. Interestingly, KLHL20 interacts with KLHL39, which adds an additional layer of regulation to this pathway, as it can block KLHL20-mediated degradation of PML and DAPK by binding to KLHL20 and disrupting

interaction of these substrates from KLHL20 (Chen et al., 2015). Although KLHL39 is a BTB-Kelch protein, it does not bind to CULLIN3 and is not able to form a functional E3 ligase. Rather, it can regulate PML and DAPK stability as an inhibitor of KLHL20-CULLIN3 complex.

A significant number of studies, as shown above, highlight the biological function of CULLIN3-RING ubiquitin ligases in cancer. More comprehensive understanding with systematic characterization of other CULLIN3 adaptors will be helpful to develop new therapeutic targets for cancer prevention. Further, it would be interesting to identify other BTB-proteins that are involved in development of other human pathologies and investigate novel insights into molecular basis of CULLIN3 E3 ligases and substrates.

Protein ubiquitylation and de-ubiquitylation in lymphoid malignancies

Emerging evidences suggest that human lymphoid cancers are derived from various stages of B-cell differentiation and where the cancers are originated dictate their biology. Mantle cell lymphoma and chronic lymphocytic leukemia are from pre-germinal center mature B-cells whereas the most of non-Hodkin's lymphomas and multiple myeloma are from germinal center B-cells or B-cells that have passed through germinal center. Gene expression profile studies have provided instructive recognition of different subtypes by specific transcriptional signatures (Staudt and Dave, 2005). Based on these signatures, the germinal center B cell-like (GCB) subtype of diffuse large B-cell lymphoma (DLBCL), follicular lymphoma, and Burkitt lymphoma appear to be from

germinal center B cells while the activated B cell-like (ABC) subtype of DLBCL appear to be from a post-germinal center B cells. A third subgroup of DLBCL, primary mediastinal B-cell lymphoma (PMBL) shares a significant similarity with Hodgkin lymphoma and is believed to arise from thymic post- germinal center B cells (Staudt and Dave, 2005).

It is conceivable that each of these lymphoid malignancies might activate oncogenic signaling pathways through different genomic alterations such as mutations, deletions, amplifications and translocations to promote their growth and survival. In some cases, the constitutive signaling comes from chromosomal rearrangements of transcription regulators such as Bcl6 and Irf4 (Pasqualucci and Dalla-Favera, 2015). Perhaps, the most common ways for lymphoid malignancies to prevent cell apoptosis is the constitutive activation of NF- κ B pathway. Various upstream of NF- κ B signaling molecules are aberrantly mutated from oncogenic events leading to more translocation of NF- κ B into the nucleus and activation of pro-survival transcription programs. These oncogenic pathways are the hallmarks of ABC-DLBCL subtype and are regulated at numerous levels by ubiquitination and deubiquitination enzymes (Staudt, 2010).

Protein ubiquitination in the oncogenic signaling pathway of ABC-DLBCLs

ABC-DLBCL cell lines are addicted to NF- κ B activation for their survival, and this subtype has gene expression profiling similar to normal B-cells that are activated by antigen recognition of the B-cell receptor (BCR). The BCR signaling triggers numerous

downstream signaling molecules to regulate proliferation and survival during B-cell development and is turned off in a tight fashion for cellular homeostasis. There are other receptors including CD40, BAFF, TNF receptor family, and various Toll-like receptors (TLRs) that can eventually converge into the NF- κ B pathway (Young et al., 2015). ABC-DLBCLs display a high activity of IKK β and knockdown of this kinase in a loss of function RNA interference (RNAi) screening showed toxicity effects specifically to ABC-DLBCL subtype. Further, previous RNAi study revealed a critical role CARD11-BCL10-MALT1 (CBM) complex, which is an upstream signalosome of IKK activation and mediator of NF- κ B activation, as knockdown of each component was also toxic to ABC-DLBCL cell lines (Ngo et al., 2006). In normal B-cells, BCR signaling activates protein kinase C β (PKC β), which in turn phosphorylates CARD11, releasing the inhibitory linker domain and changing into an active conformation. The active CARD11 translocates to the inner part of plasma membrane, recruits and associates with BCL10 and MALT1 to form an active complex. About 10% of ABC-DLBCLs carry activating mutations in the coiled-coil domain of CARD11, which causes freeing of the linker domain without PKC β phosphorylation and allows formation of CARD11 clusters that co-localize with MALT1 and IKK β (Lenz et al., 2008a). The levels of NF- κ B activity correlate with those of CARD11 clusters in the cancer cells with mutations of CARD11, supporting the relevance of the complex in pathology of ABC-DLBCLs.

Once the CBM complex is assembled, it promotes K63-linked ubiquitination chains by TRAF6 E3 ligase family. TRAF6 family contains a RING domain in the N-terminus, zinc finger domain, and TRAF domain. MALT1, a protease that is

constitutively activated in ABC-DLBCLs, brings TRAF6 to the CBM complex through TRAF6 binding domain and triggers auto-ubiquitination of TRAF6 with K63-linked chains. TRAF6 also functions as an E3 ligase for K63-polyubiquitination of MALT1 (Oeckinghaus et al., 2007). The importance of MALT1 K63-ubiquitin chains are supported by the MALT1 mutants that are not able to rescue NF- κ B signaling in MALT1-lacking cells. MALT1, acting as a scaffold protein, in the CBM complex is recently shown to be mono-ubiquitinated on lysine 644 residue, which is necessary and sufficient for activation of its protease activity (Pelzer et al., 2013). This allows MALT1 dimerization, which is critical for its enzymatic function. In ABC-DLBCLs, MALT1 is mono-ubiquitinated constitutively, and MALT1 mutant that cannot be mono-ubiquitinated is toxic to ABC-DLBCLs. Although CARD11 mutations contribute to oncogenic transformation in ABC-DLBCLs, the majority of ABC tumors do not contain mutations of the CBM complex, suggesting that upstream signaling pathways such as BCR signaling.

Another pathway relevant in ABC-DLBCLs is the Toll-like receptors (TLRs) and MYD88. About 30% of oncogenic active MYD88 mutations are found in ABC-DLBCLs, and the mutation targets the L265 residue in Toll/IL1 receptor (TIR) domain to Proline, which is essential for homo- and hetero-dimerization with TLRs (Ngo et al., 2011). This mutation induces activation of IRAK4, which in turn promotes the formation of a protein complex with IRAK4 and IRAK1 and activates NF- κ B pathway. The ectopic expression of L256P mutant form of MYD88 is shown to induce NF- κ B activation and this mutant cannot be substituted with the wild-type MYD88 in ABC-DLBCLs for their

survival. In Toll-like receptor (TLR) signaling pathway, interaction of MYD88 with IRAK4 and IRAK1 leads to recruitment of TRAF6. TRAF6 undergoes auto-ubiquitination with K63-linked ubiquitin chains that create interaction sites for other proteins such as TAK1. The recruitment of TAK1 to TRAF6 leads to activation of TAK1 itself that can phosphorylate IKK β (Bhoj and Chen, 2009). IRAK1 can also be poly-ubiquitinated by K63-linked chains in TLR signaling and mutations that impair this ubiquitination are shown to inhibit NF- κ B activation. Although mutation of MYD88 can promote ABC-DLBCL through activation of NF- κ B pathway, the evidence of MYD88-IRAK1-IRAK4 ubiquitination status is lacking. Moreover, whether TRAF6 is modified with K63-ubiquitin chains and how this might contribute to oncogenic MYD88 signaling pathway still remains open questions and will be important to understand the biology of ABC-DLBCLs.

The linear ubiquitin chain assembly complex (LUBAC) also plays an oncogenic role in activating NF- κ B signaling pathway. LUBAC consists of RNF31 (HOIP), RBCK1 (HOIL-1L), and SHARPIN, and RNF31 belongs to the RBR family of E3 ligases that promotes the formation of linear polyubiquitination (Kirisako et al., 2006). In a classical NF- κ B pathway, it targets NEMO/IKK γ to promote linear ubiquitination, which is necessary for IKK activation. LUBAC is recruited to receptor complexes including TRAFs and other ubiquitin ligases with K63-linked chains and provides binding domains for additional IKK complexes to be recruited. The auto-phosphorylation of IKK complexes due to the close proximity of each component increases NF- κ B activation. LUBAC can also associate with the CBM complex through interaction with other

ubiquitin chains attached to the complex. LUBAC induces MALT1 activity and plays a crucial role in chronic active BCR signaling in ABC-DLBCL cell lines as depletion of components of LUBAC impaired NF- κ B activity and is toxic to the cells (Yang et al., 2014). The cancer-associated mutations of LUBAC have been shown to increase ubiquitin ligase activity of LUBAC by enhancing the interaction between RBCK1 and RNF31, which in turn increases NF- κ B pathway. Given that mutations increase the binding of LUBAC components, it is conceivable that a small molecule inhibitor of RNF31-RBCK1 interaction could be a potential therapeutic target in ABC-DLBCLs.

TNFAIP3/A20 in ABC-DLBCLs

As mentioned previously, protein ubiquitination play an essential role in regulating NF- κ B activity. Ubiquitination process can be reversed by the deubiquitinating enzymes (DUBs), and there are about 100 DUBs in the human genome (Nijman et al., 2005). One of the most essential DUBs in lymphoid biology is the gene encoding A20 (also known as TNFAIP3). A20 is first identified as the primary gene induced by TNF treatment in endothelial cells and characterized as a protector from TNF-induced cell death (Dixit et al., 1990). Further studies have demonstrated the role of A20 as a negative regulator of NF- κ B activation in response to TNF, CD40, interleukin (IL-1), and B- and T-cell receptor activation (Beyaert et al., 2000). As mentioned above, NF- κ B signaling pathway is heavily dependent on protein ubiquitination and A20 is a central modulator of this ubiquitin-dependent signaling pathways. A20 is a dual function protein containing an

amino-terminal ovarian tumor (OTU) domain for deubiquitinating activity and zinc finger domain for ubiquitin ligase activity. The first substrate identified for A20 is receptor interacting protein-1 (RIP-1) (Wertz et al., 2004). The K63-ubiquitin chains of RIP-1 are modified by cellular inhibitor of apoptosis proteins (cIAP 1/2) during TNF receptor stimulation and deubiquitinated by A20. In immune cells, other identified substrates for A20 include MALT1, TRAF6, and IKK γ through poly-ubiquitination with K63-linked ubiquitin chains (Hymowitz and Wertz, 2010). A20 is recruited to CBM complex by binding to K63-linked poly-ubiquitin chains from the signalosomes upon the recognition of antigen in normal lymphocytes. CBM complex formation can activate TAK1 kinase to phosphorylate IKK β , leading to NF- κ B activation. MALT1 cleavage of A20 is also increased upon recruitment of A20 to CBM complex (Coornaert et al., 2008).

One of the critical roles of A20 is to establish a negative feedback that terminates the NF- κ B signaling. One model suggests that A20 removes K63-linked chains by its DUB activity and replacing with K48-linked chains that lead to degradation of its substrates (Wertz et al., 2004). However, other study provides an evidence that the ability of A20 to bind ubiquitin chains through its zinc finger domain is sufficient to block NF- κ B activation, suggesting its ligase activity is dispensable for IKK activation (Bosanac et al., 2010; Skaug et al., 2011). Specifically, its zinc finger #4 domain has an ability to bind K63-ubiquitin chains and this binding contributes to repression of TNF- α mediated NF- κ B activation. Therefore, it is conceivable that A20 acts in a variety of different ways such as interacting with and promoting ubiquitination and de-ubiquitination proteins involved in NF- κ B pathway. In normal mouse B-cells, deletion of A20 enhances their

response to variety of stimuli including BCR signaling activation. Consequently, mice are prone to develop autoimmunity due to increase in germinal center B-cells and plasma cells and die from the lethal inflammatory phenotypes (Turer et al., 2008).

A20 is frequently inactivated or lost by mutation, deletion, translocation and epigenetically silencing in lymphoid malignancies. ABC-DLBCL, MALT lymphomas, and classical Hodgkin's lymphoma carry inactivating mutations of A20 about 25%, 20%, and 45%, respectively (Compagno et al., 2009; Kato et al., 2009; Novak et al., 2009). A20 is well characterized as a tumor suppressor in ABC-DLBCLs as re-introduction of wild-type A20 in ABC-DLBCLs with biallelic deletion of A20 is shown to cause cellular apoptosis and growth arrest. A20 inactivation co-occurs with MYD88 and CD79B mutations, suggesting that it might contribute to oncogenic MYD88 and BCR signaling pathways (Ngo et al., 2011). In ABC-DLBCLs, it is likely that A20 mutations can enhance constitutive NF- κ B signaling with other genetic alteration events and its mutation alone may not be sufficient to activate NF- κ B signaling activity. Of note, A20 is recruited to the CBM complex when IKK γ is modified with linear ubiquitin chains via LUBAC and gain of function mutations of LUBAC increases A20 recruitment (Yang et al., 2014). Given that virtually almost all lymphoid malignancies activate NF- κ B signaling for their growth and survival, pharmacological interference with this pathway provides a strong rationale for therapeutics.

Pharmacological inhibitions in lymphoid malignancies

Given that UPS plays an important role in a variety of biological processes, it is conceivable that deregulation in this system would contribute to human diseases including lymphoid malignancies. The proteasome degradation is the final step in the UPS pathway and proteasome is investigated as the first potential target for therapeutic approaches. Proteasome inhibitors were initially synthesized to determine the function and proteolytic specificity of the proteasome (Vinitsky et al., 1994; Vinitsky et al., 1992). The possibility of proteasome inhibitors as therapeutic agents derives from the early work where the inhibitors induced apoptotic cell death in leukemic cell lines (Imajoh-Ohmi et al., 1995; Shinohara et al., 1996). This tumor inhibition effect was supported further by efficacy of the proteasome inhibitor against an *in vivo* Burkitt's lymphoma tumor model (Orlowski et al., 1998). Later on, proteasome inhibitors showed a wide spectrum of pro-apoptotic effects against hematologic malignancies and solid tumors including non-small cell lung and prostate cancer as well as follicular non-Hodgkin's lymphoma, multiple myeloma and mantle cell lymphoma (Aghajanian et al., 2002; Cortes et al., 2004; Papandreou et al., 2004; Richardson et al., 2003).

One of the mechanisms of proteasome inhibitors is to suppress nuclear factor- κ B (NF- κ B) signaling by stabilizing the inhibitory molecule I κ B that binds NF- κ B factors. This, in turn, prevents NF- κ B factors from nuclear translocation and down-regulates their target genes, resulting in anti-survival effects. Specifically, NF- κ B can induce production of growth and angiogenesis factor like interleukin-6 and increase expression of cell adhesion molecules such as ICAM-1 by plasma cells, promoting tumor microenvironment. Given that NF- κ B is involved in suppression of apoptosis,

proliferation, angiogenesis, and oncogenic transformation, it is considered that the NF- κ B pathway is central to pathogenesis of cancer and a strong rationale therapeutic target. In addition, the pro-survival effects of NF- κ B functions are activated by the chemotherapies and inhibition of this pathway enhances sensitivity to the treatment (Wang et al., 1999; Wang et al., 1996). In addition to NF- κ B inhibition, there are number of other mechanisms of proteasome inhibitors that contribute to anti-tumor effects. For instance, the inhibitors can interfere with timely degradation of cell cycle regulators such as p27 and p21, causing cell cycle arrest in cancer cells while they can also accumulate c-myc and cyclin-D1 for the proliferative effect (Adams et al., 1999; Almond and Cohen, 2002; Chauhan et al., 2005). The proteasome inhibitor can also stabilize pro-apoptotic proteins such as p53 and Bax proteins and anti-apoptotic Bcl-2, promoting a pro-survival state (Hideshima et al., 2003). It is recognized that proteasome activity is generally elevated in lymphoid malignancies, and this led to development of more potent and selective proteasome inhibitor with improved pharmacological properties, a bortezomib, which is entered into the clinic trials (Jagannath et al., 2004; Richardson et al., 2003; Richardson et al., 2006).

Bortezomib, a boronic acid dipeptide, binds with high specificity and affinity to the 20S proteasome reversibly and blocks its hydrolyzing activity. In the animal models, bortezomib did not enter the tissues such as brain, eyes and spinal cord, suggesting that these tissues are protected from toxic effects of proteasome inhibition (Adams et al., 1999). Strikingly, bortezomib potently inhibited proliferation of multiple myeloma cells and binding of these tumor cells to bone marrow stromal cells in preclinical models, thus

inhibiting tumor microenvironment. Bortezomib-induced cell death is accompanied by release of a pro-apoptotic mitochondrial protein such as cytochrome c, up-regulation of endoplasmic reticulum (ER) stress, and induction of c-Jun N-terminal kinase (JNK) (Mitsiades et al., 2002). Activation of JNK leads to Fas up-regulation and induction of caspase-8-mediated apoptotic pathway with caspase-3 activation. Caspase-3 induction results in cell apoptosis by increase of p53 activity by MDM2 degradation. Several evidences have suggested that myeloma cells are highly sensitive to bortezomib because of high level of immunoglobulin synthesis that correlates with the high level of ER stress (Nawrocki et al., 2005a; Nawrocki et al., 2005b; Obeng et al., 2006). This characteristic of myeloma cells make them more dependent on unfolded-protein response and susceptible to bortezomib compared to other B-cell malignancies. The efficacy and safety of this drug were proven through Phase 1-3 clinical trials and the impressive results led to an approval by the FDA in 2003 to use bortezomib as the third-line treatment for relapsed or refractory plasma cell myeloma (PCM) patients (Kane et al., 2003; Kane et al., 2006). Subsequently, it became the first line treatment in 2008 (Islam and Ambrus, 2008; San Miguel et al., 2008). There are extensive ongoing studies to examine the combination of bortezomib and other chemotherapy or active agents in clinical trials for blood cancers.

Given that ABC-DLBCLs harbor constitutive NF- κ B activation, combination of bortezomib treatment and cytotoxic chemotherapy (Etoposide, Prednisolone, Oncovin, Cyclophosphamide, and Hydroxydaunorubicin called EPOCH) in a clinical trial was initiated for the relapsed and refractory DLBCL patients (Dunleavy et al., 2009). Although bortezomib as a single agent did not show any efficacies, the combination

therapy yielded high responses and greatly improved overall survival rates specifically in ABC-DLBCL patients. This was remarkable achievement in that previous clinical trials with chemotherapy alone had very poorer cure rates. Another way of targeting NF- κ B is to interfere with β -TrCP ligase that recognizes the phosphorylated I κ B α and degrades in a proteasome-dependent manner. The NEDD8 modification is required for CULLIN-RING-ubiquitin ligases and small molecule (MLN4924) that inhibits NEDD8 activating enzyme (NAE) has been regarded as an attractive therapeutic approach in clinical trials (Soucy et al., 2009). Treatment with MLN4924 can inhibit neddylation and the ligase activity of β -TrCP to promote I κ B α stabilization, leading to suppression of NF- κ B transcriptional program. Additionally, inhibition of MALT1 proteolytic activity with peptide mimetics showed efficacy in decreasing NF- κ B activation and IL-2 secretion in antigen-stimulated T-cells (Rebeaud et al., 2008). Since MALT1 also cleaves and inactivate A20, the peptide inhibitors of MALT1 have also been utilized and shown some toxicity in ABC-DLBCL cell lines even in those with CARD11 mutations, providing a great rationale for development of MALT1 therapy (Ferch et al., 2009; Hailfinger et al., 2009). More recently, the most prominent therapeutic targets are upstream kinases of IKK complexes including BTK kinase that couples chronic active BCR signaling with NF- κ B activation. The BTK inhibitor, ibrutinib, is an irreversible and covalent inhibitor and shown to potently target BCR signaling and inhibit lymphocytes adhesion and tumor-promoting microenvironment (Davis et al., 2010; Yang et al., 2012). Specifically, it can prevent bone-marrow homing mechanisms of lymphoma cells and lead the cells from the tissue to the peripheral blood causing lymphocytosis. Almost all BCR signaling inhibitors

utilize this similar mechanism to attack lymphoid malignancies. Given that ABC-DLBCLs depends on BCR and NF- κ B signaling for its growth and survival, it is expected that the patients with this subtype would be more responsive to ibrutinib treatment. The phase II trials have confirmed that ibrutinib produced complete and partial response about 40% in ABC-DLBCL patients, but only 5% in GCB-DLBCL patients (Wilson et al., 2015). The interesting point of this study was that ABC tumors with concomitant MYD88 mutations with BCR mutations display greater response rates, a result confirming cooperation between BCR and MYD88 pathways. Both SYK and PKC β kinases are therapeutic targets because PKC β phosphorylates and activates the wild-type CARD11 and SYK phosphorylates many downstream effectors of BCR signaling pathway. Although SYK inhibitor, fostamatinib, showed some efficacy (22%) in phase I/II study for DLBCL patients, the follow-up phase II trial only showed 3% for refractory and relapsed DLBCL patients and no response rate for ABC-DLBCL (Flinn et al., 2016). However, BCR pathway inhibitors are very effective treating CLL and MCL and considered a major breakthrough for treating B-cell malignancies although the reasons why these particular B-cell cancers are more sensitive are not much known (Jerkeman et al., 2017). Nevertheless, BCR inhibition will be the basis for therapeutic combination therapy and understanding molecular mechanism for drug sensitivity and resistance will help to design more rational treatment for the lymphoid malignancies. In addition, going forward, evaluation of risks such as unexpected side effects along with benefits of combination therapy will be critical for the effective targeted treatment.

CHAPTER 2 : EXPERIMENTAL METHODS

Cell lines, antibodies, drugs, and other reagents

HEK293T cells were cultured using Dulbecco's modified Eagle's medium containing 10% fetal bovine serum (FBS). The following cell lines were cultured in RPMI 1640 medium containing 10% FBS: BJAB, Pfeiffer, OCI-LY8, Karpas422, ARP1, SUDHL4, SUDHL6, SUDHL10, VAL RAMOS, U2932, TMD8, HBL1, RCK8, and HLY-1. The following cell lines were cultured in Iscove's modified Dulbecco's Medium containing 10% FBS: OCI-LY1, OCI-LY7, OCI-LY10, and OCI-LY19. All antibodies were diluted with 1:1000 ratio unless otherwise specified. The following antibodies were used: anti-Roquin1/2 (MABF288), anti-Roquin2 (sc-165026) anti-Roquin2 (Bethyl Laboratories, A305-150A), anti-KLHL6 (ab182163), anti-KLHL6 (NBP1-46128), anti-Tubulin (sc-8035), anti-GAPDH (MAB374,1:5000), anti-CDK1 (sc-954), anti-CDK2 (sc-163), anti-p-AKT S473 (CST, #4051), anti-FLAG (Sigma F7425, 1:3000), anti-HA (Biolegend, #901513), anti-Cullin1 (Invitrogen, #71-8700), anti-Cullin3 (Bethyl Laboratories, A301-109A), anti-ubiquitin K48 (EMD Millipore, 05-1307), anti-p-ERK T202/Y204 (CST, #9101), anti-ERK1/2 (CST, #9102), anti-AKT (CST, #4691), anti-TNFAIP3 (CST, #5630), anti-p-IkB S32 (CST, #2859,1:500), anti-p100/p52 (CST, #4882), anti-p105/p50 (sc-7178), anti-RelA (sc-372), anti-RelB (sc-226), anti-histone H2A(EMD Millipore, 07-146) and anti-histone H3 (ab1791, 1:5000), ECL Rabbit IgG HRP-linked whole antibody (NA934-1ML, 1:5000), ECL Mouse IgG, HRP-linked whole antibody (NA931-1ML, 1:5000), Anti-Rat IgG (H+L) polyclonal antibody (Jackson ImmunoResearch, 112-035-

003, 1:5000), Anti-Goat IgG (H+L) polyclonal antibody (Jackson ImmunoResearch, 705-035-003,1:5000). The following agarose beads were used: anti-FLAG-M2 affinity gel (Sigma, A2220) and Strep-Tactin Superflow 50% suspension (Neuromics). Goat-F(ab')₂ anti-human IgM (SouthernBiotech, #2022-01) was used for BCR stimulation experiment. 150µl of Corning Matrigel Basement Membrane Matrix was used in mix of 100µl of DMEM/F12 containing 10% Knockout Serum Replacement (SR) and plated in Millicell EZ slide (Millipore) for 3D culture assays. Cell colonies were grown for 14 days and 300µl of Corning Dispase (#354235) was used to count the cell numbers according to manufacturers' protocols. The following drugs were used: ActinomycinD (Sigma Aldrich; 2µg/ml final concentration), proteasome inhibitor MG132 (Peptide Institute Inc.; 10 µM final concentration), Cycloheximide (Sigma Aldrich; 50µg/ml final concentration), Doxycycline hyclate (Sigma Aldrich; 1 µg/ml final concentration), IKK-16 (Selleckchem; 10µM final concentration), MLN4924 (Active Biochem; 5µM final concentration), Bortezomib (Selleckchem), Ibrutinib (Selleckchem; 5µM final concentration). Cells were also selected with puromycin (Sigma Aldrich; 0.5µg/ml-1µg/ml final concentration) and hygromycin (ThermoFisher; 100µg/ml) for generation of stable cell lines. MTS assays (Promega, G5421), AnnexinV staining (Thermo fisher Annexin V, Alexa Fluor® 680 conjugate; A35109) was carried out according to manufacturers' protocols. FITC mouse anti-human IgM (BD, #562029) and APC mouse anti-human IgG (BD, #562025) were used according to manufacturing instruction to detect expression of B-cell receptors.

Immunoblotting and immunoprecipitation

For immunoblotting, cell lysis was carried out with RIPA-lysis buffer (50 mM Tris pH 8.0, 150 mM NaCl, 0.1% SDS, 0.5% Na deoxycholate, 1% NP-40) supplemented with protease and phosphatase inhibitors and N-ethylmaleimide (Sigma Aldrich; 10mM). Equal amount of proteins (~15µg) were used to a 6% polyacrylamide gel for electrophoresis. Bands quantification was performed using ImageJ software and plotted using nonlinear-fit curve in Prism. For immunoprecipitation, cell lysis was carried out with NP40 buffer (15 mM Tris pH 7.4, 1 mM EDTA, 150 mM NaCl, 1 mM MgCl₂, 10% glycerol, 0.1% NP-40) containing protease inhibitors and DTT. After 5 min of lysis, the whole cell lysates were spun at 15,000 rpm for 5 min at 4 °C. The supernatants were incubated with 15 µL of anti-FLAG-M2 affinity gel agarose beads per each sample for 2 hrs at 4 °C. After 4 washes with NP-40 lysis buffer, the immunoprecipitates were eluted with 2X Laemmli buffer (240 mM Tris pH 6.8, 8% SDS, 0.04% bromophenol blue, 5% β-mercaptoethanol, 40% glycerol) and boiled for electrophoresis.

Nuclear extraction

Cell lysis was carried out in hypotonic buffer (50 mM Tris pH 8.0, 1 mM EDTA, 0.02% NP-40, 10% glycerol) containing protease inhibitors. Trypan blue was used to check nuclear isolation efficiency. Once 90% cell lysis efficiency was achieved, the whole lysates were spun at 2,400 rpm for 3 min at 4 °C. The supernatants were removed and used as a hypotonic cytoplasm fraction. The intact nuclear pellets were washed one time

with hypotonic buffer. The nuclei were lysed with RIPA buffer (50 mM Tris pH 8.0, 150 mM NaCl, 0.1% SDS, 0.5% Na deoxycholate, 1% NP-40) with protease and phosphatase inhibitors. After 5 min of nuclear lysis, the samples were spun at 15,000 rpm for 5 min at 4 °C. The supernatants were separated and used as a detergent-soluble nuclear fraction.

λ-Phosphatase treatment

After the four washes of the immunoprecipitation protocol, the beads were washed two times with the Tris-NaCl buffer (25 mM Tris pH 7.4, 50mM NaCl) and divided equally for each condition indicated. The beads were then incubated with the reaction mix (25 mM Tris pH 7.4, 50mM NaCl, 0.1 mM MnCl₂, 1X NEB buffer PMP) with or without 1 µl of λ-phosphatase (New England Biolabs, P0753, 400 U) for 30 min at 30 °C. The immunoprecipitates were eluted with 2X Laemmli buffer and were eluted with 2X Laemmli buffer.

Chromatin immunoprecipitation

Cells were collected, washed with PBS two times and cross-linked with 1% formaldehyde for 5min. Next, cross-linked cells were treated with 125 mM glycine for 5 min, washed with PBS once and lysed with the lysis buffer (0.2% NP-40, 100 mM Tris-HCl pH8, 10 mM NaCl) on ice for 10 min. The cells were centrifuged at 2500 rpm for 5min at 4 °C, and the cell pellets were re-suspended with nucleus lysis buffer (0.1% SDS, 50 mM Tris-HCl pH8, 10 mM EDTA) followed by sonication using the Covaris S220

system (Thermo Fisher Scientific, #4465653) according to the manufacturer's protocol. After the sonication, the nucleus lysates were centrifuged at 13,000 rpm for 5 min at 4 °C and the supernatants were collected. Next, 10 µl of Dynabeads Protein A (Life Technology, #10001D) were incubated with 1 mg/ml of BSA for 1 hour at 4 °C and 30 µl of Dynabeads were incubated with 5 µg of antibodies at 4 °C for 4 hours. The sonicated nuclear lysates (300µl) were incubated with 10 µl of BSA-blocked Dynabeads for 3 hours at 4 °C. These pre-cleared nuclear lysates (300µl) was incubated with 30 µl of antibody-conjugated Dynabeads overnight with addition of 700 µl of IP buffer (0.01% SDS, 1% TritonX-100, 20 mM Tris-HCl pH8, 2 mM EDTA, 150 mM NaCl). The Dynabeads were washed two times each with low salt IP wash buffer (0.01% SDS, 1% TritonX-100, 20 mM Tris-HCl pH8, 2 mM EDTA, 50 mM NaCl), with medium salt IP wash buffer (0.01% SDS, 1% TritonX-100, 20 mM Tris-HCl pH8, 2 mM EDTA, 300 mM NaCl), and with high salt IP wash buffer (0.01% SDS, 1% TritonX-100, 20 mM Tris-HCl pH8, 2 mM EDTA, 500 mM NaCl). Then, the Dynabeads were washed with LiCl buffer (1% NP-40, 1% deoxycholic acid, 10 mM Tris-HCl pH8, 1 mM EDTA, 0.25 M LiCl) and with TE buffer (10 mM Tris-HCl pH8, 1 mM EDTA) one time each. The chromatin reverse cross-linking and DNA elution were performed using IPure kit (diagenode, C03010015) according to the manufacturer's protocol.

Xenograft experiments

NOD/SCID/IL2R $\gamma^{-/-}$ (NSG) mice were purchased from the Jackson Laboratory. For KLHL6 experiment, NSG mice (6-8 weeks old) were injected sub-cutaneously with

1x10⁷ U2932 KLHL6^{-/-} (clone-derived) cells re-expressing either with KLHL6 (WT), KLHL6 (S94I) or empty vector (EV). For Roquin2 experiment, NSG mice were injected sub-cutaneously with 1x10⁷ U2932 cells infected with retroviruses encoding HA-Roquin2 (WT) or HA-Roquin2 (Y691F). Tumor volume and weight was monitored weekly by palpation and eye inspection and measured with caliper and analytical scale. All animal work was performed following the ethical guidelines and protocols approved by the Institutional Animal Care and Use Committee of the University of Pennsylvania.

KLHL6 complexes purification for mass spectrometry

HEK293T and ARP-1 cells stably expressing FLAG-tagged KLHL6 (WT) or FLAG-tagged KLHL6 (L65P) were collected and lysed in lysis buffer (50 mM Tris-HCl pH 7.5, 150 mM NaCl, 1 mM EDTA, 50 mM NaF, 0.5% NP40) with protease and phosphatase inhibitors. Flag-KLHL6 (WT) or Flag-KLHL6 (L65P) was immunoprecipitated with anti-FLAG agarose beads and washed five times with lysis buffer and proteins were eluted with FLAG peptides. 1% of protein eluates were separated by SDS-PAGE and stained by Silver Staining (Life Technology). The final eluates were precipitated with trichloroacetic acid (TCA) for mass spectrometry analysis.

In vitro binding assays

In vitro-translated FLAG-tagged KLHL6 was incubated with indicated amounts of

Roquin2 peptides in lysis buffer (50 mM Tris-HCl pH 7.5, 250 mM NaCl 0.1% Triton X-100, 1 mM EGTA). Anti-streptavidin resin was added to the samples and incubated at 4°C for 2hrs with rotation. Samples were washed three times with the lysis buffer, and protein complexes were eluted in Laemmli buffer. For another binding experiment, HEK293T cells stably expressing KLHL6 (WT) were lysed with the lysis buffer and the whole cell lysates were incubated with anti-streptavidin resin and the peptides. The protein complexes were eluted in Laemmli buffer.

In vitro and in vivo ubiquitylation assay

For *in vitro* ubiquitylation assay, FLAG-KLHL6 or FLAG-KLHL6/HA-Roquin2 complex were immunoprecipitated from HEK293T cells with anti-FLAG agarose beads. The purified proteins on the beads were incubated with 10 µl of ubiquitylation mix (50 mM Tris pH 7.6, 5 mM MgCl₂, 2 mM ATP, 1.5 ng/µl E1 (Boston Biochem), 10 ng/µl Ubc3, 10 ng/µl Ubc5, 2.5 µg/µl ubiquitin (Sigma), 1 µM ubiquitin aldehyde). The ubiquitylation reactions were incubated at 37°C for the indicated time points and subjected to SDS-PAGE analysis. When indicated, upon ubiquitylation reaction, beads were re-suspended in 1% SDS, boiled, and diluted to 0.1% SDS. The eluted proteins were immunoprecipitated with anti-FLAG agarose beads, washed, and eluted in Laemmli buffer. For *in vivo* ubiquitylation assay, U2932 *KLHL6*^{+/+} and *KLHL6*^{-/-} (clone-derived) cells were pre-treated with or without MG132 for 6hrs before cell lysis with 1% SDS and incubated in 95°C for 5 min. Then, the cell lysates were diluted to 0.1% SDS in NP-40 buffer and immunoprecipitated using a polyclonal antibody against Roquin2. The

immunocomplexes were subjected to SDS-PAGE analysis.

Transient transfections, generation of viruses for infection, and electroporation

Polyethylenimine (PEI) was used for transient transfection in HEK293T cells. For retrovirus and lentivirus production, GP-293 packaging cells (Clontech) or pCMV-DeltaR8.2 were used respectively. After 48 hours of transfection, the virus-containing medium was collected, filtered, and used to spin-infect the cells at 1800 rpm for 30 minutes. 10 µg/ml of polybrene was added to the cells with virus supernatant and incubated with six hours to overnight. RCK8 cells were electroporated using Neon transfection system according to manufacture's protocol with LentiCRISPRv2 vector carrying a GFP marker. Transfected cells were sorted by GFP positive cells. siRNA oligos transfection was also performed with Neon transfection system according to manufacture's protocol.

Generation clonal KLHL6^{-/-} cell lines

U2932 or OCI-LY10 Cas9-expressing cells were infected with lentiviruses encoding gRNAs targeting KLHL6 gene. After puromycin selection, cells were plated at a concentration of 0.5 cells/well in a 96 well plate and a single cell was grown and screened for KLHL6 knockout.

Plasmids, cloning, shRNA, gRNA, and siRNA sequences

Dr. Carola Vinuesa kindly provided human Roquin1 and Roquin2 cDNA and we sub-cloned Roquins into different vectors: pcDNA3.1-FLAG, pcDNA3.1-HA or pcDNA3.1-FLAG-Streptavidin. Human KLHL6 cDNA was purchased from Dharmacon and we sub-cloned into different vectors: pcDNA3.1-FLAG, pcDNA3.1-FLAG-Streptavidin, and pREV-TRE. QuikChange Site-directed Mutagenesis kit (Stratagene) was used to generate C-terminal deletion mutants and point mutants of Roquin2. Standard PCR methods were used to generate N-terminal deletion mutants. The pcDNA3.1 V5-PTPN14 (#61003) vector was purchased from Addgene. Dr. Elizabeth White kindly provided all MSCV-N-term V5-tagged PTPN14 deletion mutants. cDNAs encoding FLAG-tagged or HA-tagged KLHL6 and KLHL6 mutants were sub-cloned into MIGR1 retroviral vector and pREV-TRE vector. cDNAs encoding FLAG-HA-tagged or untagged Roquin2 and Roquin2 mutants were sub-cloned into pBabe Puro or pMSCV retroviral vector. shRNAs targeting human KLHL6 were sub-cloned into pSicoR-Puro lentiviral vector. shRNAs targeting human Roquin2 were sub-cloned into pSicoR-GFP lentiviral vector. KLHL6 cDNA and HA-tagged PTPN14 cDNA were sub-cloned into pTRIPZ vector.

The target sequences to knock-down human KLHL6:

hKLHL6_shRNA#1:

For: TGCAGCCAGCAACTATTTTCATTCAAGAGATGAAATAGTTGCTGGCTGCTT
TTTTC

Rev: TCGAGAAAAAAGCAGCCAGCAACTATTTTCATCTCTTGAATGAAATAGTT

GCTGGCTGCA

hKLHL6_shRNA#2:

For:TGAAGCCTTGAACCCAGAAATTCAAGAGATTTCTGGGTTCAAGGCTTCTT
TTTTTC

Rev:TCGAGAAAAAGAAGCCTTGAACCCAGAAATCTCTTGAATTTCTGGGTTCA
AAGGCTTCA

hKLHL6_shRNA#3:

For:TGCATGATGTTTGGAAATATTTCAAGAGAATATTTCCAAACATCATGCTTT
TTTTTC

Rev:TCGAGAAAAAGCATGATGTTTGGAAATATTCTCTTGAAATATTTCCAAA
CATCATGCA

hKLHL6_shRNA#4:

For:TGGATTCAGATTGAGTATTTTTCAAGAGAAAATACTCAATCTGAATCCTTT
TTTTTC

Rev:TCGAGAAAAAGGATTCAGATTGAGTATTTCTCTTGAAAATACTCAAT
CTGAATCCA

The target sequences to knock-down human Roquin2:

hRoquin2 shRNA#1:

For: TGCAGTTGTCTGCCAATCTATTCAAGAGATAGATTGGCAGACAACTGCTT
TTTTTC

Rev: TCGAGAAAAAAGCAGTTGTCTGCCAATCTATCTCTTGAATAGATTGGCAG
ACAACTGCA

hRoquin2 shRNA#2:

For: TGGACTCAGATACCCTTTGATTCAAGAGATCAAAGGGTATCTGAGTCCTT
TTTTTC

Rev: TCGAGAAAAAAGGACTCAGATACCCTTTGATCTCTTGAATCAAAGGGTA
TCTGAGTCCA

gRNAs targeting human KLHL6 were sub-cloned into Lenti-Guide-Puro vector, Lenti-Guide-GFP and LentiCRISPRv2 vector. The target sequences to knockout human KLHL6:

hKLHL6_gRNA#2 For: CAGAGCGTTTTCCATTCGCA

Rev: TCGAATGGAAAACGCTCTG

hKLHL6_gRNA#3 For: TCAGAGCGTTTTCCATTCGC

Rev: GCGAATGGAAAACGCTCTGA

hKLHL6_gRNA#4 For: AAAGGTCAAATTTGACGACG

Rev: CGTCGTCAAATTTGACCTTT

hKLHL6_gRNA#5 For: GACTTGGTCGAGATCTTAAA

Rev: TTTAAGATCTCGACCAAGTC

hKLHL6_gRNA#6 For: ACTTGGTCGAGATCTTAAAT

Rev: ATTTAAGATCTCGACCAAGT

siRNA duplexes were ordered from Dharmacon.

The target sequence for human KLHL6 siRNA: GCACGAAGGAUGAACGGUU

The target sequence for human Roquin2 siRNA: GCUUGAAAAGUAUCGAUUA

Non-targeting siRNA control sequence: UGGUUUACAUGUCGACUAA

mRNA Analysis and q-PCR primers

RNeasy Kit (Qiagen) and trizol (Invitrogen) were used for extracting RNA. Maxima first strand cDNA synthesis kit (Thermo Fisher) and RNA to cDNA Ecodry Premix kit (Clontech) were used for cDNA synthesis. Quantitative PCR analysis with SYBR Green PCR Master Mix (Applied Biosystems) was carried out according to standard procedures.

Primer sequences used for q-PCR analysis:

hGAPDH FOR: 5' GGAGCGAGATCCCTCCAAAAT 3'
REV: 5' GGCTGTTGTCATACTTCTCATGG 3'

hTNFAIP3 FOR: 5' TCCTCAGGCTTTGTATTTGAGC 3'
REV: 5' TGTGTATCGGTGCATGGTTTTA 3'

hTNFRSF14 FOR: 5' CCACTGGGTATGGTGGTTTC 3'
REV: 5' TCACCTTCTGCCTCCTGTCT 3'

hTNF FOR: 5' CTGCACTTTGGAGTGATCGGC3'
REV: 5' CACCAGCTGGTTATCTCTCAGCTCC 3'

hNFKBIE FOR: 5' TCTGGCATTGAGTCTCTGCG 3'
REV: 5' AGGAGCCATAGGTGGAATCAG 3'

hLTA FOR: 5' GCTGCTGGTTCTGCTGCC 3'
REV: 5' CAAGGAGAAACCATCCTGGAGGAAG 3'

hNEDD4L FOR: 5' ACTTCCTCCTCCTCCTCTGC 3'
REV: 5' TCCAAGTCTTCGCTGATGTG 3'

hABLIMI FOR: 5' ACTGCATCTCTCCCTGGCTA 3'
REV: 5' TGTTGGTCACCATGAGCATT 3'

hSYNGAPI FOR: 5' TCTGAGGAAAACCTGCGAGGT 3'

REV: 5' GCAAACACCTCCTTCAGCTC 3'

hNEIL2 FOR: 5' GCCTCCACAAAAAGAAGTGC 3'

REV: 5' TTGTTGGCTTTCTTGGCTCT 3'

hLGALS8 FOR: 5' CTGGGCATTTATGGCAAAGT 3'

REV: 5' GACAGTTCTGGGTGCGATTT 3'

hCD274 FOR: 5' TATGGTGGTGCCGACTACAA 3'

REV: 5' TGCTTGTCCAGATGACTTCG 3'

hKLHL6 FOR: 5' GCAGCCAGCAACTATTTTCAGG 3'

REV: 5' ACGTGTAGTCCAACAGAGTGT 3'

hNFKBIA FOR: 5' TATAAACGCTGGCTGGG 3'

REV: 5' CCCTAGTGGCTCATCGC 3'

Normalization and quantification of protein levels

Protein concentrations of whole cell lysates were quantified using a Bio-Rad DC protein assay (Lowry assay) according to the manufacturer's protocol. Equal amounts of protein (~15µg) were loaded for SDS-PAGE analyses. Additionally, equal amount of protein levels was confirmed by staining the membrane with Ponceau S and by immunoblotting for a normalization control.

Cell proliferation assay

For MTS cell proliferation assay, 2×10^3 cells were used according to manufacturers' protocols. For the long-term cell proliferation assay, $\sim 5 \times 10^4$ - 2×10^5 cells were plated, counted and re-plated every 3-5 days and cumulative cell numbers were graphed.

Flow cytometry

Flow cytometry was performed using Attune NxT Flow Cytometer and following channels were used: FITC for GFP-expressing cells, Alexa-680 AnnexinV to detect apoptosis, FITC to detect IgM or APC to detect IgG staining. All stainings were performed according to manufacturers' protocols. To measure shRNA or gRNA effects on cell proliferation and survival, 5×10^5 cells were spin-infected with 1000 μ l lentivirus supernatant with the addition polybrene (8 μ g/ml) in a 24-well plate. After the spin-infection, the supernatant was removed and replaced with regular medium and the percentage of infected cells was measured from day 2 when GFP was visible in the infected cells. The number of alive GFP-positive cells on day 2 was set to 100% to normalize for transduction efficiency and every consecutive assessment was calculated based on day 2. When indicated, AnnexinV positive cells were gated on GFP positive cells.

MudPIT analysis

TCA-precipitated proteins were urea-denatured, reduced, alkylated and digested with endoproteinase Lys-C (Roche) and modified trypsin (Roche), as previously described (Florens and Washburn, 2006; Washburn et al., 2001). Peptide mixtures were loaded onto 100- μm fused silica microcapillary columns packed with 5- μm C18 reverse phase (Aqua, Phenomenex), strong cation exchange particles (Luna, Phenomenex), and reverse phase (McDonald et al., 2002). Loaded microcapillary columns were placed in-line with a Quaternary Agilent 1100 series HPLC pump and a LTQ linear ion trap mass spectrometer equipped with a nano-LC electrospray ionization source (Thermo Scientific). Fully automated 10-step MudPIT runs were performed on the electrosprayed peptides, as previously described (Florens and Washburn, 2006). Tandem mass (MS/MS) spectra were analyzed using SEQUEST (Eng et al., 1994) against a database of 61,318 sequences, consisting of 30,449 non-redundant human proteins (downloaded from NCBI on 2012-08-27, 160 usual contaminants (such as human keratins, IgGs and proteolytic enzymes), and, to estimate false discovery rates, 30,659 randomized amino-acid sequences derived from each non-redundant protein entry. Peptide/spectrum matches were sorted and selected using DTASelect with the following criteria set: spectra/peptide matches were only retained if they had a DeltCn of at least 0.08 and a minimum XCorr of 1.8 for singly-, 2.0 for doubly-, and 3.0 for triply-charged spectra. Additionally, peptides had to be fully tryptic and at least seven amino acids long. Combining all runs, proteins had to be detected by at least two such peptides, or one peptide with two independent spectra. Under these criteria the final FDRs at the protein and spectral levels were

2.1%±0.3 and 0.94% ± 0.03, respectively. Peptide hits from multiple runs were compared via CONTRAST (Tabb et al., 2002). Normalized Spectral Abundance Factors (NSAFs) were calculated for each detected protein, as previously described (Florens et al., 2006; Paoletti et al., 2006; Zybaylov et al., 2006).

Analysis of KLHL6 expression in DLBCL patients

Raw DNA copy number data from high-resolution single nucleotide polymorphism (SNP) microarray analysis of 609 primary DLBCL tumors were used from a previously published study (Green et al., 2014). The data were visualized via the integrative genomics viewer (IGV) (Robinson et al., 2011). Cases were sorted by their KLHL6 copy number status, and those with copy number <1.8 were classified as a deletion, as previously described criteria (Monti et al., 2012). Gene expression microarray from 249 tumors with matched DNA copy number data were from a previously published study (Green et al., 2014). Their cell of origin subtype was determined via the Wright algorithm (Wright et al., 2003), as previously reported (Monti et al., 2012). Row normalized heatmaps for 4 probe sets corresponding to KLHL6 were sorted according to their average expression, and significant reduction in KLHL6 expression defined as being 1 standard deviation below the mean. Raw cel files for publicly available Affymetrix U133 plus 2.0 gene expression microarray data for diffuse large B-cell lymphoma tumors (GSE10846, GSE34171, GSE31312) were obtained from the gene expression omnibus. Data were RMA normalized using the ExpressionFileCreator module of GenePattern

(Reich et al., 2006). Scores to categorize diffuse large B-cell lymphoma tumors by cell of origin subtype were calculated according to the Wright algorithm (Wright et al., 2003). Intensities from the 4 probes for KLHL6 (1555275_a_at, 1560396_at, 1560397_s_at, 228167_at) were averaged for use in the survival analysis. Cases were dichotomized into being above or below the median expression level of KLHL6 expression within each dataset to avoid confounding batch effects. For NF- κ B signatures, Affymetrix U133 plus 2 gene expression microarrays were performed on 84 matched DLBCL tumors (Green et al., 2014; Lenz et al., 2008f). Raw cel files were RMA normalized with median scaling using the ExpressionFileCreator module of GenePattern (Reich et al., 2006). Sample-level enrichment of NF- κ B target genes was calculated using the single sample gene set enrichment analysis (Barbie et al., 2009) and the c3 TFT gene set database of mSigDB (Liberzon et al., 2011).

RNA sequencing

Total RNA was extracted using RNeasy Mini Kit (QIAGEN, #74104) and polyA+ transcripts were obtained with oligo (dT)₂₅-conjugated magnetic Dynabeads (Thermo Fisher). Preparation of strand specific RNA-seq libraries were carried out according to a published protocol (Parkhomchuk et al., 2009). In short, RNA was fragmented chemically in first strand buffer, converted to cDNA utilizing SuperScript® III reverse transcriptase (Invitrogen), end-repaired, A-tailed and ligated to custom-designed universal adapters utilizing an end-repair mix, klenow fragment, and T4 DNA ligase (all

from Enzymatics). After the ligation step, adapters were removed by SPRI purification utilizing SPRIselect beads (Beckman coulter) and amplified with Q5 Hot Start DNA polymerase (New England Biolabs) while introducing custom dual indexes. Three biological replicates were used to sequence on a NextSeq 500 (Illumina) at a depth of at least 2×10^7 reads each. Reads were mapped and analyzed via a custom bioinformatic pipeline based on STAR (Dobin et al., 2013), SAMTOOLS (Li et al., 2009), and the R packages DEGseq (Wang et al., 2010) and DEseq2 (Love et al., 2014). We used human genome version GRCh38 and gene annotations from the ENSEMBL release 83. GO analyses were performed using version 6.8 of the DAVID web server (Huang et al., 2009a, c).

CHIP sequencing

The previously published data were obtained from the NCBI's Gene Expression Omnibus (Zhao et al., 2014) and they are accessible through GEO at Series accession numbers GSE55105. FASTQs were downloaded and mapped to hg19 with bowtie2 (v2.1.0). Genome browser tracks were generated using custom scripts. When available, biological replicates were merged by taking the mean of the reads density at each position. The data were visualized via the integrative genomics viewer (IGV) (Robinson et al., 2011).

Statistics and reproducibility

Mean values with error bars indicating standard deviation (s.d.) were shown in the graphs. Unless otherwise noted, all the experiments were successfully repeated at least

three times. One-tailed *t*-test, two-tailed *t*-test, one-way or two-way ANOVA was performed as indicated in the figure legends. DEseq2 was performed for RNA-seq analysis in Fig. 4.3b and Table 4.1. Weighted Exclusivity Test (WExT) was performed for Table 4.3. Mantel-Cox was performed for survival analysis in Fig. 4.11. Pearson Correlation Coefficient was used in Fig. 3.5b.

CHAPTER 3 : BIOCHEMICAL ANALYSIS OF KLHL6 AND ROQUIN2 AS AN E3 LIGASE-SUBSTRATE PAIR

Chapter Summary

Research described in this chapter was performed in collaboration with the laboratories of Dr. Michael Washburn and Dr. Michael Green. Mass Spectrometry (MS) sample preparations were carried out in our laboratory, and MS analysis was performed by Anita Saraf and Laurance Florens in Dr. Michael Washburn lab (Stowers Institute). Re-analysis of published SNP array data and KLHL6 transcript expression in DLBCL tumors were performed in collaboration with Saber Tadros, a graduate student in Dr. Michael Green lab (MD Anderson Cancer Center).

The work described here forms the body of a manuscript that is currently accepted at Nature Cell Biology. This chapter is heavily focused on biochemical approaches to understand KLHL6 as a CULLIN3-RING-ubiquitin Ligase for Roquin2 protein and is written and arranged differently from the original manuscript.

Jaewoo Choi, Kyutae Lee, Kristin Ingvarsdottir, Roberto Bonasio, Anita Saraf, Laurence Florens, Michael P. Washburn, Saber Tadros, Michael R. Green, and Luca Busino. Loss of KLHL6 promotes diffuse large B-cell lymphoma growth and survival by stabilizing the mRNA decay factor Roquin2

Introduction

Kelch-like protein 6 (KLHL6) is a highly conserved and uncharacterized BTB-Kelch protein with a lymphoid tissue-restricted expression pattern (Gupta-Rossi et al., 2003). Although expressed at all stages of B-cell development, *Klhl6* levels are highly up-regulated in sheep Peyer's patch, human tonsil B cells and germinal center (GC) B-cells, suggesting a functional relevance in GC reaction (Kroll et al., 2005). In line with this expression profile, *Klhl6*^{-/-} mice fail to mount a full GC formation *in vivo* (Kroll et al., 2005). Recently, whole-genome and exome sequencing have revealed cancer-associated mutations of the *KLHL6* gene in mature B-cell malignancies, including diffuse large B-cell lymphoma (DLBCL) (Lohr et al., 2012; Morin et al., 2011). The somatic mutations tend to localize to the N-terminus of the protein, namely the BTB domain and the relevance of these mutations or the molecular function of KLHL6 is currently not known. The BTB protein family can be sub-divided into BTB-BACK-Kelch (BBK), MATH-BTB, BTB-NPH3, Kelch repeat and BTB-domain containing proteins (KBTBD), BTB-zinc finger (BTB-ZF), and Kelch family (KLHL)(Pintard et al., 2004). Many of these BTB proteins interact with CULLIN3, but not with other CULLIN scaffold proteins, to induce ubiquitination of target proteins involved in a variety of biological processes such as cell cycle regulation, oxidative stress, and others (Anderica-Romero et al., 2013). Although approximately 500 BTB-domain proteins have been identified, little is known about the physiological and molecular functions of these proteins.

The Roquin family of proteins consists of Roquin1 (Rc3h1) and Roquin2 (Rc3h2). The N-terminal region of Roquin proteins comprises a RING finger, a

conserved ROQ domain, and a CCCH-type zinc finger (Vinuesa et al., 2005). Specifically, mRNAs that display a 3' UTR sequence conserved a stem-loop motif, called a constitutive-decay element (CDE), which are recognized by the ROQ domain of Roquin1 and 2 (Leppek et al., 2013; Schlundt et al., 2014; Tan et al., 2014). Upon recognition, Roquin proteins recruit the mRNA decapping and deadenylation complexes through their C-terminal effector domains leading to the destabilization of their target mRNAs. CDEs are reported to be highly conserved in the 3' UTRs of more than 50 vertebrate genes, suggesting that CDE is a ubiquitous regulatory element (Leppek et al., 2013). Genome-wide identification of Roquin targets by crosslinked-immunoprecipitation (CLIP)-Seq revealed that many mRNAs associated with the roquin encode for proteins are important for immunity, inflammation, and development (Leppek et al., 2013). Accordingly, in the context of lymphocyte biology, tissue-specific ablation of Roquin1 in T cells causes expansion of CD8 effector-like T cells with up-regulation of essential T-cell co-stimulatory receptor, ICOS, which is a well-known target for Roquin proteins (Bertossi et al., 2011; Glasmacher et al., 2010; Yu et al., 2007). Mice with a T-cell-specific combined deficiency of Roquin1 and Roquin2 exhibit lymphadenopathy and splenomegaly with spontaneous development of follicular T-helper cells (Tfh) and GC B-cells, suggesting the function of these cells in the control of T-cell activation and Tfh differentiation. This autoimmunity phenotype is partially caused by elevated levels of ICOS.

Many studies defining the role of Roquin proteins have focused on T-cell biology and T-cell differentiation. Recent studies on the regulation of Roquin protein stability

have suggested that it is regulated by the paracaspase MALT1 (Jeltsch et al., 2014). Stimulation of wild-type CD4⁺ T cells by the pharmacological agents PMA and ionomycin mimic for activation of T-cell receptor and co-stimulation causes the cleavage of Roquin proteins by MALT1 and this phenomenon is blocked by the specific peptide inhibitor z-VPR-fmk. Both Roquin1 and Roquin2 are cleaved and inactivated to control post-transcriptional targets for promoting T_H17 differentiation. However, the regulation of Roquin protein abundance in B-cell biology has not been investigated.

Based on a proteomic analysis of the purified KLHL6 complex, we show that KLHL6 assembles a functional multi-subunit E3 ligase based on CULLIN3. We have found that binding CULLIN3 to KLHL6 requires an intact BTB-domain and the cancer-associated mutations of KLHL6 inhibit its ubiquitin ligase activity by disrupting this interaction. Furthermore, we have identified Roquin2 as a novel substrate and found that the integrity of a specific tyrosine residue (Y691) in Roquin2 is crucial for KLHL6 binding. In addition, degradation of Roquin2 is dependent on B-cell receptor activation. These findings identify KLHL6 as the E3 ligase for Roquin2 and can provide critical evidence and implements to uncover the connection between the ubiquitin proteasome system and mRNA decay in B-cell cancers.

Results

Cancer-associated mutations of KLHL6 in B-cell malignancies

KLHL6 is a lymphoid-tissue expressed gene (Gupta-Rossi et al., 2003; Kroll et al., 2005) with uncharacterized function. Mutations of the *KLHL6* gene were observed in DLBCL (<http://cancergenome.nih.gov/> and (Idoia et al., 2016; Lohr et al., 2012; Morin et al., 2011; Reddy et al., 2017), chronic lymphocytic leukemia (CLL) (Puente et al., 2015) and multiple myeloma (MM) (Lohr et al., 2014) (Fig. 3.1A) via analysis of genomic databases of B-cell cancer patients. DLBCL cohorts from UNMC, TCGA and CMSGSC revealed the highest rate of genetic mutations with 10%, 14.5%, and 12.5%, respectively (Fig. 3.1A), which are stratified in a similar rate amongst GCB-DLBCL, ABC-DLBCL and uncharacterized DLBCL (Fig. 3.1B). Majority of the cancer-associated mutations are missense and monoallelic mutations as non-sense and frameshift mutations exhibit a very low frequency (Fig. 3.1C, Table 3.1) (Idoia et al., 2016; Lohr et al., 2012; Morin et al., 2011; Reddy et al., 2017). Most of mutations occur near and inside the BTB-domain of *KLHL6*, and the residues Leucines 65 and 90 of *KLHL6* are mutational hotspots as shown (Fig. 3.1C). Additionally, infrequent deletion of the *KLHL6* locus was observed upon re-analysis of previously published SNP array data (Green et al., 2014) (Fig. 3.1D). Gene expression microarray analysis showed that ~6% of DLBCL tumors have lower expression of *KLHL6* transcript (Fig. 3.1E), suggesting that there might be possible role of transcriptional silencing as a way to inactivate *KLHL6* function.

KLHL6 assembles a *CULLIN3*-based *E3* ligase

To gain insight into the molecular function of KLHL6 and to understand the impact of the cancer associated mutations, we first compared the protein interactome change between KLHL6 (WT) and the cancer mutant KLHL6 (L65P). FLAG-KLHL6 (WT) or FLAG-KLHL6 (L65P) complexes were immunopurified from two different cell lines (HEK293T and ARP-1) and the tryptic digestion of each protein eluate was measured by mass spectrometry (Table 3.2). In the two cell lines, high unique spectral counts corresponding to CULLIN3 were identified in KLHL6 (WT) immunoprecipitates as opposed to none in the KLHL6 (L65P) purifications (Fig. 3.2A and Table 3.2), indicating that CULLIN3 is a novel KLHL6 binding partner and that a hotspot BTB-domain mutation of KLHL6 (L65P) abolishes this interaction.

To validate the mass spectrometric analyses, we expressed and immunoprecipitated FLAG-tagged KLHL6 from HEK293T cells and confirmed interaction with endogenous CULLIN3 (Fig. 3.2B), similarly to the established CULLIN3 interactor IBTK (Bennett et al., 2010) (Fig. 3.2B). KLHL14 was used as a negative control of a BTB-containing protein that did not interact with CULLIN3. In contrast, CULLIN1 was detected in FBXW7 and FBXL15 immunoprecipitations (Fig. 3.2B), as previously shown (Busino et al., 2012; Cui et al., 2011), but not in association with KLHL6, suggesting that KLHL6 specifically assembles a CULLIN3-based ubiquitin ligase complex.

To determine whether KLHL6 is capable of catalyzing polyubiquitylation, we carried out an *in vitro* ubiquitylation assay where we incubated purified KLHL6 (WT) or KLHL6 (Δ Kelch), a deletion mutant that contains only the BTB-domain, with a

ubiquitylation mix consisting of E1 enzyme, Ubch5a (E2) enzyme, ATP and ubiquitin. As expected, KLHL6 promoted self-ubiquitylation, and, notably, its BTB-domain alone was sufficient in catalyzing self-polyubiquitylation to a higher degree as recognized by an antibody specific to K-48 linked ubiquitin chains (Fig. 3.2C). These data revealed that the KLHL6 complex catalyzes ubiquitin transfer *in vitro*, further supporting the notion of assembling a functional CULLIN3-RING ubiquitin Ligase (CRL3) (Lydeard et al., 2013).

BTB-domain mutations of KLHL6 abolishes its ligase activity

Having established above that KLHL6 is a CRL3 ligase, we tested the effect of BTB-domain mutations on ligase assembly and activity. First, we confirmed our initial proteomic data by showing that the KLHL6 (L65P) mutant did not co-immunoprecipitate endogenous CULLIN3 (Fig. 3.3A). We also found that two other cancer mutants (KLHL6 (S94I) and KLHL6 (F97L)) did not interact with CULLIN3 (Fig. 3.3A). Secondly, we showed that mutations in the BTB-domain were sufficient in inhibiting self-polyubiquitylation *in vitro* (Fig. 3.3B), as a result of a loss of catalytic activity due to endogenous CULLIN3 dissociation.

The latter findings prompted us to determine whether loss of KLHL6 self-ubiquitylation would affect its turnover in cells. To this end, we expressed KLHL6 (WT) or BTB-domain KLHL6 mutants (L65P, S94I and F97L) in OCI-LY10 *KLHL6*^{-/-} and assessed protein half-life in cycloheximide (CHX) chase experiments (Fig. 3.3C).

Consistent with our *in vitro* findings, the protein levels of BTB-domain KLHL6 mutants were remarkably high at steady state and displayed extended half-lives as compared to that of KLHL6 (WT) (Fig. 3.3C). These results suggested that KLHL6 promotes auto-ubiquitylation and degradation via CULLIN3 interaction (Fig. 3.3D).

Together, our data show that (i) KLHL6 is a CRL3 that promotes self-ubiquitylation and degradation, and (ii) cancer-associated mutations within the BTB-domain abrogate the interaction with CULLIN3, resulting in the loss of ubiquitin ligase activity (Fig.3.3D)

KLHL6 specifically interacts with Roquin2

Based on our previous findings, we hypothesized that the molecular function of KLHL6 is to ubiquitylate and degrade one or more substrates. Since KLHL6 (L65P) mutant is unable to promote ubiquitylation, we reasoned that it might trap (i.e. interact with, but not ubiquitylate or degrade) natural KLHL6 substrates offering an opportunity to identify them. Thus, we ranked the identified proteins by the number of unique spectral counts associated to KLHL6 (L65P) and compared them to KLHL6 (WT) (Fig. 3.4A and Table 3.2). Roquin2 was enriched in the KLHL6 (L65P) complex in both HEK293T cells and ARP-1 cells. Notably, Roquin1 was not detected, suggesting that KLHL6 interacts preferentially with Roquin2 (Fig 3.4A).

To investigate whether the binding between Roquin2 and KLHL6 is specific, we screened a panel of human F-box proteins, as well as BTB-domain containing proteins (Fig. 3.4B). We found that only KLHL6 co-immunoprecipitated endogenous Roquin2

(but not Roquin1 despite its higher expression), in agreement with our mass spectrometry results (Fig. 3.4B). To further confirm this finding, we expressed FLAG-tagged Roquin1 or Roquin2 in HEK293T cells stably expressing exogenous KLHL6 (HEK293T cells do not express KLHL6 at the endogenous level). Analysis of FLAG immunoprecipitates confirmed that Roquin2, but not Roquin1, interacted with KLHL6 (Fig. 3.4C). We also confirmed the endogenous KLHL6 and Roquin2 interaction in DLBCL cells (Fig. 3.4D). KLHL6 required an intact Kelch domain to interact with Roquin2 (Fig. 3.4E), further supporting substrate-like interaction between KLHL6 and Roquin2 (Lo et al., 2006). Consistent with the proteomic data, mutations in the BTB-domain did not affect binding of KLHL6 to Roquin2 (Fig. 3.4E).

KLHL6 promotes ubiquitylation and degradation of Roquin2.

To investigate whether KLHL6 regulates Roquin2 protein levels, we first analyzed Roquin2 abundance in a panel of DLBCL cell lines. Interestingly, higher levels of KLHL6 protein in OCI-LY1, SUDHL4, SUDHL6 and U2932 cell lines correlated with lower levels of Roquin2 protein (Fig. 3.5A and 3.5B). Inversely, lower levels of KLHL6 protein in OCI-LY7, OCI-LY10, OCI-LY19, TMD8, HLB1, Pfeiffer, and Karpas422 cell lines correlated with higher levels of Roquin2 protein (Fig. 3.5A and 3.5B). We further assessed Roquin2 protein turnover by analysis of its half-life in two ABC-DLBCL cell lines (OCI-LY10 and U2932) (Fig. 3.5C and Fig. 3.5D respectively). In both cell lines, down-regulation of KLHL6 via siRNAs or ablation via gRNAs significantly extended Roquin2 half-life. Roquin1 half-life was not significantly changed upon KLHL6 down-

regulation or ablation, further confirming that KLHL6 specifically promotes Roquin2 but not Roquin1 degradation (Fig. 3.5C and Fig. 3.5D).

Gain of function experiments also confirmed that Roquin2 protein levels were negatively regulated by expression of KLHL6 using a doxycycline-dependent promoter in cell lines with low *KLHL6* expression (*i.e.*; HEK293T and HBL1) (Fig. 3.5E). Moreover, overexpression of KLHL6 (WT), but not BTB-domain KLHL6 mutants, in OCI-LY8 (a DLBCL cell line with undetectable KLHL6 levels), induced Roquin2 down-regulation (Fig. 3.5F), indicating that loss of function cancer-associated mutations of KLHL6 is incapable of promoting Roquin2 degradation.

To explore whether KLHL6 directly controls Roquin2 ubiquitylation *in vitro*, we purified KLHL6-Roquin2 complex from HEK293T cells by immunoprecipitations and incubated with a ubiquitylation mix. High-molecular species of Roquin2 were detected only upon incubation with the KLHL6 (WT) complex, but not with the KLHL6 (L65P) complex, suggesting that Roquin2 is conjugated with polyubiquitin chains in a CULLIN3-dependent manner (Fig. 3.5G). Furthermore, we investigated whether Roquin2 ubiquitylation is regulated by KLHL6 *in vivo*. The K48-linked polyubiquitin chains of Roquin2 were only detected in *KLHL*^{+/+} cell lines, but not in *KLHL6*^{-/-} cell lines (Fig. 3.5H).

Hence, we have shown that Roquin2 is the first identified bona fide substrate of the CRL3^{KLHL6} E3 ubiquitin ligase complex.

BTB-mutations of KLHL6 are not dominant-negative

First, we utilized HEK293T cells stably expressing BTB-mutants of KLHL6. We infected these cells with lentiviruses encoding a doxycycline (DOX) inducible expression of KLHL6 (WT) and found that the expression KLHL6 (WT) still promoted Roquin2 degradation, suggesting these BTB-domain mutations of KLHL6 are not dominant negative (Fig. 3.6A).

Next, we utilized B-cell lymphoma cell lines harboring endogenous *KLHL6* mutations. VAL cells harbor two endogenous BTB-mutations: N60T and T72R (Fig. 3.6B). We found that only the KLHL6 (T72R) mutant lost interaction with CULLIN3 (Fig. 3.6B) while KLHL6 (N60T) mutant was still able to interact. Interestingly, knockdown of KLHL6 in VAL cells did not have any effects on Roquin2 protein levels (Fig. 3.6C), suggesting that KLHL6 is not functional in VAL cells. Additionally, retroviral expression of KLHL6 (WT) in VAL cells still promoted degradation of Roquin2 (Fig. 3.6D), suggesting this mutation as non-dominant. In VAL cells, expression of *KLHL6* at the mRNA level was comparatively low (Fig. 3.6E). Overall, this suggests that VAL cells display one *KLHL6* allele inactivated by a mutation in the BTB-domain and an additional down-regulation of *KLHL6* mRNA, a scenario suggestive of a loss of function.

We have also analyzed the effect of KLHL6 mutations in SUDHL10 cells with two mutations (L24R and A25E). Both the KLHL6 (L24R) and KLHL6 (A25E) mutants retained interaction with CULLIN3, suggesting an intact KLHL6 function (Fig. 3.6B).

Indeed, knockdown of KLHL6 in SUDHL10 cells induced stabilization of Roquin2 (Fig. 3.6C) and over-expression of KLHL6 WT had a minor effect on Roquin2 degradation, likely because endogenous KLHL6 is already functional (Fig. 3.6D).

Taken together, our biochemical analyses on mutations suggest that the BTB-domain mutations of KLHL6 do not have dominant-negative effects on KLHL6 (WT).

Interaction between KLHL6 and Roquin2 requires a functional tyrosine residue Y691 in Roquin2

Next, we investigated the KLHL6 binding region in Roquin2 by performing an unbiased mutagenesis screening. To this end, we generated a set of C-terminal deletion mutants in Roquin2 and identified that a region between amino acids 640 and 700 is required for interaction with KLHL6 (Fig. 3.7A). Consistently, deletion of N-terminal residues up to amino acids 439 did not alter KLHL6-Roquin2 interaction (Fig. 3.7B). We performed more refined deletions and further narrowed down the interaction motif between amino acids 690 and 695 (Fig. 3.7C). By carrying out alanine scanning mutagenesis of the individual residues of Roquin2 from 691 to 704 region, we identified a specific and conserved tyrosine residue, in position 691. The single alanine mutation at this specific tyrosine completely abrogated the interaction between Roquin2 and KLHL6 (Fig. 3.7D). *In-vitro* binding assays confirmed that a Roquin2 peptide containing the region from 686 to 700 directly interacts with KLHL6 (Fig. 3.7E-H). Further, mutations of tyrosine 691 into alanine (Y691A) or phenylalanine (Y691F) disrupts the ability of

Roquin2 to co-immunoprecipitate with KLHL6 both *in vitro* and *in vivo*. This suggests that the intact tyrosine hydroxyl group is required for the KLHL6-Roquin2 interaction (Fig 3.7G and I).

To determine whether tyrosine 691 controls Roquin2 stability in DLBCL cells, we retrovirally-transduced a DLBCL cell line, BJAB, with Roquin2 (WT) or Roquin2 (Y691F). Strikingly, Roquin2 (Y691F) displayed increased protein levels at steady state as well as an extended half-life when compared to that of Roquin2 (WT) (Fig. 3.7J), suggesting that the integrity of tyrosine 691 controls Roquin2 protein turnover. To further validate this finding, we expressed KLHL6 (WT) or KLHL6 (L65P) in HEK293T cells and assessed the effect on Roquin2 protein levels. While Roquin2 (WT) was effectively down-regulated by the expression of KLHL6 (WT), Roquin2 (Y691F) was not (Fig. 3.7K). Expression of KLHL6 (L65P) had no effects on protein levels of Roquin2 (WT) or Roquin2 (Y691F) (Fig. 3.7K).

Collectively, these data show that tyrosine 691 in Roquin2 is required for KLHL6-mediated degradation of Roquin2 in DLBCL.

KLHL6 promotes Roquin2 degradation upon BCR stimulation

KLHL6 was shown to be involved in the B-cell Receptor (BCR) signaling and a part of BCR signalosome (Satpathy et al., 2015). Also, KLHL6 was induced upon antigen stimulation in the germinal center (Kroll et al., 2005), so we first investigated whether mRNA and protein levels of KLHL6 and Roquin2 were affected by BCR stimulation in

DLBCL cell lines. We first screened DLBCL cell lines for IgM or IgG surface expression (Fig. 3.8A). Consistent with previous findings, ABC-DLBCL cells predominantly express an IgM-BCR as opposed to GCB-DLBCL cells, which are positive for IgG-BCR (Lenz et al., 2007). Amongst the DLBCL cell lines screened, we analyzed levels of KLHL6 and Roquin2 in IgM-positive ABC- DLBCL cell lines (U2932, OCI-LY10 and HBL1) (Fig 3.8B). BCR activation using the fragment affinity-purified antibody F(ab')₂-IgM induced up-regulation of KLHL6 and down-regulation of Roquin2 protein levels in OCI-LY10 and U2932, but not in HBL1, lacking KLHL6 mRNA and protein (Fig.3.8B). Thus, Roquin2 down-regulation upon BCR stimulation correlated with KLHL6 expression in DLBCLs.

To further prove that BCR-dependent down-regulation of Roquin2 protein in ABC-DLBCLs is controlled by CRLs, we pre-treated U2932 cells with MLN4924, a NEDD8-activating enzyme (NAE) inhibitor blocking neddylation of CULLINs (Milhollen et al., 2010). MLN4924 treatment rescued Roquin2 down-regulation induced by BCR-crosslinking, suggesting that a functional CRL-complex is necessary to promote degradation of Roquin2 (Fig. 3.8C). As a positive control, phosphorylation of ERK is shown to assess the efficacy of BCR-crosslinking. Notably, BCR stimulation induced KLHL6 up-regulation at transcriptional levels (Fig. 3.8D), revealing KLHL6 as a BCR-signaling dependent gene. Consistently, BCR-crosslinking in both U2932 and OCI-LY10 induced KLHL6 expression in a time and dose-dependent manner, which inversely correlated with Roquin2 protein levels (Fig. 3.8E and 3.8F). Furthermore, silencing the expression of KLHL6 via siRNA ablated F(ab')₂-IgM-induced Roquin2 degradation

(Fig. 3.8E and 3.8F), indicating that BCR-signaling promotes Roquin2 degradation in a KLHL6-dependent manner. BCR-induced Roquin2 degradation was also impaired in *KLHL6*^{-/-} cells (Fig. 3.8G)

Consistent with degradation of endogenous Roquin2, we found that exogenous Roquin2 (WT) was also degraded in a dose-dependent manner upon BCR stimulation (Fig 3.8H). In contrast, levels of Roquin2 (Y691F) mutant were higher already at steady state and unaffected by BCR stimulation, confirming that BCR-signaling induces KLHL6-mediated degradation of Roquin2.

Discussion

Our work uncovers, for the first time, uncovers a functional link between KLHL6 and Roquin2 protein as an E3 ligase-substrate pair. KLHL6 is a BTB-Kelch domain protein mutated in human DLBCLs. BTB domain-containing zinc finger proteins and Kelch domain are evolutionarily conserved from *Drosophila melanogaster* to *Homo sapiens* (Adams et al., 2000; Siggs and Beutler, 2012). The common function of the BTB/Kelch domain is to facilitate protein binding and associated proteins control various biological processes such as transcription repression, protein degradation, and organization and binding of actin filaments, and cellular morphology (Albagli et al., 1995; Kang et al., 2004; Melnick et al., 2000; Perez-Torrado et al., 2006). Somatic mutations localize to the BTB-domain with relevant hotspots at amino acid residue 65 and 90 (Idoia et al., 2016; Lohr et al., 2012; Morin et al., 2011; Reddy et al., 2017). Most

KLHL6 genetic alterations in DLBCL contain monoallelic missense mutations and infrequent copy loss (Idoia et al., 2016; Lohr et al., 2012; Morin et al., 2011; Reddy et al., 2017). It is likely that most of cancer-associated mutations *KLHL6* are the consequence of aberrant hypersomatic mutation (Puente et al., 2011), similarly to those of *BCL6* and *MYC* (Pasqualucci et al., 2001). More importantly, we have shown that the hotspot mutations and other deleterious BTB-domain mutations cause a dissociation of *CULLIN3* and loss of E3 ligase activity. Although cancer-associated mutations in the Kelch-domain, which can serve as a substrate-binding domain, are observed in DLBCLs, mutation such as T440A is not able to disrupt binding of Roquin2 with *KLHL6* completely (Fig 3.4E). This observation suggests that somatic mutations in the BTB-domain are more potent than the ones in the Kelch-domain in terms of disrupting the ligase activity and leading to substrate accumulation. This might be the reason that *KLHL6* alterations in DLBCLs happen more frequently in the BTB-domain.

Furthermore, we identified Roquin2 as the bona fide substrate of *KLHL6*. *KLHL6* interacts specifically with Roquin2, ubiquitylates and triggers its degradation upon BCR stimulation. It is noticeable that Roquin1, which is a Roquin2 paralog and has highly similar amino acid sequence across RING, ROQ, and CCCH (C3H) domains (Pratama et al., 2013), is not a target of *KLHL6*. Indeed, the binding domain of *KLHL6* in Roquin2 is in the proline rich region, which has only about ~40% sequence similarity with Roquin1. Therefore, it is conceivable that this sequence difference only allows *KLHL6* to recognize Roquin2 via tyrosine 691 residue. The Roquin-1 and Roquin-2 proteins in T-cell activation and Tfh differentiation have been reported to be functionally

redundant as both can regulate and act together to degrade key mRNAs and control inflammation and autoimmunity such as ICOS and Ox40 costimulatory receptors and TNF (Vogel et al., 2013). These redundant functions serve as a critical safety mechanism for preventing cancer development and autoimmune diseases. However, systemic Roquin1 knockout mice are born with a caudal spine defect and impaired lung development, resulting in a poor perinatal survival (Bertossi et al., 2011), implying a role of Roquin1 in embryonic development that extends beyond the immune system. Moreover, systemic Roquin2 deficient mice are born at a Mendelian ratio, but very few individual mice reach adulthood. Notably, a large proportion of Roquin2 deficient mice died within the first few days after birth (Vogel et al., 2013). This suggests that Roquin1 and Roquin2 redundancy varies in a cell-context dependent manner. Therefore, it is possible that, in B-cell biology where Roquin2 is specifically degraded by KLHL6, Roquin1 and Roquin2 might have a functional difference, adding new aspects of the regulation of Roquin proteins.

Notably, cancer-associated mutations of KLHL6 in the BTB-domain are not dominant negative as KLHL6 (WT) is still able to degrade Roquin2 in the presence of these BTB-domain mutants. Moreover, N-terminal mutations outside of the BTB-domain do not disrupt the function of KLHL6, suggesting that it is mainly BTB-domain mutations that lead to loss of function. We have not investigated whether these BTB-domain mutations affect the dimerization of KLHL6 and whether KLHL6 is functional in the dimer form. Indeed, SPOP, a MATH-BTB protein, generates a dimeric ubiquitin ligase to recognize a single substrate, and a dimerization defective SPOP mutant is not

able to promote ubiquitination of the substrate (Zhuang et al., 2009). Dimerization and conformational variability is an important factor to facilitate elongation of ubiquitin chain on the substrate and to provide a variety of orientation flexibility as previously shown by the SCF ligase, Cdc4 (Tang et al., 2007). The dimerization of Cdc4 affects the positioning of the substrate for the formation of the ligase complex rather than the affinity with its substrate. It is possible that KLHL6 works as a homodimer and mutations in the BTB-domain disrupt interaction between the wild-type KLHL6s in addition to disrupting the CULLIN3 association. Furthermore, we have not characterized the function of the BACK domain as no somatic mutations for this domain are found in KLHL6. It has been shown that single mutation in the BACK domain results in decreased efficiency of CULLIN3-KLHL7 ligase complex in autoimmune diseases (Kigoshi et al., 2011). How KLHL6 protein exists in cells in terms of its complex formation and whether the cancer-associated mutations have any impacts on dimerization or other regulation part of KLHL6 remain to be elucidated.

KLHL6 has been shown to be a novel component of BCR signalosomes (Satpathy et al., 2015). Our study demonstrates that KLHL6 transcription is up-regulated upon BCR stimulation leading to corresponding degradation of Roquin2 protein. Furthermore, the protein levels of non-degradable Roquin2 mutant are insensitive to BCR stimulation. Although we have not investigated whether this regulation exists similarly in primary B-cells, we have, for the first time, identified the physiological condition where Roquin2 protein abundance is controlled by proteasomal degradation in B-cell cancers. The

mechanism of how KLHL6 expression is up-regulated by BCR signaling will be explored further in chapter 4.

Taken together, our findings indicate that KLHL6 is an E3 ligase for Roquin2. Cancer-associated mutations of KLHL6 inhibit its ubiquitin ligase activity, leading to CULLIN3 dissociation. The integrity of the tyrosine 691 in Roquin2 is critical for the KLHL6-Roquin2 interaction, and B-cell receptor activation induces degradation of Roquin2. How the KLHL6-Roquin2 axis functions in DLBCL biology and how alteration of this pathway affects cancer cell proliferation and survival will be discussed in chapter 4.

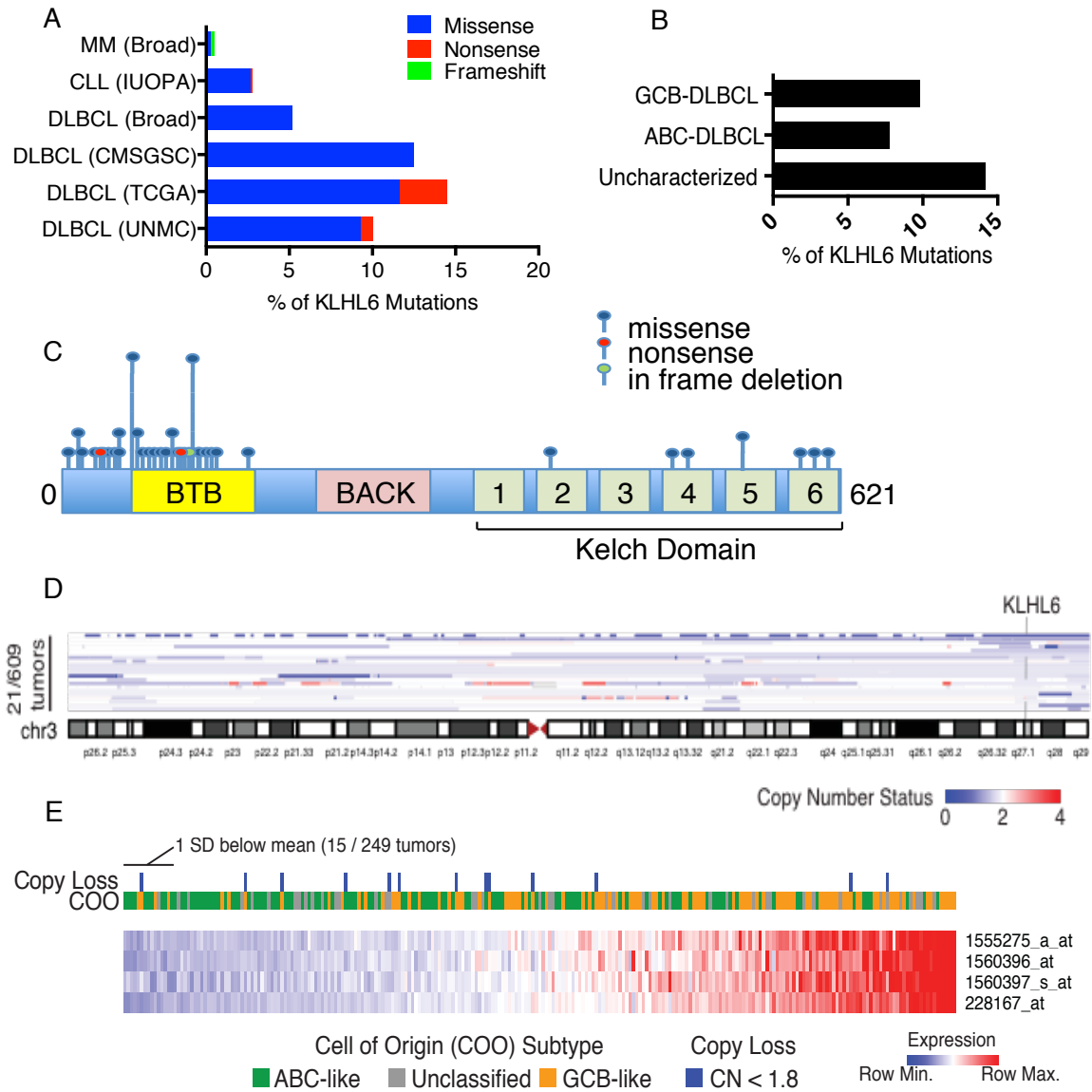


Figure 3.1 Analyses of KLHL6 cancer mutations in B-cell malignancies

(A) KLHL6 mutations occur most frequently in DLBCL. The graph shows the percentage of KLHL6 mutations found in different B-cell cancer patients. Diffuse Large B-cell Lymphoma DLBCL [University of Nebraska Medical Center (UNMC), n=140, The Cancer Genome Atlas (TCGA), n=48, Canada's Michael Smith Genome Sciences Centre

(CMSGSC), n=96, and Broad Institute (Broad), n=58], Chronic Lymphocytic Leukemia (CLL) [Departamento de Bioquímica y Biología Molecular, Instituto Universitario de Oncología (IUOPA), n=586] and Multiple Myeloma (MM) [Broad Institute (Broad), n=205]. In blue, missense mutations; in red, nonsense mutations; in green, frameshift mutations. (B) *KLHL6* mutations occur in a similar rate among different DLBCL subtypes. UNMC and CMSGSC cohorts were pooled and sub-classified as Activated B-cell-like (ABC), Germinal Center B-cell-like (GC) and Unclassified DLBCL. (C) Schematic representation of *KLHL6* protein (BTB, Broad-Complex, Tramtrack and Bric-a-brac; BACK, BTB and C-terminal Kelch plant homeodomain; Kelch domain, Kelch motif). In blue, missense mutations; in red, nonsense mutations; in green, frameshift mutations. (D) DNA copy number (chromosome 3) data were used from previously published high-resolution single nucleotide polymorphism (SNP) microarray analysis of 609 primary DLBCL tumors (Green et al., 2014). The position of *KLHL6* is annotated for 21 DLBCL tumors with copy number <1.8. About 3.4% of patients show *KLHL6* loss. (E) A row-normalized heat map is shown for probe sets of *KLHL6*. 249 tumors with matched DNA copy number data from a previously published study (Green et al., 2014) were analyzed for gene expression microarray and annotated for the cell of origin subtype and DNA copy loss of *KLHL6* as shown in (D). 6% of DLBCL patient cases have a lower expression of *KLHL6* transcripts defined as expression ≤ 1 standard deviation below the mean.

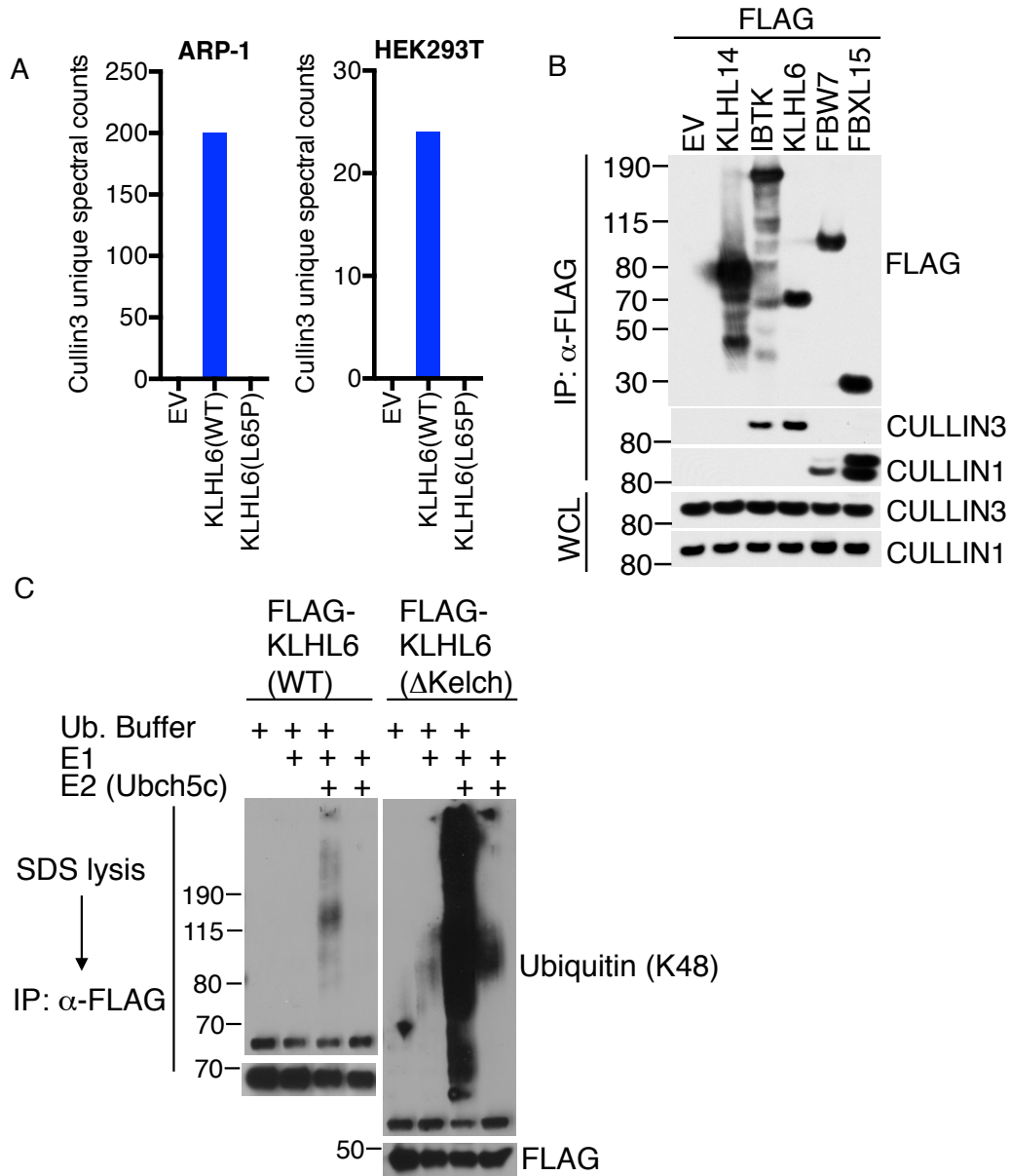


Figure 3.2 KLHL6 assembles a CULLIN3-based E3 ligase

(A) CULLIN3 interacts with KLHL6 (WT) and not with KLHL6 BTB-mutant (L65P). The graphs show results from mass spectrometry analysis of KLHL6 immunoprecipitations in two different cell lines (HEK293T and ARP-1). Unique spectral

counts numbers for CULLIN3 protein are shown. EV, empty vector control. (B) KLHL6 is a CULLIN3-Ring-Ligase (CRL3). HEK293T cells were transfected with FLAG-tagged E3 ligases. Proteins were immunoprecipitated (IP) from cell extracts with an anti-FLAG resin, and immunocomplexes were probed with antibodies to the indicated proteins. Bottom panels show whole cell lysates (WCL). EV, empty vector control. (C) KLHL6 promotes self-ubiquitylation. FLAG-KLHL6 (WT) or FLAG-KLHL6 (Δ Kelch) was immunopurified (IP) from transfected HEK293T cells. The IP was incubated with E1, Ubch5c (E2), Ubiquitin and ATP as indicated. After 30 minutes, reactions were denatured with SDS-lysis buffer and further immunopurified using an anti-FLAG resin and stopped by addition of Laemmli buffer. IPs were subjected to immunoblotting for the indicated proteins.

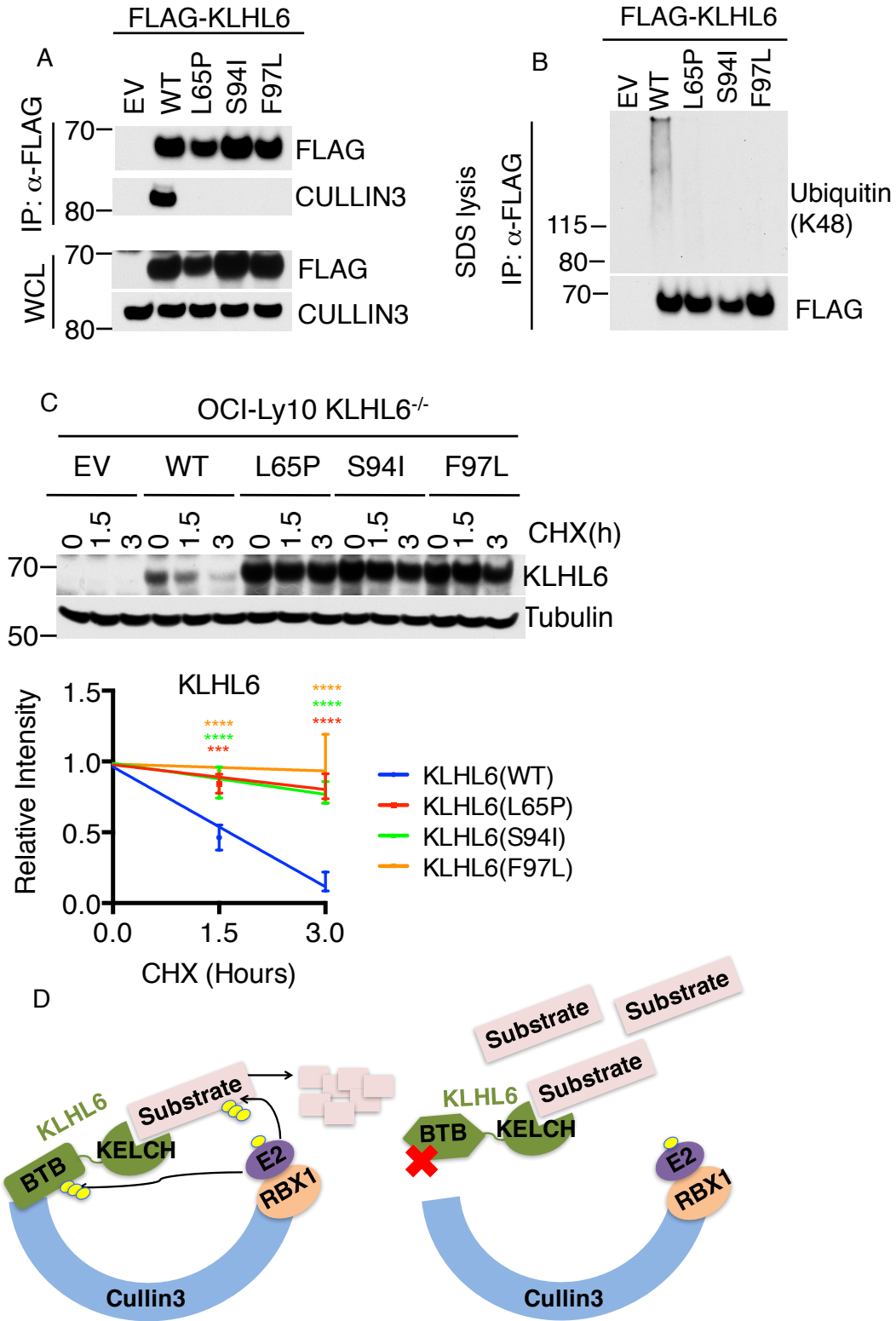
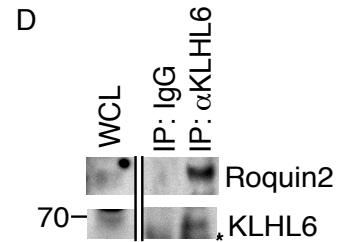
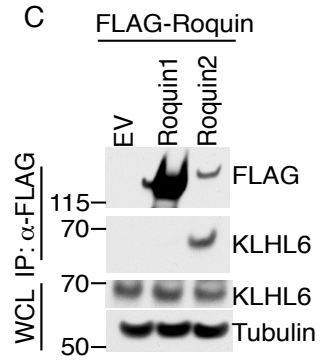
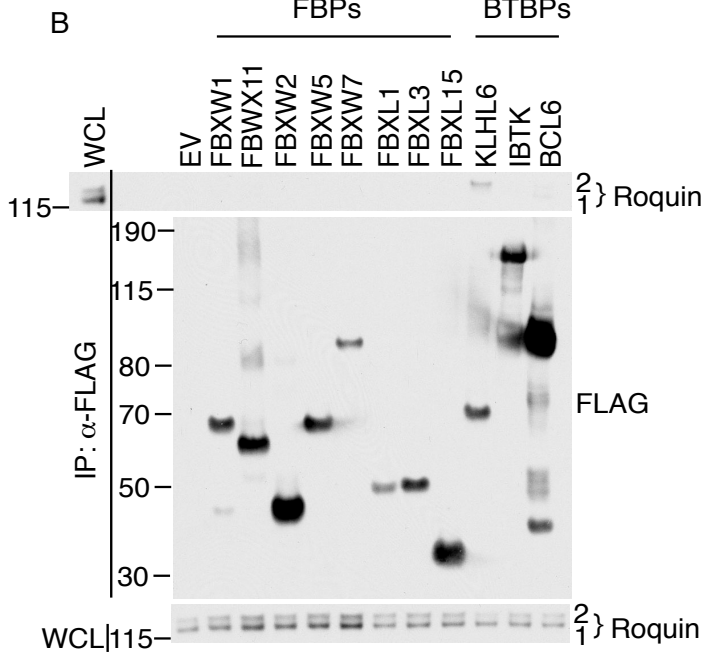
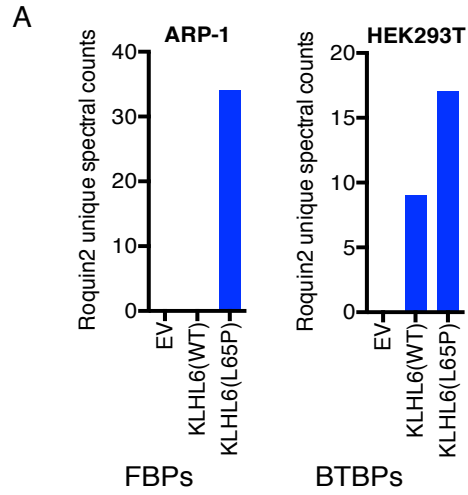


Figure 3.3 BTB-domain mutations of KLHL6 abolishes its ligase activity

(A) Cancer-associated mutations in the BTB-domain inhibit interaction with CULLIN3. HEK293T cells were transfected with FLAG-tagged KLHL6 wild-type (WT), BTB-mutants (L65P, S94I and F97L), or empty vector control (EV). Proteins were immunoprecipitated (IP) from cell extracts with an anti-FLAG resin, and immunocomplexes were probed with antibodies to the indicated proteins. Bottom panels show whole cell lysates (WCL). (B) Mutations in the BTB-domain impair KLHL6 self-ubiquitylation. FLAG-KLHL6 (WT and BTB-mutants) was immunopurified (IP) from transfected HEK293T. The IP was incubated with E1, Ubch5c (E2), Ubiquitin and ATP as indicated. After 30 minutes, reactions were denatured with SDS-lysis buffer and further immunopurified using an anti-FLAG resin and stopped by addition of Laemmli buffer. IPs were subjected to immunoblotting for the indicated proteins. (C) Mutations in the BTB-domain extend KLHL6 half-life. A DLBCL cell line, OCI-LY10, was engineered by CRISPR to generate a OCI-LY10 *KLHL6*^{-/-} cell line. Cells were retrovirally transduced with cDNAs encoding an empty vector (EV), KLHL6 (WT) or BTB-mutants (L65P, S94I and F97L). Cells were treated with cycloheximide (CHX) for the indicated times, and whole cell lysates were analyzed by immunoblotting for the indicated proteins. Bottom panel shows quantification of KLHL6 protein levels using ImageJ and their relative intensities were plotted over time. (D) Schematic model of CULLIN3-Ring-Ligase (CRL3)-KLHL6. KLHL6 assembles a functional CRL via interaction with CULLIN3 and promotes ubiquitylation of itself and a substrate. Cancer-associated mutations in the BTB-domain displace CULLIN3 interaction.



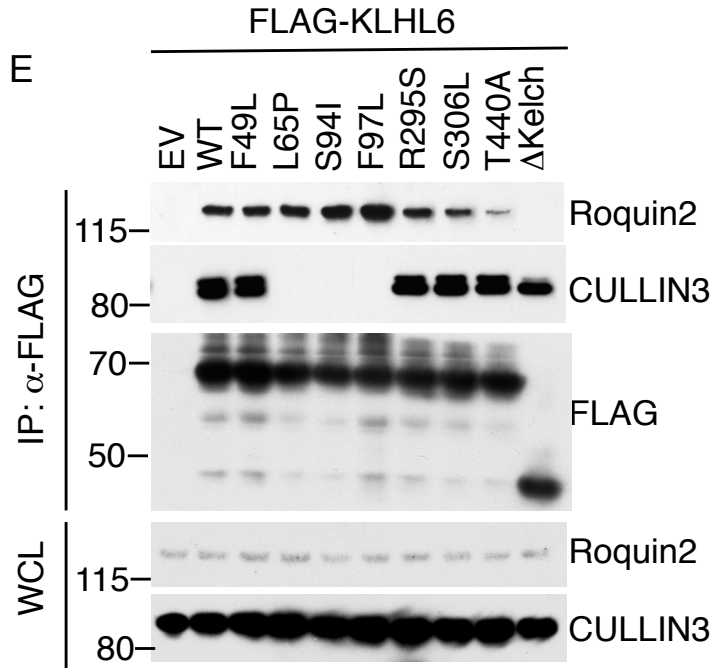
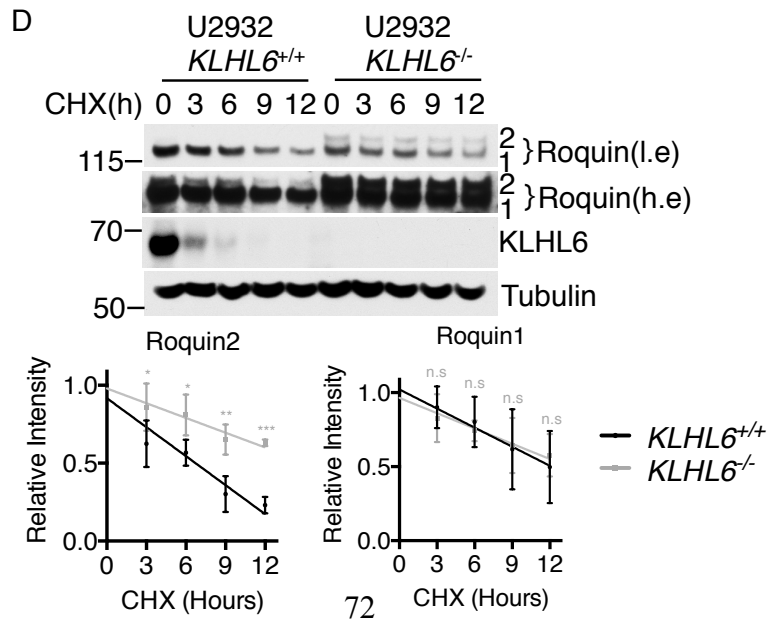
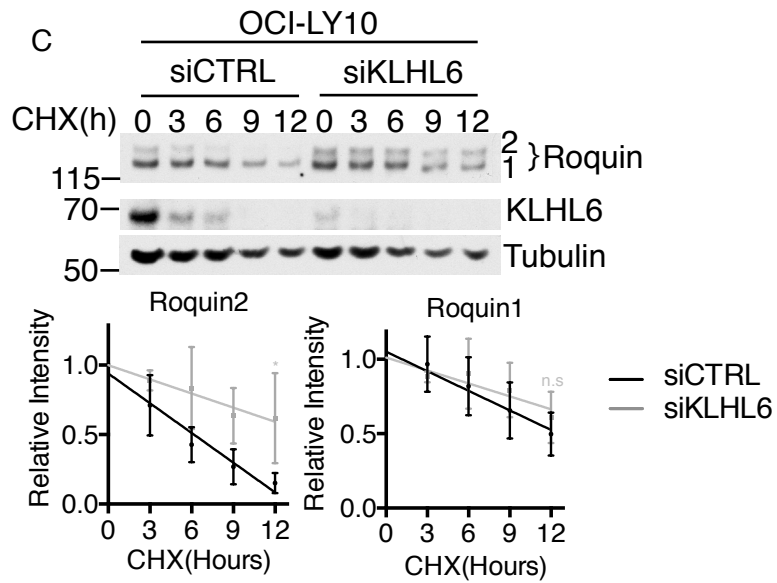
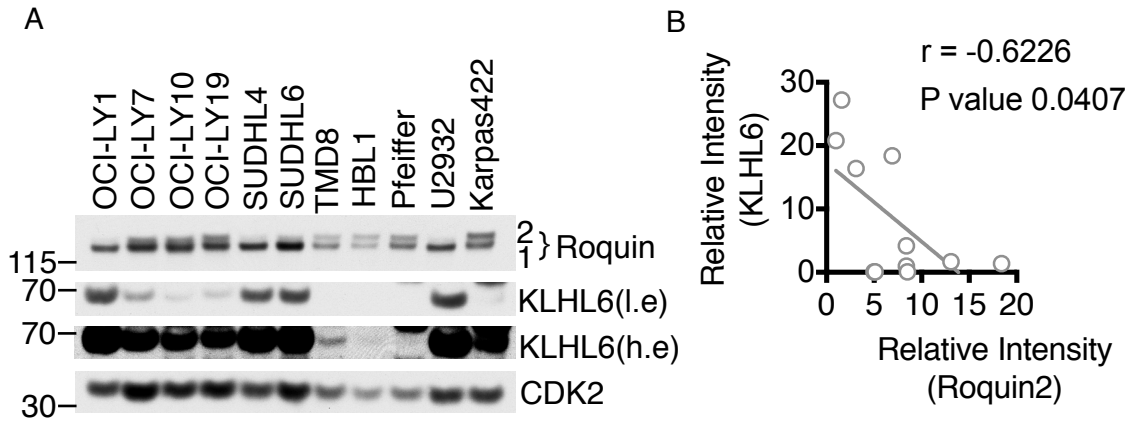


Figure 3.4 KLHL6 specifically interacts with Roquin2.

(A) Roquin2, but not Roquin1, is highly enriched in catalytic inactive KLHL6 (L65P) mutant complex. The graphs show mass spectrometry analysis of KLHL6 immunoprecipitations in two different cell lines (HEK293T and ARP-1). Unique spectral counts for Roquin2 proteins are shown. EV, empty vector control. (B) Roquin2 interacts with KLHL6 specifically. HEK293T cells were transfected with cDNAs encoding the indicated FLAG-tagged F-box proteins (FBPs) or BTB proteins (BTBPs). Exogenous proteins were immunoprecipitated (IP) from cell extracts with an anti-FLAG resin, and immunocomplexes were probed with antibodies to the indicated endogenous proteins. Lane 1 shows a whole cell lysates (WCL) from cells transfected with an empty vector (EV). (C) Roquin2, but not Roquin1, interacts with KLHL6. HEK293T cells stably

expressing KLHL6 were transfected with cDNAs encoding the FLAG-Roquin1 or FLAG-Roquin2. Exogenous proteins were immunoprecipitated (IP) from cell extracts with an anti-FLAG resin, and immunocomplexes were probed with antibodies to the indicated proteins. Bottom panels show whole cell lysates (WCL). (D) Endogenous Roquin2 and KLHL6 complex is detectable in DLBCL cells. Endogenous KLHL6 was immunoprecipitated from U2932 cells and immunocomplexes were probed with antibodies to the indicated proteins. IgG antibody immunoprecipitates=negative control. A representative blot from two independent experiments is shown. * indicates non-specific band. (E) KLHL6 binds Roquin2 through the Kelch domain. HEK293T cells were transfected with constructs encoding FLAG-tagged KLHL6 (WT) or mutants as indicated and empty vector (EV). KLHL6 was immunoprecipitated (IP) from cell extracts with an anti-FLAG resin, and immunocomplexes were probed with antibodies to the indicated proteins.



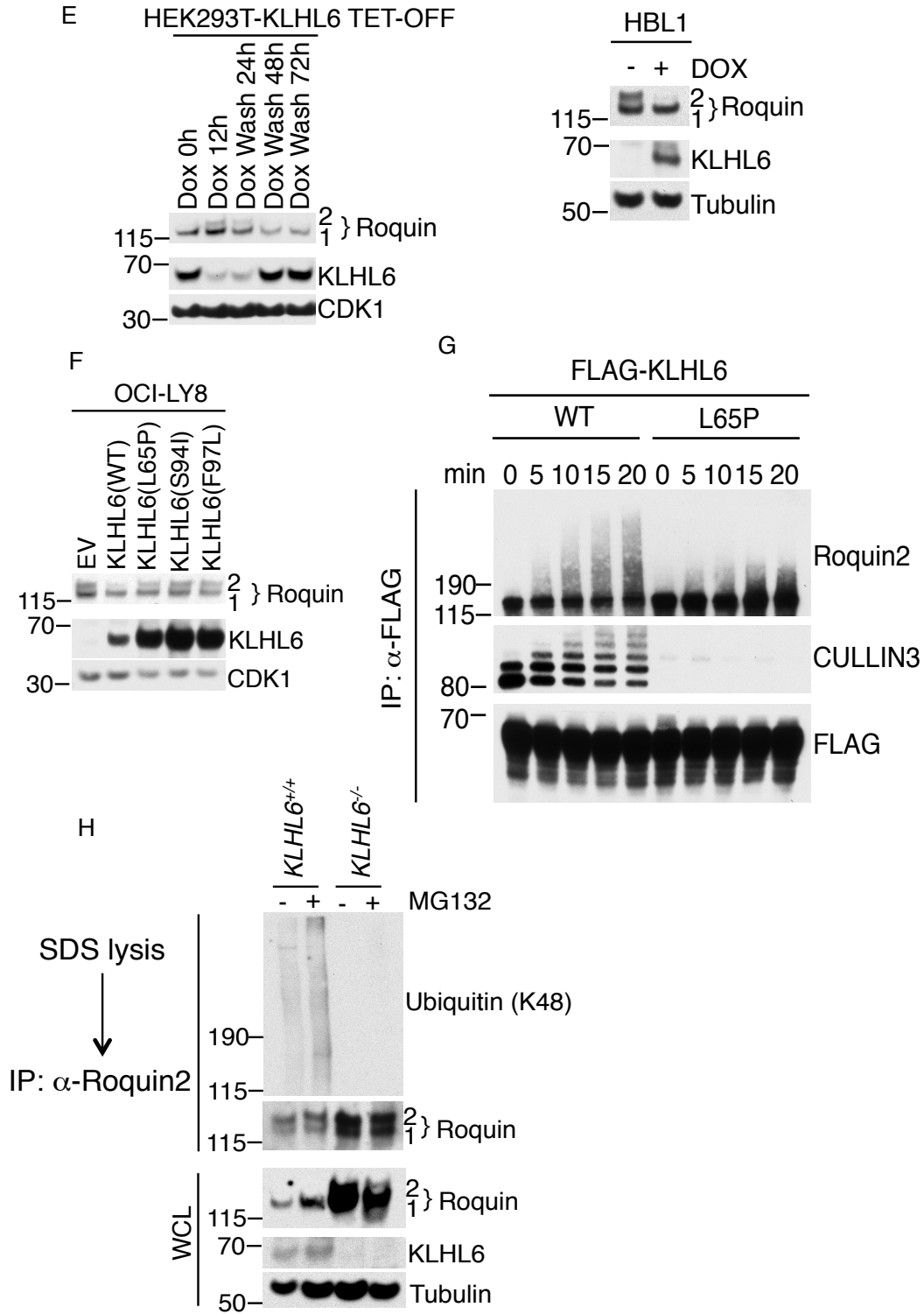


Figure 3.5 KLHL6 promotes ubiquitylation and degradation of Roquin2.

(A) Protein levels of Roquin2 and KLHL6 are inversely correlated in human DLBCL cells. Indicated human DLBCL cell lysates were analyzed by immunoblotting for the indicated proteins. (B) Quantification of Roquin2 (x-axis) and KLHL6 (y-axis) protein levels in each DLBCL cell line. n=11 DLBCL cell lines. r, Pearson correlation coefficient (95% confidence interval). (C) Knockdown of KLHL6 extends Roquin2 half-life in OCI-LY10 cells. OCI-LY10 cells were electroporated with siRNA scramble (siCTRL) or targeting KLHL6 (siKLHL6). Cells were treated with cycloheximide (CHX) for the indicated times. Whole cell lysates were analyzed by immunoblotting for the indicated proteins (top panel). Bottom panel shows quantification of Roquin1 and Roquin2 protein levels using ImageJ and their relative intensities were plotted over time. (D) Loss of KLHL6 extends Roquin2 half-life in U2932 cells. U2932 *KLHL6*^{+/+} and *KLHL6*^{-/-} cells were treated with cycloheximide (CHX) for the indicated times. Whole cell lysates were analyzed by immunoblotting for the indicated proteins (top panel). Bottom panel shows quantification of Roquin1 and Roquin2 protein levels using ImageJ and their relative intensities were plotted over time. (E) Roquin2 protein levels were negatively regulated by expression of KLHL6. HEK293T (TET)-OFF cells were transduced with retroviruses encoding a doxycycline (DOX) inducible expression of FLAG-tagged KLHL6 carrying a hygromycin cassette (left panel). DOX was added and/or washed at the indicated times. Whole cell lysates were analyzed by immunoblotting for the indicated proteins (left panel). HBL1 cells were transduced with lentiviruses encoding a doxycycline (DOX) inducible expression of KLHL6 wild-type (WT) carrying a puromycin cassette. The cells

were treated with DOX for 12 hours. Whole cell lysates were analyzed by immunoblotting for the indicated proteins (right panel). (F) Cancer-associated mutations of KLHL6 are incapable of promoting Roquin2 degradation. OCI-LY8 cells were transduced with retroviruses encoding empty vector (EV), KLHL6 wild type (WT) or BTB-mutants (L65P, S94I and F97L). Whole cell extracts were subjected to immunoblotting for the indicated proteins. (G) Roquin2 is ubiquitylated *in vitro* in a KLHL6 and CULLIN3-dependent manner. FLAG-KLHL6 and Roquin2 were immunopurified from HEK293T cells and incubated at 30°C with a ubiquitylation mix containing E1, UbcH5c, ubiquitin, and ATP. Reactions were stopped by addition of Laemmli buffer at the indicated times, and analyzed by immunoblotting for the indicated proteins. (H) Roquin2 ubiquitylation is regulated by KLHL6 *in vivo*. Endogenous Roquin2 was immunoprecipitated from U2932 *KLHL6*^{+/+} or *KLHL6*^{-/-} (clone-derived) cell extracts pre-treated with or without MG132 for 6 hours, and immunocomplexes were probed with antibodies to the indicated proteins. A representative blot from two independent experiments is shown.

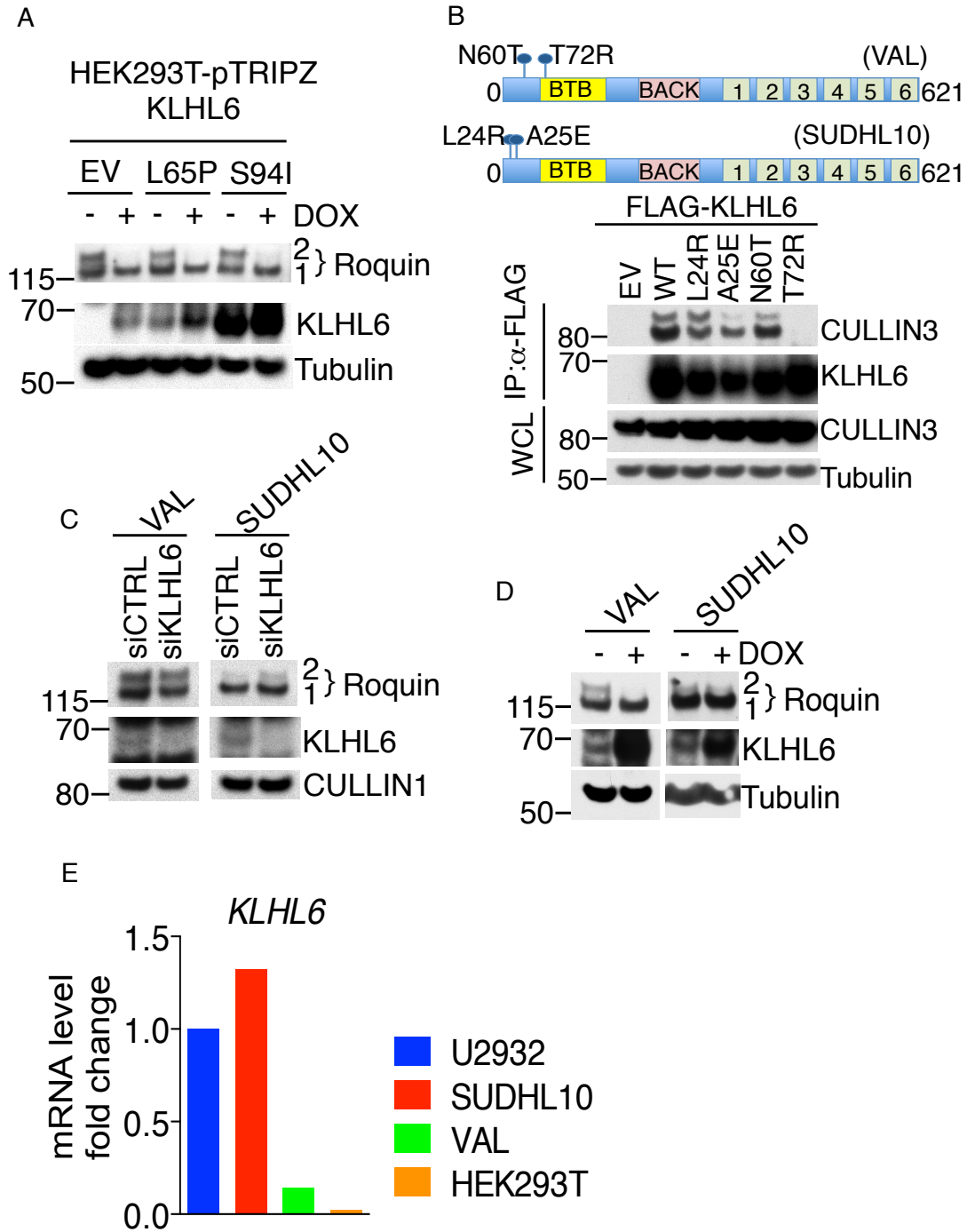


Figure 3.6 BTB-mutations of KLHL6 are not dominant-negative

(A) Expression KLHL6 (WT) promotes Roquin2 degradation even in the presence of BTB-mutations of KLHL6. HEK293T cells were transduced with lentiviruses encoding a doxycycline (DOX) inducible expression of KLHL6 carrying a puromycin cassette and then infected with lentiviruses encoding empty vector (EV) or KLHL6 BTB-mutants (L65P and S94I) carrying a GFP marker. The cells were treated with DOX for 12 hours, and whole cell extracts were subjected to immunoblotting for the indicated proteins. (B) BTB-mutations of KLHL6 are not dominant-negative. Top panel shows the schematic representation of KLHL6 protein displaying endogenous mutations in two different cell lines (VAL and SUDHL10). HEK293T cells were transfected with constructs encoding FLAG-tagged KLHL6 wild-type (WT), KLHL6 mutants (L24R, A25E, N60T, and T72R), or empty vector (EV). Exogenous proteins were immunoprecipitated (IP) from cell extracts with an anti-FLAG resin, and immunocomplexes were probed with antibodies to the indicated proteins. (C) KLHL6 is not functional in VAL cells. VAL and SUDHL10 cells were electroporated with siRNA scramble (siCTRL) or targeting KLHL6 (siKLHL6) and whole cell extracts were subjected to immunoblotting for the indicated proteins. (D) KLHL6 is not functional in VAL cells. VAL and SUDHL10 cells stably expressing KLHL6 under a doxycycline (DOX) inducible promoter with a puromycin cassette were treated with DOX for 12hrs and whole cell extracts were subjected to immunoblotting for the indicated proteins. (E) KLHL6 mRNA levels were comparably low in VAL cells. Analysis of KLHL6 expression by quantitative PCR (qPCR) in different cell lines is shown, and the value for the PCR product from U2932 cells was set as 1. A representative graph from two independent experiments is shown.

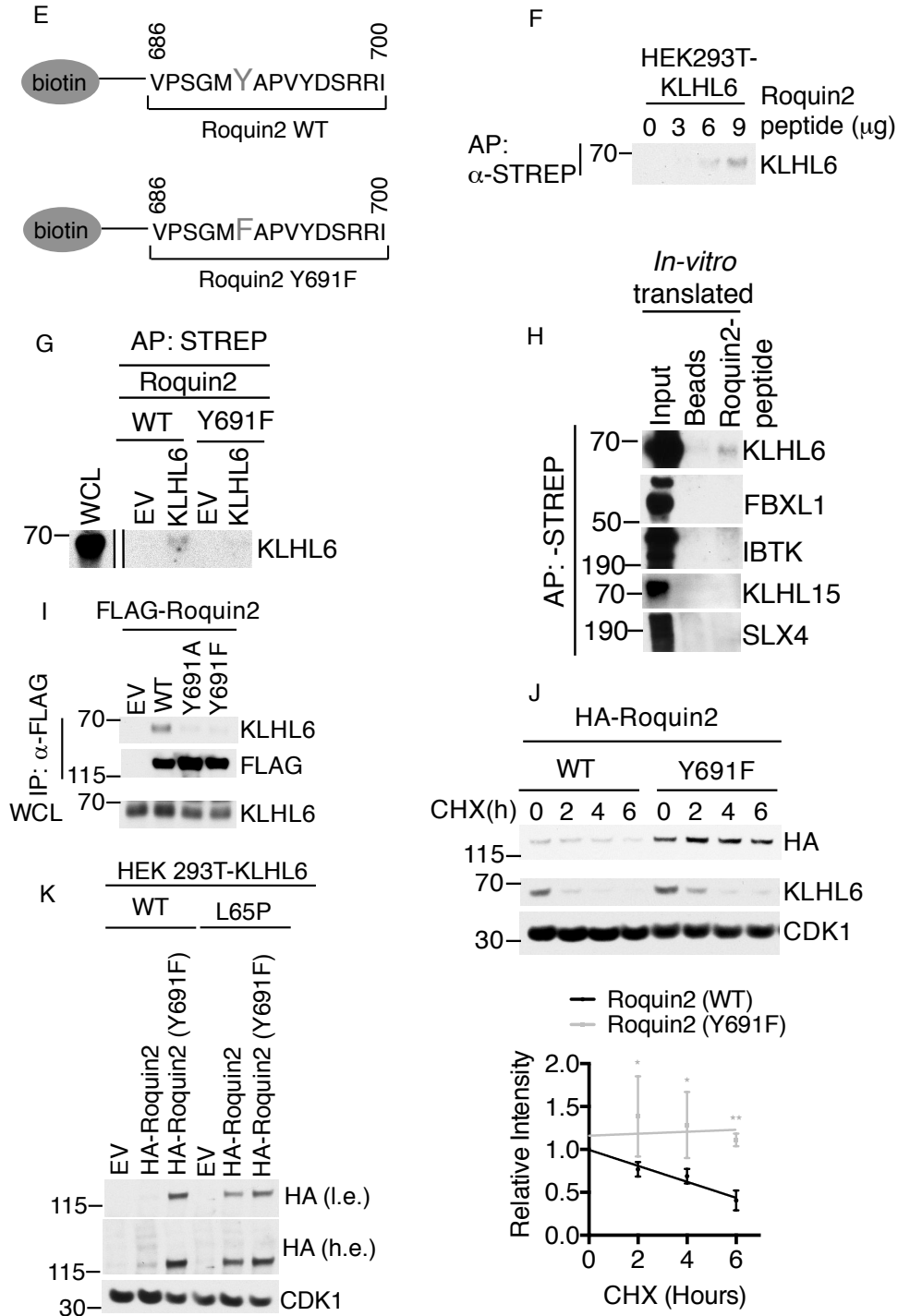
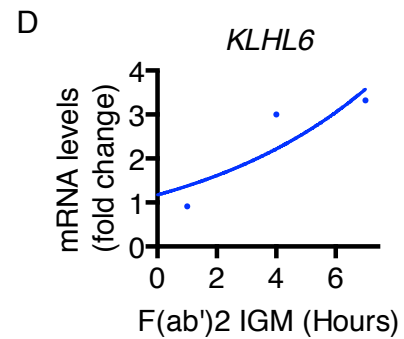
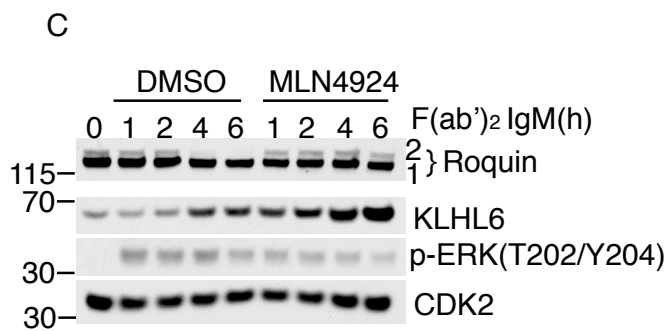
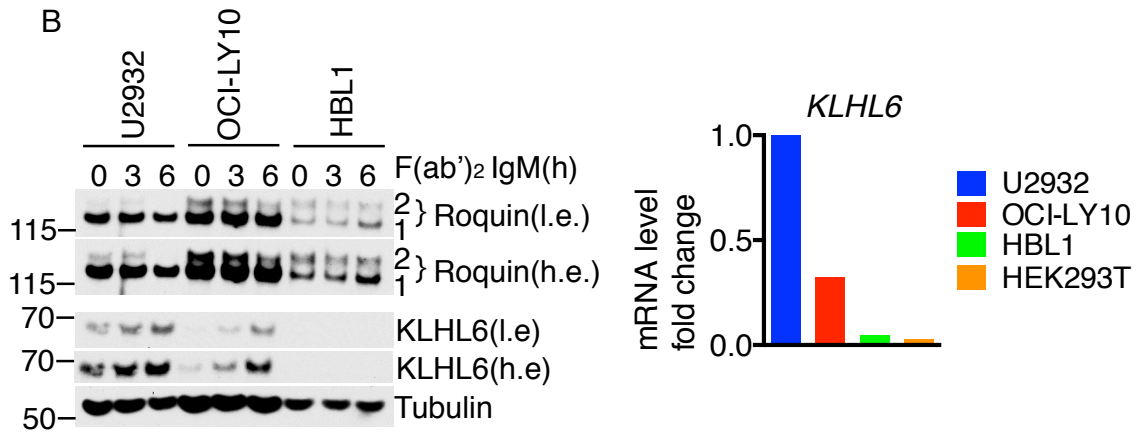
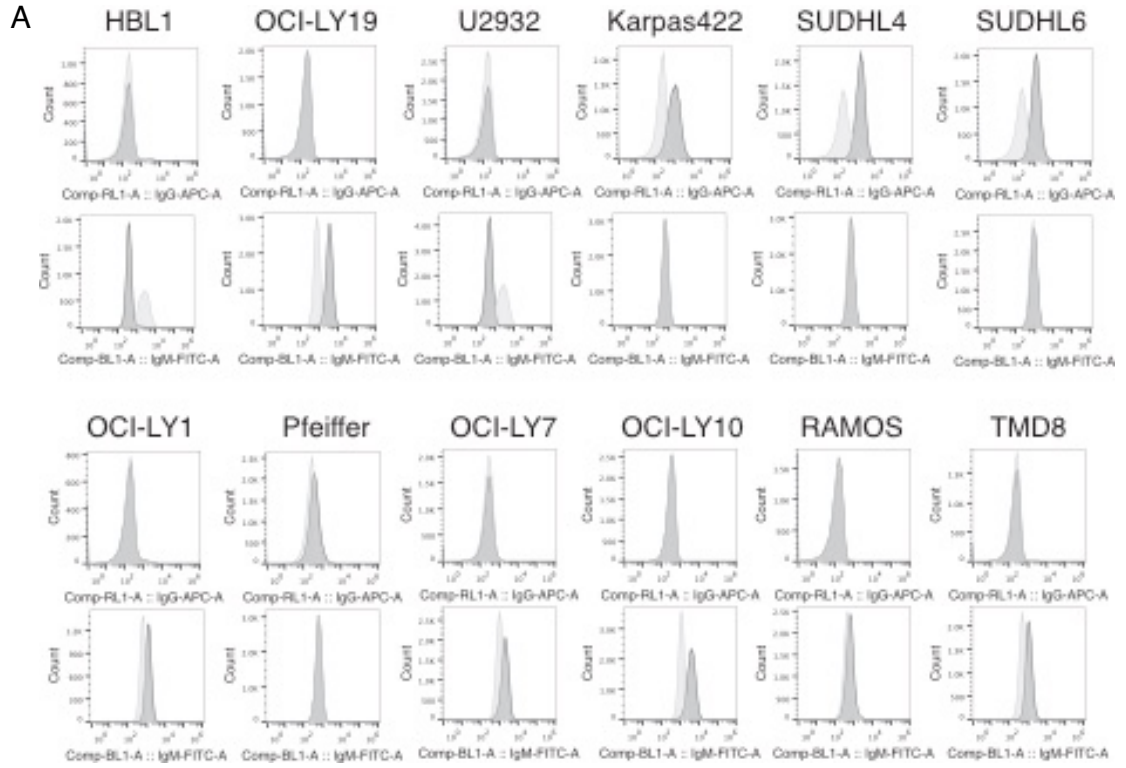


Figure 3.7 Interaction between KLHL6 and Roquin2 requires a functional tyrosine residue Y691 in Roquin2

(A) Mapping strategy for KLHL6 binding motif in Roquin2. HEK293T cells stably expressing KLHL6 were transfected with constructs encoding an empty vector (EV), FLAG-tagged Roquin2 wild type (WT) or mutants as indicated. Left panel shows a schematic representation of Roquin2 mutants. Roquin2 mutants that interact (+) or do not interact (-) with KLHL6 are shown. Right panel shows immunoblot analysis of FLAG-Roquin2 immunoprecipitation (IP). Immunocomplexes were probed with antibodies to the indicated proteins. Asterisk indicates non-specific bands. (B) Same as in (A). (C) Same as in (A). (D) Roquin2 binds KLHL6 through tyrosine 691. Left panel shows conservation of tyrosine 691 in lower species. HEK293T cells stably expressing KLHL6 were transfected with constructs encoding an empty vector (EV), FLAG-tagged Roquin2 wild type (WT) and mutants as indicated. Roquin2 was immunoprecipitated (IP) from cell extracts with an anti-FLAG resin, and immunocomplexes were probed with antibodies to the indicated proteins (right panel). (E) Schematic representation of the biotinylated Roquin2 peptide sequences. (F) KLHL6 directly interacts with Roquin2 in *in vitro* pull-down assay. The indicated amount of biotinylated Roquin2 peptides were incubated with whole cell extracts from HEK293T cells stably expressing KLHL6. Affinity Purification, AP. (G) and (H) KLHL6 directly interacts with Roquin2 in *in vitro* pull-down assay. Same as in (F) except that FLAG-tagged *in-vitro* translated proteins were utilized instead of whole cell extracts as indicated. Immunocomplexes were probed with anti-FLAG antibody to the indicated proteins as all *in-vitro* translated proteins were FLAG-tagged. (I) Mutation of tyrosine 691 into alanine or phenylalanine inhibits interaction with KLHL6. HEK293T cells stably expressing KLHL6 were transfected with

constructs encoding an empty vector (EV), FLAG-tagged Roquin2 wild type (WT) or mutants as indicated. Roquin2 was immunoprecipitated (IP) from cell extracts with an anti-FLAG resin, and immunocomplexes were probed with antibodies to the indicated proteins. (J) A mutant of Roquin2 incapable of interacting with KLHL6 displays a prolonged half-life in DLBCL cells. A DLBCL cell line, BJAB, was retrovirally transduced with cDNAs encoding Roquin2 (WT) or Roquin2 (Y691F). Cells were treated with cycloheximide (CHX) for the indicated times, and whole cell lysates were analyzed by immunoblotting for the indicated proteins (top panel). Roquin2 protein levels were quantified using Image J and their relative intensities were plotted over time (bottom panel). (K) KLHL6 (WT) induces degradation of Roquin2 (WT), but not Roquin2 (Y691F), while KLHL6 (L65P) has no effect. HEK2932T cells stably expressing KLHL6 (WT) or KLHL6 (L65P) were further infected with retroviruses encoding an empty vector (EV), Roquin2 (WT) or Roquin2 (Y691F). Whole cell lysates were analyzed by immunoblotting for the indicated proteins. A low exposure (l.e) and high exposure (h.e) are shown for HA-tagged Roquin2.



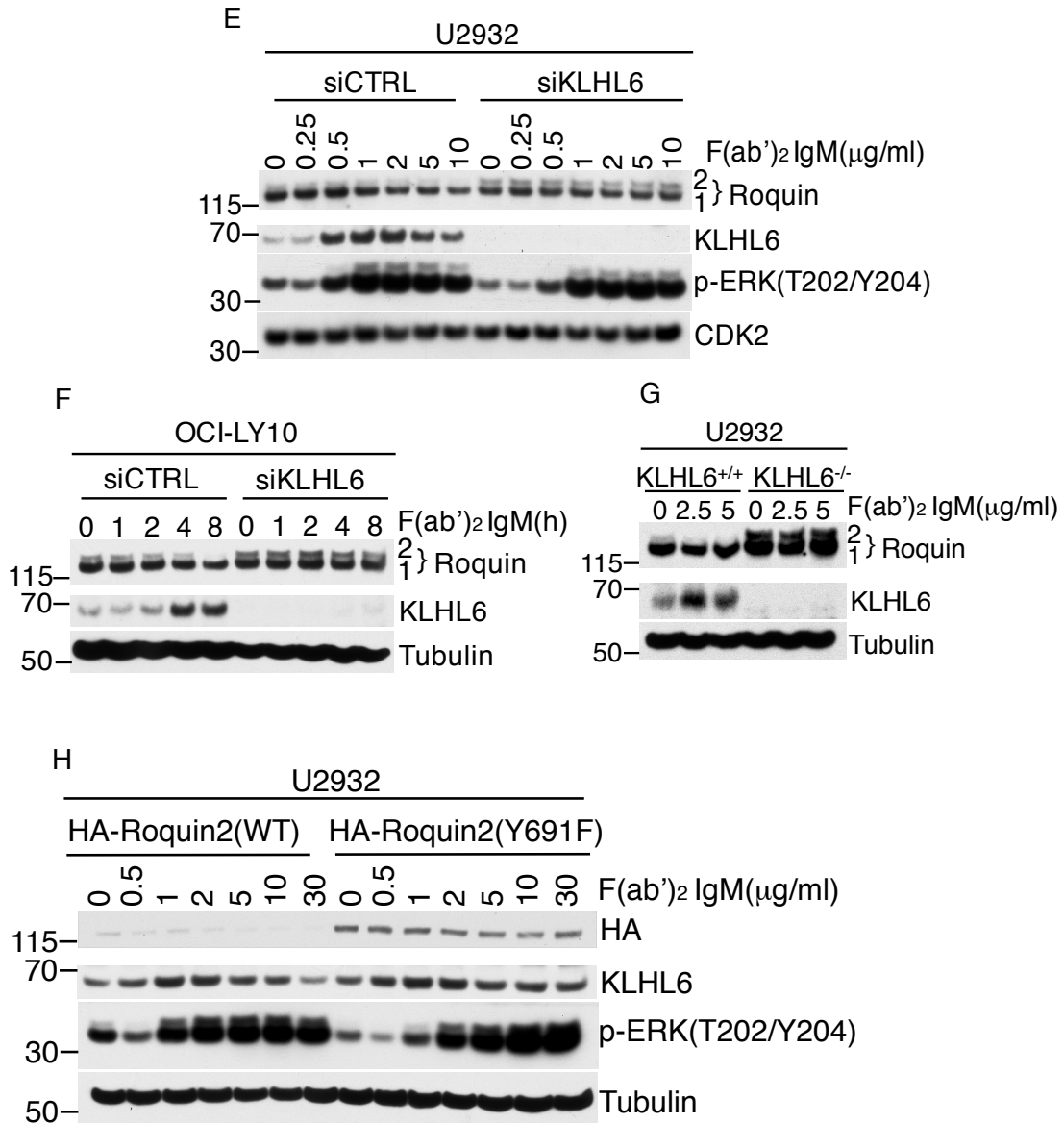


Figure 3.8 KLHL6 promotes Roquin2 degradation upon BCR stimulation

(A) ABC-DLBCLs and GCB-DLBCLs express IgM and IgG on their cell surfaces, respectively. A panel of human DLBCLs were stained either with anti-IgM or anti-IgG antibody to detect surface expression. A darker curve indicates a positive signal. A representative image from two independent experiments is shown. (B) B-cell receptor

activation induces Roquin2 down-regulation in DLBCL cells. KLHL6-expressing ABC-DLBCL cell lines, OCI-LY10 and U2932, and a non-expressing cell line, HBL1, were stimulated with 10 $\mu\text{g/ml}$ of F(ab')₂-IgM for 3 and 6 hours. Whole cell lysates were analyzed by immunoblotting for the indicated proteins. A low exposure (l.e.) and high exposure (h.e.) are shown for Roquin2 (Left Panel). Right panel shows levels of *KLHL6* mRNA analyzed by qPCR. The value for the PCR product from U2932 was set as 1. A representative graph from two independent experiments is shown. (C) Degradation of Roquin2 is blocked upon chemical inhibition of CULLIN neddylation. U2932 cells were treated with 10 $\mu\text{g/ml}$ of F(ab')₂-IgM for the indicated times. Where indicated, cells were pre-treated with 5 μM MLN4932 for 1 hour. Whole cell lysates were analyzed by immunoblotting for the indicated proteins. (D) BCR stimulation up-regulates KLHL6 transcriptionally. U2932 cells were treated with 10 $\mu\text{g/ml}$ of F(ab')₂-IgM for the indicated times. Levels of KLHL6 mRNA were analyzed by real time PCR. The value for PCR product present without treatment was set as 1. A representative graph from two independent experiments is shown. (E) Roquin2 is degraded in a dose-dependent BCR signaling- and KLHL6-dependent manner. U2932 cells were electroporated with a siRNA scramble (siCTRL) or targeting KLHL6 (siKLHL6) and treated with increasing concentrations of F(ab')₂-IgM for 6 hours. Whole cell lysates were analyzed by immunoblotting for the indicated proteins. (F) Degradation kinetics of Roquin2 are dependent on BCR signaling and KLHL6 expression. OCI-LY10 cells were treated with 10 $\mu\text{g/ml}$ F(ab')₂-IgM for the indicated times. Where indicated, cells were electroporated with a siRNA scramble (siCTRL) or targeting KLHL6 (siKLHL6). Whole cell lysates

were analyzed by immunoblotting for the indicated proteins. (G) Roquin2 is degraded in a KLHL6-dependent manner. U2932 *KLHL6*^{+/+} and *KLHL6*^{-/-} (clone-derived) cells were treated with increasing concentrations of F(ab')₂-IgM for 6 hours. Whole cell lysates were analyzed by immunoblotting for the indicated proteins. (H) Roquin2 (Y691F) mutant is insensitive to BCR-induced degradation. U2932 cells were stably transduced with retroviruses encoding HA-Roquin2 (WT) or HA-Roquin2 (Y691F). Cells were treated with increasing concentrations of F(ab')₂-IgM for 6 hours, and whole cell lysates were analyzed by immunoblotting for the indicated proteins.

University of Nebraska Medical Center(UNMC)				
Type	Chromosome	Sample ID	Variant Classification	Amino Acid Change
DLBCL		3 DLBCL-36539	missense	C85W
DLBCL		3 DLBCL-43092	missense	M67I
DLBCL		3 S02-2857	missense	A135V
DLBCL		3 S02-312	missense	V78E
DLBCL		3 S08-4728	missense	N69D
DLBCL		3 S08-4728	missense	D73H
DLBCL		3 S08-4728	missense	I80M
DLBCL		3 SC06-1631	missense	M3R
DLBCL		3 SC06-1631	missense	E17A
DLBCL		3 SC06-1631	stop-gained	L42*
DLBCL		3 SC06-3802	missense	D29N
DLBCL		3 SC07-2866	missense	G475E
DLBCL		3 SC08-2147	missense	L90F
DLBCL		3 SP01-10756	missense	E568K

Canada's Michael Smith Genome Sciences Centre(CMSGSC)				
Type	Chromosome	Sample ID	Variant Classification	Amino Acid Change
DLBCL(GCB)		3 98-22532/DLBCL-	missense	S83T, S94T
DLBCL(GCB)		3 95-32814	not-classified	2
DLBCL(GCB)		3 05-24561	not-classified	1
DLBCL(GCB)		3 96-20883	missense	L54V, L65V
DLBCL(ABC)		3 02-22991	missense, stop	L45*, L56*, T53I, T64I
DLBCL(ABC)		3 07-37968	not-classified	1
DLBCL(GCB Line)		3 OCI-Ly1	not-classified	1
DLBCL(GCB)		3 05-24904	not-classified	1
DLBCL(ABC)		3 06-16716	missense	T53S, T64S
DLBCL(U)		3 82-57570	not-classified	1
DLBCL(U)		3 04-20644	not-classified	1

For CMSGSC data, the total numbers of cSNV detected are reported (the exact change of cSNV is not reported)

Broad Institute(Broad)				
Type	Chromosome	Sample ID	Variant Classification	Amino Acid Change
DLBCL		3	4 missense	R566W
DLBCL		3	5 missense	C578S
DLBCL		3	47 missense	C508R
DLBCL		3	49 missense	F83L
DLBCL		3	49 missense	D14N

The Cancer Genome Atlas(TCGA)				
Type	Chromosome	Sample ID	Variant Classification	Amino Acid Change
DLBCL		3 TCGA-GR-A4D6-01	missense	T387A
DLBCL		3 TCGA-FM-8000-01	missense	L90P
DLBCL		3 TCGA-FF-8047-01	missense	A91V
DLBCL		3 TCGA-G8-6914-01	missense	L65P
DLBCL		3 TCGA-GR-A4D9-01	missense	E547K
DLBCL		3 TCGA-FF-A7CW-01	missense	L90F
DLBCL		3 TCGA-FF-8062-01	missense	E547Q

Duke Cancer Institute				
Type	Chromosome	Sample ID	Variant Classification	Amino Acid Change
DLBCL	3	3620*	frameshift substitution	exon1:c.268_280CA
DLBCL	3	3582*	nonframeshift substitution	exon1:c.60_75A
DLBCL	3	2613	nonsynonymous SNV	exon1:c.A126C:p.L42F
DLBCL	3	3593	nonsynonymous SNV	exon1:c.A152G:p.D51G
DLBCL	3	3593*	nonsynonymous SNV	exon1:c.A168C:p.L56F
DLBCL	3	3401	nonsynonymous SNV	exon1:c.A179T:p.N60I
DLBCL	3	2217, 3439	nonsynonymous SNV	exon1:c.A236T:p.D79V
DLBCL	3	2290, 3703	nonsynonymous SNV	exon1:c.A246T:p.E82D
DLBCL	3	705*	nonsynonymous SNV	exon1:c.A287C:p.Y96S
DLBCL	3	3506*	stopgain	exon1:c.C175T:p.Q59X
DLBCL	3	3625	nonsynonymous SNV	exon1:c.C209G:p.A70G
DLBCL	3	2158, 2213	nonsynonymous SNV	exon1:c.C211G:p.L71V
DLBCL	3	2809*	stopgain	exon1:c.C241T:p.Q81X
DLBCL	3	2243, 2559, 2901, 2945, 3634*	nonsynonymous SNV	exon1:c.C268T:p.L90F
DLBCL	3	2649*	nonsynonymous SNV	exon1:c.G217A:p.D73N
DLBCL	3	2901	nonsynonymous SNV	exon1:c.G232C:p.V78L
DLBCL	3	3681*	nonsynonymous SNV	exon1:c.G254A:p.C85Y
DLBCL	3	2827, 3627*	nonsynonymous SNV	exon1:c.G281A:p.S94N
DLBCL	3	2073*	nonsynonymous SNV	exon1:c.T161C:p.L54P
DLBCL	3	705, 2158, 2302, 2522, 2544, 2613, 3548, 3601, 3614, 3819*	nonsynonymous SNV	exon1:c.T194C:p.L65P
DLBCL	3	2048*	nonsynonymous SNV	exon1:c.T200A:p.M67K
DLBCL	3	3739*	nonsynonymous SNV	exon1:c.T247A:p.F83I
DLBCL	3	2556, 3739*	nonsynonymous SNV	exon1:c.T286G:p.Y96D
DLBCL	3	2613*	stopgain	exon1:c.T288A:p.Y96X
DLBCL	3	2654*	nonsynonymous SNV	exon2:c.A320G:p.E107G
DLBCL	3	2286	nonsynonymous SNV	exon3:c.C743T:p.S248L
DLBCL	3	2952, 3542	nonsynonymous SNV	exon4:c.G1040A:p.R347H
DLBCL	3	3609	nonsynonymous SNV	exon4:c.G1105A:p.E369K
DLBCL	3	3741	nonsynonymous SNV	exon5:c.A1184G:p.N395S
DLBCL	3	2826, 2840	nonsynonymous SNV	exon5:c.C1231T:p.R411C
DLBCL	3	2676, 3468, 3495	nonsynonymous SNV	exon5:c.G1324A:p.D442N
DLBCL	3	2543	nonsynonymous SNV	exon5:c.T1313A:p.V438E
DLBCL	3	3903	nonsynonymous SNV	exon6:c.G1427A:p.G476E
DLBCL	3	3718, 3832	nonsynonymous SNV	exon7:c.A1640G:p.E547G
DLBCL	3	3944	nonsynonymous SNV	exon7:c.C1675T:p.R559W
DLBCL	3	2455	nonsynonymous SNV	exon7:c.C1724T:p.T575M
DLBCL	3	3883	nonsynonymous SNV	exon7:c.G1639A:p.E547K
DLBCL	3	705, 2083, 2120, 2153, 2269, 2709, 2785, 2912, 2944, 3401, 3484	nonsynonymous SNV	exon7:c.G1702A:p.E568K
DLBCL	3	2867, 3595	nonsynonymous SNV	exon7:c.G1781A:p.R594Q
DLBCL	3	3542, 3585, 3627	nonsynonymous SNV	exon7:c.G1804A:p.V602I
DLBCL	3	2654	nonsynonymous SNV	exon7:c.T1685C:p.I562T
DLBCL	3	2827	nonsynonymous SNV	exon7:c.T1735G:p.W579G
DLBCL	3	2816	nonsynonymous SNV	:exon7:c.T1819G:p.S607A

* BTB mutations experimentally verified to abolish CULLIN3 interaction.
 These mutations were utilized to calculate statistical association with TNFAIP3 mutations

Instituto Universitario de Oncologia(IUOPA)				
Type	Chromosome	Sample ID	Variant Classification	Amino Acid Change
CLL	3	3	missense	L65P
CLL	3	3	missense	F49L
CLL	3	287	missense	V47G
CLL	3	287	missense(synonymous)	D14D
CLL	3	338	missense	T6S4
CLL	3	338	missense	F49I
CLL	3	338	missense	L38S
CLL	3	381	missense	L65P
CLL	3	535	missense	I75F
CLL	3	535	missense	M67V
CLL	3	594	missense	L90F
CLL	3	669	missense	L6P5
CLL	3	770	missense	S94I
CLL	3	884	missense	L65P
CLL	3	1237	missense	L90R
CLL	3	1353	missense	L90V
CLL	3	1462	stop	Q81*
CLL	3	1465	missense	Y96F
CLL	3	1465	missense	Q81K
CLL	3	1471	missense	A93G

Broad Institute(Broad)				
Type	Chromosome	Sample ID	Variant Classification	Amino Acid Change
MM	3	MM-0308-Tumor	missense	F97L
MM	3	MM-0335-Tumor	Intron	n/a
MM	3	MM-0338-Tumor	Intron	n/a
MM	3	MM-0389-Tumor	Intron	n/a
MM	3	MM-0389-Tumor	Intron	n/a
MM	3	MM-0408-Tumor	Intron	n/a
MM	3	MM-0447-Tumor	Intron	n/a
MM	3	MM-0456-Tumor	Intron	n/a
MM	3	MM-0456-Tumor	Intron	n/a
MM	3	MM-0633-Tumor	3'UTR	n/a
MM	3	MM-0510-Tumor	In frame deletion	V89

Table 3.1 KLHL6 mutations in DLBCLs

List of *KLHL6* mutations in B-cell cancer patients [University of Nebraska Medical Center (UNMC), The Cancer Genome Atlas (TCGA), Canada's Michael Smith Genome Sciences Centre (MSGSC), Broad Institute (Broad), Duke Cancer Institute (DCI) and Instituto Universitario de Oncología (IUOPA)].

Data set	Cell Type	Condition	# Replicates	Accession Code
Mass Spectrometry	HEK293T cells	Empty Vector, KLHL6 (WT), KLHL6 (L65P)	1	PXD008963
Mass Spectrometry	ARP-1 cells	Empty Vector, KLHL6 (WT), KLHL6 (L65P)	1	PXD008963

Table 3.2 Proteomic analyses of KLHL6 complexes generated in this dissertation

List of KLHL6 interacting proteins identified by proteomic analyses of KLHL6 complexes purified from ARP-1 and HEK293T cells.

CHAPTER 4 : THE BIOLOGICAL FUNCTION OF KLHL6-ROQUIN2 AXIS IN ABC-DLBCLS

Chapter summary

Research described in this chapter was performed in collaboration with the laboratories of Dr. Roberto Bonasio and Dr. Michael Green. RNA-seq sample preparations and analyses were carried out in collaboration with Kristin Ingvarsdottir, a postdoctoral fellow in Dr. Roberto Bonasio's laboratory (Upenn). The mutual exclusivity analysis for DLBCL patients was carried out in collaboration with Dr. Roberto Bonasio laboratory (Upenn) and Dr. Michael Green laboratory (MD Anderson Cancer Center)

Some of works presented here forms the body of a manuscript that is currently accepted at Nature Cell Biology. Experiments on GCB-DLBCL cell growth and survival are unpublished and establish the basis for the ongoing projects in our laboratory to investigate whether KLHL6 has a function beyond cell autonomous regulation. This chapter is focused on elucidating the role of the KLHL6-Roquin2 axis on ABC-DLBCL biology and is written and arranged differently from the original manuscript.

Jaewoo Choi, Kyutae Lee, Kristin Ingvarsdottir, Roberto Bonasio, Anita Saraf, Laurence Florens, Michael P. Washburn, Saber Tadros, Michael R. Green, and Luca Busino. Loss of KLHL6 promotes diffuse large B-cell lymphoma growth and survival by stabilizing the mRNA decay factor Roquin2

Introduction

DLBCL is the most common lymphoid malignancy accounting for ~30% of lymphoma cases and can be sub-divided into three distinct molecular subtypes: activated B cell-like (ABC) DLBCL, germinal center B cell-like (GCB) DLBCL, and primary mediastinal B cell lymphoma (PMBL) (Alizadeh et al., 2000; Rosenwald et al., 2003). These subtypes arise from different stages of B-cell differentiation and are characterized by reliance on completely distinctive oncogenic signaling pathways. GCB-DLBCLs are arising from centroblasts within the germinal center and generally expresses lower NF- κ B target genes than ABC-DLBCL (Staudt, 2010). One of the key features of GCB-DLBCLs is the amplification of chromosome 2 encoding *c-rel* with 27% of occurrence and translocation involving *bcl2* gene (Lenz et al., 2008f). Furthermore, GCB-DLBCLs are characterized by deletion of PTEN, a tumor suppressor gene, and amplification of mir-17-92, an oncogenic micro-RNAs with deregulated expression of Bcl-6 (Parekh et al., 2007; Shaffer et al., 2002). *BCL6* gene plays an important role in germinal center (GC) formation and suppresses genes involved in cell cycle arrest, apoptosis, and DNA checkpoint genes (Cerchietti et al., 2010; Phan and Dalla-Favera, 2004). This suggests that Bcl-6 is a potential target gene in GCB-DLBCL. In fact, inhibitors of Bcl-6 BTB domain, histone deacetylase, and topoisomerase II have shown some efficacies in down-regulating Bcl6 expression and improved survival of younger DLBCL patients (Cerchietti et al., 2010; Kurosu et al., 2003; Parekh et al., 2007).

On the other hand, key features of human ABC-DLBCLs are hyper-activation of the inhibitor of I κ B kinase (IKK) and the NF- κ B transcription factor program (Staudt,

2010). ABC-DLBCL cell lines depend on chronic active B-cell receptor (BCR) signaling that mediates NF- κ B activation for their proliferation and survival (Staudt, 2010; Young et al., 2015). This is evidenced by frequent mutations occurrence in the BCR pathway, including activating mutations of positive (*CD79A/B* and *CARD11* (Davis et al., 2010; Lenz et al., 2008a)) and inactivating mutations of negative (*TNFAIP3* (Compagno et al., 2009; Davis et al., 2010; Kato et al., 2009; Lenz et al., 2008a)) NF- κ B regulators. This suggests that ABC-DLBCLs might have increased BCR antigenic response and targeting the components of the BCR pathway such as Bruton's tyrosine kinase (Btk) would be a great therapeutic approach. In fact, ibrutinib, which is a covalent inhibitor of Btk, is selectively toxic to ABC-DLBCL cell lines with an anti-proliferative activity (Davis et al., 2010). More importantly, in a phase 1/2 clinical trial, ibrutinib has shown to produce complete or partial responses with relapsed or refractory ABC-DLBCL patients with more frequent response rate for the patients with BCR mutations and concomitant myeloid differentiation primary response 88 (MYD88) mutations (Wilson et al., 2015).

ABC-DLBCLs are also dependent on MYD88, which is an adaptor protein that mediates NF- κ B pathway after activation of toll-like receptors and IL-1 and IL-8 receptors (Iwasaki and Medzhitov, 2010). RNA interference screening has shown that MYD88 and the IRAK1 and IRAK4 (IL-1 receptor-associated kinases) are critical for ABC DLBCL survival (Ngo et al., 2011). About 29% of ABC DLBCL tumors harbors L265P mutation in MYD88, which is a gain of function mutation that activates NF- κ B signaling, JAK-STAT3 and cytokine signaling such as IL-6, IL-10, and interferon- β , promoting survival of ABC-DLBCLs. More recently, integrative analysis of whole-

exome and transcriptome sequencing have identified novel genetic drivers and defined oncogenes that promote DLBCL growth and survival, including well-known genes described above such as MYD88 and CARD11 (Reddy et al., 2017) along with unknown gene like *KLHL6* with 10-15% of cases in DLBCLs. We have analyzed the biochemical aspects of cancer-associated mutations in *KLHL6* and found that mutations completely disrupt its ligase activity and interaction with CULLIN3 in chapter 3. However, exact mechanisms of how *KLHL6* contributes to the pathology of human DLBCL and whether the stabilization of *KLHL6* substrate, Roquin2, influences NF- κ B activation or BCR signaling pathways is currently unknown.

One another common target of genetic alteration in ABC-DLBCLs is tumor necrosis factor- α -inducible gene 3 (TNFAIP3 or A20), a negative regulator of NF- κ B signaling pathway. Roughly 30% of ABC-DLBCL patients show nonsense mutations and biallelic inactivation of this gene, and re-introduction of wild-type A20 in A20-null ABC-DLBCL cell lines induces cellular apoptosis and growth arrest. This suggests that A20 is a relevant tumor suppressor in ABC-DLBCLs (Compagno et al., 2009). A20 belongs to deubiquitinating enzymes with ovarian tumour (OTU) domain and serves as a terminator of NF- κ B responses by deubiquitinating TRAF2/6, IKK γ subunit, and MALT1 proteins (Boone et al., 2004; Lin et al., 2008; Wertz et al., 2004). The fact that A20-deficient mice die from spontaneous inflammation suggests that A20 mutations alone might not be sufficient to induce constitutive NF- κ B signaling pathway (Boone et al., 2004). Instead, they might rather cooperate with other genetic alteration events such as CARD11 or CD79A/B mutations to enhance NF- κ B programs. Although there are many cases

reported for genetic mutation and inactivation of A20, whether there are additional mechanisms to inhibit its function in B-cell malignancies remain to be determined.

In chapter 4, we have identified a novel role for KLHL6-Roquin2 axis in ABC-DLBCLs. We found that KLHL6 is a tumor suppressor gene where loss of KLHL6 favors cancer cell growth and survival both *in vitro* and in xenograft models. Correspondingly, ABC-DLBCL cell lines expressing non-degradable Roquin2 (Y691F) mutant exhibit a similar growth advantage compared to cells expressing Roquin2 (WT). These proliferative and growth effects were dependent on RNA binding ability of Roquin2. Mechanistically, stabilization of Roquin2 promotes mRNA decay of the tumor suppressor and NF- κ B pathway inhibitor, tumor necrosis factor- α -inducible gene 3 (TNFAIP3), thereby enhancing NF- κ B programs in ABC-DLBCLs. All together, our study shows a previously uncharacterized molecular mechanism whereby the KLHL6-Roquin2 axis affects B-cell cancer cell proliferation through modulation of the NF- κ B activity via mRNA decay.

Results

KLHL6 is a tumor suppressor in ABC-DLBCL subtype

Given that cancer-associated mutations of KLHL6 result in loss of E3 ubiquitin ligase activity, we hypothesized that KLHL6 acts as a tumor suppressor by promoting

Roquin2 degradation. *KLHL6* mutations are equally distributed among the two molecular subtypes of DLBCL, even though *KLHL6* mutations are predictive of poor patient survival mainly in the ABC-DLBCL cohorts (Meriranta et al., 2016). First, we investigated the dependency of GCB-DLBCL cells on Roquin2. We utilized shRNA-mediated knockdown of Roquin2 in SUDHL10, which display a functional *KLHL6*. Loss of Roquin2 had no significant effects on cell proliferation (Fig 4.1A). Similar data were obtained in VAL cells (Fig 4.1B), which harbor a *KLHL6* loss of function mutation. Furthermore, we edited the *KLHL6* locus in the GCB-DLBCL cell line BJAB, which carries wild-type *KLHL6* alleles, and showed that concomitant knockdown of Roquin2 had no significant effects on cell proliferation in both *KLHL6*^{+/+} and *KLHL6*^{-/-} cells (Fig 4.1C). To analyze the impact of Roquin2 stabilization in GCB-DLBCL cells, we generated BJAB cells stably expressing Roquin2 (WT) or Roquin2 (Y691F) and measured differential gene expression in these cells via RNA sequencing. GO enrichment analysis revealed minor pathway alteration (Fig 4.1D). Thus, although the mutational pattern in GCB-DLBCL patients suggests *KLHL6* as a tumor suppressor in this subtype, the survival data (Meriranta et al., 2016) together with our functional characterization indicate that the *KLHL6*-Roquin2 axis does not play a role in cellular proliferation and survival in the GCB-DLBCL subtype.

Since somatic mutations of *KLHL6* are clinically relevant in the ABC-DLBCL subtype (Leo Meriranta, 2016), we assessed the biological effect of *KLHL6* loss by infecting Cas9-expressing U2932, OCI-LY10 and TMD8 cells with lentiviruses encoding three different gRNAs targeting the *KLHL6* gene locus. Loss of *KLHL6* in all three ABC-

DLBCL cell lines resulted in an increase in cellular proliferation with a corresponding decrease in apoptosis (Fig. 4.1E and 4.1F). This effect was confirmed in 3D cultures as measured by a larger number and size of colonies (Fig. 4.1G). To rule out the possible off-target effects of gRNAs, we utilized shRNA-mediated knockdown of *KLHL6* in U2932 and OCI-LY10 and observed similar results (Fig. 4.1H and 4.1I).

Having established that *KLHL6* loss promotes ABC-DLBCL growth and survival, we next investigated whether cancer mutations in the BTB-domain of *KLHL6* would affect cell growth. To this aim, we re-introduced *KLHL6* (WT) or *KLHL6* BTB-domain mutants (L65P, S94I and F97L) along with an empty vector (EV) in U2932 *KLHL6*^{-/-} cells (Fig. 4.1J). Re-expression of *KLHL6* (WT) in *KLHL6*^{-/-} cells decreased the rate of cancer cell proliferation, confirming *KLHL6* as a tumor suppressor in DLBCLs. However, *KLHL6* BTB-domain mutants displayed similar proliferative effects compared to *KLHL6* (EV), phenocopying the loss of *KLHL6* (Fig. 4.1J). This confirms the fact that mutations in the BTB-domain of *KLHL6* are loss of function mutation in ABC-DLBCLs. Furthermore, we injected these U2932 *KLHL6*^{-/-} cells re-expressing either EV, *KLHL6* (WT) or *KLHL6* (S94I) subcutaneously into NOD/SCID/IL2Rγ^{-/-} (NSG) mice. In agreement with the cell proliferation data, expression of *KLHL6* (WT) decreased tumor burden, measured by tumor volume and tumor weight (Fig. 4.1K). In contrast, DLBCL cells expressing *KLHL6* (S94I) displayed a similar tumor burden compared to *KLHL6*^{-/-} cells (EV).

Lastly, to examine whether *KLHL6* expression correlates with better survival of ABC-DLBCL patients, we combined gene expression data sets from three different

studies (Lenz et al., 2008f; Monti et al., 2012; Visco et al., 2012) and found that low KLHL6 expression correlated with significantly poorer survival in ABC-DLBCL patients (Fig. 4.1L). This analysis further supports the notion that KLHL6 is a tumor suppressor in ABC-DLBCL cells.

Roquin2 stabilization promotes ABC-DLBCL growth and survival

Since loss of KLHL6 induces stabilization of Roquin2, we investigated the significance of the KLHL6-Roquin2 axis by analyzing the effect of Roquin2 stabilization on ABC-DLBCL growth. We generated U2932 cells stably expressing Roquin2 (WT) or Roquin2 (Y691F) for use in xenograft experiments. Consistent with the hypothesis that loss of KLHL6 promotes cell proliferation and survival via stabilization of Roquin2, expression of the non-degradable Roquin2 (Y691F) mutant increased tumor burden when inoculated sub-cutaneously in *NSG* mice as monitored by tumor volume and weight at the experimental endpoint (Fig. 4.2A). This effect was not due to an overexpression artifact because the levels of Roquin2 (Y691F) were similar (actually even lower) to those of endogenous Roquin2 in *KLHL6*^{-/-} cells (Fig. 4.2B).

Furthermore, we utilized shRNA-mediated knockdown of Roquin2 in *KLHL6*^{-/-} U2932 and OCI-LY10 cells and found that ablation of Roquin2 impaired the cell growth advantage of both *KLHL6*^{-/-} cells (Fig. 4.2C, and 4.2D). Importantly, loss of Roquin2 increased cell toxicity preferentially in *KLHL6*^{-/-} cells (Fig. 4.2E), supporting the notion that loss of *KLHL6* promotes cell proliferation in a Roquin2-dependent manner.

Stabilization of Roquin2 down-regulate BCR responsive genes

Roquin proteins act broadly as regulators of mRNA deadenylation and degradation by recognizing stem-loop RNA degradation motifs through a ROQ domain (Leppek et al., 2013). We generated a double mutant Roquin2 (Y691F Δ ROQ) lacking the ROQ domain (Fig. 4.3A) to examine whether the pro-proliferative effect of Roquin2 (Y691F) mutant depends on its RNA binding ability. Remarkably, concomitant deletion of the ROQ domain in non-degradable Roquin2 mutant (Y691F) completely abolished the growth advantage induced by this mutant, implying that the effect of Roquin2 stabilization on cell growth requires an intact RNA binding domain.

BCR signaling is a major pathway driving ABC-DLBCL survival (Staudt, 2010). Since stabilization of Roquin2 promotes DLBCL proliferation in a manner dependent on the mRNA binding ability of Roquin2, we hypothesized that deregulation of Roquin2 proteolysis would result in aberrant BCR-dependent transcriptional program. Since Roquin2 is targeted for protein degradation in a KLHL6-dependent manner upon activation of BCR signaling, we reasoned that expression of the non-degradable Roquin2 (Y691F) mutant would result in constitutive mRNA decay of Roquin2 targets upon BCR activation. We treated U2932 cells expressing Roquin2 (WT) or Roquin2 (Y691F) with F(ab')₂-IgM and measured differential gene expression via RNA sequencing analysis (Fig. 4.3B and Table 4.1). We performed a pairwise comparison of RNA reads and found that 133 mRNAs were significantly down-regulated in Roquin2 (Y691F) expressing cells

as compared to Roquin2 (WT). Since Roquin2 is degraded upon BCR stimulation, we specifically searched for the BCR dependent transcripts whose expression was up-regulated by at least two-fold upon BCR activation (Fig. 4.3C). Among 133 genes, we identified 64 genes whose expression was BCR-responsive and down-regulated when Roquin2 is not properly degraded in DLBCL cells.

Additionally, we performed gene ontology (GO) enrichment analysis (Fig. 4.3D and Table 4.2) and found that Roquin2 putative mRNA targets are involved in immune and inflammatory responses, including genes implicated in the NF- κ B pathway and as lymphoid tumor suppressors (e.g., *TNF*, *NFKBIE*, *TNFAIP3*, *LTA*, *TNFRSF14*) (Boice et al., 2016; Compagno et al., 2009; Mansouri et al., 2016; Tian et al., 2005; Zhou et al., 2003). Further, we ranked the final 64 genes by the genetic alteration frequencies in human DLBCLs (TCGA, <http://cancergenome.nih.gov/>) and base mean expression in our RNA-Seq analysis to identify relevant targets in DLBCL biology (Fig. 4.3E and Table 4.1). We identified 11 potential candidates that were additionally validated in a secondary screen to evaluate dependency on a functional ROQ domain. We confirmed that all 11 transcripts were down-regulated by expression of non-degradable Roquin2 (Y691F), with 7 transcripts rescued upon expression of the double mutant Roquin2 (Y691FAROQ) (Fig. 4.3F), suggesting their dependency on Roquin2 mRNA binding/decay activity. We concluded that these 7 transcripts were likely direct mRNA targets of Roquin2.

Amongst the putative mRNA targets we identified, we decided to focus on tumor necrosis factor- α -inducible gene 3 (*TNFAIP3*) with the consideration that human ABC-DLBCLs frequently harbor inactivating mutations or deletions in the *TNFAIP3* gene

(Compagno et al., 2009; Davis et al., 2010; Kato et al., 2009; Lenz et al., 2008a). Kinetic analysis of mRNA expression in response to BCR stimulation revealed a time-dependent up-regulation of *TNFAIP3* (Fig. 4.3G), consistent with its function as a negative feedback regulator of the NF- κ B program (Chu et al., 2011). This response was mitigated in cells expressing the non-degradable Roquin2 (Y691F) mutant, suggesting that degradation of Roquin2 contributes to a build up *TNFAIP3* mRNA levels upon BCR signaling. Notably, *TNFAIP3* mRNA levels were partially rescued in cells expressing Roquin2 double mutant (Y691F Δ ROQ), indicating that down-regulation of Roquin2 specific targets are dependent on the ability of Roquin2 to bind RNA. These data are consistent with previous findings that *TNFAIP3* mRNA directly interacts with Roquin proteins (Murakawa et al., 2015). Moreover, similar results were obtained with the NF- κ B target genes (*NFKBIE* and *LTA*) and the tumor suppressor gene *TNFRSF14* (Fig. 4.3G).

Lastly, we investigated whether the KLHL6-Roquin2 axis can directly control *TNFAIP3* mRNA levels and its stability. The mRNA half-life of *TNFAIP3* was shortened upon knockdown of KLHL6 and was partially rescued by concomitant knockdown of Roquin2 (Fig. 4.3H). When we re-expressed of KLHL6 (WT) in VAL cells carrying, endogenous BTB-domain mutations of KLHL6, the mRNA half-life of *TNFAIP3* (Fig. 4.3I) was greatly extended. Our findings suggest that *TNFAIP3* is a target of Roquin2 and reveal that loss of KLHL6 promotes down-regulation of *TNFAIP3* mRNA in ABC-DLBCLs.

KLHL6-Roquin2 axis controls NF-κB activation via TNFAIP3

TNFAIP3 is a ubiquitin-editing enzyme that inhibits the NF-κB signaling pathway via catalytic and non-catalytic inhibition of the IKK complex (Srinivasula and Ashwell, 2011). Since we observed that KLHL6 loss promotes *TNFAIP3* mRNA down-regulation, we expected that loss of KLHL6 might result into a higher NF-κB activation in ABC-DLBCLs. First, we investigated whether the TNFAIP3 protein levels are regulated in a similar way as the *TNFAIP3* transcriptional levels. BCR stimulation induced degradation of Roquin2 (WT) with the corresponding up-regulation of TNFAIP3 protein levels (Fig. 4.4A). More importantly, TNFAIP3 up-regulation upon BCR stimulation was abolished in cells stably expressing the non-degradable Roquin2 (Y691F) mutant, reflecting its transcriptional changes.

Since KLHL6 levels are also dependent on BCR activation and the KLHL6-Roquin2 axis regulates the NF-κB pathway through *TNFAIP3* decay, we hypothesized that *KLHL6* itself is regulated by NF-κB. To explore this hypothesis, we analyzed previously published CHIP-seq datasets for NF-κB factors (Zhao et al., 2014) and found that p50, p52, RelA, RelB and cRel were indeed enriched at the *KLHL6* gene locus. This suggests that KLHL6 is a bona fide NF-κB target gene (Fig. 4.4B). Correspondingly, IKK or a BTK inhibitor (ibrutinib) treatment (Davis et al., 2010) induced a down-regulation of KLHL6 both at mRNA and protein levels (Fig. 4.4C). Interestingly, we found that *KLHL6*^{-/-} cells are less sensitive to ibrutinib treatment (Fig. 4.4D). These data support a model in which BCR signaling induces KLHL6 up-regulation, Roquin2

degradation and *TNFAIP3* mRNA stabilization. In agreement with this model, TNFAIP3 protein levels were down-regulated in *KLHL6*^{-/-} cells as compared to *KLHL6*^{+/+} cells, both at steady state and in response to BCR stimulation (Fig. 4.4E), phenocopying the effect of the non-degradable Roquin2 mutant on TNFAIP3 protein. Knockdown of Roquin2 in U2932 *KLHL6*^{-/-} cells increased TNFAIP3 levels similar to those of *KLHL6*^{+/+} cells (Fig. 4.4F), suggesting a direct regulation of TNFAIP3 protein levels by Roquin2. Likewise, depletion of Roquin2 increased TNFAIP3 protein levels in HBL1 cells along with more robust up-regulation upon BCR stimulation (Fig. 4.4G). Correspondingly, re-introduction of KLHL6 (WT) in *KLHL6*^{-/-} cells increased TNFAIP3 levels (Fig. 4.4H).

Further, we investigated whether KLHL6-dependent down-regulation of TNFAIP3 would result in increased IKK activation utilizing IκBα phosphorylation as readout. Although IκBα was rapidly phosphorylated in both *KLHL6*^{+/+} and *KLHL6*^{-/-} cells following BCR activation, the amplitude of phosphorylation was higher in *KLHL6*^{-/-} cells, suggesting an increased activity of IKK (Fig. 4.4I). Importantly, the increase in phosphorylation was mitigated after re-introduction of KLHL6 (WT) (Fig. 4.4J). More importantly, the increase in phosphorylation correlated with more nuclear translocation of the NF-κB transcriptional factors in *KLHL6*^{-/-} cells (Fig. 4.4K). The increase in nuclear translocation was partially mitigated by the concomitant knockdown of Roquin2 (Fig. 4.4L). Correspondingly, we also observed that loss of KLHL6 increased DNA-binding of RelA to its target promoter, *NFKB1A*, and this effect was reversed upon concomitant knockdown of Roquin2 (Fig. 4.4M).

KLHL6 BTB-domain mutations and TNFAIP3 mutations are mutually exclusive in DLBCL patients

If KLHL6-Roquin2 axis acts through TNFAIP3 as a main downstream effector, it is likely that loss of function mutation of KLHL6 would be mutually exclusive with TNFAIP3 inactivating mutation or deletion. Correspondingly, when we performed the mutual exclusivity analysis on BTB-associated *KLHL6* mutations with *TNFAIP3* alterations in DLBCL patients, we observed no overlap with deleterious *KLHL6* BTB-mutations and *TNFAIP3* biallelic deletion or mutation (Fig. 4.5A and 4.5B). Using a weighted test (Leiserson et al., 2016), we found there was a trend toward significance for *KLHL6* and *TNFAIP3* mutual exclusivity with the *p*-value of 0.085 (Table 4.3). Notably, there were cases where deleterious BTB-domain mutations of *KLHL6* did co-occur with monoallelic deletion of *TNFAIP3*. This suggests that these mutations might cooperate to increase NF- κ B activation in the cases where only one *TNFAIP3* allele is lost. This is in line with the fact that patients with *KLHL6* mutations tended to have a higher NF- κ B activity, although this signature was not only restricted to *KLHL6* mutated cases (Fig. 4.5C).

Next, we investigated whether the tumor suppressing effects of *KLHL6* would be decreased in *TNFAIP3*-null ABC-DLBCLs (RCK8 and HLY1 cells). Loss of *KLHL6* in RCK8 cells (Compagno et al., 2009) did not show any noticeable effects on cellular proliferation (Fig. 4.5D) and apoptosis (Fig. 4.5E). Correspondingly, knockdown of Roquin2 in HLY1 cells (*TNFAIP3*-null (Fontan et al., 2012)) resulted into a greater cellular apoptosis compared to HBL1 cells (*TNFAIP3*-WT) (Fig. 4.5F). All together, this

indicates the functional relevance of Roquin2 in cells harboring a wild-type *TNFAIP3* gene.

Discussion

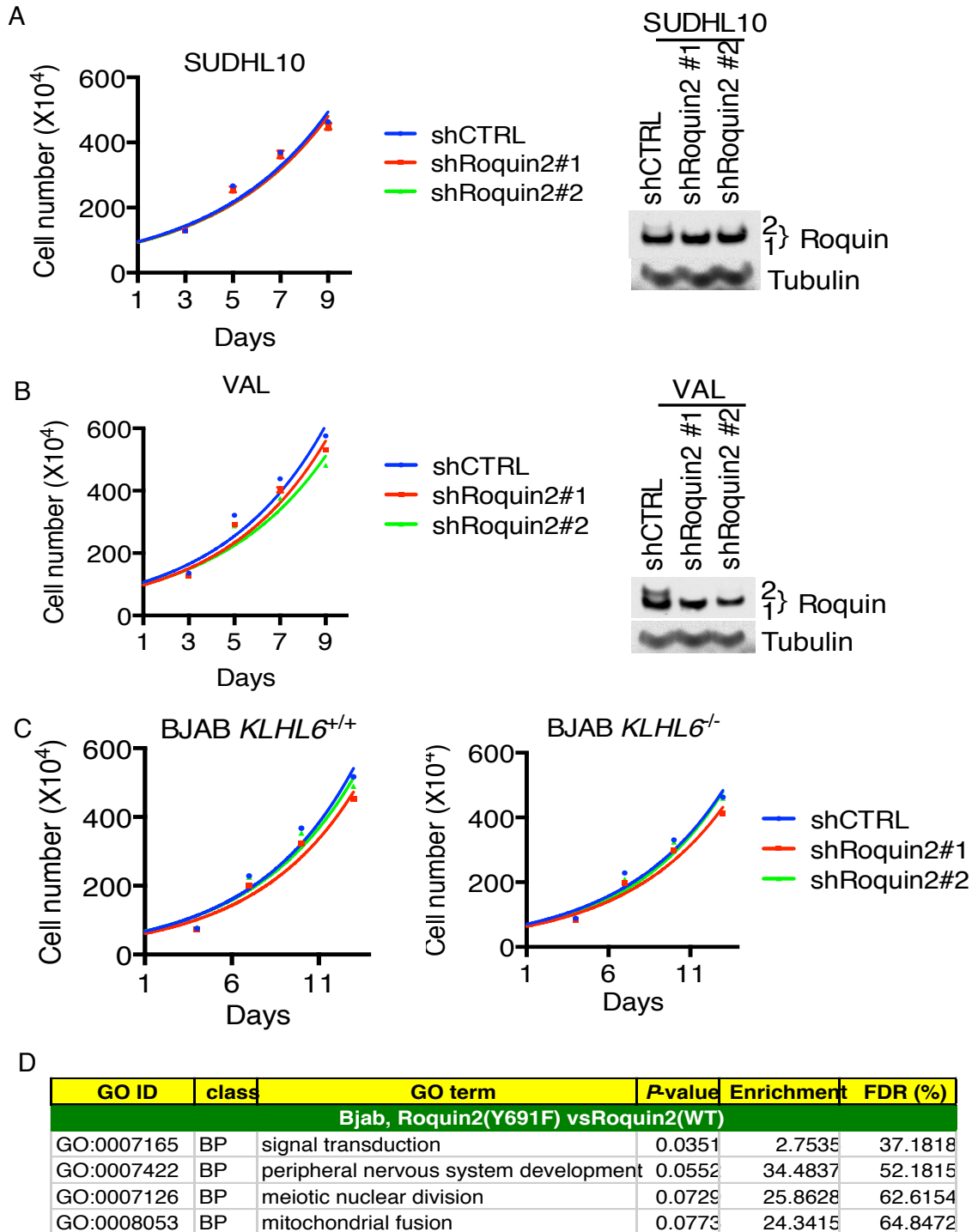
Although KLHL6 mutations occur at a similar frequency in GCB-DLBCL, we have shown that the KLHL6-Roquin2 axis does not play a significant role in cell proliferation and survival in the GCB-DLBCL subtype. In contrast, ablation of *KLHL6* in ABC-DLBCL cell lines promotes cell growth both *in vitro* and *in vivo*, supporting a tumor suppressor role of KLHL6. These findings are indeed consistent with low *KLHL6* expression levels correlating with poorer survival in ABC-DLBCL patients (Kunder et al., 2017; Leo Meriranta, 2016). Furthermore, expression of a non-degradable Roquin2 (Y691F) mutant phenocopies loss of KLHL6 in ABC-DLBCLs and concomitant ablation of Roquin2 in *KLHL6*^{-/-} cells results in an inhibition of cell proliferation. This pro-proliferative effect depends on the ability of Roquin2 to bind RNA (Glasmacher et al., 2010; Leppek et al., 2013; Murakawa et al., 2015; Schlundt et al., 2014; Vogel et al., 2013). Although Roquin1 and Roquin2 are reported to be functionally redundant in the T-cells (Vogel et al., 2013), no studies so far have examined the functional redundancy of Roquin proteins in mature B-cell cancers. The fact that KLHL6 targets only Roquin2 suggests that, in the context of B-cell cancers, Roquin2 might play a non-redundant role

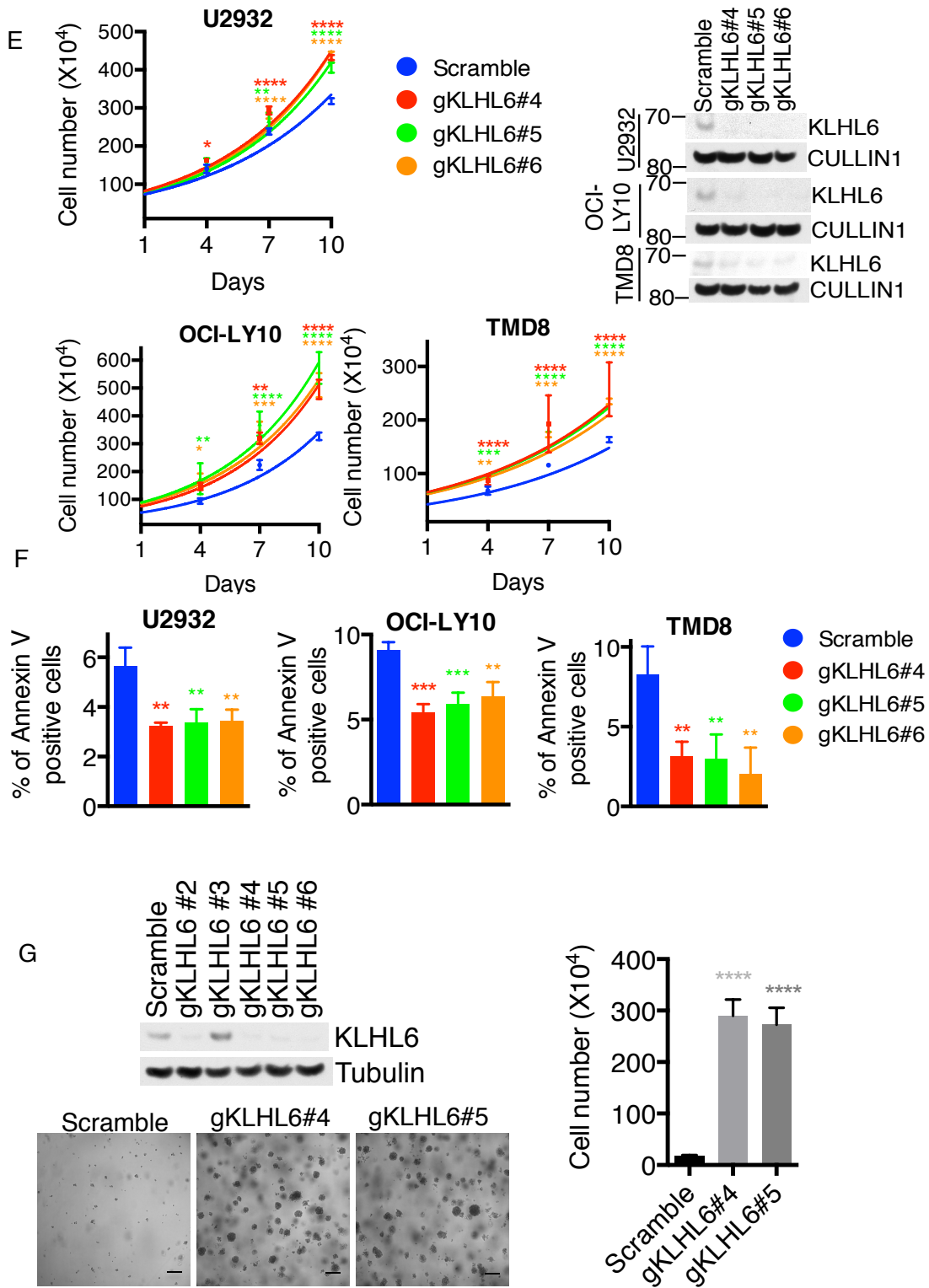
from Roquin1. Consistent with this hypothesis, the expression of Roquin2 is higher in germinal center B-cells, which is the origin of DLBCL (data not shown).

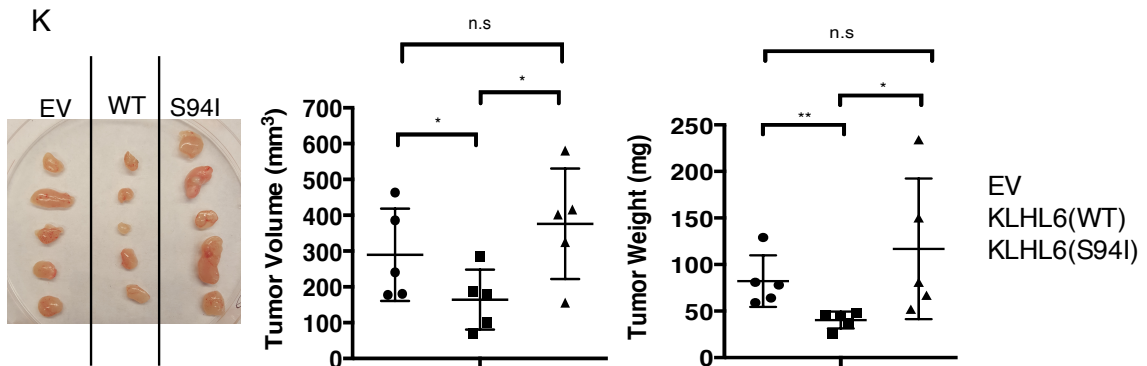
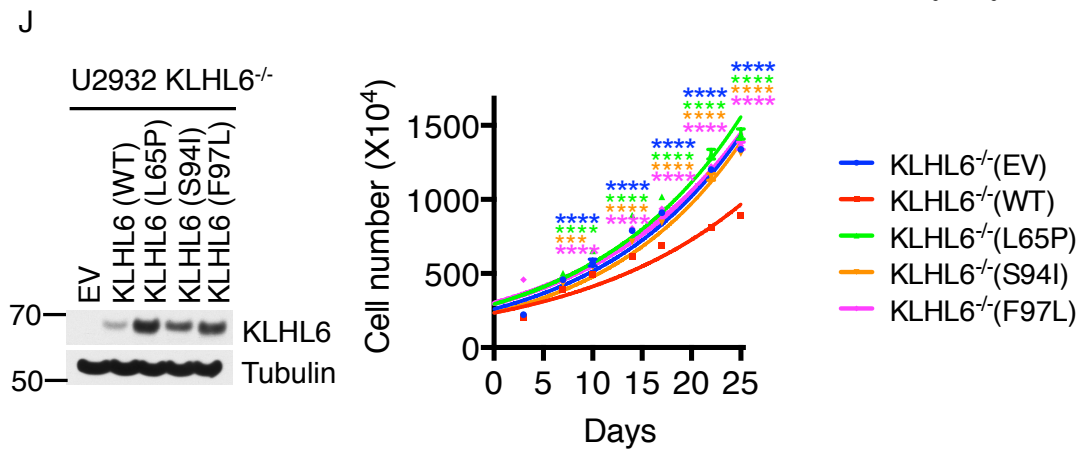
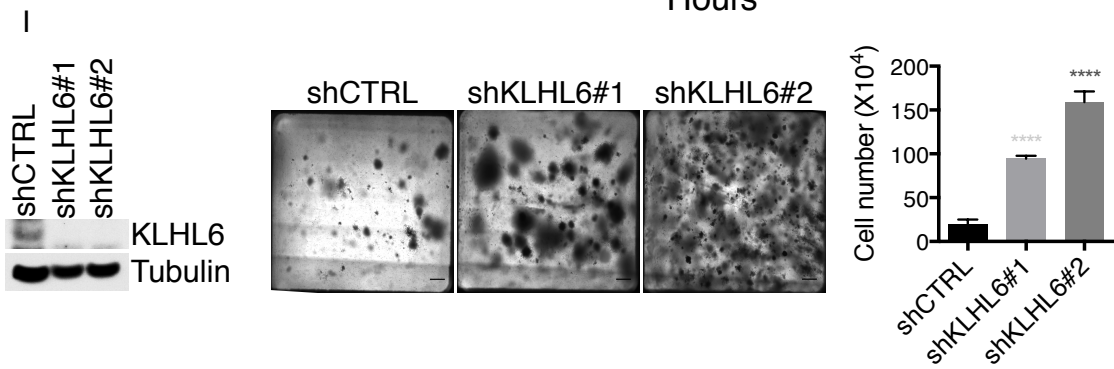
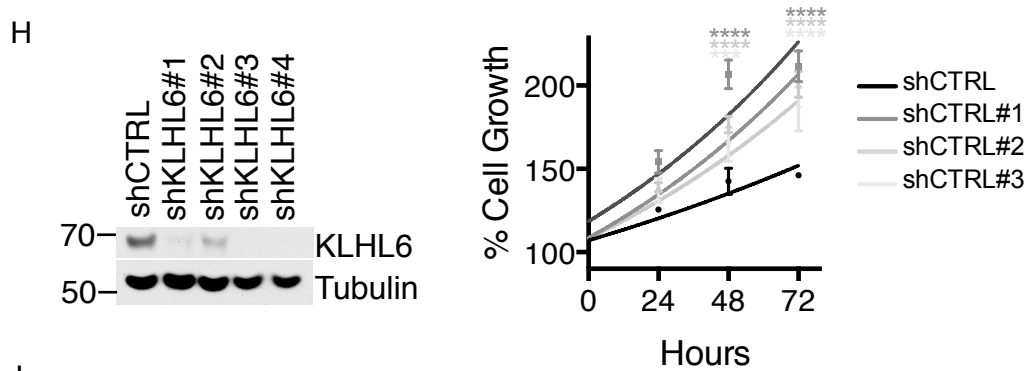
Genetic screens based on loss of function via CRISPR technology have identified negative regulators of NF- κ B (such as TNFAIP3, CD83 and CBLB) as tumor suppressors in ABC-DLBCL cells (Reddy et al., 2017). This suggests that the degrees of NF- κ B activation in DLBCL cells can vary as a consequence of changes in the negative regulators of NF- κ B. Furthermore, ABC-DLBCL cell lines can respond to BCR-stimulation and further activate the NF- κ B pathway (Yang et al., 2016). We have used U2932 cells, which harbors *KLHL6* wild-type and a hemi-deletion of *TNFAIP3* (Ferch et al., 2009) along with a basal level of NF- κ B activation (Ferch et al., 2009). Although featured as a single wild-type allele, U2932 cells express detectable levels of *TNFAIP3* both at mRNA and protein levels. This emphasizes that *TNFAIP3* is a relevant target of Roquin-mediated mRNA decay (Murakawa et al., 2015) in ABC-DLBCLs. BCR-signaling triggers up-regulation of *KLHL6* transcripts, leading to down-regulation of Roquin2 protein and de-repression of *TNFAIP3* mRNA. We expect that *KLHL6* suppresses *TNFAIP3* mRNA decay via Roquin2 degradation to establish a negative feedback loop and fine-tune the NF- κ B signaling pathways (Fig 4.5G). Therefore, it is conceivable that loss of *KLHL6* promotes BCR-signaling dependent NF- κ B activation by down-regulation of *TNFAIP3* mRNA and protein levels, disengaging this negative feedback loop in ABC-DLBCLs. Correspondingly, we found that DLBCL patients with BTB-domain mutations of *KLHL6* are likely to have high NF- κ B signatures. Therefore, *KLHL6* mutation spectrum could serve as a resistance marker to NF- κ B pathway

inhibitors such as ibrutinib (Davis et al., 2010), MLN4924 (Milhollen et al., 2010) or bortezomib (Yang and Staudt, 2015). Interestingly, we have found that loss of *KLHL6* predisposes ABC-DLBCL cells to ibrutinib desensitization. A complete characterization of *KLHL6* loss in the ibrutinib mechanism remains to be further elucidated.

TNFAIP3 genetic alterations including inactivation mutations and deletions are frequently observed in ABC-DLBCLs (Compagno et al., 2009; Davis et al., 2010; Kato et al., 2009; Lenz et al., 2008a). Several studies have shown that *TNFAIP3* is a tumor suppressor by re-introduction of functional *TNFAIP3* (WT) in *TNFAIP3*-null DLBCLs as the reconstitution causes cellular apoptosis and growth arrest (Honma et al., 2009; Schmitz et al., 2009). Interestingly, *KLHL6* BTB-mutations and *TNFAIP3* biallelic deletion or mutations do not co-occur in DLBCL patients, suggesting that these two genes might have similar downstream NF- κ B effectors. The fact that there was a partial overlap between *KLHL6* BTB-mutations and *TNFAIP3* monoallelic deletion further supports a notion of possible synergy of these mutations towards increasing NF- κ B activity. On the other hand, neither Roquin2 amplification nor sequence mutation of *TNFAIP3* mRNA at the 3' UTR of Roquin2 binding site has been observed in DLBCLs. This suggests that *KLHL6* could play a tumor suppressor role via other mechanisms beyond de-regulation of Roquin2 proteolysis and *TNFAIP3* mRNA decay. Furthermore, additional genetic lesions that could cooperate with the loss of *KLHL6* in promoting tumorigenesis in B-cell cancers remain open questions.







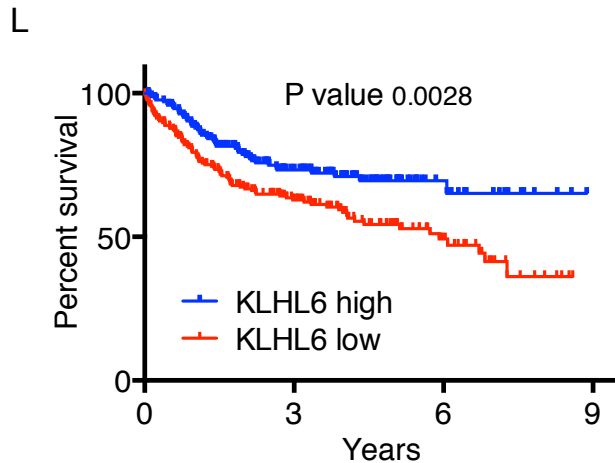


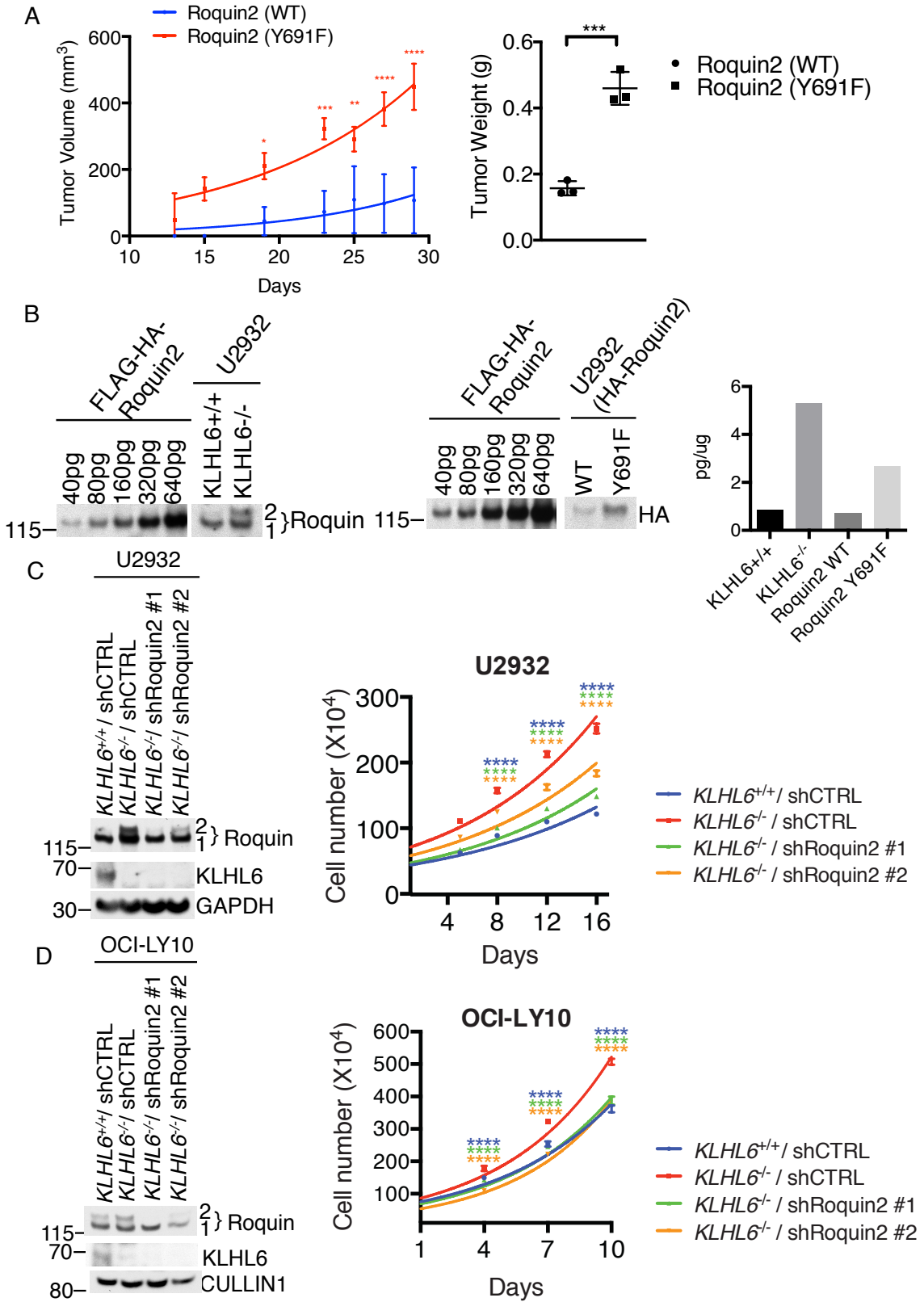
Fig 4.1 KLHL6 is a tumor suppressor in ABC-DLBCL subtype

(A) Loss of Roquin2 had no significant effects on cell proliferation in SUDHL10 cells. Left panel shows cell number counts of SUDHL10 expressing shRNA control or shRNAs targeting Roquin2 (#1 and #2) (mean± s.d., n=3 independent experiments). Whole cell lysates were analyzed by immunoblotting for the indicated proteins (Right panel). (B) Loss of Roquin2 had no significant effects on cell proliferation in VAL cells. Same as in (a) except that VAL cells were used. (C) Loss of Roquin2 had no significant effects on cell proliferation in BJAB cells. Same as in (a) except that BJAB *KLHL6*^{+/+} and *KLHL6*^{-/-} were used. (D) Gene ontology (GO) analysis of genes regulated by the non-degradable Roquin2 (Y691F) mutant in BJAB cells. (E) Ablation of *KLHL6* in all three ABC-DLBCL cell lines resulted in an increase in cellular proliferation. Left panel shows cell counts of U2932-, OCI-LY10- and TMD8-Cas9 cells expressing the indicated gRNAs and carrying a puromycin cassette (mean±s.d., n=3 independent experiments, two-way ANOVA, *P value≤0.05; **P value≤0.01; *** P value≤0.001; ****P value≤0.0001). Cells were grown in media containing 1μg/ml (U2932 and OCI-LY10) or 4μg/ml

(TMD8) of F(ab')₂-IgM. Whole cell lysates were analyzed by immunoblotting for the indicated proteins (Right panel). (F) Ablation of *KLHL6* in all three ABC-DLBCL cell lines resulted in a decrease in cellular apoptosis. U2932-, OCI-LY10-, and TMD8-Cas9 cells expressing the indicated gRNAs and carrying a GFP marker were grown as in (b) and analyzed for cell apoptosis rates. Apoptosis was quantified on GFP⁺ and Annexin V⁺ cells (mean±s.d., n=3 independent experiments, one-way ANOVA, **P value≤0.01; ***P value≤0.001). (G) Ablation of *KLHL6* in U2932 cells resulted in an increase in cell numbers and large colonies in 3D cultures. U2932-Cas9 cells were infected with lentiviruses encoding scrambled gRNA or gRNAs against *KLHL6* exon 1 carrying a puromycin cassette. Whole cell lysates were analyzed by immunoblotting for the indicated proteins (left top panel). Left bottom panel shows representative image of U2932 cell colonies expressing indicated gRNAs and plated into a matrigel. After 14 days, the matrigel was dissolved and recovered. Cells were counted and plotted as shown on the right panel (mean±s.d., n=4 independent experiments, one-way ANOVA, ****P value≤0.0001). Scale bar 150µm. (H) Ablation of *KLHL6* in U2932 cells resulted in an increase in cellular proliferation. U2932 cells were infected with lentiviruses encoding the indicated shRNAs carrying a puromycin cassette. Whole cell lysates were analyzed by immunoblotting for the indicated proteins (left panel). Right panel shows MTS assay for U2932 cells infected with lentiviruses encoding the indicated shRNAs and grown in media containing 1µg/ml of F(ab')₂-IgM. Values were normalized to the shCTRL cells at time 0 hour and set as 100% (mean±s.d., n=3 independent experiments, two-way ANOVA; *** P value≤0.001, ****P value≤0.0001). (I) Ablation of *KLHL6* in OCI-

LY10 cells resulted in an increase in cellular growth and survival. OCI-LY10 cells were infected with lentiviruses encoding indicated shRNAs carrying a puromycin cassette. Whole cell lysates were analyzed by immunoblotting for the indicated proteins (left panel). Middle panel shows representative image of OCI-LY10 cell colonies infected with indicated shRNAs and plated into a matrigel. After 14 days, the matrigel was dissolved and recovered. Cells were counted and plotted as shown on the right panel (mean±s.d., n=4 independent experiments, one-way ANOVA, ****P value ≤0.0001). Scale bar 150µm. (J) Expression of BTB-mutants phenocopies loss of *KLHL6* in promoting ABC-DLBCL cell proliferation *in vitro*. U2932 *KLHL6*^{-/-} cells were infected with retroviruses encoding an empty vector (EV) or *KLHL6* WT or BTB-mutants (L65P, S94I and F97L). Whole cell lysates were analyzed by immunoblotting for the indicated proteins (left panel). Right panel shows cell growth as measured by counting the number of cells over time. Error bars represent s.d., n=3. Asterisks indicate: ****P value ≤0.001 calculated with ANOVA. (K) Expression of *KLHL6* BTB-mutants phenocopies loss of *KLHL6* in promoting ABC-DLBCL growth in xenograft models. U2932 *KLHL6*^{-/-} cells were infected with retroviruses encoding an empty vector (EV), *KLHL6* (WT) or *KLHL6* (S94I) prior to sub-cutaneous injection of NOD/SCID/IL2Rγ^{-/-} (NSG) mice. Left panel shows a picture of the tumors after the experimental endpoint. Middle panel shows tumor volume calculated by caliper measurements. Right panel shows tumor weight calculated by the weight of the excised tumors at the experimental endpoint. Error bars represent s.d., n=5. Asterisks indicate: *P value ≤0.05, **P value ≤0.01, and n.s. indicates non-significant P value. Statistical analysis was performed using the t-test. (L) Low level of

KLHL6 expression correlates with poor survival in ABC-DLBCL patients. Gene expression microarray data (diffuse large B-cell lymphoma tumors) were obtained from GSE10846, GSE34171 and GSE31312 (Lenz et al., 2008f; Monti et al., 2012; Visco et al., 2012). Kaplan–Meier analyses of ABC-DLBCL patients based on *KLHL6* expression is shown (n=367, cases were dichotomized into being above or below the median expression level of *KLHL6* expression within each dataset to avoid confounding batch effects). Statistical analysis was performed using the Log-rank (Mantel-Cox) test.



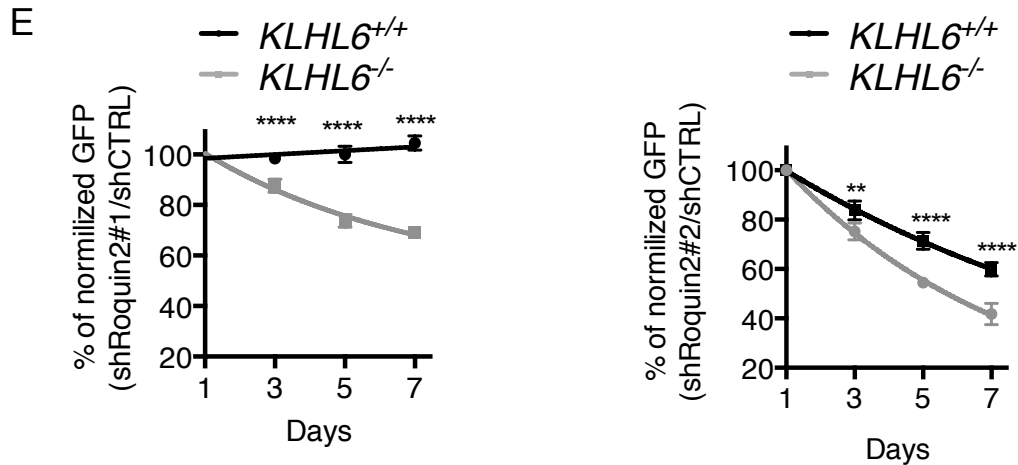
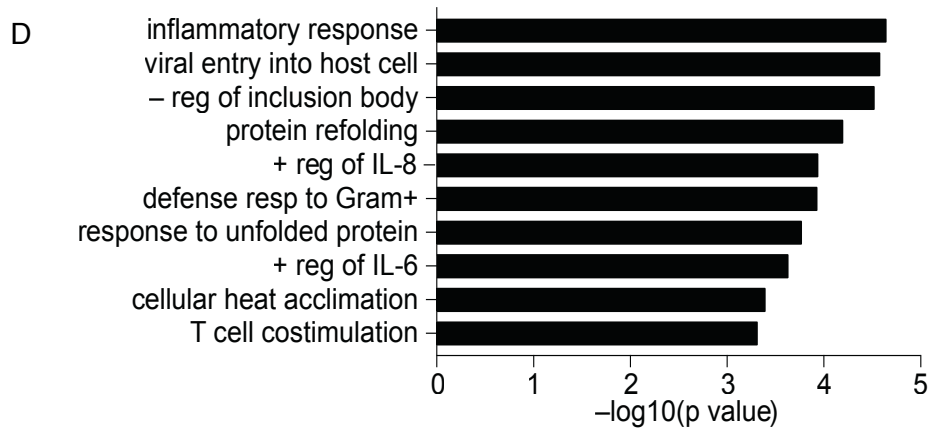
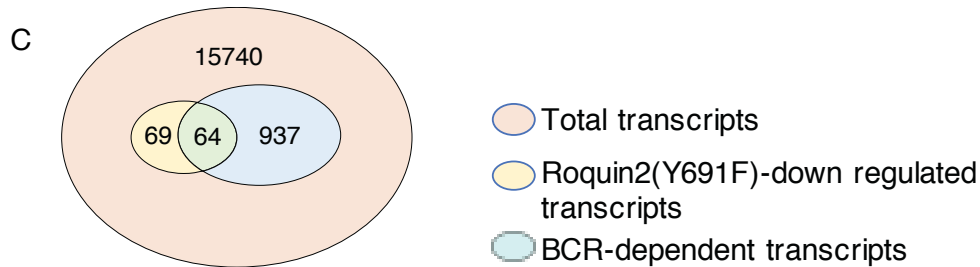
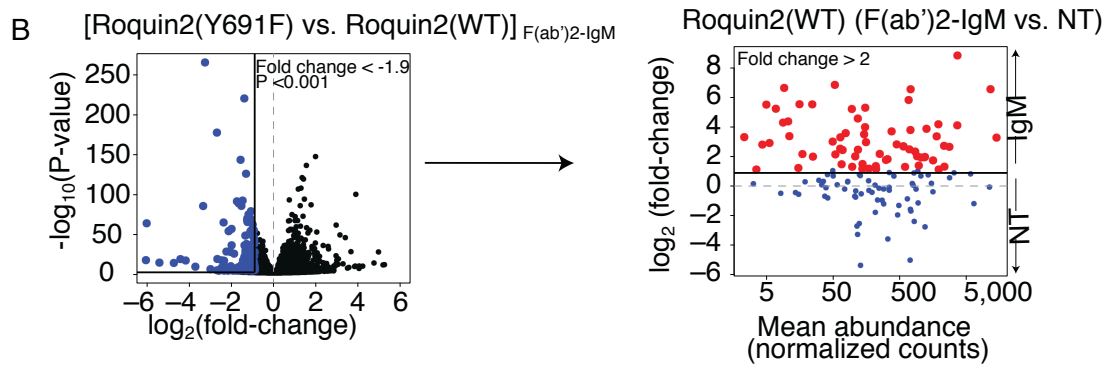
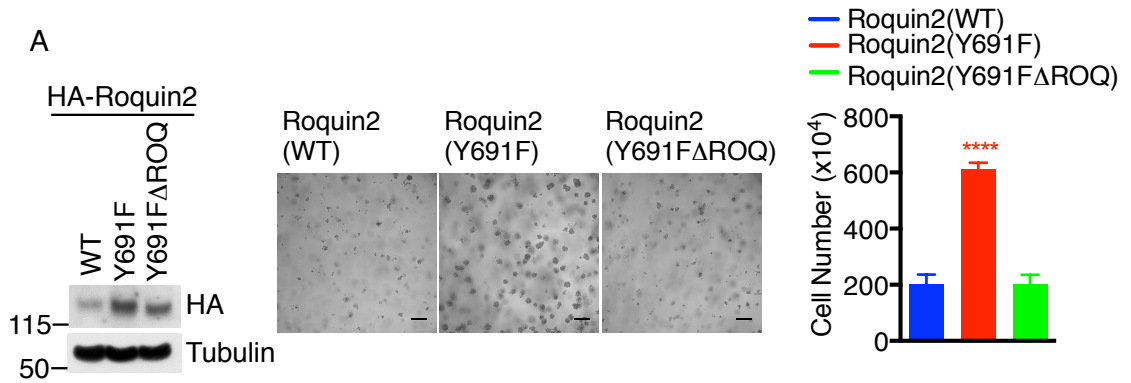


Fig 4.2 Roquin2 stabilization promotes ABC-DLBCL growth and survival

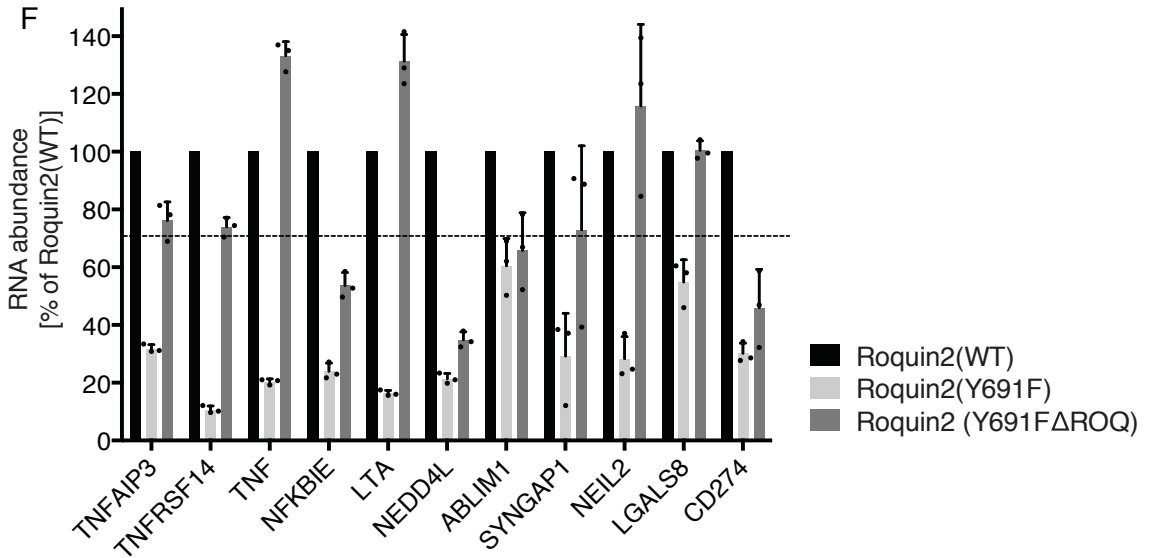
(A) Stabilization of Roquin2 promotes ABC-DLBCL growth in xenograft models. U2932 cells were infected with retroviruses encoding HA-Roquin2 (WT) or HA-Roquin2 (Y691F) and 1×10^7 cells were sub-cutaneously injected in NSG mice. On the left panel, tumor volume was calculated by caliper measurements. On the right panel, tumor weight was determined on the excised tumors at the experimental endpoint. Error bars represent s.d., $n=3$. Statistical analysis was performed using ANOVA and the t-test for tumor volume and tumor weight, respectively. Asterisks indicate: *P value ≤ 0.05 , **P value ≤ 0.01 , *** P value ≤ 0.001 , ****P value ≤ 0.001 . (B) Roquin2 (Y691F) protein levels are similar to endogenous Roquin2 protein levels in *KLHL6*^{-/-} cells. Indicated amounts of recombinant Roquin2 (set as the standard) along with whole cell lysates from U2932 *KLHL6*^{+/+} and *KLHL6*^{-/-} cells (clone-derived) (left panel) or U2932 stably expressing HA-Roquin2 (WT) and HA-Roquin2 (Y691F) cells (middle panel) were analyzed for immunoblotting. Right panel shows intensity of quantified Roquin2 bands compared to the standard. A representative blot from one experiment is shown. (C) Loss of *KLHL6*

promotes cell proliferation in a Roquin2-dependent manner in U2932 cells. Whole cell lysates were analyzed by immunoblotting for the indicated proteins (left panel). Right panel shows cell number counts of GFP-sorted U2932 *KLHL6*^{+/+} and *KLHL6*^{-/-} (clone-derived) cells infected with scramble shRNA (shCTRL) or shRNA targeting Roquin2 (ShRoquin2#1 or #2) carrying a GFP marker. GFP⁺ cells were grown in media containing 1µg/ml of F(ab')₂-IgM. (mean±s.d., n=3 independent experiments, two-way ANOVA, ****P value≤0.0001). A representative blot from two independent experiments is shown. (D) Same as (c) except that OCI-LY10 *KLHL6*^{+/+} and *KLHL6*^{-/-} cells were utilized. (E) Loss of Roquin2 increased toxicity of *KLHL6*^{-/-} cells. GFP⁺-live OCI-LY10 *KLHL6*^{+/+} and *KLHL6*^{-/-}(clone-derived) cells were infected with lentiviruses encoding the indicated shRNAs carrying a GFP marker and monitored over time by flow cytometry. Cells were grown in media containing 2µg/ml of F(ab')₂-IgM and normalized to the shCTRL cells set as 100% (mean±s.d., n=3 independent experiments, two-way ANOVA, **P value≤0.01; ****P value≤0.0001).

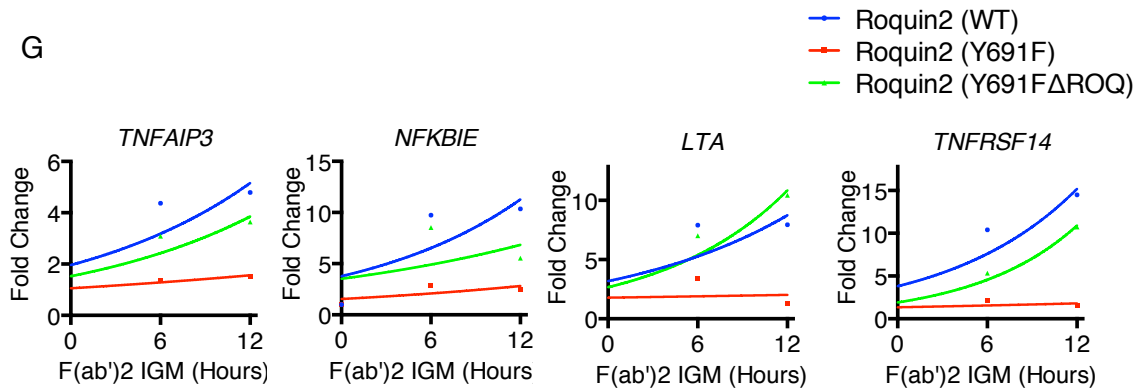


E

Gene	% Genetic Alteration	Base Mean	Rescue (>70%)
TNFAIP3	31%	1215.26	Yes
TNFRSF14	17%	733.84	Yes
TNF	15%	609.03	Yes
NFKBIE	13%	2832.97	No
LTA	10%	1609.40	Yes
NEDD4L	6%	14540.3	No
ABLIM1	6%	1958.09	No
SYNGAP1	6%	980.44	Yes
NEIL2	6%	253.09	Yes
LGALS8	6%	221.05	Yes
CD274	6%	152.22	No



G



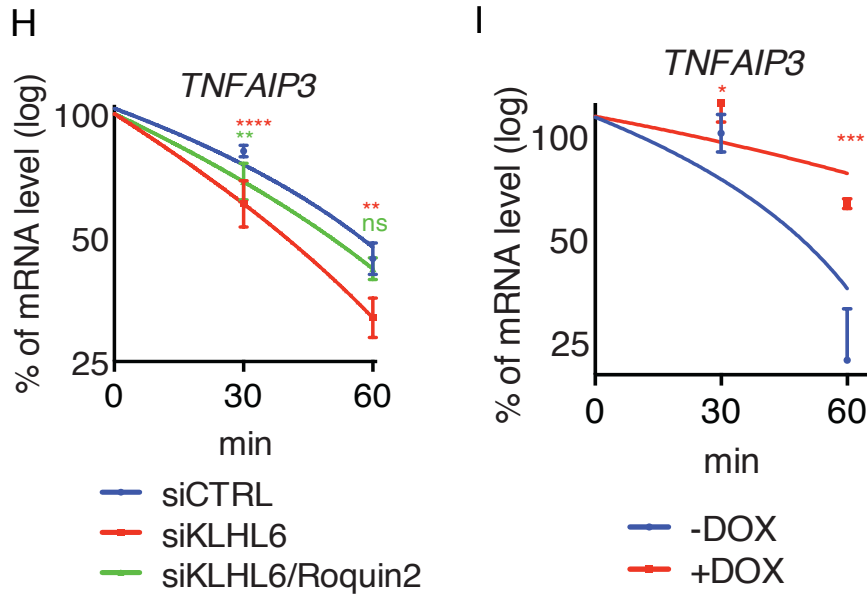
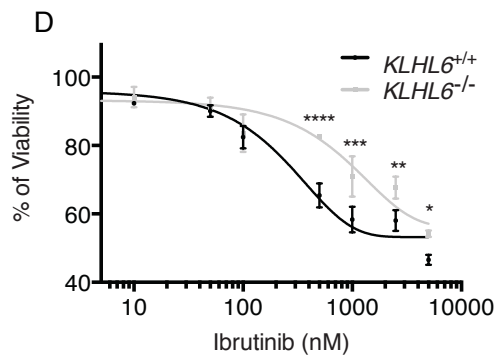
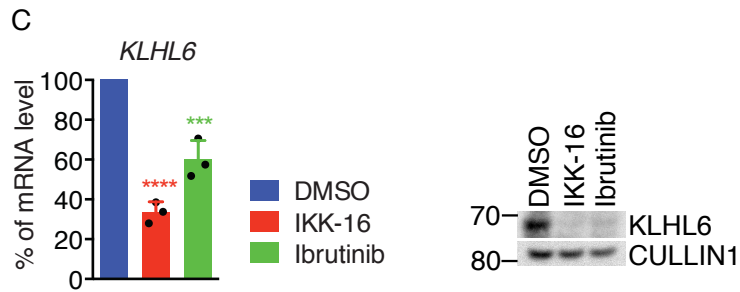
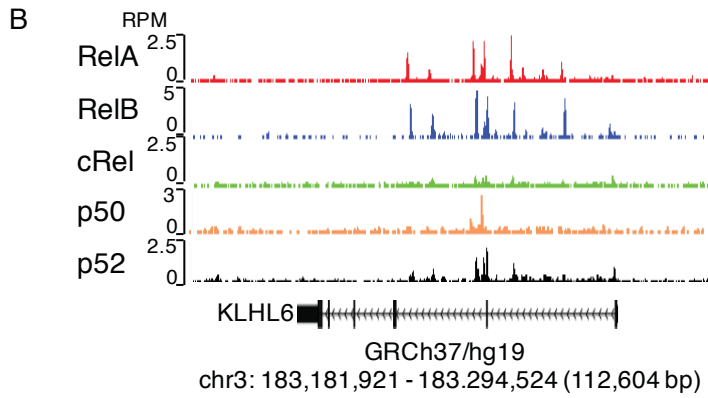
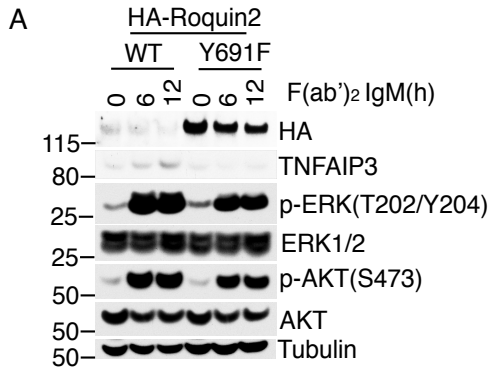


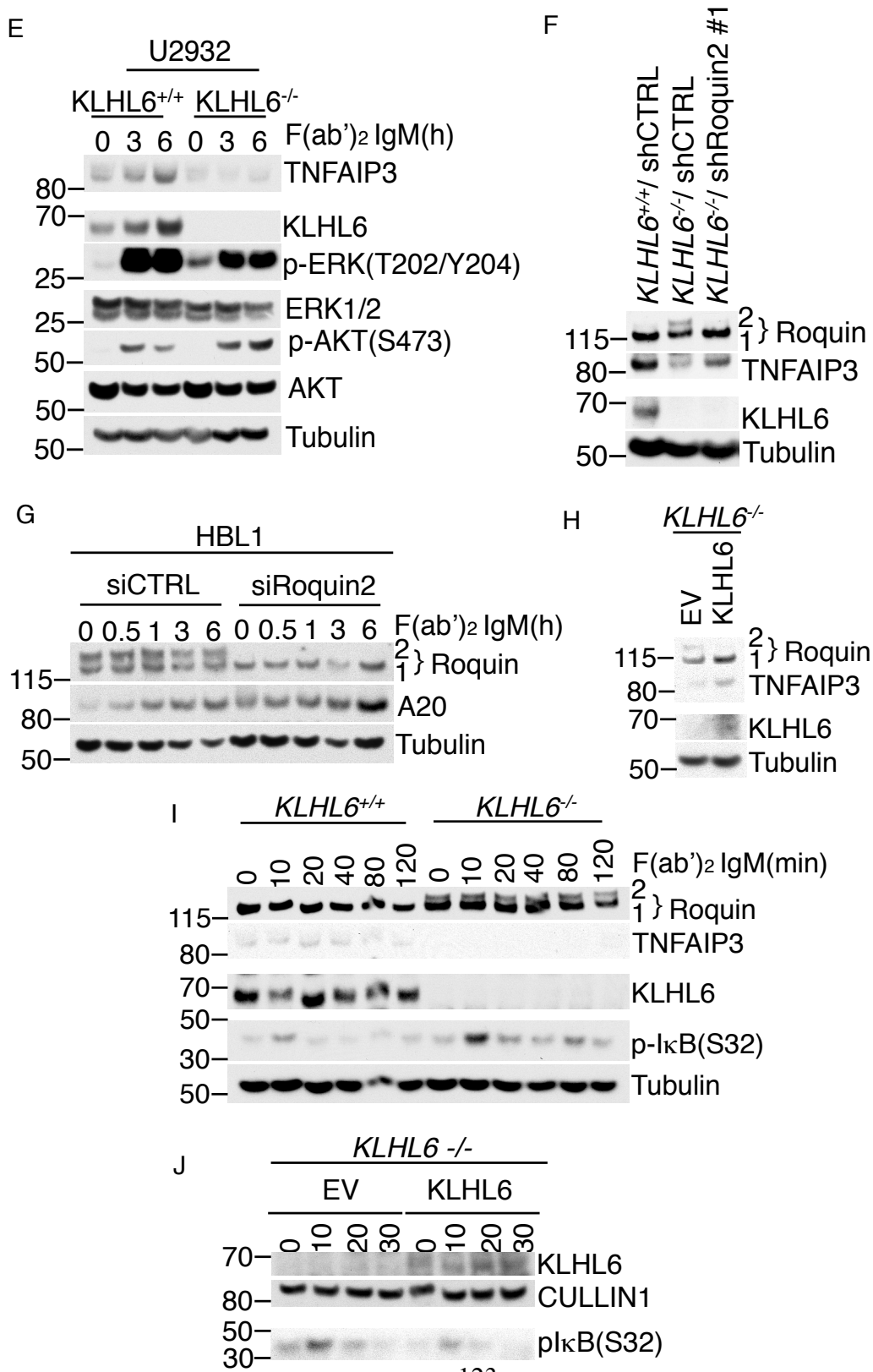
Figure 4.3 Stabilization of Roquin2 down-regulate BCR responsive genes

(A) Concomitant deletion of the ROQ domain abolished the proliferative effect of Roquin2 (Y691F). U2932 cells were infected with retroviruses encoding HA-Roquin2 (WT), HA-Roquin2 (Y691F) or HA-Roquin2 (Y691FΔROQ). Whole cell lysates were analyzed by immunoblotting for the indicated proteins (left panel). Middle panel shows a representative image of cell colonies. Cells were plated into a matrigel matrix and were allowed to grow for 14 days. After 14 days, the matrigel matrix was dissolved with dispase to recover the cells, which were counted and plotted on the right panel. Error bars represent s.d., $n=4$. Scale bar 150 μ m. (B) Identification of mRNA targets affected by stabilization of Roquin2 and BCR stimulation. The volcano plot (left panel) shows the mRNAs (blue) down-regulated in U2932 cells stably expressing Roquin2 (Y691F) as compared to Roquin2 (WT) after 12 hours of treatment with 10 μ g/ml of F(ab')₂-IgM ($\log_2(\text{fold-change}) < -0.9$; P value < 0.001; $n=3$). Down-regulated mRNAs were further

plotted in an MA (log ratio, mean average)-plot (right panel) to identify mRNAs (red) up-regulated upon treatment with F(ab')₂-IgM in cells expressing Roquin (WT) ($\log_2(\text{fold-change}) > 1$; $P \text{ value} < 0.001$). (C) 64 genes are BCR responsive transcripts controlled by Roquin2 degradation. A venn diagram shows the overlap between genes down-regulated by expression of non-degradable Roquin2 (Y691F) mutant and BCR responsive genes. (D) Gene ontology (GO) analysis was performed on genes regulated by the non-degradable Roquin2 (Y691F) mutant. Bar plot shows the $-\log_{10}$ of the P value of the top 10 enriched GO terms of genes regulated by Roquin2 (Y691F) as determined by the hypergeometric distribution. -reg., negative regulation; + reg., positive regulation. (E) The list of Roquin2-regulated genes ranked by the percentage of genetic alteration/mutation in human DLBCLs from the TCGA database and the base mean expression from the RNA-seq analysis. The cut-off was set at 6% for genetic mutation frequency. "Yes" indicates down-regulation of transcript is dependent on the ROQ domain of Roquin2 and rescued at least 70%; "No" indicates down-regulation of transcript is not dependent and not rescued. (F) Secondary q-PCR screening for mRNAs levels of U2932 cells stably expressing HA-Roquin2 (WT), HA-Roquin2 (Y691F) or HA-Roquin2 (Y691FΔROQ). The cells were treated with 10 μg/ml of F(ab')₂-IgM for 12 hours and the value for each PCR product present in HA-Roquin2 (WT) cells was set as 100%. Rescued transcripts are considered as the ones whose mRNA levels reach at least 70% of the Roquin2 (WT) control (dashed line in the graph=70% rescue) (mean±s.d., n=3 independent experiments). (G) *TNFAIP3* mRNA levels are regulated by Roquin2 degradation and mRNA decay activity. U2932 cells stably expressing encoding HA-

Roquin2 (WT), HA-Roquin2 (Y691F) or HA-Roquin2 (Y691F Δ ROQ) were treated with 10 μ g/ml of F(ab')₂-IgM for indicated times. Levels of the indicated mRNAs were analyzed by real time PCR. A representative experiment from two biological replicates is shown. Value for PCR product present at time 0 hour was arbitrarily set as 1 for each condition. (H) Ablation of *KLHL6* shortened the half-life of *TNFAIP3*. U2932 cells were electroporated with indicated siRNAs (left panel) and treated with actinomycinD for the indicated times for qPCR analysis of *TNFAIP3* mRNA. The value for PCR product present at time 0 hour was arbitrarily set as 100% (mean \pm s.d., n=3 independent experiments, two-way ANOVA, **P value \leq 0.01, ****P value \leq 0.0001, n.s, not significant). (I) Overexpression of *KLHL6* increases the half-life of *TNFAIP3*. Same analysis was performed in VAL cells expressing *KLHL6* under a DOX-inducible promoter. Cells were pre-treated with DOX for 12 hours and actinomycinD for the indicated times (mean \pm s.d., n=3 independent experiments, two-way ANOVA, *P value \leq 0.05; *** P value \leq 0.001).





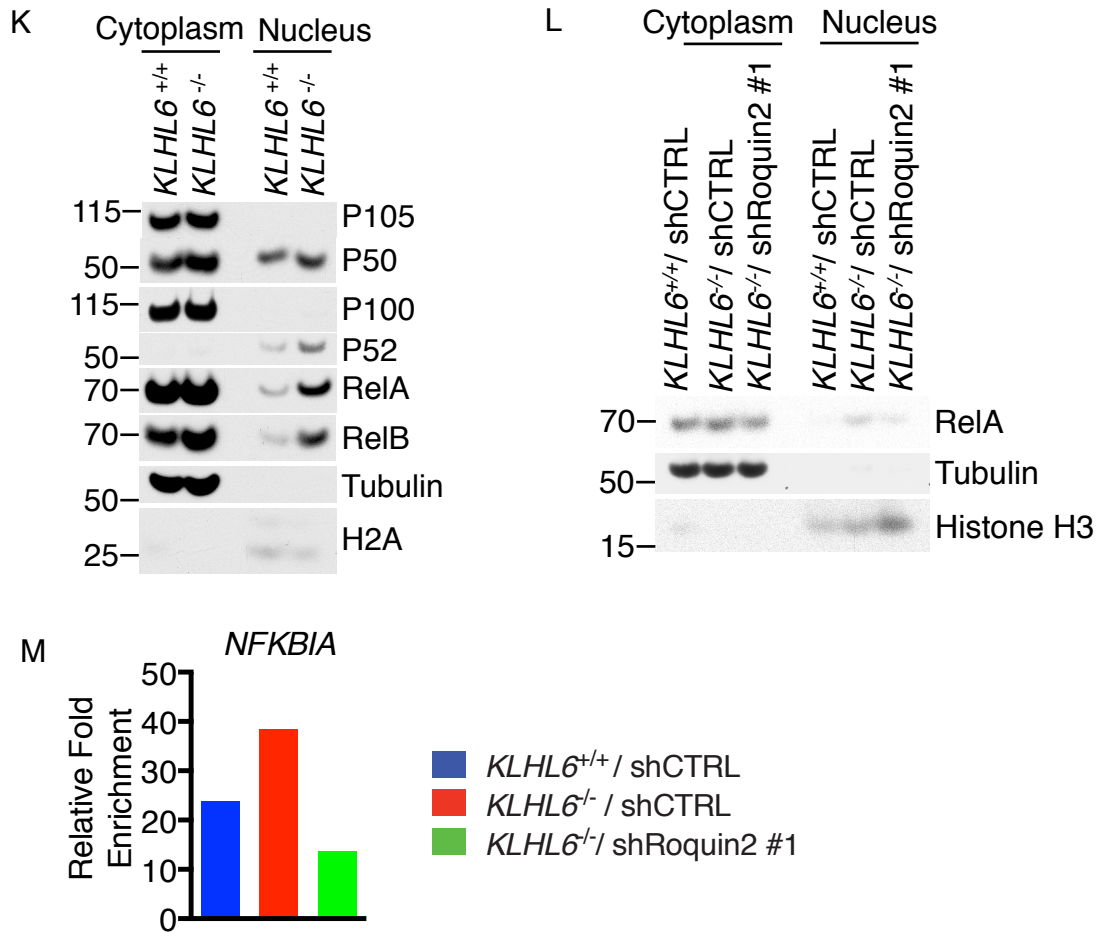
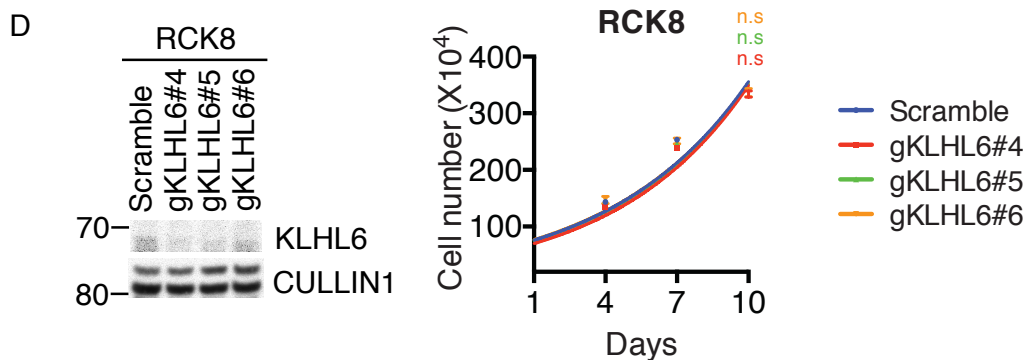
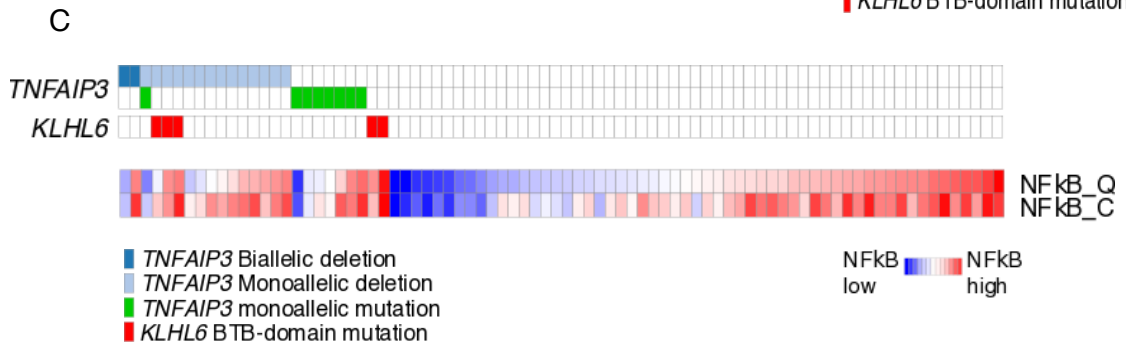
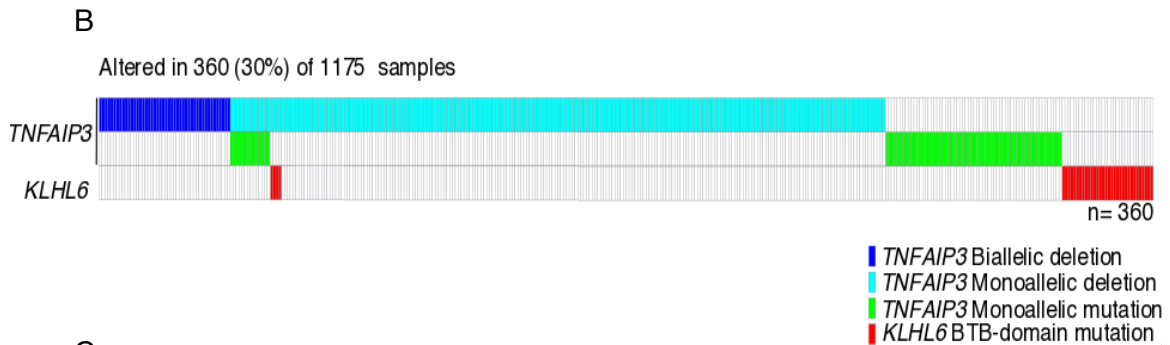
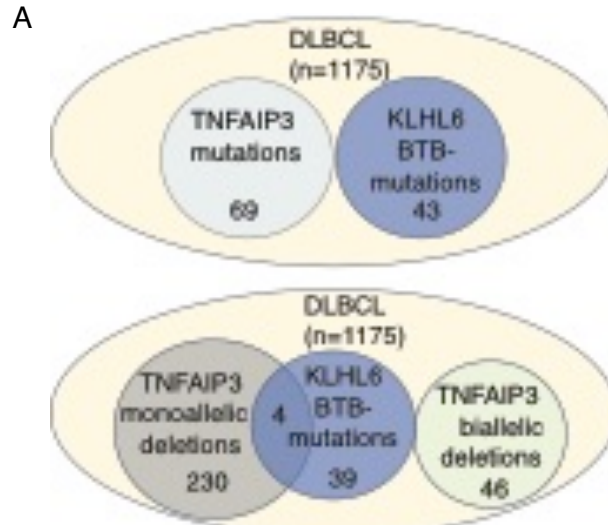


Figure 4.4 KLHL6-Roquin2 axis controls NF- κ B activation via TNFAIP3

(A) Roquin2 stabilization induces a decrease in TNFAIP3 protein levels. U2932 cells stably expressing HA-Roquin2 (WT) or HA-Roquin2 (Y691F) were treated with 10 μ g/ml of F(ab')₂-IgM for the indicated times. Whole cell lysates were analyzed by immunoblotting for the indicated proteins. (B) ChIP-seq peaks were analyzed and visualized by using University of California Santa Cruz (UCSD) Genome browser (GEO Series accession GSE55105). RPM, reads per million mapped. (C) KLHL6 is a bona fide NF- κ B target gene. Left panel shows analysis of level of *KLHL6* mRNA by qPCR in

U2932 cells treated with DMSO, 10 μ M of IKK inhibitor (IKK-16) or 5 μ M of BTK inhibitor (ibrutinib) for 6 hours. The value for PCR product present without treatment (DMSO) was set as 100% (mean \pm s.d., n=3 independent experiments, one-way ANOVA, *** P value \leq 0.001; ****P value \leq 0.0001). Whole cell lysates were analyzed by immunoblotting for the indicated proteins (Right panel). (D) *KLHL6*^{-/-} cells are less sensitive to ibrutinib. U2932 cells *KLHL6*^{+/+} and *KLHL6*^{-/-} treated with increasing amounts of ibrutinib for 48 hours, and cell proliferation was analyzed by MTS assay. Values were normalized to the non-treated cells and set as 100% (mean \pm s.d., n=3 independent experiments, two-way ANOVA; *P value \leq 0.05, **P value \leq 0.01, *** P value \leq 0.001, ****P value \leq 0.0001). (E) Loss of *KLHL6* induces a decrease in TNFAIP3 protein levels. U2932 cells *KLHL6*^{+/+} or *KLHL6*^{-/-} were treated with 10 μ g/ml of F(ab')₂-IgM for the indicated times. Whole cell lysates were analyzed by immunoblotting for the indicated proteins. (F) Knockdown of Roquin2 in U2932 *KLHL6*^{-/-} cells rescues TNFAIP3 levels. GFP-sorted U2932 *KLHL6*^{+/+}, *KLHL6*^{-/-} or *KLHL6*^{-/-} cells were infected with lentiviruses encoding the indicated shRNAs carrying a GFP marker and treated with 10 μ g/ml of F(ab')₂-IgM for 6 hours. The whole cell lysates were analyzed by immunoblotting for the indicated proteins. (G) Knockdown of Roquin2 increases TNFAIP3 levels in HBL1 cells. HBL1 cells were electroporated with indicated siRNAs and treated as in (E) for the indicated times. The whole cell lysates were analyzed by immunoblotting for the indicated proteins. (H) Re-expression of *KLHL6* (WT) in U2932 *KLHL6*^{-/-} cells rescues TNFAIP3 levels. GFP-sorted U2932 *KLHL6*^{-/-} (clone-derived) cells were infected with retroviruses encoding empty vector (EV) or *KLHL6* (WT)

carrying a GFP marker and treated with 10µg/ml of F(ab')₂-IgM for 6 hours. The whole cell lysates were analyzed by immunoblotting for the indicated proteins. (I) Loss of *KLHL6* enhances phosphorylation of IκBα. U2932 cells *KLHL6*^{+/+} or *KLHL6*^{-/-} were treated with 10µg/ml of F(ab')₂-IgM for the indicated times. Whole cell lysates were analyzed by immunoblotting for the indicated proteins. (J) Re-expression of *KLHL6* (WT) in U2932 *KLHL6*^{-/-} cells mitigates IκBα phosphorylation. Same as in (h) except that cells were treated with 10µg/ml F(ab')₂-IgM for the indicated times (min). (K) Loss of *KLHL6* promotes nuclear translocation of NF-κB transcription factors. U2932 cells *KLHL6*^{+/+} or *KLHL6*^{-/-} were fractionated into cytoplasmic and nuclear extracts. The indicated cell lysates were analyzed by immunoblotting for the indicated proteins. (L) Concomitant knockdown of Roquin2 in *KLHL6*^{-/-} cells mitigated nuclear translocation of NF-κB transcription factors. GFP-sorted U2932 *KLHL6*^{+/+}, *KLHL6*^{-/-} or *KLHL6*^{-/-} cells infected with lentiviruses encoding the indicated shRNAs carrying a GFP marker were fractionated into cytoplasmic and nuclear extracts and analyzed by immunoblotting for the indicated proteins. (M) Loss of *KLHL6* increases RelA DNA-binding at the *NFKB1A* promoter. U2932 *KLHL6*^{+/+}, *KLHL6*^{-/-} or *KLHL6*^{-/-} cells were infected with indicated shRNAs and analyzed for RelA binding degrees to its target *NFKB1A* promoter by chromatin immunoprecipitation followed by qPCR. Data are displayed as fold enrichment relative to IgG control. A representative graph from two independent experiments is shown.



127

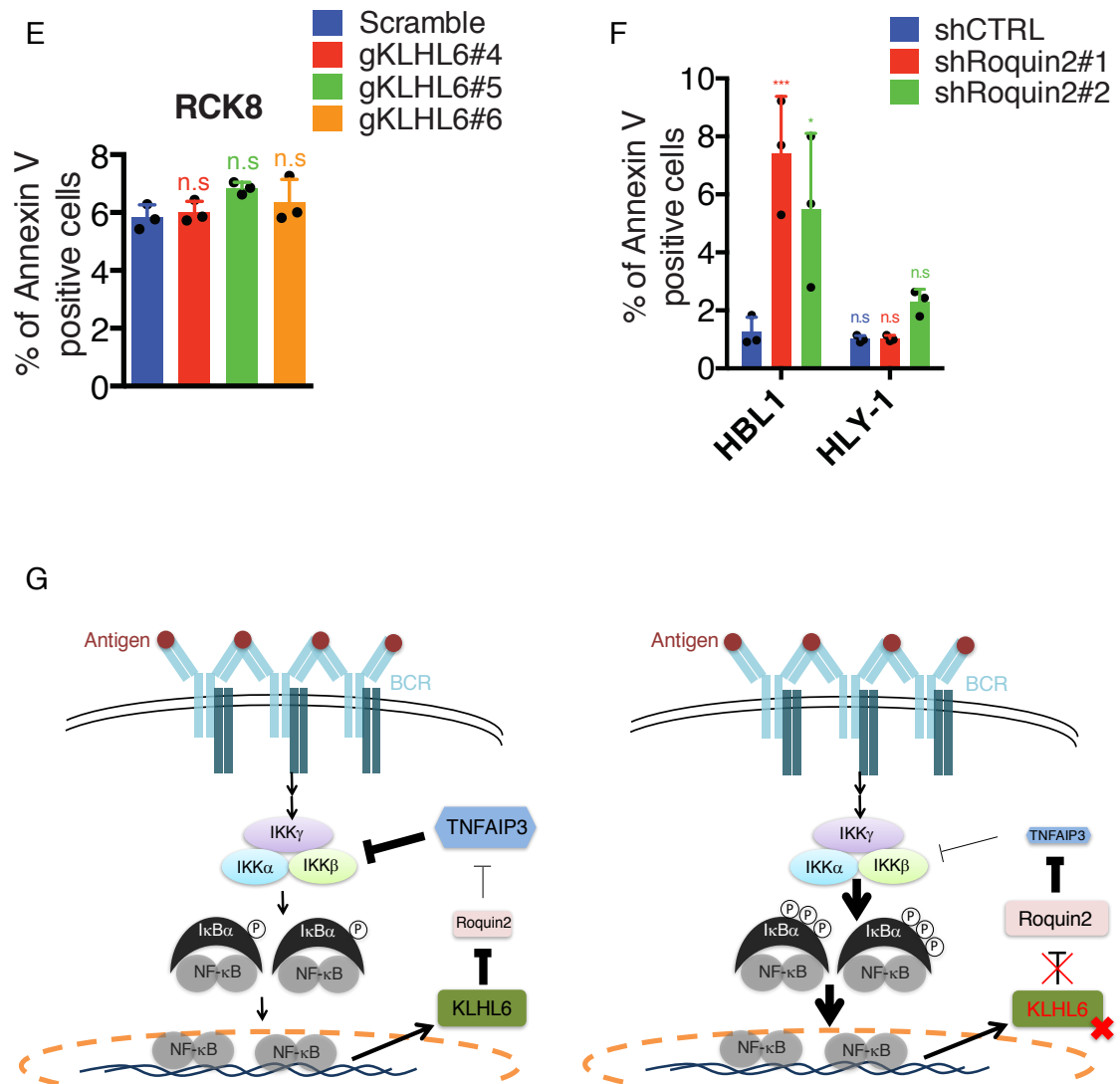


Figure 4.5 KLHL6 BTB-domain mutations and TNFAIP3 mutations are mutually exclusive in DLBCL patients

(A) BTB-associated mutations of *KLHL6* with *TNFAIP3* alterations do not overlap in DLBCLs. Top panel shows tumors sequenced at UNMC (Idoia et al., 2016) and DCI (Reddy et al., 2017) (n=1175) with deleterious mutations of *KLHL6* in the BTB-domain

and *TNFAIP3* mutations. Bottom panel shows the *TNFAIP3* subset with biallelic and monoallelic deletions. (B) Some overlaps occur between deleterious BTB-domain mutations of *KLHL6* and monoallelic deletion of *TNFAIP3*. A heat map shows the presence of biallelic deletion (dark blue), monoallelic deletion (light blue) and monoallelic mutation (green) of *TNFAIP3* in DLBCL tumors sequenced at UNMC (Idoia et al., 2016) and DCI (Reddy et al., 2017) (n=1175). Deleterious mutations of *KLHL6* BTB-domain are shown in these same cases. (C) The DLBCL patients with *KLHL6* mutations exhibit higher NF- κ B signatures. A heat map shows the tumor gene alterations matched with gene expression profiling data available at UNMC. Single sample gene set enrichment analysis (GSEA) was utilized to infer NF- κ B activity using expression of target gene sets from the molecular signatures database (NF κ B_Q and NF κ B_C) (Green et al., 2014; Lenz et al., 2008f). The enrichment score is displayed as a row-normalized heat map. (D) Tumor suppressor role of *KLHL6* is abolished in *TNFAIP3*-null ABC-DLBCLs. GFP-sorted RCK8 cells expressing Cas9, the indicated gRNAs and a GFP marker, were grown in media containing 1 μ g/ml of F(ab')₂-IgM and cell numbers were counted and graphed (right panel) (mean \pm s.d., n=3 independent experiments, two-way ANOVA, n.s, not significant). Whole cell lysates were analyzed by immunoblotting for the indicated proteins (Left panel). (E) Tumor suppressor role of *KLHL6* is reduced in *TNFAIP3*-null ABC-DLBCLs. Cells from (d) were analyzed for cell apoptosis rates (mean \pm s.d., n=3 independent experiments, one-way ANOVA, n.s, not significant). (F) Elevated apoptosis by knockdown of Roquin2 is only observed in cells harboring a functional *TNFAIP3* gene. GFP⁺ and AnnexinV⁺ HBL1 and HLY-1 cells expressing the

indicated shRNAs were for cell apoptosis rates (mean±s.d., n=3 independent experiments, one-way ANOVA, *P value≤0.05; *** P value≤0.001, n.s, not significant).

(G) KLHL6 is a tumor suppressor in ABC-DLBCLs. In ABC-DLBCL cells, active BCR signaling sustains the NF-κB pathway. KLHL6 is a target of NF-κB and promotes degradation of Roquin2 and *TNFAIP3* mRNA stabilization, establishing a negative feedback loop on NF-κB activity (left panel). Loss of *KLHL6* disengages this negative feedback by promoting Roquin2 stabilization, *TNFAIP3* mRNA decay and higher IKK activity, which further enhances the NF-κB activity (right panel).

Data set	Cell type	# Replicates	Accession number
RNA-seq	U2932 cells expressing Roquin2 (WT) and Roquin2 (Y691F) with 0h and 12h of 10µg/ml of anti-IgM treatment	3	GSE93675

Table 4.1 RNA-seq data sets generated in this dissertation

The table lists the mRNA fold changes in U2932 cells expressing Roquin2 (Y691F) vs Roquin2 (WT) upon 12 hours treatment with 10 µg/ml of F(ab')₂-IgM. Quantification analysis of RNA reads was performed using of R packages DEseq2 (n= 3 independent experiments) (Love et al., 2014).

GO ID	GO class	GO term	P-value	Enrichment	FDR (%)
Background: genes with average expression > 1 RPKM					
GO:0006954	BP	inflammatory response	2.29E-05	7.43	0.03528
GO:0046718	BP	viral entry into host cell	2.65E-05	16.47	0.04078
GO:0090084	BP	negative regulation of inclusion body assembly	3.03E-05	59.03	0.04668
GO:0042026	BP	protein refolding	6.42E-05	47.23	0.09881
GO:0032757	BP	positive regulation of interleukin-8 production	1.16E-04	39.36	0.17893
GO:0050830	BP	defense response to Gram-positive bacterium	1.19E-04	19.04	0.18228
GO:0006986	BP	response to unfolded protein	1.71E-04	17.36	0.26353
GO:0032755	BP	positive regulation of interleukin-6 production	2.36E-04	31.49	0.36314
GO:0070370	BP	cellular heat acclimation	4.08E-04	88.55	0.62632
GO:0034605	BP	cellular response to heat	4.92E-04	24.86	0.75366
GO:0031295	BP	T cell costimulation	5.60E-04	12.83	0.85748
GO:0045080	BP	positive regulation of chemokine biosynthetic process	6.77E-04	70.84	1.03623
GO:0007267	BP	cell-cell signaling	9.61E-04	11.14	1.46831
GO:0006955	BP	immune response	9.89E-04	5.99	1.51131
GO:0070374	BP	positive regulation of ERK1 and ERK2 cascade	0.0017	9.52	2.62922
GO:0042110	BP	T cell activation	0.0017	16.29	2.653
GO:0032496	BP	response to lipopolysaccharide	0.0035	7.87	5.21571
GO:0050731	BP	positive regulation of peptidyl-tyrosine phosphorylation	0.0035	12.76	5.31
GO:0043536	BP	positive regulation of blood vessel endothelial cell migration	0.0036	32.20	5.40275
GO:0051092	BP	positive regulation of NF-kappaB transcription factor activity	0.0054	6.95	8.04951
GO:0050829	BP	defense response to Gram-negative bacterium	0.0059	25.30	8.65474
GO:0001666	BP	response to hypoxia	0.0064	6.63	9.40337
GO:0008284	BP	positive regulation of cell proliferation	0.0068	4.07	9.96367
GO:2001240	BP	negative regulation of extrinsic apoptotic signaling pathway in absence of ligand	0.0086	20.84	12.4802
GO:0071222	BP	cellular response to lipopolysaccharide	0.0107	8.59	15.3085
GO:0042594	BP	response to starvation	0.0119	17.71	16.7694
GO:0031663	BP	lipopolysaccharide-mediated signaling pathway	0.0143	16.10	19.8324
GO:0032729	BP	positive regulation of interferon-gamma production	0.0155	15.40	21.413
GO:0043406	BP	positive regulation of MAP kinase activity	0.0155	15.40	21.413
GO:0045785	BP	positive regulation of cell adhesion	0.0155	15.40	21.413
GO:0002925	BP	positive regulation of humoral immune response mediated by circulating immunoglobulin	0.0166	118.07	22.7502
GO:0048566	BP	embryonic digestive tract development	0.0166	118.07	22.7502
GO:0002876	BP	positive regulation of chronic inflammatory response to antigenic stimulus	0.0166	118.07	22.7502
GO:1902380	BP	positive regulation of endoribonuclease activity	0.0166	118.07	22.7502
GO:1904722	BP	positive regulation of mRNA endonucleolytic cleavage involved in unfolded protein response	0.0166	118.07	22.7502
GO:0071230	BP	cellular response to amino acid stimulus	0.0169	14.76	23.0212
GO:0006959	BP	humoral immune response	0.0182	14.17	24.6533
GO:0043410	BP	positive regulation of MAPK cascade	0.0226	12.65	29.656
GO:0030890	BP	positive regulation of B cell proliferation	0.0226	12.65	29.656
GO:0048661	BP	positive regulation of smooth muscle cell proliferation	0.0241	12.21	31.3475
GO:0038033	BP	positive regulation of endothelial cell chemotaxis by VEGF-activated vascular endothelial growth factor receptor signaling pathway	0.0249	78.71	32.1053
GO:0070434	BP	positive regulation of nucleotide-binding oligomerization domain containing 2 signaling pathway	0.0249	78.71	32.1053
GO:0031397	BP	negative regulation of protein ubiquitination	0.0274	11.43	34.747
GO:0033209	BP	tumor necrosis factor-mediated signaling pathway	0.0329	5.62	40.2216
GO:0046641	BP	positive regulation of alpha-beta T cell proliferation	0.0330	59.03	40.3284
GO:0010038	BP	response to metal ion	0.0330	59.03	40.3284
GO:0007568	BP	aging	0.0339	5.56	41.1695
GO:0030968	BP	endoplasmic reticulum unfolded protein response	0.0380	9.57	44.8682
GO:0019221	BP	cytokine-mediated signaling pathway	0.0380	9.57	44.8682
GO:0045766	BP	positive regulation of angiogenesis	0.0399	9.32	46.517
GO:0045732	BP	positive regulation of protein catabolic process	0.0399	9.32	46.517
GO:0050869	BP	negative regulation of B cell activation	0.0411	47.23	47.5563
GO:1901029	BP	negative regulation of mitochondrial outer membrane permeabilization involved in apoptotic signaling pathway	0.0411	47.23	47.5563
GO:1903265	BP	positive regulation of tumor necrosis factor-mediated signaling pathway	0.0411	47.23	47.5563
GO:0010460	BP	positive regulation of heart rate	0.0411	47.23	47.5563
GO:0043433	BP	negative regulation of sequence-specific DNA binding transcription factor activity	0.0438	8.86	49.7626

GO:0070936	BP	protein K48-linked ubiquitination	0.0478	8.43	52.9269
GO:0033138	BP	positive regulation of peptidyl-serine phosphorylation	0.0478	8.43	52.9269
GO:0006972	BP	hyperosmotic response	0.0491	39.36	53.9094
GO:0097190	BP	apoptotic signaling pathway	0.0520	8.05	55.9972
GO:0050862	BP	positive regulation of T cell receptor signaling pathway	0.0570	33.73	59.4935
GO:0043123	BP	positive regulation of I-kappaB kinase/NF-kappaB signaling	0.0613	4.37	62.1967
GO:0000122	BP	negative regulation of transcription from RNA polymerase II promoter	0.0621	2.23	62.7059
GO:0032722	BP	positive regulation of chemokine production	0.0649	29.52	64.4016
GO:0010941	BP	regulation of cell death	0.0649	29.52	64.4016
GO:0044130	BP	negative regulation of growth of symbiont in host	0.0649	29.52	64.4016
GO:0048010	BP	vascular endothelial growth factor receptor signaling pathway	0.0698	6.81	67.161
GO:0006928	BP	movement of cell or subcellular component	0.0698	6.81	67.161
GO:0007165	BP	signal transduction	0.0714	2.02	68.0057
GO:0060333	BP	interferon-gamma-mediated signaling pathway	0.0722	6.68	68.4184
GO:0002548	BP	monocyte chemotaxis	0.0727	26.24	68.7155
GO:0043122	BP	regulation of I-kappaB kinase/NF-kappaB signaling	0.0727	26.24	68.7155
GO:0003009	BP	skeletal muscle contraction	0.0805	23.61	72.5071
GO:0007193	BP	adenylate cyclase-inhibiting G-protein coupled receptor signaling pathway	0.0805	23.61	72.5071
GO:0045662	BP	negative regulation of myoblast differentiation	0.0805	23.61	72.5071
GO:0042787	BP	protein ubiquitination involved in ubiquitin-dependent protein catabolic process	0.0864	3.78	75.1133
GO:0001819	BP	positive regulation of cytokine production	0.0882	21.47	75.8394
GO:0006970	BP	response to osmotic stress	0.0882	21.47	75.8394
GO:0042981	BP	regulation of apoptotic process	0.0929	3.66	77.6925
GO:0007275	BP	multicellular organism development	0.0931	2.87	77.7523
GO:0035924	BP	cellular response to vascular endothelial growth factor stimulus	0.0958	19.68	78.7682
GO:0010628	BP	positive regulation of gene expression	0.0962	3.61	78.9129

Table 4.2 GO enrichments of Roquin2 regulated genes

U2932 cells expressing Roquin2 (Y691F) vs Roquin2 (WT) were treated with 10 µg/ml of F(ab')₂-IgM for 12 hrs (n= 3 independent experiments). GO analyses were performed using version 6.8 of the DAVID web server (Huang et al., 2009a, c). Exact P values are shown.

#Gene set	WRE (Saddlepoint) P-value
KLHL6, TP53	0.007296593
KLHL6, MLL2	0.009864889
ARID1B, KLHL6	0.013723417
INO80, KLHL6	0.071010277
KLHL6, TNFAIP3	0.085828689
BCL6, KLHL6	0.085828689
BTG1, KLHL6	0.116142985
CHD1, KLHL6	0.127426758
KLHL6, SPEN	0.142065165
KLHL6, TAF1	0.146780171
CCND3, KLHL6	0.154272416
KLHL6, NF1	0.154272416
KLHL6, PRDM1	0.161910743
ARID5B, KLHL6	0.161910743
DDX3X, KLHL6	0.161910743
KLHL6, SETD5	0.170053834
KLHL6, TET2	0.185069315
KLHL6, MCL1	0.186363405
CDKN2A, KLHL6	0.186363405
BTK, KLHL6	0.197108625
CBLB, KLHL6	0.217375064
KLHL6, UBR5	0.228611023
DDX10, KLHL6	0.228611023
KLHL6, MLL3	0.230162112
KLHL6, MEF2B	0.236302759
KLHL6, MEF2BNB-MEF2B	0.236302759
KLHL6, PTPN6	0.25167532
IKBKB, KLHL6	0.25167532
KLHL6, TMSB4X	0.264893745
KLHL6, TOX	0.264893745
KLHL6, ZFAT	0.264893745
KLHL6, MAGT1	0.264893745
CD58, KLHL6	0.264893745
DICER1, KLHL6	0.264893745
GNAI2, KLHL6	0.264893745
KLHL6, TNFRSF14	0.271707356
KLHL6, WAC	0.276026659
CHD8, KLHL6	0.283441479
KLHL6, MYB	0.291571234

#Gene set	WRE (Saddlepoint) P-value
HRAS, KLHL6	0.291571234
CD22, KLHL6	0.291571234
KLHL6, RARA	0.306825911
BRAF, KLHL6	0.306825911
HIST1H2BC, KLHL6	0.306825911
CD79B, KLHL6	0.313455867
DNMT3A, KLHL6	0.313455867
KLHL6, STAT5B	0.321352706
BCL7A, KLHL6	0.331514193
KLHL6, RUNX1	0.339731515
KLHL6, MAP2K1	0.358658894
KLHL6, ZNF608	0.366771011
KLHL6, LIN54	0.398063455
CXCR4, KLHL6	0.398063455
CREBBP, KLHL6	0.405364718
IRF8, KLHL6	0.408385843
ACTB, KLHL6	0.415044201
ATR, KLHL6	0.431749456
KCMF1, KLHL6	0.439622268
KLHL6, PTEN	0.439622268
KLHL6, TGFBR2	0.439622268
EZH2, KLHL6	0.442419554
ETS1, KLHL6	0.459153037
KLHL6, STAT3	0.472592121
KLHL6, ZBTB7A	0.472592121
EP300, KLHL6	0.483090559
KLHL6, MAP4K4	0.487558531
KLHL6, UBE2A	0.487558531
CASP8, KLHL6	0.493686666
CD70, KLHL6	0.496622919
B2M, KLHL6	0.496622919
IL16, KLHL6	0.502377438
DCAF6, KLHL6	0.502377438
JAK1, KLHL6	0.51773029
KLHL6, PTPRK	0.51773029
JUNB, KLHL6	0.51773029
CDC73, KLHL6	0.518526498
KLHL6, SGK1	0.530599488
KLHL6, SMARCA4	0.530599488

#Gene set	WRE (Saddlepoint) P-value
KLHL6, MGA	0.530599488
KLHL6, NFKBIA	0.532770403
KLHL6, RHOA	0.532770403
GOLGA5, KLHL6	0.532770403
GNAS, KLHL6	0.540277952
KLHL6, PIM2	0.565577169
BCL10, KLHL6	0.565577169
ATM, KLHL6	0.57551293
KLHL6, RB1	0.587675935
IKZF3, KLHL6	0.598550468
KLHL6, MECOM	0.598550468
FOXO1, KLHL6	0.604824556
HNRNPU, KLHL6	0.615881531
CARD11, KLHL6	0.624780346
KLHL6, MYC	0.625882038
KLHL6, RRAGC	0.649495031
JAK3, KLHL6	0.650624883
BIRC6, KLHL6	0.655684962
FAM5C, KLHL6	0.661914103
KLHL6, PIK3CD	0.663416907
KLHL6, PHF6	0.667627082
KLHL6, POU2F2	0.667627082
EBF1, KLHL6	0.679660224
KLHL6, TMEM30A	0.688893946
KLHL6, MYD88	0.70470071
KLHL6, ZNF292	0.706970359
KLHL6, MSH2	0.715851297
KLHL6, NCOR1	0.715851297
ETV6, KLHL6	0.715851297
FOXP1, KLHL6	0.72033584
KLHL6, S1PR2	0.72033584
KLHL6, ZEB2	0.729192934
FUBP1, KLHL6	0.737060758
ARID1A, KLHL6	0.750943182
FAS, KLHL6	0.757016267
KLHL6, STAT6	0.763453997
KLHL6, TBL1XR1	0.763453997
KLHL6, NOTCH2	0.763849993
CD83, KLHL6	0.765570173

#Gene set	WRE (Saddlepoint) P-value
KLHL14, KLHL6	0.774720583
FBXW7, KLHL6	0.776384508
KLHL6, TCL1A	0.776384508
BTBD3, KLHL6	0.792343414
HNRNPD, KLHL6	0.792343414
CIITA, KLHL6	0.792343414
KLHL6, ZFX	0.792343414
KLHL6, MSH6	0.813216926
KLHL6, PIK3R1	0.813216926
HIST1H1E, KLHL6	0.831918553
KLHL6, MTOR	0.836996935
KLHL6, SETD1B	0.839606965
GNA13, KLHL6	0.839606965
KLHL6, TIPARP	0.847348818
KLHL6, SYK	0.847348818
KLHL6, SETD2	0.850989763
KLHL6, MARK1	0.859572181
KLHL6, SF3B1	0.870536694
ANKRD17, KLHL6	0.873998924
DUSP2, KLHL6	0.880002839
IRF4, KLHL6	0.895653425
KLHL6, MET	0.900090752
KLHL6, NFKB2	0.90060563
KLHL6, NFKBIE	0.903203366
KLHL6, XPO1	0.908495003
KLHL6, PAX5	0.908495003
KLHL6, YY1	0.927248212
CHST2, KLHL6	0.945672185
BCL2, KLHL6	0.96295551
KLHL6, SOCS1	0.986246166
BTG2, KLHL6	0.986948128
KLHL6, PIM1	0.987391459
KLHL6, KRAS	0.990970456

Table 4.3 Mutual exclusive analyses of KLHL6 BTB-mutations in DLBCL

The Weighted Exclusivity Test (WExT, <http://compbio.cs.brown.edu/software/>) (Leiserson et al., 2016) was utilized to calculate the mutual exclusivity significance of deleterious BTB-domain mutations of *KLHL6* with the 150 genetic drivers of DLBCL described in the DCI datasets (n=1001) (Reddy et al., 2017). Exact P values are shown.

CHAPTER 5 : TYROSINE PHOSPHATASE PTPN14 REGULATES ROQUIN2 PROTEIN STABILITY

Chapter summary

Research described in this chapter was performed in collaboration with the laboratories of Dr. Michael Washburn. Mass Spectrometry (MS) sample preparations were carried out in our laboratory, and Anita Saraf and Laurance Florens performed MS analysis in Dr. Michael Washburn laboratory (Stowers Institute).

The work described in this chapter is all unpublished and forms the body of manuscript that I am currently planning to submit in a small journal. This chapter is focused on elucidating regulation for Roquin2 protein stability by studying post-translational modification of tyrosine 691 residue of Roquin2.

Jaewoo Choi, Anita Saraf, Laurence Florens, Michael P. Washburn, Luca Busino.
Tyrosine phosphatase PTPN14 regulates Roquin2 protein stability

Introduction

Protein post-translational modifications (PTMs) regulate a variety of biological processes such as switching protein activity, intracellular trafficking of transporters, signal transduction, and other fundamental cellular mechanisms (Hunter, 2007; Moeller et al., 2010; Nguyen et al., 2011). Phosphorylation and ubiquitylation are most predominant and ubiquitous PTMs in eukaryotic proteomes. Crosstalk between phosphorylation and ubiquitylation can take many different forms. For example, phosphorylation can activate E3 ligase activity or be a priming event to promote the subsequent ubiquitylation and degradation of the substrates (Fuchs et al., 1996; Khosravi et al., 1999; Sehat et al., 2007). Alternatively, ubiquitylation can influence protein phosphorylation by regulating kinase activity (Hunter, 2007), suggesting that multiple PTMs can work in a *cis*-regulatory manner to fine tune a plethora of complex cellular processes. Phosphorylation is a direct and single step of addition of the phosphate group by protein kinases. However, ubiquitylation is catalyzed in a stepwise manner through an enzymatic cascade requiring an E1 ubiquitin activating-enzyme, an E2 ubiquitin-conjugating enzyme, and an E3 ubiquitin-ligating enzymes (Deshaies and Joazeiro, 2009). Both phosphorylation and ubiquitylation are reversible by protein phosphatases and deubiquitylation enzymes (DUBs), respectively (Alonso et al., 2004; Hershko and Ciechanover, 1998).

Protein tyrosine phosphatases (PTPs) can contribute to the dynamic signal transduction and protein regulation. Increasing evidence has suggested that PTPs have essential roles in tumorigenesis and are primarily considered as tumor suppressors (Julien

et al., 2011). For example, many studies have shown protein tyrosine phosphatase non-receptor type 14 (PTPN14) is mutated in multiple types of cancers including colorectal, breast, ovarian, liver cancers (Sjoblom et al., 2006; Wang et al., 2012; Wang et al., 2004; Zhang et al., 2013). The most well known function of PTPN14 is to inhibit the oncogenic function of yes-associated protein 1 (YAP1), a protein involved in the hippo-signaling pathway (Liu et al., 2013; Wang et al., 2012). Recently, the p53-PTPN14-YAP1 pathway has shown to suppress pancreatic cancer progression and PTPN14 also suppresses metastasis by limiting protein trafficking in breast cancer (Belle et al., 2015; Mello et al., 2017). PTPN14 (also known as PTPD2 or PEZ) has an N-terminal FERM domain and a C-terminal phosphatase domain and plays critical roles in cellular proliferation and growth, cell-cell adhesion and cell migration (Smith et al., 1995; Wadham et al., 2000, 2003) Only three substrates (YAP1, B-catenin, and p130Cas) have been identified so far, and the other biological function of PTPN14 in different genetic and cellular context still remains to be determined (Liu et al., 2013; Wadham et al., 2003; Zhang et al., 2013).

The Roquin family of proteins consists of Roquin1 (Rc3h1) and Roquin2 (Rc3h2). The N-terminal region of Roquin proteins comprises a RING finger, a conserved ROQ domain, and a CCCH-type zinc finger. Mechanistically, mRNAs that contain a constitutive-decay element (CDE) in a 3' UTR sequence are recognized by the ROQ domain of Roquin1 and 2 and undergo mRNA deadenylation and ultimately degradation (Leppek et al., 2013; Schlundt et al., 2014; Tan et al., 2014). Most of Roquin mRNA targets identified by the genome-wide crosslinked-immunoprecipitation (CLIP)-Seq are involved in immunity, inflammation, and development. The recent study on the

paracaspase MALT1 has revealed a regulatory control of Roquin proteins in T cells. When CD4⁺ T cells are stimulated with pharmacological agents PMA and ionomycin, Roquin proteins are cleaved by MALT1 and the specific MALT1 inhibitor, z-VPR-fmk, blocks this cleavage (Jeltsch et al., 2014). Moreover, our study in the chapter 3 shows that Roquin2 protein is targeted by CULLIN3-KLHL6 complex for proteasomal degradation. Whether there are any other regulation components for Roquin2 protein stability remain open questions.

Here, we show that tyrosine 691 of Roquin2 is directly phosphorylated in cells and this phosphorylation disrupts interaction between Roquin2 and KLHL6. We also present evidence that PTPN14 forms a trimeric complex with Roquin2 and KLHL6 and enhances the KLHL6-Roquin2 interaction. Specifically, PTPN14 binds to the end of C-terminus domain of Roquin2 via its phosphatase domain. Overexpression of the wild-type PTPN14 in B-cell lymphomas decreases the Roquin2 protein abundance compared to that of trapping mutant PTPN14. These findings reveal PTPN14 as a novel regulator for Roquin2 protein stability and add another layer of regulation on KLHL6-mediated Roquin2 protein degradation.

Results

Tyrosine 691 in Roquin2 is phosphorylated in vivo

Our previous data in the chapter 3 shows that the integrity of tyrosine 691 residue (Y691) in Roquin2 is critical for KLHL6 interaction as mutation to alanine and

phenylalanine increases the protein stability. Since the tyrosine residue is often modified post-translationally by phosphorylation (Hunter, 2007), we generated a phospho-specific antibody against Y691 residue to test this hypothesis. HEK293T cells were transfected with FLAG-STREP-tagged wild-type (WT) or FLAG-STREP-tagged Roquin2 (Y691F) mutant, a non-phosphorylatable form of tyrosine. To increase the level of cellular tyrosine phosphorylation, we treated the transfected cells with or without pervanadate, a complex from vanadate and hydrogen peroxide, (Heffetz et al., 1990; Secrist et al., 1993) for 15 min before SDS-lysis and affinity purification by streptavidin beads. After the purification, the beads were treated with or without lamda (λ)-phosphatase (Fig 5.1A). Pre-treatment of cells with pervanadate induced a strong phosphorylation of proteins in tyrosine as detected by analysis of whole cell lysates with a phospho-tyrosine antibody (Fig. 5.1B). Under pervanadate treatment conditions, our phospho-antibody specifically recognized Roquin2 (WT), but not the Roquin2 (Y691F) mutant (Fig. 5.1C). To further assess the phospho-specificity of our antibody, we de-phosphorylated Roquin2 (WT) with λ -phosphatase (Fig 5.1A and 5.1C). This treatment abrogated the ability of our antibody to recognize Roquin2 (WT) isolated from pervanadate treated cells, suggesting that the antibody, indeed, recognizes a phosphorylated moiety in position 691. Notably, the antibody could not detect the phosphorylation of tyrosine 691 at the steady state. This could mean that the basal level of Roquin2 phosphorylation is very low or that our antibody is not sensitive enough to detect the basal phosphorylation.

All together, our data suggest that the tyrosine in position 691 of Roquin2 is phosphorylated in cells.

Tyrosine 691 phosphorylation in Roquin2 is inhibitory for KLHL6 interaction

Most PTMs function is a creation of binding sites to promote recognition domains for the protein interaction (Seet et al., 2006). Given that tyrosine 691 is critical for interaction between KLHL6 and Roquin2 (chapter 3), we, next, investigated to assess the effect of tyrosine 691 phosphorylation on the KLHL6-Roquin2 interaction. Since we have found that tyrosine 691 is phosphorylated upon the pervanadate treatment (Fig 5.1B and 5.1C), we examined the interaction between Roquin2 and KLHL6 in the same condition. Interestingly, the pervanadate treatment disrupted the binding between Roquin2 and KLHL6, suggesting that tyrosine phosphorylation negatively regulates the interaction of the two proteins (Fig 5.2A). Next, to directly assess whether tyrosine phosphorylation is inhibitory for the KLHL6-Roquin2 interaction, we synthesized an unphospho- and phospho-peptide in tyrosine 691 (Fig 5.2B). Utilizing these peptides, we performed *in vitro* binding assays and demonstrated that phosphorylation of tyrosine 691 impaired the ability to Roquin2 to associate with KLHL6 (Fig 5.2B). We also confirmed that the peptide without the phosphorylation efficiently interacted with *in vitro*-translated recombinant KLHL6 protein.

Collectively, these data show that phosphorylation at tyrosine 691 in Roquin2 negatively regulates the KLHL6-Roquin2 interaction.

PTPN14 specifically interacts with Roquin2

Since Roquin2, but not its paralog Roquin1, specifically interacts with KLHL6, we hypothesized that tyrosine 691 could be modified by a kinase or phosphatase specific to Roquin2. To gain insight into the regulation components of tyrosine 691 phosphorylation in Roquin2, we compared the protein interactome of Roquin1 (WT) to that of Roquin2 (WT) in HEK293T cells. FLAG-Roquin1 or FLAG-Roquin2 complexes were biochemically immunopurified and the tryptic digestion of each protein eluate was analyzed by mass spectrometry (Fig 5.3A and Supplementary table 5.1). It has been established that Roquin proteins recruit the CCR4-NOT complex through C-terminal region of the proteins (Leppek et al., 2013; Sgromo et al., 2017). Our proteomic analysis validated that Roquin1 and Roquin2 function by recruiting deadenylation factors such as CNOT1, CNOT2, CNOT3, CNOT7, CNOT10, and CNOT11 (Figure 5.3B). Additionally, we also identified a variety of ribosomal protein genes that are essential for eukaryotic ribosome assembly such as RPS or RPL genes (Provost et al., 2013; Warner, 1999). More importantly, we identified PTPN14 as a specific binding partner of Roquin2 immunoprecipitates as opposed to Roquin1 immunoprecipitates, suggesting that PTPN14 is a novel interactor of Roquin2 (Fig 5.3B). PTPN14 is a non-receptor type of tyrosine phosphatase (Smith et al., 1995). To validate the mass spectrometric analysis, we expressed and immunoprecipitated FLAG-tagged Roquin1 or Roquin2 from HEK293T cells and confirmed interaction of endogenous PTPN14 with Roquin2 specifically. Roquin1, although expressed at a higher level than Roquin2, is incapable of binding with PTPN14 (Fig 5.3C).

Altogether, we identified PTPN14 as a specific binding partner of Roquin2.

PTPN14 binds the C-terminal region of the Roquin2 protein through its phosphatase domain

To determine the regions of Roquin2 that contribute to the interaction with PTPN14, we generated a set of refined C-terminal deletion mutants in Roquin2 by site-directed mutagenesis. Given that Roquin1 and Roquin2 have a high sequence similarity including the RING, ROQ, and zinc finger domains (Pratama et al., 2013) and that PTPN14 specifically interacts with Roquin2, we predicted that the binding region should be confined in the C-terminal region of Roquin2. Consistent with our hypothesis, all C-terminal deletions eliminated the ability of Roquin2 to bind to PTPN14 up to the mutant lacking the very C-terminal 50 amino acids (Fig 5.4A) (Pratama et al., 2013). Interestingly, Roquin1 differs from Roquin2 in its C-terminal region as Roquin1 contains a coiled-coil domain instead of a hydrophobic rich region domain that might be responsible for binding to PTPN14.

Next, we utilized a panel of PTPN14 deletion mutants described from the previous study (Szalmas et al., 2017). These mutants include deletions of FERM domain (important for cell adhesion and cytoskeletal function), the linker 1 region, the linker 2 region (required for YAP1 interaction), the linker 3 region, and the phosphatase (PTP) domain (Ogata et al., 1999; Wang et al., 2012). We co-transfected HEK293T cells with N-terminal V5 tagged-PTPN14 wild-type and mutants with FLAG-tagged Roquin2, and FLAG immunoprecipitates were probed with V5 and FLAG antibodies. FLAG-Roquin2

efficiently co-precipitated wild-type and deletion mutants of PTPN14, except for the mutant lacking the PTP domain (Fig 5.4B).

Thus, we concluded that the PTP phosphatase domain of PTPN14 is required to bind the C-terminus of Roquin2.

PTPN14 enhances interaction between KLHL6 and Roquin2

Next, we investigated whether PTPN14 affects the interaction between KLHL6 and Roquin2. KLHL6 is an E3 ligase that specifically binds, ubiquitylates and degrades Roquin2 as shown in the chapter 3. We transfected HEK293T cells stably expressing HA-KLHL6 with FLAG-tagged Roquin2 and V5-tagged PTPN14. Cell lysates were immunoprecipitated with anti-FLAG, and the precipitates were probed with FLAG, KLHL6, or V5 antibodies. As expected, FLAG-Roquin2 co-immunopurified both V5-tagged PTPN14 and HA-tagged KLHL6, indicating that Roquin2, KLHL6 and PTPN14 form a trimeric complex (Fig 5.5A). Furthermore, expression of PTPN14 increased the binding of KLHL6 and Roquin2. These results suggest that PTPN14 might play a role in promoting KLHL6 and Roquin2 interaction for the efficient degradation of Roquin2. Given that phosphorylation at tyrosine 691 of Roquin2 is inhibitory for KLHL6 binding, we expected that PTPN14 might regulate tyrosine 691 directly to bring KLHL6 and Roquin2 together.

Thus, we propose a model where PTPN14 binds at the hydrophobic rich region of Roquin2 and dephosphorylates tyrosine 691 phosphorylation to enhance KLHL6-Roquin2 interaction (Fig 5.5B).

PTPN14 regulates Roquin2 protein stability

Having established that PTPN14 forms a trimeric complex with Roquin2 and KLHL6, we, then, investigated whether PTPN14 promotes degradation of Roquin2 via KLHL6. We transfected HA-tagged Roquin2, V5-tagged PTPN14, Flag-tagged KLHL6 in HEK293T cells in different combinations and see whether PTPN14 has any effects on Roquin2 protein levels. As shown in Figure 5.6A, expression of KLHL6 induced degradation of Roquin2 and, more importantly, the degradation was enhanced when Roquin2 was co-expressed with PTPN14. This suggests that PTPN14 promotes Roquin2 degradation dependent on KLHL6.

We next examined the kinetics of Roquin2 degradation by expressing PTPN14 using a doxycycline-dependent promoter in OCI-LY10, a human DLBCL cell line expressing both endogenous KLHL6 and Roquin2. We generated two different cell lines: one expressing PTPN14 (WT) and the other expressing PTPN14 (D1079A) mutant. This mutant traps the phospho-substrates by keeping them from being dephosphorylated (Blanchetot et al., 2005) (Zhang et al., 2013). We stimulated these cells with the fragment affinity-purified antibody F(ab')₂-IgM to activate B-cell receptor (BCR) signaling pathway after pre-treatment with the doxycycline for 12 hours. We have shown that BCR crosslinking induces degradation of Roquin2 in a KLHL6-dependent manner in ABC-DLBCLs in chapter 3. As shown in Figure 5.6B, Roquin2 was degraded upon BCR stimulation in cells expressing PTPN14 (WT) while this degradation was diminished in cells expressing PTPN14 (D1079A) mutant. This suggests that the trapping mutant might

potentially enrich phosphorylated Roquin2, which might be insensitive to KLHL6-mediated degradation, thus leading to accumulation of Roquin2 substrate.

All together, we conclude that PTPN14 functions in promoting Roquin2 degradation.

Discussion

By generating a phospho-specific antibody against tyrosine 691 in Roquin2, we have demonstrated that Roquin2 is phosphorylated *in vivo*. Upon phosphorylation, KLHL6 dissociates from Roquin2, so phosphorylation directly inhibits the KLHL6-mediated protein degradation. Using a proteomic analysis to analyze co-associated proteins to Roquin2, we have identified the tyrosine phosphatase PTPN14. PTPN14 interacts with Roquin2 and regulates Roquin2 protein stability, as the trapping mutant is able to inhibit BCR-mediated degradation of Roquin2.

Furthermore, we have shown that the integrity of tyrosine 691 residue in Roquin2 is critical for KLHL6 and Roquin2 interaction as both mutation of tyrosine to alanine or phenylalanine can disrupt interaction of two proteins in chapter 3. Now, we have the evidence that phosphorylation at this site inhibits its binding to KLHL6. Consistent with this data, we show that phosphorylated Roquin2 peptide abrogated the ability to Roquin2 to co-immunoprecipitate with KLHL6, suggesting phosphorylation-dependent substrate stabilization. Several other studies have shown that phosphorylation disrupts interaction between E3 ligases and substrates. Although most of substrates of SCF ubiquitin ligases

are recognized in a phosphorylation-dependent manner, phosphorylation of p85 β at tyrosine residue has been shown to inhibit the interaction with its ligase FBXL2 (Kuchay et al., 2013). Furthermore, Aurora A is phosphorylated in serine residue within “A-box” that inhibits APC/C (the ubiquitin ligase anaphase-promoting complex)-dependent degradation (Song and Rape, 2011).

The role of tyrosine 691 phosphorylation prompts us to search for tyrosine kinases or phosphatases, and we are able to identify PTPN14 as a binding partner for Roquin2 by mass spectrometry analysis. Since Roquin2 can form a trimeric complex with PTPN14 and KLHL6, it is conceivable that PTPN14 can bring Roquin2 and KLHL6 together to ensure de-phosphorylation and efficient degradation of Roquin2. In further support of this idea, expression of PTPN14 makes Roquin2 interact with KLHL6 more strongly, suggesting that tyrosine phosphorylation can play a role in protein-protein interaction.

Our mapping experiments show that PTPN14 binds at the C-terminus of Roquin2 through its PTP domain. This is in line with the fact that PTPN14 binds only Roquin2, but not Roquin1. The sequence of RING, ROQ, and CCCH (C3H) domain in Roquin1 and Roquin2 has similarity of 82%, 99%, 81%, respectively (Pratama et al., 2013), so it is likely that PTPN14 binds the C-terminus of Roquin2 where sequence similarity with Roquin1 is only about 45%. Although we have not determined the structure of this trimeric complex, it would be interesting to investigate where this tyrosine phosphorylation is located within the complex and how conformational change occurs upon binding of PTPN14 to KLHL6-Roquin2 complexes.

The fact that tyrosine 691 can be phosphorylated in cells suggests that there might be potential tyrosine kinases involved in this process. In agreement with this hypothesis, we are able to see the effects of overexpression of PTPN14 in both HEK293T cells and human DLBCL cell line in terms of Roquin2 down-regulation, suggesting there might be a basal level of tyrosine 691 phosphorylation in cells. Recent study shows that Roquin1 can specifically interact with the $\alpha 1$ subunit of AMPK kinase and negatively regulate AMPK kinase activity in follicular helper T cells (Ramiscal et al., 2015). Furthermore, Roquin2 can interact and promote ubiquitylation and proteasomal degradation of ASK1 kinase upon the oxidative stress to inhibit reactive oxygen species (ROS)-induced cell death (Maruyama et al., 2014). Although, to date, there are no tyrosine kinases identified that associate with Roquin2 proteins, it is possible that PTM crosstalk between potential tyrosine kinase and PTPN14 phosphatase exists to fine-tune regulation of Roquin2 stability. Furthermore, in chapter 3, we have found that BCR signaling induces degradation of Roquin2 in a KLHL6-dependent manner. It is conceivable that dephosphorylation at tyrosine 691 of Roquin2 might happen in this specific context to promote degradation. Moreover, it would be also interesting to examine whether Roquin2 is constitutively phosphorylated by unknown tyrosine kinases in ABC-DLBCL cell lines that exhibit chronic active BCR signaling.

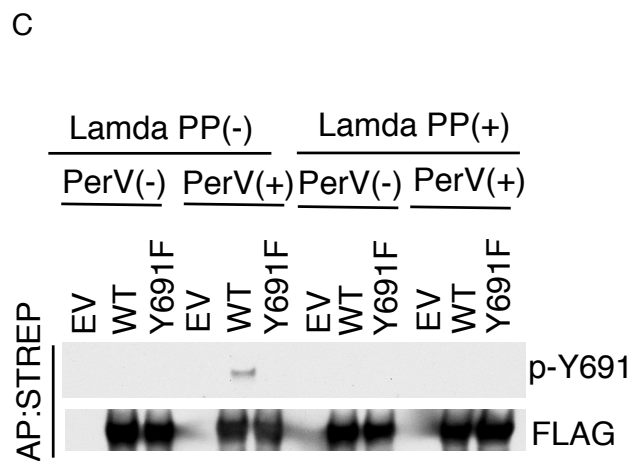
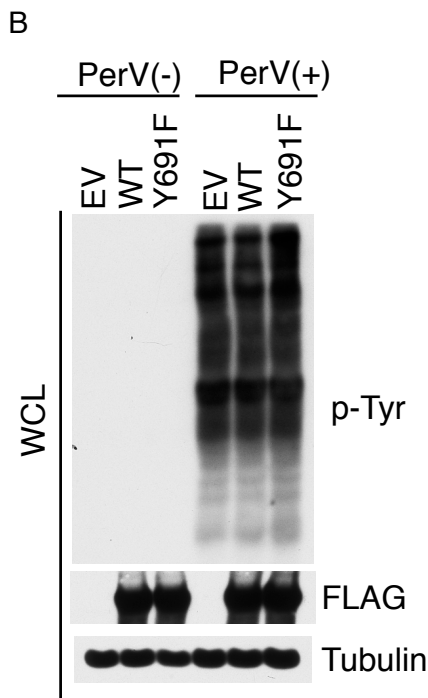
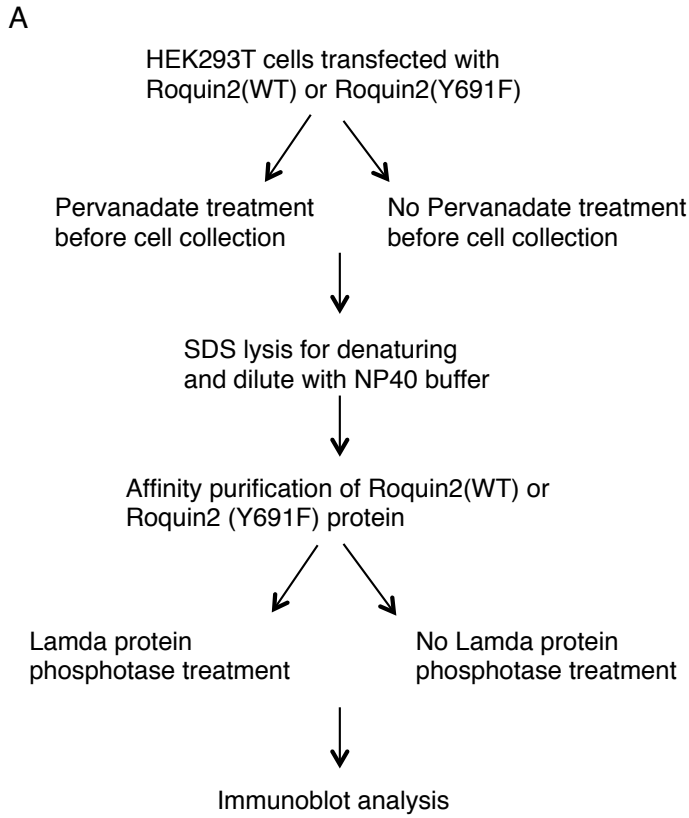


Figure 5.1 Tyrosine 691 in roquin2 is phosphorylated in vivo

(A) A schematic model of validation for phospho-antibody against tyrosine 691 residue in Roquin2. (B) HEK293T cells were transfected with cDNAs encoding FLAG-STREP-tagged Roquin2 (WT), Roquin2 (Y691F) or empty vector (EV). The transfected cells were treated with 100 μ M of pervanadate for 15 min and lysed in a denatured condition (1% SDS-lysis). Cell lysis was diluted with NP-40 buffer (0.1% SDS final concentration) and whole cell lysates were used for immunoblot analysis. (C) Exogenous proteins were affinity-purified (AP) from cell extracts of (b) with an anti-streptavidin resin. The purified complexes were, then, treated with lambda (λ)-phosphatase and probed with antibodies to the indicated proteins.

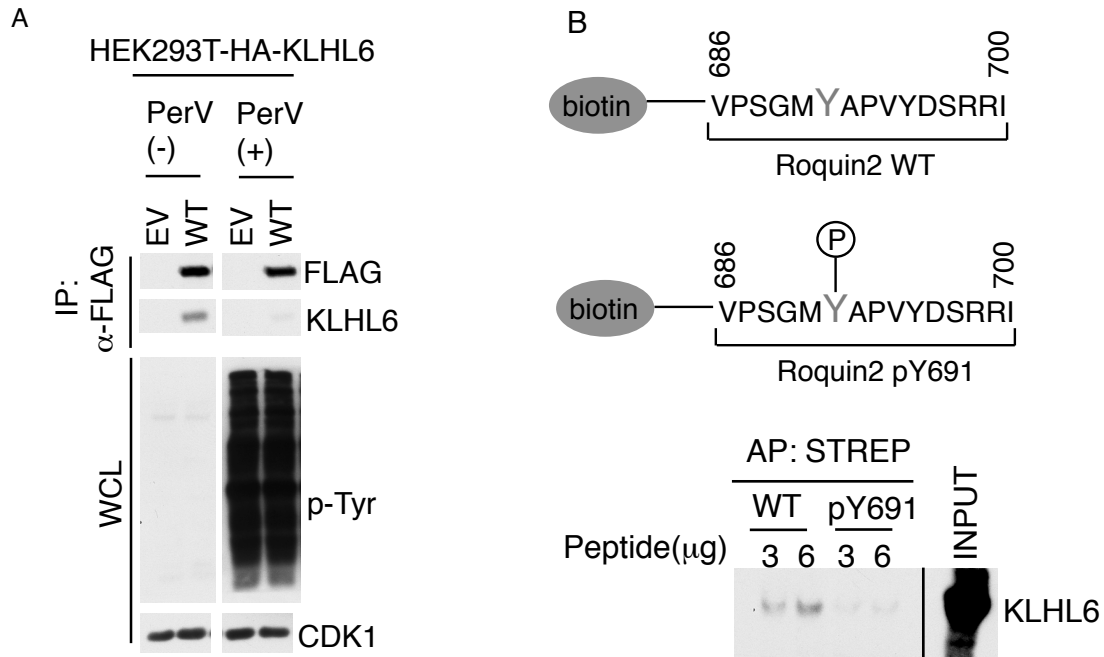


Figure 5.2 Tyrosine 691 phosphorylation in Roquin2 is inhibitory for KLHL6 interaction

(A) HEK293T cells stably expressing HA-tagged KLHL6 were transfected with cDNAs encoding FLAG-tagged Roquin2. The transfected cells were treated with 100μM of pervanadate for 15 min and exogenous proteins were immunopurified from cell extracts with an anti-FLAG resin. Immunocomplexes were probed with antibodies to the indicated proteins. Bottom panel shows whole cell lysates (WCL). (B) Top panel shows a schematic representation of the sequence of the biotinylated unphosphorylated-Roquin2 peptides or phosphorylated-Roquin2 peptides. Bottom panel shows a streptavidin pull-down assay using the indicated amount of biotinylated Roquin2 peptides incubated with FLAG-tagged *in-vitro* translated KLHL6 protein. Affinity Purification,

AP. Immunoblot analysis for the indicated proteins was performed using KLHL6 antibody.

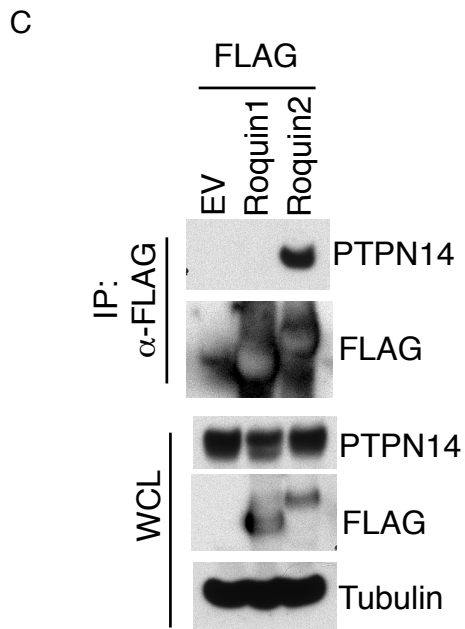
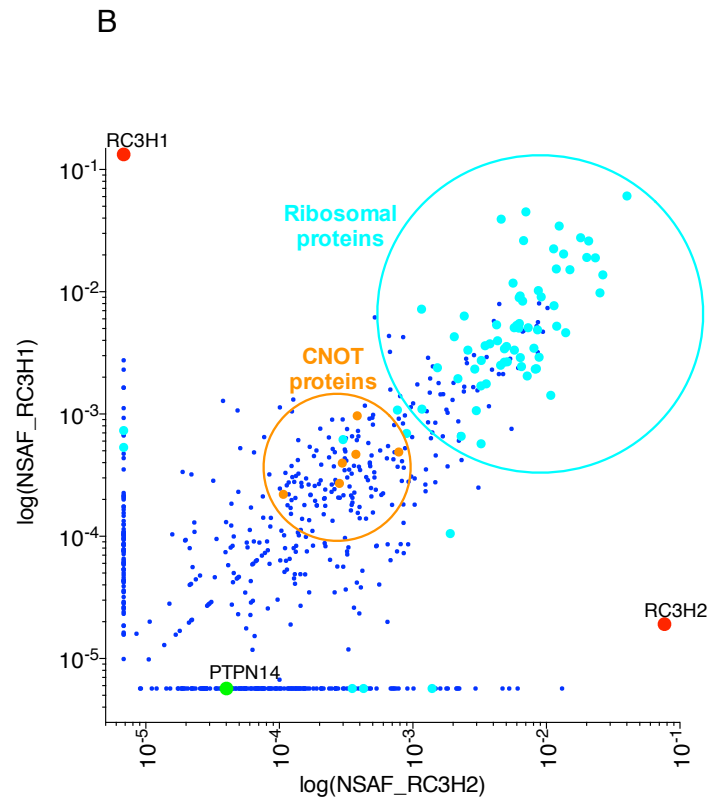
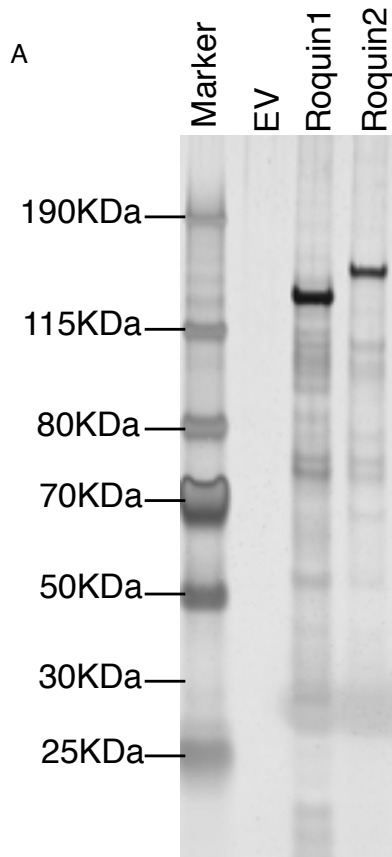
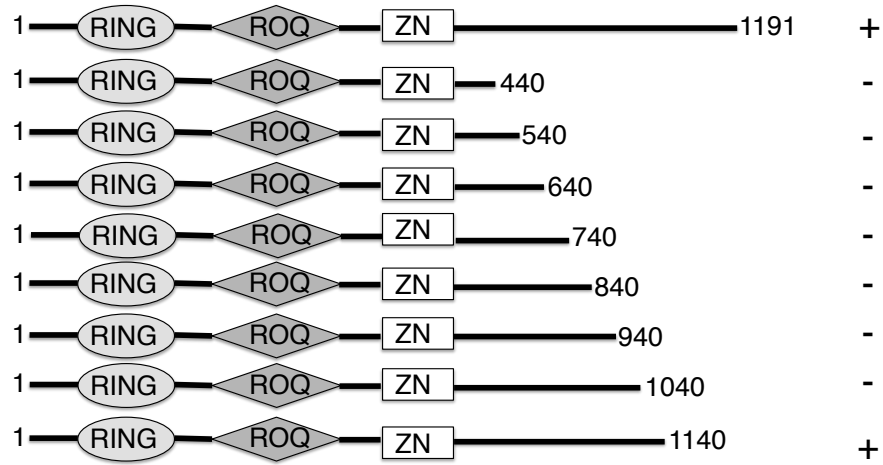


Figure 5.3 PTPN14 specifically interacts with Roquin2

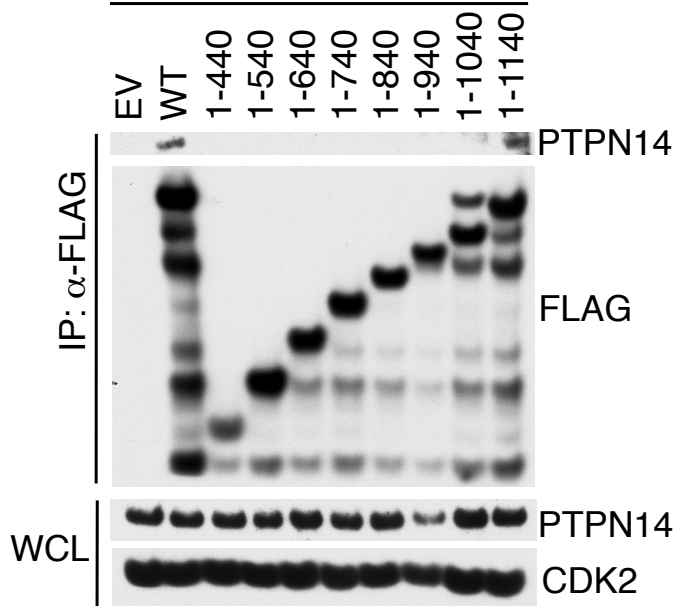
(A) Biochemical purification of Roquin1 or Roquin2 protein complexes. HEK293T cells were transfected with cDNAs encoding FLAG-Roquin1 (WT) or FLAG-Roquin2 (WT). Proteins were immunoprecipitated (IP) with an anti-FLAG resin, eluted with a FLAG peptide. 1% of samples were resolved by SDS-PAGE. The gel was stained with silver staining for protein visualization. (B) Mass spectrometry analysis of Roquin1 (WT) and Roquin2 (WT). Normalized Spectral Abundance Factors (NSAFs) were calculated for each detected protein and plotted on a log scale. X-axis represents NSAF scores distribution of all proteins detected from Roquin2 protein complexes while Y-axis represents NSAF scores distribution of all proteins detected from Roquin1 protein complexes. Red dots represent NSAF scores for the baits such as Roquin1 and Roquin2. The green dot represents the NSAF score for PTPN14. The orange and cyan dots and circles represent common interactors between Roquin1 and Roquin2. (C) HEK293T cells were transfected with cDNAs encoding empty vector (EV), FLAG-tagged Roquin1 or FLAG-tagged Roquin2. Exogenous proteins were immunopurified from cell extracts with an anti-FLAG resin and immunocomplexes were probed with antibodies to the indicated proteins. Bottom panel shows whole cell lysates (WCL).

A

PTPN14 binding



FLAG-STREP Roquin2



B

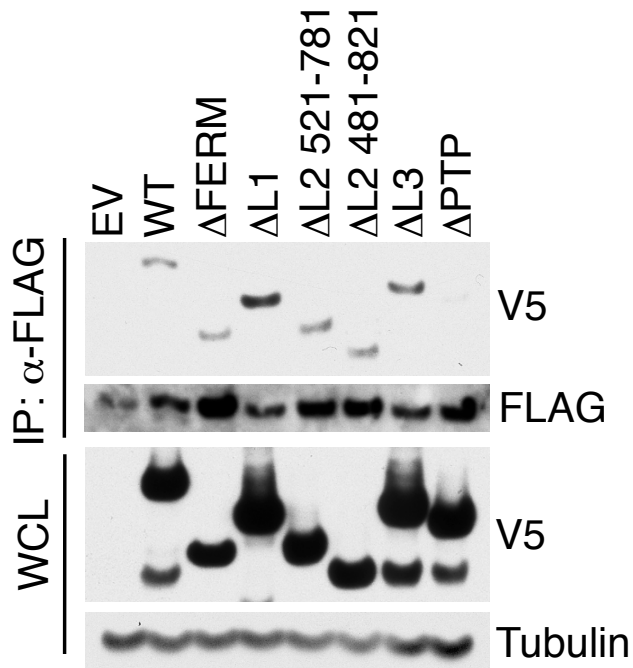
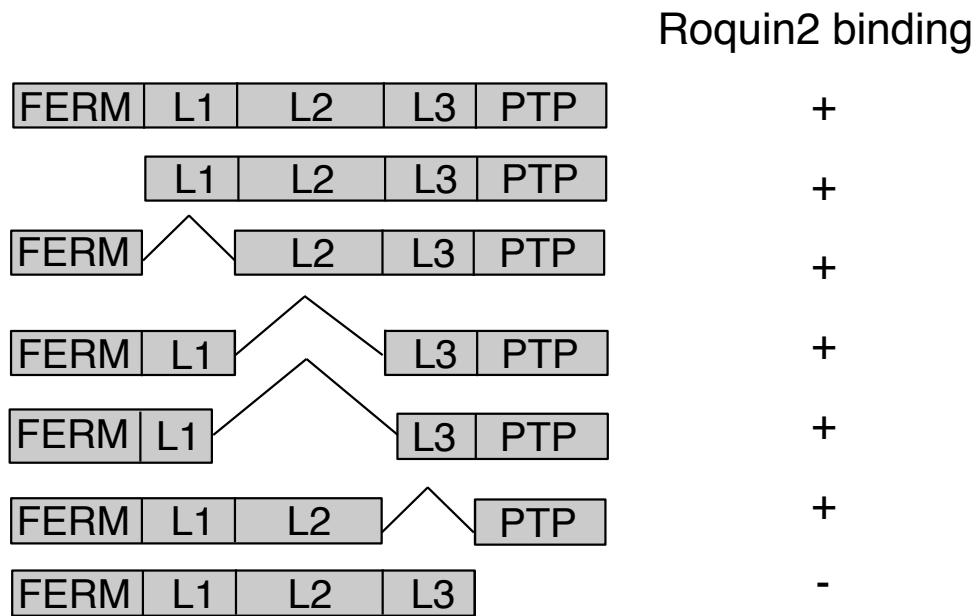


Figure 5.4 PTPN14 binds the C-terminal region of the Roquin2 protein through its phosphatase domain

(A) HEK293T cells were transfected with constructs encoding an empty vector (EV), FLAG-tagged Roquin2 (WT) or FLAG-tagged Roquin2 deletion mutants as indicated. Top panel shows a schematic representation of Roquin2 (WT) or Roquin2 deletion mutants. Roquin2 mutants that interact (+) or do not interact (-) with endogenous PTPN14 are shown. Bottom panel shows immunoblot analysis of FLAG-Roquin2 immunoprecipitation (IP). Immunocomplexes were probed with antibodies to the indicated proteins. (B) HEK293T cells were co-transfected with constructs encoding an empty vector (EV), V5-tagged PTPN14 (WT) or V5-tagged PTPN14 deletion mutants and FLAG-tagged Roquin2 as indicated. Top panel shows a schematic representation of PTPN14 (WT) or PTPN14 internal deletion mutants. PTPN14 mutants that interact (+) or do not interact (-) with exogenous Roquin2 are shown. Bottom panel shows immunoblot analysis of FLAG-Roquin2 immunoprecipitation (IP). Immunocomplexes were probed with antibodies to the indicated proteins.

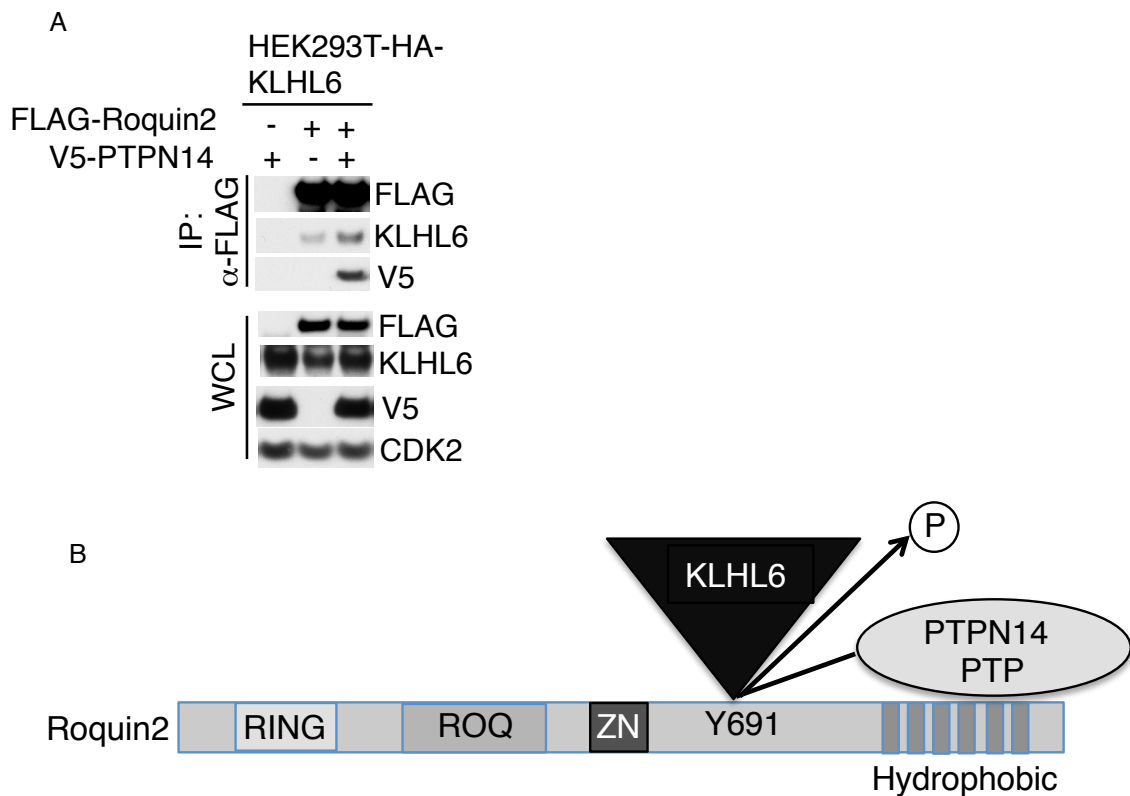


Figure 5.5 PTPN14 enhances interaction between KLHL6 and Roquin2

(A) HEK293T cells stably expressing HA-tagged KLHL6 were co-transfected with cDNAs encoding FLAG-tagged Roquin2 and V5-tagged PTPN14. Exogenous Roquin2 proteins were immunopurified from cell extracts with an anti-FLAG resin and immunocomplexes were probed with antibodies to the indicated proteins. Bottom panel shows whole cell lysates (WCL). (B) A schematic model of trimeric complex composed of Roquin2, KLHL6 and PTPN14. PTPN14 binds Roquin2 through its PTP domain and KLHL6 binds Roquin2 at tyrosine 691 residue. PTPN14 might regulate Roquin2 and KLHL6 interaction by direct de-phosphorylation of tyrosine 691 in Roquin2. Phosphorylation, P.

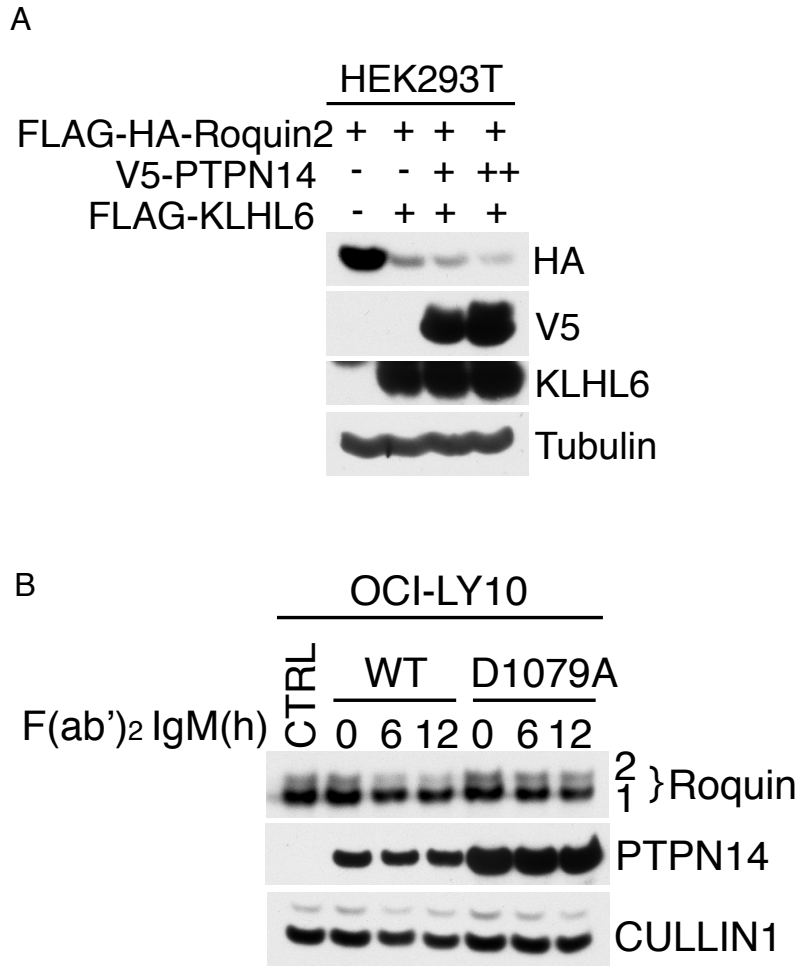


Figure 5.6 PTPN14 regulates Roquin2 protein stability

(A) HEK293T cells were co-transfected with cDNAs encoding FLAG-HA-tagged Roquin2 (WT), FLAG-tagged KLHL6, and increasing amounts of V5-tagged PTPN14 in different combinations. Whole cell lysates were probed with antibodies to the indicated proteins. (B) OCI-LY10 cells were lenti-virally transduced to express doxycycline (DOX) controllable HA-tagged PTPN14 (WT) or PTPN14 (D1079A) mutant. DOX was pre-added for 12 hours and, then, cells were stimulated with anti-IgM (10 μ g/ml) with indicated time points. Whole cell lysates were probed with antibodies to the indicated proteins.

Data set	Cell Type	Condition	# Replicates	Accession Code
Mass Spectrometry	HEK293T cells	Empty Vector, Roquin1 (WT), Roquin2 (WT)	1	PXD009312

Table 5.1 Proteomic analyses of Roquin1 and Roquin2 complexes generated in this dissertation

List of Roquin1 and Roquin2 interacting proteins identified by proteomic analysis of Roquin1 and Roquin2 complexes purified from HEK293T cells.

CHAPTER 6 : CONCLUSIONS AND FUTURE DIRECTIONS

KLHL6 as a tumor suppressor in DLBCL

Here, we find that KLHL6 is a novel CULLIN3-based E3 ligase and reveal that KLHL6 cancer-associated mutations are loss of function. We also demonstrate that loss of KLHL6 (WT) promotes cancer cell proliferation and survival with anti-apoptotic effects while re-expression of KLHL6 (WT) in *KLHL6-null* cells has an opposite effect. Although these data suggest that KLHL6, at least, is a tumor suppressor in terms of tumor maintenance in cancer cells, we do not have any evidence whether loss of *KLHL6* plays a significant role in DLBCL tumor initiation or maintenance in genetic mouse models.

Our laboratory has generated *Klhl6*-null animals using heterozygous embryos from the EMMA consortium. Consistent with the fact that KLHL6 is specifically expressed in lymphoid tissues, *Klhl6*-null mice show several defects in B-cell development. The population of immature B-cells is increased while the frequency of mature B-cells is decreased two- to three-fold in the *Klhl6*-null mice. We also found that the frequencies of progenitor B (pro-B) and precursor B (pre-B) cells in bone marrow of *Klhl6*^{-/-} mice are normal with no defects in hematopoietic stem cells and thymic T-cells, suggesting that there is a specific block in B-cell differentiation from the immature to mature transition. All of results above are indeed in agreement with previous observations that *Klhl6* is not required for the early stages of B-cell development (Kroll et al., 2005). In addition to the B-cell defect in the bone marrow, *Klhl6*-null animals show a cell-intrinsic defect in GC-cell expansion upon immunization (Kroll et al., 2005). More

importantly, aging these *Klhl6*^{-/-} mice did not show any symptoms of lymphoma and we thus concluded that loss of KLHL6 is not sufficient to induce cellular transformation and there likely needs to be other genetic alterations to contribute to lymphomagenesis.

Genome analysis of DLBCL revealed co-occurrence of KLHL6 mutations with translocation of BCL6 under the IgH promoter (Morin et al., 2011), thus we expect that loss of *KLHL6* is required for germinal center tumorigenesis induced by BCL6. The *EμHA-Bcl6* mice mimicking a chromosomal translocation detected in human DLBCL patients develop lympho-proliferative diseases with increased germinal center formation and dysregulated post-germinal center differentiation. Starting at the age of 13 months, *EμHA-Bcl6* show increased mortality, with tumors displaying morphological and immunophenotypic features reminiscent of the human DLBCL (Cattoretti et al., 2005).

We thus generated *EμHA-Bcl6/Klhl6*^{-/-} mice by breeding our *Klhl6*-null mice with *EμHA-Bcl6* mice (Cattoretti et al., 2005) and have now three cohorts of *EμHA-Bcl6/Klhl6*^{-/-}, *EμHA-Bcl6/Klhl6*^{+/-}, *EμHA-Bcl6/Klhl6*^{+/+} mice for ongoing projects in our laboratory. We are monitoring these mice for any signs of lymphoma progression and will consider morbidity of mice at the end-point of the experiment to calculate the median survival and construct a Kaplan-Meier curve. We expect that the onset and penetrance of *EμHA-Bcl6*-induced tumors will be accelerated in *Klhl6*-null mice. Moreover, since loss of KLHL6 promotes the survival of cancer cells, we expect that *Klhl6*-null mice have a survival advantage in producing secondary tumors. It will be also important to determine whether KLHL6-negative lymphomas are addicted to or dependent on Roquin2 for the growth and survival. We plan to perform a rescue experiment similar to *in vitro* system

where we will isolate splenic tumors from *EμHA-Bcl6/Klhl6^{-/-}* mice and utilize shRNA against Roquin2 to knockdown before transplanting into syngeneic mice. Since loss of Roquin2 induces cellular apoptosis in ABC-DLBCL, we expect the lower penetrance and/or longer tumor latency in *EμHA-Bcl6/Klhl6^{-/-}* mice with knockdown of Roquin2.

It would be also interesting to investigate whether deleting *Klhl6* in the context of B-cell lineage p53 deletion could uncover the tumor suppressive role of KLHL6. This experiment can be carried out by crossing *Klhl6*-null mice with CD19-Cre p53^{flox/flox} mice. All of these *in vivo* investigations are required to shed light on how KLHL6 contributes to pathogenesis of mature B-cell tumors and some of these further studies are ongoing in our laboratory. In the future, we will have direct evidence to state that KLHL6 is a tumor suppressor in DLBCL biology. It is also worth noting that *KLHL6* mutations are not observable at a high frequency in non-B-cell cancers, suggesting a possibly differential role for KLHL6 in a different genetic and cellular context.

Roquin2 as an oncogene in DLBCL

We have demonstrated that deregulation of Roquin2 proteolysis or Roquin2 stabilization affects Roquin2 target mRNA stability, which is dependent on a ROQ domain necessary for RNA recognition. More specifically, we show that KLHL6-Roquin2 axis controls NF-κB activation in ABC-DLBCLs by controlling TNFAIP3/A20 mRNA decay. However, Roquin proteins bind and degrade other NF-κB inhibitors mRNAs such as NFKBIZ and NFKBID (Leppek et al., 2013). NFKBID did not score in our RNA-sequencing analysis whereas NFKBIZ did score in our primary screen as a

gene that was down-regulated in non-degradable Roquin2 mutant (Y691F) but failed to score as a BCR-dependent transcript. Moreover, we also found that another NF- κ B inhibitor, NFKBIE, scored in our primary RNA-sequencing screening, but was not effectively rescued in the secondary q-PCR screening. Despite the fact that some of these NF- κ B pathway inhibitors might not be the direct targets of Roquin2, they are indirectly down-regulated by Roquin2 and may contribute to increased NF- κ B activation for the survival of ABC-DLBCLs. We specifically chose to further study A20 and its downstream effects on the NF- κ B signaling pathway, as it is the most well known tumor suppressor and negative regulator of NF- κ B in ABC-DLBCL biology. However, we cannot exclude the possibility that the growth advantages induced by stabilization of Roquin2 could be due to combinatorial effects of multiple Roquin2 specific mRNA targets. It would be interesting to see whether any other NF- κ B pathway inhibitors are affected by the KLHL6-Roquin2 axis in ABC-DLBCLs.

Additionally, we also found TNFRSF14 (the tumor necrosis factor receptor superfamily member herpesvirus entry mediator, HVEM) as Roquin2 specific mRNA targets that might play a role in GCB-DLBCLs since it is frequently mutated in GC lymphomas, especially follicular lymphoma (Launay et al., 2012; Lohr et al., 2012). TNFRSF14 regulates the immune response in T-cells by activation of inhibitory and inflammatory responses. TNFRSF14 can act as a receptor by binding TNF-related ligands such as lymphotoxin- α and LIGHT (lymphotoxin-like, exhibits inducible expression, and competes with herpes simplex virus glycoprotein D for HVEM, a receptor expressed by T lymphocytes). It also can act as a ligand by engaging with the immunoglobulin

superfamily, B and T lymphocyte attenuator (BTLA) and CD160, and regulate diverse signaling pathways for the immune responses (Murphy and Murphy, 2010). A recent study reveals that TNFRSF14 loss increases production of TNF family of cytokines that activate lymphoid stromal cells and recruitment of T follicular help (T_{FH}) cells. This, in turn, provides a tumor-supportive microenvironment via production of IL-4, IL-21 and CD40L (Ame-Thomas and Tarte, 2014; Boice et al., 2016). Therefore, it is conceivable that mutations of KLHL6 with Roquin2 stabilization might contribute to the pathogenesis of follicular lymphoma by linking tumor microenvironment. In line with this, we cannot exclude the fact that KLHL6 might have other substrates that are involved in different biological processes such as cellular migration, adhesion or immune surveillance in patients. We plan to study other unknown KLHL6 substrates or different Roquin2 mRNA targets and further evaluate the functional impact of the KLHL6-Roquin2 axis in GCB-DLBCLs. We have defined the interactome landscape of KLHL6 for putative substrates and interactors, and we plan to validate these novel candidate substrates similarly to what we have performed with Roquin2. The characterization of these novel substrates will constitute the basis for new projects, and future studies will address another molecular mechanisms controlled by KLHL6-mediated degradation in the context of B-cell cancers.

Although Roquin2 stabilization or deregulation of Roquin2 proteolysis promotes cancer cell proliferation and survival and loss of Roquin2 causes cellular apoptosis in ABC-DLBCLs, we do not have genetic mouse evidence to state that Roquin2 is an oncogene. Several studies have shown that overexpression of Roquin1 in T-cell lymphoma cell lines or Roquin1 transgenic mice in T-cells promotes production of

inflammatory cytokines such as IL-2, TNF- α , IFN- γ and develop more severe collagen-induced arthritis with autoimmune symptoms (Ji et al., 2012; Kim et al., 2012). Moreover, T-lymphoma cell lines overexpressing Roquin were hyper-responsive to T-cell receptor stimulation with anti-CD3/CD28 *in vitro*. This is in line with the fact that Roquin proteins might play an oncogenic role by regulating inflammatory and immune-related mRNA targets in T-cells. Although Roquin1 protein alterations or mutations are not seen in angioimmunoblastic T-cell lymphoma (AITL), Roquin2 missense mutation at tyrosine residue (Y691) was recently uncovered in thymic lymphoma from TCGA data analysis. This suggests that Roquin1 and Roquin2 might play a non-redundant role in T-cell cancers. This is also in line with the fact that KLHL6 mutation only affects Roquin2 proteolysis in B-cell cancers and not Roquin1, implying that there is a specific function of Roquin2 in the development of DLBCLs. Transgenic mice overexpressing Roquin2 or the non-degradable Roquin2 mutant (Y691F) in the germinal center or in mature B-cells might be helpful to model the oncogenic role of Roquin2 in DLBCL *in vivo*. Moreover, our collaborators and we are currently breeding Roquin2 knockout mice with mouse model of murine DLBCLs. We expect that knockout of Roquin2 will decrease the oncogenic progression of DLBCL tumors with lower tumor penetrance and longer tumor latency.

PTPN14 as a tumor suppressor in DLBCL

We have demonstrated that Roquin2 protein stability is decreased by overexpression tyrosine phosphatase, PTPN14. Moreover, Roquin2 is phosphorylated in tyrosine 691 residue in cells and this phosphorylation disrupts KLHL6-Roquin2 interaction. Although we do not have direct evidence that PTPN14 dephosphorylates tyrosine 691 of Roquin2 at this point, we are currently performing *in vitro* phosphatase assay to link the mechanism of phosphorylation and protein degradation. PTPN14 has been regarded as a tumor suppressor in a variety of cancers as mutation and deletion are identified (Sjoblom et al., 2006; Wang et al., 2004; Zhang et al., 2013). Consistent with this idea, PTPN14 negatively regulates the stability of Roquin2, which plays an oncogenic role in ABC-DLBCL cell lines. In chapter 3, we have shown that stabilization of Roquin2 by cancer-associated mutations of KLHL6 or loss of *KLHL6* promotes DLBCL growth and survival by regulation of mRNA decay of the tumor suppressor and NF- κ B pathway inhibitor, TNFAIP3. The role of protein tyrosine phosphatases in lymphoma has not been extensively studied. However, there are some cases reported where PTPN1 that is frequently mutated in Hodgkin lymphoma, and primary mediastinal B cell lymphoma with loss of function mutations, suggesting a tumor suppressor role (Gunawardana et al., 2014). Furthermore, inactivating mutations and epigenetic silencing of PTPN13 have been reported in non-Hodgkin's and Hodgkin's lymphoma (Ying et al., 2006).

Interestingly, we have noticed PTPN14 protein is also expressed at very low levels and almost non-detectable in ABC-DLBCL cell lines (data not shown). As a future direction, it would be interesting to determine whether there are unknown mechanism to

down-regulate PTPN14 mRNA or protein in human B-lymphomas. Alternatively, whether overexpression of PTPN14 in ABC-DLBCLs has any impacts on cancer cell proliferation and whether it can regulate NF- κ B pathway through Roquin2 degradation remain open questions.

Concluding remarks

The studies presented in this dissertation focus on defining molecular mechanisms by which the KLHL6-Roquin2 axis contributes to growth and survival of ABC-DLBCLs. This work provides insight into the distinct role of KLHL6 as an E3 ligase for Roquin2 and how misregulation of this pathway impacts maintenance of mature B-cell cancers in *in vitro* and *in vivo* xenograft experiments. The identification of KLHL6 as the E3 ligase for Roquin2 provides essential information and tools to elucidate the molecular link between the ubiquitin proteasome system and mRNA decay. Understanding whether deregulation of Roquin2 proteolysis has any functional consequences in terms of mRNA decay will allow us to understand its role in B-cell biology further. Additionally, the studies here highlight the post-translational modifications that add another layer of regulation on KLHL6-Roquin2 axis. As targeting specific ubiquitin ligases is therapeutically feasible and relevant to human cancers, a deeper molecular understanding of KLHL6-mediated proteolysis of Roquin2 in cancers can potentially broaden therapeutic approaches for the treatment of B-cell malignancies.

CHAPTER 7 : REFERENCES

- Adams, J., Kelso, R., and Cooley, L. (2000). The kelch repeat superfamily of proteins: propellers of cell function. *Trends Cell Biol* 10, 17-24.
- Adams, J., Palombella, V.J., Sausville, E.A., Johnson, J., Destree, A., Lazarus, D.D., Maas, J., Pien, C.S., Prakash, S., and Elliott, P.J. (1999). Proteasome inhibitors: a novel class of potent and effective antitumor agents. *Cancer Res* 59, 2615-2622.
- Aghajanian, C., Soignet, S., Dizon, D.S., Pien, C.S., Adams, J., Elliott, P.J., Sabbatini, P., Miller, V., Hensley, M.L., Pezzulli, S., *et al.* (2002). A phase I trial of the novel proteasome inhibitor PS341 in advanced solid tumor malignancies. *Clin Cancer Res* 8, 2505-2511.
- Albagli, O., Dhordain, P., Deweindt, C., Lecocq, G., and Leprince, D. (1995). The BTB/POZ domain: a new protein-protein interaction motif common to DNA- and actin-binding proteins. *Cell Growth Differ* 6, 1193-1198.
- Alizadeh, A.A., Eisen, M.B., Davis, R.E., Ma, C., Lossos, I.S., Rosenwald, A., Boldrick, J.C., Sabet, H., Tran, T., Yu, X., *et al.* (2000). Distinct types of diffuse large B-cell lymphoma identified by gene expression profiling. *Nature* 403, 503-511.
- Almond, J.B., and Cohen, G.M. (2002). The proteasome: a novel target for cancer chemotherapy. *Leukemia* 16, 433-443.
- Alonso, A., Sasin, J., Bottini, N., Friedberg, I., Friedberg, I., Osterman, A., Godzik, A., Hunter, T., Dixon, J., and Mustelin, T. (2004). Protein tyrosine phosphatases in the human genome. *Cell* 117, 699-711.
- Ambroggio, X.I., Rees, D.C., and Deshaies, R.J. (2004). JAMM: a metalloprotease-like zinc site in the proteasome and signalosome. *PLoS Biol* 2, E2.
- Ame-Thomas, P., and Tarte, K. (2014). The yin and the yang of follicular lymphoma cell niches: role of microenvironment heterogeneity and plasticity. *Semin Cancer Biol* 24, 23-32.
- An, J., Wang, C., Deng, Y., Yu, L., and Huang, H. (2014). Destruction of full-length androgen receptor by wild-type SPOP, but not prostate-cancer-associated mutants. *Cell Rep* 6, 657-669.
- Anderica-Romero, A.C., Gonzalez-Herrera, I.G., Santamaria, A., and Pedraza-Chaverri, J. (2013). Cullin 3 as a novel target in diverse pathologies. *Redox Biol* 1, 366-372.
- Barbie, D.A., Tamayo, P., Boehm, J.S., Kim, S.Y., Moody, S.E., Dunn, I.F., Schinzel, A.C., Sandy, P., Meylan, E., Scholl, C., *et al.* (2009). Systematic RNA interference reveals that oncogenic KRAS-driven cancers require TBK1. *Nature* 462, 108-U122.
- Beck, J., Maerki, S., Posch, M., Metzger, T., Persaud, A., Scheel, H., Hofmann, K., Rotin, D., Pedrioli, P., Swedlow, J.R., *et al.* (2013). Ubiquitylation-dependent localization of PLK1 in mitosis. *Nat Cell Biol* 15, 430-439.
- Belle, L., Ali, N., Lonic, A., Li, X., Paltridge, J.L., Roslan, S., Herrmann, D., Conway, J.R., Gehling, F.K., Bert, A.G., *et al.* (2015). The tyrosine phosphatase PTPN14 (Pez) inhibits metastasis by altering protein trafficking. *Sci Signal* 8, ra18.
- Bennett, E.J., Rush, J., Gygi, S.P., and Harper, J.W. (2010). Dynamics of Cullin-RING Ubiquitin Ligase Network Revealed by Systematic Quantitative Proteomics. *Cell* 143, 951-965.

- Bernardi, R., Guernah, I., Jin, D., Grisendi, S., Alimonti, A., Teruya-Feldstein, J., Cordon-Cardo, C., Simon, M.C., Rafii, S., and Pandolfi, P.P. (2006). PML inhibits HIF-1alpha translation and neoangiogenesis through repression of mTOR. *Nature* 442, 779-785.
- Bertossi, A., Aichinger, M., Sansonetti, P., Lech, M., Neff, F., Pal, M., Wunderlich, F.T., Anders, H.J., Klein, L., and Schmidt-Supprian, M. (2011). Loss of Roquin induces early death and immune deregulation but not autoimmunity. *J Exp Med* 208, 1749-1756.
- Beyaert, R., Heyninck, K., and Van Huffel, S. (2000). A20 and A20-binding proteins as cellular inhibitors of nuclear factor-kappa B-dependent gene expression and apoptosis. *Biochem Pharmacol* 60, 1143-1151.
- Bhoj, V.G., and Chen, Z.J. (2009). Ubiquitylation in innate and adaptive immunity. *Nature* 458, 430-437.
- Blanchetot, C., Chagnon, M., Dube, N., Halle, M., and Tremblay, M.L. (2005). Substrate-trapping techniques in the identification of cellular PTP targets. *Methods* 35, 44-53.
- Boice, M., Salloum, D., Mourcin, F., Sanghvi, V., Amin, R., Oricchio, E., Jiang, M., Mottok, A., Denis-Lagache, N., Ciriello, G., *et al.* (2016). Loss of the HVEM Tumor Suppressor in Lymphoma and Restoration by Modified CAR-T Cells. *Cell* 167, 405-418 e413.
- Boone, D.L., Turer, E.E., Lee, E.G., Ahmad, R.C., Wheeler, M.T., Tsui, C., Hurley, P., Chien, M., Chai, S., Hitotsumatsu, O., *et al.* (2004). The ubiquitin-modifying enzyme A20 is required for termination of Toll-like receptor responses. *Nat Immunol* 5, 1052-1060.
- Bosanac, I., Wertz, I.E., Pan, B., Yu, C., Kusam, S., Lam, C., Phu, L., Phung, Q., Maurer, B., Arnott, D., *et al.* (2010). Ubiquitin binding to A20 ZnF4 is required for modulation of NF-kappaB signaling. *Mol Cell* 40, 548-557.
- Braun, B.C., Glickman, M., Kraft, R., Dahlmann, B., Kloetzel, P.M., Finley, D., and Schmidt, M. (1999). The base of the proteasome regulatory particle exhibits chaperone-like activity. *Nat Cell Biol* 1, 221-226.
- Busino, L., Millman, S.E., Scotto, L., Kyratsous, C.A., Basrur, V., O'Connor, O., Hoffmann, A., Elenitoba-Johnson, K.S., and Pagano, M. (2012). Fbxw7alpha- and GSK3-mediated degradation of p100 is a pro-survival mechanism in multiple myeloma. *Nature cell biology*.
- Cardozo, T., and Pagano, M. (2004). The SCF ubiquitin ligase: insights into a molecular machine. *Nat Rev Mol Cell Biol* 5, 739-751.
- Cattoretti, G., Pasqualucci, L., Ballon, G., Tam, W., Nandula, S.V., Shen, Q., Mo, T., Murty, V.V., and Dalla-Favera, R. (2005). Deregulated BCL6 expression recapitulates the pathogenesis of human diffuse large B cell lymphomas in mice. *Cancer Cell* 7, 445-455.
- Cerchiatti, L.C., Ghetu, A.F., Zhu, X., Da Silva, G.F., Zhong, S., Matthews, M., Bunting, K.L., Polo, J.M., Fares, C., Arrowsmith, C.H., *et al.* (2010). A small-molecule inhibitor of BCL6 kills DLBCL cells in vitro and in vivo. *Cancer Cell* 17, 400-411.
- Chauhan, D., Hideshima, T., Mitsiades, C., Richardson, P., and Anderson, K.C. (2005). Proteasome inhibitor therapy in multiple myeloma. *Mol Cancer Ther* 4, 686-692.

- Chen, H.Y., Hu, J.Y., Chen, T.H., Lin, Y.C., Liu, X., Lin, M.Y., Lang, Y.D., Yen, Y., and Chen, R.H. (2015). KLHL39 suppresses colon cancer metastasis by blocking KLHL20-mediated PML and DAPK ubiquitination. *Oncogene* 34, 5141-5151.
- Chen, H.Y., Lee, Y.R., and Chen, R.H. (2014). The functions and regulations of DAPK in cancer metastasis. *Apoptosis* 19, 364-370.
- Chu, Y.Y., Vahl, J.C., Kumar, D., Heger, K., Bertossi, A., Wojtowicz, E., Soberon, V., Schenten, D., Mack, B., Reutelshofer, M., *et al.* (2011). B cells lacking the tumor suppressor TNFAIP3/A20 display impaired differentiation and hyperactivation and cause inflammation and autoimmunity in aged mice. *Blood* 117, 2227-2236.
- Compagno, M., Lim, W.K., Grunn, A., Nandula, S.V., Brahmachary, M., Shen, Q., Bertoni, F., Ponzoni, M., Scandurra, M., Califano, A., *et al.* (2009). Mutations of multiple genes cause deregulation of NF-kappaB in diffuse large B-cell lymphoma. *Nature* 459, 717-721.
- Coornaert, B., Baens, M., Heyninck, K., Bekaert, T., Haegman, M., Staal, J., Sun, L., Chen, Z.J., Marynen, P., and Beyaert, R. (2008). T cell antigen receptor stimulation induces MALT1 paracaspase-mediated cleavage of the NF-kappaB inhibitor A20. *Nat Immunol* 9, 263-271.
- Cope, G.A., Suh, G.S., Aravind, L., Schwarz, S.E., Zipursky, S.L., Koonin, E.V., and Deshaies, R.J. (2002). Role of predicted metalloprotease motif of Jab1/Csn5 in cleavage of Nedd8 from Cul1. *Science* 298, 608-611.
- Correale, S., Pirone, L., Di Marcotullio, L., De Smaele, E., Greco, A., Mazza, D., Moretti, M., Alterio, V., Vitagliano, L., Di Gaetano, S., *et al.* (2011). Molecular organization of the cullin E3 ligase adaptor KCTD11. *Biochimie* 93, 715-724.
- Cortes, J., Thomas, D., Koller, C., Giles, F., Estey, E., Faderl, S., Garcia-Manero, G., McConkey, D., Ruiz, S.L., Guerciolini, R., *et al.* (2004). Phase I study of bortezomib in refractory or relapsed acute leukemias. *Clin Cancer Res* 10, 3371-3376.
- Cui, Y., He, S., Xing, C., Lu, K., Wang, J., Xing, G., Meng, A., Jia, S., He, F., and Zhang, L. (2011). SCFFBXL(1)(5) regulates BMP signalling by directing the degradation of HECT-type ubiquitin ligase Smurf1. *EMBO J* 30, 2675-2689.
- Cullinan, S.B., Gordan, J.D., Jin, J., Harper, J.W., and Diehl, J.A. (2004). The Keap1-BTB protein is an adaptor that bridges Nrf2 to a Cul3-based E3 ligase: oxidative stress sensing by a Cul3-Keap1 ligase. *Mol Cell Biol* 24, 8477-8486.
- Davis, R.E., Ngo, V.N., Lenz, G., Tolar, P., Young, R.M., Romesser, P.B., Kohlhammer, H., Lamy, L., Zhao, H., Yang, Y.D., *et al.* (2010). Chronic active B-cell-receptor signalling in diffuse large B-cell lymphoma. *Nature* 463, 88-U97.
- DeNicola, G.M., Karreth, F.A., Humpton, T.J., Gopinathan, A., Wei, C., Frese, K., Mangal, D., Yu, K.H., Yeo, C.J., Calhoun, E.S., *et al.* (2011). Oncogene-induced Nrf2 transcription promotes ROS detoxification and tumorigenesis. *Nature* 475, 106-109.
- Deshaies, R.J., and Joazeiro, C.A. (2009). RING domain E3 ubiquitin ligases. *Annu Rev Biochem* 78, 399-434.
- Dias, D.C., Dolios, G., Wang, R., and Pan, Z.Q. (2002). CUL7: A DOC domain-containing cullin selectively binds Skp1.Fbx29 to form an SCF-like complex. *Proc Natl Acad Sci U S A* 99, 16601-16606.

Dixit, V.M., Green, S., Sarma, V., Holzman, L.B., Wolf, F.W., O'Rourke, K., Ward, P.A., Prochownik, E.V., and Marks, R.M. (1990). Tumor necrosis factor- α induction of novel gene products in human endothelial cells including a macrophage-specific chemotaxin. *J Biol Chem* 265, 2973-2978.

Dobin, A., Davis, C.A., Schlesinger, F., Drenkow, J., Zaleski, C., Jha, S., Batut, P., Chaisson, M., and Gingeras, T.R. (2013). STAR: ultrafast universal RNA-seq aligner. *Bioinformatics* 29, 15-21.

Dunleavy, K., Pittaluga, S., Czuczman, M.S., Dave, S.S., Wright, G., Grant, N., Shovlin, M., Jaffe, E.S., Janik, J.E., Staudt, L.M., *et al.* (2009). Differential efficacy of bortezomib plus chemotherapy within molecular subtypes of diffuse large B-cell lymphoma. *Blood* 113, 6069-6076.

Eades, G., Yang, M., Yao, Y., Zhang, Y., and Zhou, Q. (2011). miR-200a regulates Nrf2 activation by targeting Keap1 mRNA in breast cancer cells. *J Biol Chem* 286, 40725-40733.

Elowe, S., Hummer, S., Uldschmid, A., Li, X., and Nigg, E.A. (2007). Tension-sensitive Plk1 phosphorylation on BubR1 regulates the stability of kinetochore microtubule interactions. *Genes Dev* 21, 2205-2219.

Eng, J.K., McCormack, A.L., and Yates, J.R. (1994). An approach to correlate tandem mass spectral data of peptides with amino acid sequences in a protein database. *J Am Soc Mass Spectrom* 5, 976-989.

Errington, W.J., Khan, M.Q., Bueler, S.A., Rubinstein, J.L., Chakrabarty, A., and Prive, G.G. (2012). Adaptor protein self-assembly drives the control of a cullin-RING ubiquitin ligase. *Structure* 20, 1141-1153.

Faraonio, R., Vergara, P., Di Marzo, D., Pierantoni, M.G., Napolitano, M., Russo, T., and Cimino, F. (2006). p53 suppresses the Nrf2-dependent transcription of antioxidant response genes. *J Biol Chem* 281, 39776-39784.

Ferch, U., Kloo, B., Gewies, A., Pfander, V., Duwel, M., Peschel, C., Krappmann, D., and Ruland, J. (2009). Inhibition of MALT1 protease activity is selectively toxic for activated B cell-like diffuse large B cell lymphoma cells. *J Exp Med* 206, 2313-2320.

Flinn, I.W., Bartlett, N.L., Blum, K.A., Ardeschna, K.M., LaCasce, A.S., Flowers, C.R., Shustov, A.R., Thress, K.S., Mitchell, P., Zheng, F., *et al.* (2016). A phase II trial to evaluate the efficacy of fostamatinib in patients with relapsed or refractory diffuse large B-cell lymphoma (DLBCL). *Eur J Cancer* 54, 11-17.

Florens, L., Carozza, M.J., Swanson, S.K., Fournier, M., Coleman, M.K., Workman, J.L., and Washburn, M.P. (2006). Analyzing chromatin remodeling complexes using shotgun proteomics and normalized spectral abundance factors. *Methods* 40, 303-311.

Florens, L., and Washburn, M.P. (2006). Proteomic analysis by multidimensional protein identification technology. *Methods Mol Biol* 328, 159-175.

Fontan, L., Yang, C.H., Kabaleeswaran, V., Volpon, L., Osborne, M.J., Beltran, E., Garcia, M., Cerchietti, L., Shaknovich, R., Yang, S.N., *et al.* (2012). MALT1 Small Molecule Inhibitors Specifically Suppress ABC-DLBCL In Vitro and In Vivo. *Cancer Cell* 22, 812-824.

Fuchs, S.Y., Dolan, L., Davis, R.J., and Ronai, Z. (1996). Phosphorylation-dependent targeting of c-Jun ubiquitination by Jun N-kinase. *Oncogene* 13, 1531-1535.

Glasmacher, E., Hoefig, K.P., Vogel, K.U., Rath, N., Du, L., Wolf, C., Kremmer, E., Wang, X., and Heissmeyer, V. (2010). Roquin binds inducible costimulator mRNA and effectors of mRNA decay to induce microRNA-independent post-transcriptional repression. *Nat Immunol* *11*, 725-733.

Green, M.R., Vicente-Duenas, C., Romero-Camarero, I., Long Liu, C., Dai, B., Gonzalez-Herrero, I., Garcia-Ramirez, I., Alonso-Escudero, E., Iqbal, J., Chan, W.C., *et al.* (2014). Transient expression of Bcl6 is sufficient for oncogenic function and induction of mature B-cell lymphoma. *Nat Commun* *5*, 3904.

Gunawardana, J., Chan, F.C., Telenius, A., Woolcock, B., Kridel, R., Tan, K.L., Ben-Neriah, S., Mottok, A., Lim, R.S., Boyle, M., *et al.* (2014). Recurrent somatic mutations of PTPN1 in primary mediastinal B cell lymphoma and Hodgkin lymphoma. *Nat Genet* *46*, 329-335.

Guo, D., Wu, B., Yan, J., Li, X., Sun, H., and Zhou, D. (2012). A possible gene silencing mechanism: hypermethylation of the Keap1 promoter abrogates binding of the transcription factor Sp1 in lung cancer cells. *Biochem Biophys Res Commun* *428*, 80-85.

Gupta-Rossi, N., Storck, S., Griebel, P.J., Reynaud, C.A., Weill, J.C., and Dahan, A. (2003). Specific over-expression of deltex and a new Kelch-like protein in human germinal center B cells. *Mol Immunol* *39*, 791-799.

Hailfinger, S., Lenz, G., Ngo, V., Posvitz-Fejfar, A., Rebeaud, F., Guzzardi, M., Penas, E.M., Dierlamm, J., Chan, W.C., Staudt, L.M., *et al.* (2009). Essential role of MALT1 protease activity in activated B cell-like diffuse large B-cell lymphoma. *Proc Natl Acad Sci U S A* *106*, 19946-19951.

Hatzivassiliou, G., Zhao, F., Bauer, D.E., Andreadis, C., Shaw, A.N., Dhanak, D., Hingorani, S.R., Tuveson, D.A., and Thompson, C.B. (2005). ATP citrate lyase inhibition can suppress tumor cell growth. *Cancer Cell* *8*, 311-321.

Heffetz, D., Bushkin, I., Dror, R., and Zick, Y. (1990). The insulinomimetic agents H₂O₂ and vanadate stimulate protein tyrosine phosphorylation in intact cells. *J Biol Chem* *265*, 2896-2902.

Hershko, A., and Ciechanover, A. (1998). The ubiquitin system. *Annu Rev Biochem* *67*, 425-479.

Hideshima, T., Mitsiades, C., Akiyama, M., Hayashi, T., Chauhan, D., Richardson, P., Schlossman, R., Podar, K., Munshi, N.C., Mitsiades, N., *et al.* (2003). Molecular mechanisms mediating antimyeloma activity of proteasome inhibitor PS-341. *Blood* *101*, 1530-1534.

Honma, K., Tsuzuki, S., Nakagawa, M., Tagawa, H., Nakamura, S., Morishima, Y., and Seto, M. (2009). TNFAIP3/A20 functions as a novel tumor suppressor gene in several subtypes of non-Hodgkin lymphomas. *Blood* *114*, 2467-2475.

Huang, D.W., Sherman, B.T., and Lempicki, R.A. (2009a). Bioinformatics enrichment tools: paths toward the comprehensive functional analysis of large gene lists. *Nucleic Acids Research* *37*, 1-13.

Huang, D.W., Sherman, B.T., and Lempicki, R.A. (2009c). Systematic and integrative analysis of large gene lists using DAVID bioinformatics resources. *Nature Protocols* *4*, 44-57.

- Hunter, T. (2007). The age of crosstalk: phosphorylation, ubiquitination, and beyond. *Mol Cell* 28, 730-738.
- Hymowitz, S.G., and Wertz, I.E. (2010). A20: from ubiquitin editing to tumour suppression. *Nat Rev Cancer* 10, 332-341.
- Idoia, G.R., Shrishrimal, S., Gonzalez-Herrero, I., Martin-Lorenzo, A., Rodriguez-Hernandez, G., Duval, R., Moore, D., Ruiz-Roca, L., Blanco, O., Alonso-Lopez, D., *et al.* (2016). CREBBP Loss Cooperates with BCL2 Over-Expression to Promote Lymphoma in Mice. *Blood* 128.
- Imajoh-Ohmi, S., Kawaguchi, T., Sugiyama, S., Tanaka, K., Omura, S., and Kikuchi, H. (1995). Lactacystin, a specific inhibitor of the proteasome, induces apoptosis in human monoblast U937 cells. *Biochem Biophys Res Commun* 217, 1070-1077.
- Islam, A., and Ambrus, J.L. (2008). Bortezomib plus melphalan and prednisone for multiple myeloma. *N Engl J Med* 359, 2613; author reply 2613-2614.
- Itoh, K., Wakabayashi, N., Katoh, Y., Ishii, T., Igarashi, K., Engel, J.D., and Yamamoto, M. (1999). Keap1 represses nuclear activation of antioxidant responsive elements by Nrf2 through binding to the amino-terminal Neh2 domain. *Genes Dev* 13, 76-86.
- Iwasaki, A., and Medzhitov, R. (2010). Regulation of adaptive immunity by the innate immune system. *Science* 327, 291-295.
- Jagannath, S., Barlogie, B., Berenson, J., Siegel, D., Irwin, D., Richardson, P.G., Niesvizky, R., Alexanian, R., Limentani, S.A., Alsina, M., *et al.* (2004). A phase 2 study of two doses of bortezomib in relapsed or refractory myeloma. *Br J Haematol* 127, 165-172.
- Jeltsch, K.M., Hu, D., Brenner, S., Zoller, J., Heinz, G.A., Nagel, D., Vogel, K.U., Rehage, N., Warth, S.C., Edelmann, S.L., *et al.* (2014). Cleavage of roquin and regnase-1 by the paracaspase MALT1 releases their cooperatively repressed targets to promote T(H)17 differentiation. *Nat Immunol* 15, 1079-1089.
- Jerkeman, M., Hallek, M., Dreyling, M., Thieblemont, C., Kimby, E., and Staudt, L. (2017). Targeting of B-cell receptor signalling in B-cell malignancies. *J Intern Med* 282, 415-428.
- Ji, L., Li, H., Gao, P., Shang, G., Zhang, D.D., Zhang, N., and Jiang, T. (2013). Nrf2 pathway regulates multidrug-resistance-associated protein 1 in small cell lung cancer. *PLoS One* 8, e63404.
- Ji, Y.R., Kim, H.J., Yu, D.H., Bae, K.B., Park, S.J., Yi, J.K., Kim, N., Park, S.J., Oh, K.B., Hwang, S.S., *et al.* (2012). Enforced expression of roquin protein in T cells exacerbates the incidence and severity of experimental arthritis. *J Biol Chem* 287, 42269-42277.
- Julien, S.G., Dube, N., Hardy, S., and Tremblay, M.L. (2011). Inside the human cancer tyrosine phosphatome. *Nat Rev Cancer* 11, 35-49.
- Kan, Z., Jaiswal, B.S., Stinson, J., Janakiraman, V., Bhatt, D., Stern, H.M., Yue, P., Haverty, P.M., Bourgon, R., Zheng, J., *et al.* (2010). Diverse somatic mutation patterns and pathway alterations in human cancers. *Nature* 466, 869-873.
- Kane, R.C., Bross, P.F., Farrell, A.T., and Pazdur, R. (2003). Velcade: U.S. FDA approval for the treatment of multiple myeloma progressing on prior therapy. *Oncologist* 8, 508-513.

Kane, R.C., Farrell, A.T., Sridhara, R., and Pazdur, R. (2006). United States Food and Drug Administration approval summary: bortezomib for the treatment of progressive multiple myeloma after one prior therapy. *Clin Cancer Res* 12, 2955-2960.

Kang, M.I., Kobayashi, A., Wakabayashi, N., Kim, S.G., and Yamamoto, M. (2004). Scaffolding of Keap1 to the actin cytoskeleton controls the function of Nrf2 as key regulator of cytoprotective phase 2 genes. *Proc Natl Acad Sci U S A* 101, 2046-2051.

Kato, M., Sanada, M., Kato, I., Sato, Y., Takita, J., Takeuchi, K., Niwa, A., Chen, Y., Nakazaki, K., Nomoto, J., *et al.* (2009). Frequent inactivation of A20 in B-cell lymphomas. *Nature* 459, 712-716.

Kawakami, T., Chiba, T., Suzuki, T., Iwai, K., Yamanaka, K., Minato, N., Suzuki, H., Shimbara, N., Hidaka, Y., Osaka, F., *et al.* (2001). NEDD8 recruits E2-ubiquitin to SCF E3 ligase. *EMBO J* 20, 4003-4012.

Khosravi, R., Maya, R., Gottlieb, T., Oren, M., Shiloh, Y., and Shkedy, D. (1999). Rapid ATM-dependent phosphorylation of MDM2 precedes p53 accumulation in response to DNA damage. *Proc Natl Acad Sci U S A* 96, 14973-14977.

Kigoshi, Y., Tsuruta, F., and Chiba, T. (2011). Ubiquitin ligase activity of Cul3-KLHL7 protein is attenuated by autosomal dominant retinitis pigmentosa causative mutation. *J Biol Chem* 286, 33613-33621.

Kim, H.J., Ji, Y.R., Kim, M.O., Yu, D.H., Shin, M.J., Yuh, H.S., Bae, K.B., Park, S., Yi, J.K., Kim, N.R., *et al.* (2012). The role of Roquin overexpression in the modulation of signaling during in vitro and ex vivo T-cell activation. *Biochem Biophys Res Commun* 417, 280-286.

Kirisako, T., Kamei, K., Murata, S., Kato, M., Fukumoto, H., Kanie, M., Sano, S., Tokunaga, F., Tanaka, K., and Iwai, K. (2006). A ubiquitin ligase complex assembles linear polyubiquitin chains. *EMBO J* 25, 4877-4887.

Kobayashi, A., Kang, M.I., Okawa, H., Ohtsuji, M., Zenke, Y., Chiba, T., Igarashi, K., and Yamamoto, M. (2004). Oxidative stress sensor Keap1 functions as an adaptor for Cul3-based E3 ligase to regulate proteasomal degradation of Nrf2. *Mol Cell Biol* 24, 7130-7139.

Kominami, K., and Toda, T. (1997). Fission yeast WD-repeat protein pop1 regulates genome ploidy through ubiquitin-proteasome-mediated degradation of the CDK inhibitor Rum1 and the S-phase initiator Cdc18. *Genes Dev* 11, 1548-1560.

Konstantinopoulos, P.A., Spentzos, D., Fountzilas, E., Francoeur, N., Sanisetty, S., Grammatikos, A.P., Hecht, J.L., and Cannistra, S.A. (2011). Keap1 mutations and Nrf2 pathway activation in epithelial ovarian cancer. *Cancer Res* 71, 5081-5089.

Kroll, J., Shi, X., Caprioli, A., Liu, H.H., Waskow, C., Lin, K.M., Miyazaki, T., Rodewald, H.R., and Sato, T.N. (2005). The BTB-kelch protein KLHL6 is involved in B-lymphocyte antigen receptor signaling and germinal center formation. *Mol Cell Biol* 25, 8531-8540.

Kuchay, S., Duan, S., Schenkein, E., Peschiaroli, A., Saraf, A., Florens, L., Washburn, M.P., and Pagano, M. (2013). FBXL2- and PTPL1-mediated degradation of p110-free p85beta regulatory subunit controls the PI(3)K signalling cascade. *Nat Cell Biol* 15, 472-480.

- Kunder, C.A., Roncador, G., Advani, R.H., Gualco, G., Bacchi, C.E., Sabile, J.M., Lossos, I.S., Nie, K., Tibshirani, R.J., Green, M.R., *et al.* (2017). KLHL6 Is Preferentially Expressed in Germinal Center-Derived B-Cell Lymphomas. *Am J Clin Pathol* 148, 465-476.
- Kurosu, T., Fukuda, T., Miki, T., and Miura, O. (2003). BCL6 overexpression prevents increase in reactive oxygen species and inhibits apoptosis induced by chemotherapeutic reagents in B-cell lymphoma cells. *Oncogene* 22, 4459-4468.
- Kurz, T., Pintard, L., Willis, J.H., Hamill, D.R., Gonczy, P., Peter, M., and Bowerman, B. (2002). Cytoskeletal regulation by the Nedd8 ubiquitin-like protein modification pathway. *Science* 295, 1294-1298.
- Launay, E., Pangault, C., Bertrand, P., Jardin, F., Lamy, T., Tilly, H., Tarte, K., Bastard, C., and Fest, T. (2012). High rate of TNFRSF14 gene alterations related to 1p36 region in de novo follicular lymphoma and impact on prognosis. *Leukemia* 26, 559-562.
- Lee, Y.R., Yuan, W.C., Ho, H.C., Chen, C.H., Shih, H.M., and Chen, R.H. (2010). The Cullin 3 substrate adaptor KLHL20 mediates DAPK ubiquitination to control interferon responses. *EMBO J* 29, 1748-1761.
- Leiserson, M.D.M., Reyna, M.A., and Raphael, B.J. (2016). A weighted exact test for mutually exclusive mutations in cancer. *Bioinformatics* 32, 736-745.
- Lenz, G., Davis, R.E., Ngo, V.N., Lam, L., George, T.C., Wright, G.W., Dave, S.S., Zhao, H., Xu, W., Rosenwald, A., *et al.* (2008a). Oncogenic CARD11 mutations in human diffuse large B cell lymphoma. *Science* 319, 1676-1679.
- Lenz, G., Nagel, I., Siebert, R., Roschke, A.V., Sanger, W., Wright, G.W., Dave, S.S., Tan, B., Zhao, H., Rosenwald, A., *et al.* (2007). Aberrant immunoglobulin class switch recombination and switch translocations in activated B cell-like diffuse large B cell lymphoma. *Journal of Experimental Medicine* 204, 633-643.
- Lenz, G., Wright, G., Dave, S.S., Xiao, W., Powell, J., Zhao, H., Xu, W., Tan, B., Goldschmidt, N., Iqbal, J., *et al.* (2008f). Stromal gene signatures in large-B-cell lymphomas. *N Engl J Med* 359, 2313-2323.
- Leo Meriranta, A.P., Alejandra Cervera, Harald Holte Jr., Rainer Lehtonen, Sampsa Hautaniemi and Sirpa Leppä (2016). Low Expression and Somatic Mutations of the KLHL6 Gene Predict Poor Survival in Patients with Activated B-Cell like Diffuse Large B-Cell Lymphoma. *Blood vol. 128 no. 22* 2926.
- Leppek, K., Schott, J., Reitter, S., Poetz, F., Hammond, M.C., and Stoecklin, G. (2013). Roquin promotes constitutive mRNA decay via a conserved class of stem-loop recognition motifs. *Cell* 153, 869-881.
- Li, G., Ci, W., Karmakar, S., Chen, K., Dhar, R., Fan, Z., Guo, Z., Zhang, J., Ke, Y., Wang, L., *et al.* (2014). SPOP promotes tumorigenesis by acting as a key regulatory hub in kidney cancer. *Cancer Cell* 25, 455-468.
- Li, H., Handsaker, B., Wysoker, A., Fennell, T., Ruan, J., Homer, N., Marth, G., Abecasis, G., Durbin, R., and Genome Project Data Processing, S. (2009). The Sequence Alignment/Map format and SAMtools. *Bioinformatics* 25, 2078-2079.
- Liberzon, A., Subramanian, A., Pinchback, R., Thorvaldsdottir, H., Tamayo, P., and Mesirov, J.P. (2011). Molecular signatures database (MSigDB) 3.0. *Bioinformatics* 27, 1739-1740.

- Lin, S.C., Chung, J.Y., Lamothe, B., Rajashankar, K., Lu, M., Lo, Y.C., Lam, A.Y., Darnay, B.G., and Wu, H. (2008). Molecular basis for the unique deubiquitinating activity of the NF-kappaB inhibitor A20. *J Mol Biol* 376, 526-540.
- Liu, X., Yang, N., Figel, S.A., Wilson, K.E., Morrison, C.D., Gelman, I.H., and Zhang, J. (2013). PTPN14 interacts with and negatively regulates the oncogenic function of YAP. *Oncogene* 32, 1266-1273.
- Lo, S.C., Li, X.C., Henzl, M.T., Beamer, L.J., and Hannink, M. (2006). Structure of the Keap1 : Nrf2 interface provides mechanistic insight into Nrf2 signaling. *Embo Journal* 25, 3605-3617.
- Lohr, J.G., Stojanov, P., Carter, S.L., Cruz-Gordillo, P., Lawrence, M.S., Auclair, D., Sougnez, C., Knoechel, B., Gould, J., Saksena, G., *et al.* (2014). Widespread genetic heterogeneity in multiple myeloma: implications for targeted therapy. *Cancer Cell* 25, 91-101.
- Lohr, J.G., Stojanov, P., Lawrence, M.S., Auclair, D., Chapuy, B., Sougnez, C., Cruz-Gordillo, P., Knoechel, B., Asmann, Y.W., Slager, S.L., *et al.* (2012). Discovery and prioritization of somatic mutations in diffuse large B-cell lymphoma (DLBCL) by whole-exome sequencing. *Proc Natl Acad Sci U S A* 109, 3879-3884.
- Love, M.I., Huber, W., and Anders, S. (2014). Moderated estimation of fold change and dispersion for RNA-seq data with DESeq2. *Genome Biol* 15, 550.
- Luke-Glaser, S., Pintard, L., Lu, C., Mains, P.E., and Peter, M. (2005). The BTB protein MEL-26 promotes cytokinesis in *C. elegans* by a CUL-3-independent mechanism. *Curr Biol* 15, 1605-1615.
- Lydeard, J.R., Schulman, B.A., and Harper, J.W. (2013). Building and remodelling Cullin-RING E3 ubiquitin ligases. *EMBO Rep* 14, 1050-1061.
- Maerki, S., Olma, M.H., Staubli, T., Steigemann, P., Gerlich, D.W., Quadroni, M., Sumara, I., and Peter, M. (2009). The Cul3-KLHL21 E3 ubiquitin ligase targets aurora B to midzone microtubules in anaphase and is required for cytokinesis. *J Cell Biol* 187, 791-800.
- Mani, R.S. (2014). The emerging role of speckle-type POZ protein (SPOP) in cancer development. *Drug Discov Today* 19, 1498-1502.
- Mansouri, L., Noerenberg, D., Young, E., Mylonas, E., Abdulla, M., Frick, M., Asmar, F., Ljungstrom, V., Schneider, M., Yoshida, K., *et al.* (2016). Frequent NFKBIE deletions are associated with poor outcome in primary mediastinal B-cell lymphoma. *Blood* 128, 2666-2670.
- Maruyama, T., Araki, T., Kawarazaki, Y., Naguro, I., Heynen, S., Aza-Blanc, P., Ronai, Z., Matsuzawa, A., and Ichijo, H. (2014). Roquin-2 promotes ubiquitin-mediated degradation of ASK1 to regulate stress responses. *Sci Signal* 7, ra8.
- McDonald, W.H., Ohi, R., Miyamoto, D.T., Mitchison, T.J., and Yates, J.R. (2002). Comparison of three directly coupled HPLC MS/MS strategies for identification of proteins from complex mixtures: single-dimension LC-MS/MS, 2-phase MudPIT, and 3-phase MudPIT. *International Journal of Mass Spectrometry* 219, 245-251.
- McMahon, M., Thomas, N., Itoh, K., Yamamoto, M., and Hayes, J.D. (2006). Dimerization of substrate adaptors can facilitate cullin-mediated ubiquitylation of

proteins by a "tethering" mechanism: a two-site interaction model for the Nrf2-Keap1 complex. *J Biol Chem* *281*, 24756-24768.

Mello, S.S., Valente, L.J., Raj, N., Seoane, J.A., Flowers, B.M., McClendon, J., Bieging-Rolett, K.T., Lee, J., Ivanochko, D., Kozak, M.M., *et al.* (2017). A p53 Super-tumor Suppressor Reveals a Tumor Suppressive p53-Ptpn14-Yap Axis in Pancreatic Cancer. *Cancer Cell* *32*, 460-473 e466.

Melnick, A., Ahmad, K.F., Arai, S., Polinger, A., Ball, H., Borden, K.L., Carlile, G.W., Prive, G.G., and Licht, J.D. (2000). In-depth mutational analysis of the promyelocytic leukemia zinc finger BTB/POZ domain reveals motifs and residues required for biological and transcriptional functions. *Mol Cell Biol* *20*, 6550-6567.

Menendez, J.A., and Lupu, R. (2007). Fatty acid synthase and the lipogenic phenotype in cancer pathogenesis. *Nat Rev Cancer* *7*, 763-777.

Meriranta, L., Pasanen, A., Cervera, A., Holte, H., Lehtonen, R., Hautaniemi, S., and Leppa, S. (2016). Low Expression and Somatic Mutations of the KLHL6 Gene Predict Poor Survival in Patients with Activated B-Cell like Diffuse Large B-Cell Lymphoma. *Blood* *128*.

Michel, J.J., McCarville, J.F., and Xiong, Y. (2003). A role for *Saccharomyces cerevisiae* Cul8 ubiquitin ligase in proper anaphase progression. *J Biol Chem* *278*, 22828-22837.

Milgram, L.Z., Witters, L.A., Pasternack, G.R., and Kuhajda, F.P. (1997). Enzymes of the fatty acid synthesis pathway are highly expressed in in situ breast carcinoma. *Clin Cancer Res* *3*, 2115-2120.

Milhollen, M.A., Traore, T., Adams-Duffy, J., Thomas, M.P., Berger, A.J., Dang, L., Dick, L.R., Garnsey, J.J., Koenig, E., Langston, S.P., *et al.* (2010). MLN4924, a NEDD8-activating enzyme inhibitor, is active in diffuse large B-cell lymphoma models: rationale for treatment of NF-kappa B-dependent lymphoma. *Blood* *116*, 1515-1523.

Mitsiades, N., Mitsiades, C.S., Poulaki, V., Chauhan, D., Fanourakis, G., Gu, X., Bailey, C., Joseph, M., Libermann, T.A., Treon, S.P., *et al.* (2002). Molecular sequelae of proteasome inhibition in human multiple myeloma cells. *Proc Natl Acad Sci U S A* *99*, 14374-14379.

Moeller, H.B., Praetorius, J., Rutzler, M.R., and Fenton, R.A. (2010). Phosphorylation of aquaporin-2 regulates its endocytosis and protein-protein interactions. *Proc Natl Acad Sci U S A* *107*, 424-429.

Moghe, S., Jiang, F., Miura, Y., Cerny, R.L., Tsai, M.Y., and Furukawa, M. (2012). The CUL3-KLHL18 ligase regulates mitotic entry and ubiquitylates Aurora-A. *Biol Open* *1*, 82-91.

Monti, S., Chapuy, B., Takeyama, K., Rodig, S.J., Hao, Y., Yeda, K.T., Inguilizian, H., Mermel, C., Currie, T., Dogan, A., *et al.* (2012). Integrative analysis reveals an outcome-associated and targetable pattern of p53 and cell cycle deregulation in diffuse large B cell lymphoma. *Cancer Cell* *22*, 359-372.

Morin, R.D., Mendez-Lago, M., Mungall, A.J., Goya, R., Mungall, K.L., Corbett, R.D., Johnson, N.A., Severson, T.M., Chiu, R., Field, M., *et al.* (2011). Frequent mutation of histone-modifying genes in non-Hodgkin lymphoma. *Nature*.

Motohashi, H., and Yamamoto, M. (2004). Nrf2-Keap1 defines a physiologically important stress response mechanism. *Trends Mol Med* *10*, 549-557.

Murakawa, Y., Hinz, M., Mothes, J., Schuetz, A., Uhl, M., Wyler, E., Yasuda, T., Mastrobuoni, G., Friedel, C.C., Dolken, L., *et al.* (2015). RC3H1 post-transcriptionally regulates A20 mRNA and modulates the activity of the IKK/NF-kappaB pathway. *Nat Commun* 6, 7367.

Murphy, T.L., and Murphy, K.M. (2010). Slow down and survive: Enigmatic immunoregulation by BTLA and HVEM. *Annu Rev Immunol* 28, 389-411.

Nawrocki, S.T., Carew, J.S., Dunner, K., Jr., Boise, L.H., Chiao, P.J., Huang, P., Abbruzzese, J.L., and McConkey, D.J. (2005a). Bortezomib inhibits PKR-like endoplasmic reticulum (ER) kinase and induces apoptosis via ER stress in human pancreatic cancer cells. *Cancer Res* 65, 11510-11519.

Nawrocki, S.T., Carew, J.S., Pino, M.S., Highshaw, R.A., Dunner, K., Jr., Huang, P., Abbruzzese, J.L., and McConkey, D.J. (2005b). Bortezomib sensitizes pancreatic cancer cells to endoplasmic reticulum stress-mediated apoptosis. *Cancer Res* 65, 11658-11666.

Ngo, V.N., Davis, R.E., Lamy, L., Yu, X., Zhao, H., Lenz, G., Lam, L.T., Dave, S., Yang, L., Powell, J., *et al.* (2006). A loss-of-function RNA interference screen for molecular targets in cancer. *Nature* 441, 106-110.

Ngo, V.N., Young, R.M., Schmitz, R., Jhavar, S., Xiao, W., Lim, K.H., Kohlhammer, H., Xu, W., Yang, Y., Zhao, H., *et al.* (2011). Oncogenically active MYD88 mutations in human lymphoma. *Nature* 470, 115-119.

Nguyen, L.K., Munoz-Garcia, J., Maccario, H., Ciechanover, A., Kolch, W., and Kholodenko, B.N. (2011). Switches, excitable responses and oscillations in the Ring1B/Bmi1 ubiquitination system. *PLoS Comput Biol* 7, e1002317.

Nijman, S.M., Luna-Vargas, M.P., Velds, A., Brummelkamp, T.R., Dirac, A.M., Sixma, T.K., and Bernards, R. (2005). A genomic and functional inventory of deubiquitinating enzymes. *Cell* 123, 773-786.

Novak, U., Rinaldi, A., Kwee, I., Nandula, S.V., Rancoita, P.M., Compagno, M., Cerri, M., Rossi, D., Murty, V.V., Zucca, E., *et al.* (2009). The NF- κ B negative regulator TNFAIP3 (A20) is inactivated by somatic mutations and genomic deletions in marginal zone lymphomas. *Blood* 113, 4918-4921.

Obeng, E.A., Carlson, L.M., Gutman, D.M., Harrington, W.J., Jr., Lee, K.P., and Boise, L.H. (2006). Proteasome inhibitors induce a terminal unfolded protein response in multiple myeloma cells. *Blood* 107, 4907-4916.

Oeckinghaus, A., Wegener, E., Welteke, V., Ferch, U., Arslan, S.C., Ruland, J., Scheidereit, C., and Krappmann, D. (2007). Malt1 ubiquitination triggers NF-kappaB signaling upon T-cell activation. *EMBO J* 26, 4634-4645.

Ogata, M., Takada, T., Mori, Y., Oh-hora, M., Uchida, Y., Kosugi, A., Miyake, K., and Hamaoka, T. (1999). Effects of overexpression of PTP36, a putative protein tyrosine phosphatase, on cell adhesion, cell growth, and cytoskeletons in HeLa cells. *J Biol Chem* 274, 12905-12909.

Ohta, T., Iijima, K., Miyamoto, M., Nakahara, I., Tanaka, H., Ohtsuji, M., Suzuki, T., Kobayashi, A., Yokota, J., Sakiyama, T., *et al.* (2008). Loss of Keap1 function activates Nrf2 and provides advantages for lung cancer cell growth. *Cancer Res* 68, 1303-1309.

Orlowski, R.Z., Eswara, J.R., Lafond-Walker, A., Grever, M.R., Orlowski, M., and Dang, C.V. (1998). Tumor growth inhibition induced in a murine model of human Burkitt's lymphoma by a proteasome inhibitor. *Cancer Res* 58, 4342-4348.

Osaka, F., Saeki, M., Katayama, S., Aida, N., Toh, E.A., Kominami, K., Toda, T., Suzuki, T., Chiba, T., Tanaka, K., *et al.* (2000). Covalent modifier NEDD8 is essential for SCF ubiquitin-ligase in fission yeast. *EMBO J* 19, 3475-3484.

Paoletti, A.C., Parmely, T.J., Tomomori-Sato, C., Sato, S., Zhu, D., Conaway, R.C., Conaway, J.W., Florens, L., and Washburn, M.P. (2006). Quantitative proteomic analysis of distinct mammalian Mediator complexes using normalized spectral abundance factors. *Proc Natl Acad Sci U S A* 103, 18928-18933.

Papandreou, C.N., Daliani, D.D., Nix, D., Yang, H., Madden, T., Wang, X., Pien, C.S., Millikan, R.E., Tu, S.M., Pagliaro, L., *et al.* (2004). Phase I trial of the proteasome inhibitor bortezomib in patients with advanced solid tumors with observations in androgen-independent prostate cancer. *J Clin Oncol* 22, 2108-2121.

Parekh, S., Polo, J.M., Shakhovich, R., Juszczynski, P., Lev, P., Ranuncolo, S.M., Yin, Y., Klein, U., Cattoretti, G., Dalla Favera, R., *et al.* (2007). BCL6 programs lymphoma cells for survival and differentiation through distinct biochemical mechanisms. *Blood* 110, 2067-2074.

Parkhomchuk, D., Borodina, T., Amstislavskiy, V., Banaru, M., Hallen, L., Krobitch, S., Lehrach, H., and Soldatov, A. (2009). Transcriptome analysis by strand-specific sequencing of complementary DNA. *Nucleic Acids Res* 37, e123.

Pasqualucci, L., and Dalla-Favera, R. (2015). The genetic landscape of diffuse large B-cell lymphoma. *Semin Hematol* 52, 67-76.

Pasqualucci, L., Neumeister, P., Goossens, T., Nanjangud, G., Chaganti, R.S., Kupperts, R., and Dalla-Favera, R. (2001). Hypermethylation of multiple proto-oncogenes in B-cell diffuse large-cell lymphomas. *Nature* 412, 341-346.

Pelzer, C., Cabalzar, K., Wolf, A., Gonzalez, M., Lenz, G., and Thome, M. (2013). The protease activity of the paracaspase MALT1 is controlled by monoubiquitination. *Nat Immunol* 14, 337-345.

Perez-Torrado, R., Yamada, D., and Defossez, P.A. (2006). Born to bind: the BTB protein-protein interaction domain. *Bioessays* 28, 1194-1202.

Petroski, M.D., and Deshaies, R.J. (2005a). Function and regulation of cullin-RING ubiquitin ligases. *Nat Rev Mol Cell Biol* 6, 9-20.

Petroski, M.D., and Deshaies, R.J. (2005c). Function and regulation of cullin-RING ubiquitin ligases. *Nature reviews. Molecular cell biology* 6, 9-20.

Phan, R.T., and Dalla-Favera, R. (2004). The BCL6 proto-oncogene suppresses p53 expression in germinal-centre B cells. *Nature* 432, 635-639.

Pintard, L., Willems, A., and Peter, M. (2004). Cullin-based ubiquitin ligases: Cul3-BTB complexes join the family. *EMBO J* 23, 1681-1687.

Pratama, A., Ramiscal, R.R., Silva, D.G., Das, S.K., Athanasopoulos, V., Fitch, J., Botelho, N.K., Chang, P.P., Hu, X., Hogan, J.J., *et al.* (2013). Roquin-2 shares functions with its paralog Roquin-1 in the repression of mRNAs controlling T follicular helper cells and systemic inflammation. *Immunity* 38, 669-680.

- Provost, E., Weier, C.A., and Leach, S.D. (2013). Multiple ribosomal proteins are expressed at high levels in developing zebrafish endoderm and are required for normal exocrine pancreas development. *Zebrafish* 10, 161-169.
- Puente, X.S., Bea, S., Valdes-Mas, R., Villamor, N., Gutierrez-Abril, J., Martin-Subero, J.I., Munar, M., Rubio-Perez, C., Jares, P., Aymerich, M., *et al.* (2015). Non-coding recurrent mutations in chronic lymphocytic leukaemia. *Nature* 526, 519-524.
- Puente, X.S., Pinyol, M., Quesada, V., Conde, L., Ordonez, G.R., Villamor, N., Escaramis, G., Jares, P., Bea, S., Gonzalez-Diaz, M., *et al.* (2011). Whole-genome sequencing identifies recurrent mutations in chronic lymphocytic leukaemia. *Nature* 475, 101-105.
- Ramiscal, R.R., Parish, I.A., Lee-Young, R.S., Babon, J.J., Blagih, J., Pratama, A., Martin, J., Hawley, N., Cappello, J.Y., Nieto, P.F., *et al.* (2015). Attenuation of AMPK signaling by ROQUIN promotes T follicular helper cell formation. *Elife* 4.
- Read, M.A., Brownell, J.E., Gladysheva, T.B., Hottelet, M., Parent, L.A., Coggins, M.B., Pierce, J.W., Podust, V.N., Luo, R.S., Chau, V., *et al.* (2000). Nedd8 modification of cul-1 activates SCF(beta(TrCP))-dependent ubiquitination of I kappa B alpha. *Mol Cell Biol* 20, 2326-2333.
- Rebeaud, F., Hailfinger, S., Posevitz-Fejfar, A., Tapernoux, M., Moser, R., Rueda, D., Gaide, O., Guzzardi, M., Iancu, E.M., Rufer, N., *et al.* (2008). The proteolytic activity of the paracaspase MALT1 is key in T cell activation. *Nat Immunol* 9, 272-281.
- Reddy, A., Zhang, J., Davis, N.S., Moffitt, A.B., Love, C.L., Waldrop, A., Leppa, S., Pasanen, A., Meriranta, L., Karjalainen-Lindsberg, M.L., *et al.* (2017). Genetic and Functional Drivers of Diffuse Large B Cell Lymphoma. *Cell* 171, 481-494 e415.
- Reich, M., Liefeld, T., Gould, J., Lerner, J., Tamayo, P., and Mesirov, J.P. (2006). GenePattern 2.0. *Nat Genet* 38, 500-501.
- Reineke, E.L., Liu, Y., and Kao, H.Y. (2010). Promyelocytic leukemia protein controls cell migration in response to hydrogen peroxide and insulin-like growth factor-1. *J Biol Chem* 285, 9485-9492.
- Richardson, P.G., Barlogie, B., Berenson, J., Singhal, S., Jagannath, S., Irwin, D., Rajkumar, S.V., Srkalovic, G., Alsina, M., Alexanian, R., *et al.* (2003). A phase 2 study of bortezomib in relapsed, refractory myeloma. *N Engl J Med* 348, 2609-2617.
- Richardson, P.G., Barlogie, B., Berenson, J., Singhal, S., Jagannath, S., Irwin, D.H., Rajkumar, S.V., Srkalovic, G., Alsina, M., and Anderson, K.C. (2006). Extended follow-up of a phase II trial in relapsed, refractory multiple myeloma: final time-to-event results from the SUMMIT trial. *Cancer* 106, 1316-1319.
- Robinson, J.T., Thorvaldsdottir, H., Winckler, W., Guttman, M., Lander, E.S., Getz, G., and Mesirov, J.P. (2011). Integrative genomics viewer. *Nat Biotechnol* 29, 24-26.
- Rosenwald, A., Wright, G., Leroy, K., Yu, X., Gaulard, P., Gascoyne, R.D., Chan, W.C., Zhao, T., Haioun, C., Greiner, T.C., *et al.* (2003). Molecular diagnosis of primary mediastinal B cell lymphoma identifies a clinically favorable subgroup of diffuse large B cell lymphoma related to Hodgkin lymphoma. *J Exp Med* 198, 851-862.
- San Miguel, J.F., Schlag, R., Khuageva, N.K., Dimopoulos, M.A., Shpilberg, O., Kropff, M., Spicka, I., Petrucci, M.T., Palumbo, A., Samoilova, O.S., *et al.* (2008). Bortezomib

plus melphalan and prednisone for initial treatment of multiple myeloma. *N Engl J Med* 359, 906-917.

Satpathy, S., Wagner, S.A., Beli, P., Gupta, R., Kristiansen, T.A., Malinova, D., Francavilla, C., Tolar, P., Bishop, G.A., Hostager, B.S., *et al.* (2015). Systems-wide analysis of BCR signalosomes and downstream phosphorylation and ubiquitylation. *Mol Syst Biol* 11, 810.

Schlundt, A., Heinz, G.A., Janowski, R., Geerlof, A., Stehle, R., Heissmeyer, V., Niessing, D., and Sattler, M. (2014). Structural basis for RNA recognition in roquin-mediated post-transcriptional gene regulation. *Nat Struct Mol Biol* 21, 671-678.

Schmitz, R., Hansmann, M.L., Bohle, V., Martin-Subero, J.I., Hartmann, S., Mechttersheimer, G., Klapper, W., Vater, I., Giefing, M., Gesk, S., *et al.* (2009). TNFAIP3 (A20) is a tumor suppressor gene in Hodgkin lymphoma and primary mediastinal B cell lymphoma. *J Exp Med* 206, 981-989.

Scott, D.C., Monda, J.K., Bennett, E.J., Harper, J.W., and Schulman, B.A. (2011). N-terminal acetylation acts as an avidity enhancer within an interconnected multiprotein complex. *Science* 334, 674-678.

Secrist, J.P., Burns, L.A., Karnitz, L., Koretzky, G.A., and Abraham, R.T. (1993). Stimulatory effects of the protein tyrosine phosphatase inhibitor, pervanadate, on T-cell activation events. *J Biol Chem* 268, 5886-5893.

Seet, B.T., Dikic, I., Zhou, M.M., and Pawson, T. (2006). Reading protein modifications with interaction domains. *Nat Rev Mol Cell Biol* 7, 473-483.

Sehat, B., Andersson, S., Vasilcanu, R., Girnita, L., and Larsson, O. (2007). Role of ubiquitination in IGF-1 receptor signaling and degradation. *PLoS One* 2, e340.

Semenza, G.L. (2012). Hypoxia-inducible factors: mediators of cancer progression and targets for cancer therapy. *Trends Pharmacol Sci* 33, 207-214.

Sgromo, A., Raisch, T., Bawankar, P., Bhandari, D., Chen, Y., Kuzuoglu-Ozturk, D., Weichenrieder, O., and Izaurralde, E. (2017). A CAF40-binding motif facilitates recruitment of the CCR4-NOT complex to mRNAs targeted by Drosophila Roquin. *Nat Commun* 8, 14307.

Shaffer, A.L., Rosenwald, A., and Staudt, L.M. (2002). Lymphoid malignancies: the dark side of B-cell differentiation. *Nat Rev Immunol* 2, 920-932.

Shibata, T., Kokubu, A., Gotoh, M., Ojima, H., Ohta, T., Yamamoto, M., and Hirohashi, S. (2008). Genetic alteration of Keap1 confers constitutive Nrf2 activation and resistance to chemotherapy in gallbladder cancer. *Gastroenterology* 135, 1358-1368, 1368 e1351-1354.

Shibata, T., Kokubu, A., Saito, S., Narisawa-Saito, M., Sasaki, H., Aoyagi, K., Yoshimatsu, Y., Tachimori, Y., Kushima, R., Kiyono, T., *et al.* (2011). NRF2 mutation confers malignant potential and resistance to chemoradiation therapy in advanced esophageal squamous cancer. *Neoplasia* 13, 864-873.

Shinohara, K., Tomioka, M., Nakano, H., Tone, S., Ito, H., and Kawashima, S. (1996). Apoptosis induction resulting from proteasome inhibition. *Biochem J* 317 (Pt 2), 385-388.

Siggs, O.M., and Beutler, B. (2012). The BTB-ZF transcription factors. *Cell Cycle* 11, 3358-3369.

- Silverman, J.S., Skaar, J.R., and Pagano, M. (2012). SCF ubiquitin ligases in the maintenance of genome stability. *Trends Biochem Sci* 37, 66-73.
- Singer, J.D., Gurian-West, M., Clurman, B., and Roberts, J.M. (1999). Cullin-3 targets cyclin E for ubiquitination and controls S phase in mammalian cells. *Genes Dev* 13, 2375-2387.
- Singh, A., Misra, V., Thimmulappa, R.K., Lee, H., Ames, S., Hoque, M.O., Herman, J.G., Baylin, S.B., Sidransky, D., Gabrielson, E., *et al.* (2006). Dysfunctional KEAP1-NRF2 interaction in non-small-cell lung cancer. *PLoS Med* 3, e420.
- Sjoblom, T., Jones, S., Wood, L.D., Parsons, D.W., Lin, J., Barber, T.D., Mandelker, D., Leary, R.J., Ptak, J., Silliman, N., *et al.* (2006). The consensus coding sequences of human breast and colorectal cancers. *Science* 314, 268-274.
- Skaar, J.R., Pagan, J.K., and Pagano, M. (2013). Mechanisms and function of substrate recruitment by F-box proteins. *Nat Rev Mol Cell Biol* 14, 369-381.
- Skaug, B., Chen, J., Du, F., He, J., Ma, A., and Chen, Z.J. (2011). Direct, noncatalytic mechanism of IKK inhibition by A20. *Mol Cell* 44, 559-571.
- Smith, A.L., Mitchell, P.J., Shipley, J., Gusterson, B.A., Rogers, M.V., and Crompton, M.R. (1995). Pez: a novel human cDNA encoding protein tyrosine phosphatase- and ezrin-like domains. *Biochem Biophys Res Commun* 209, 959-965.
- Song, L., and Rape, M. (2011). Substrate-specific regulation of ubiquitination by the anaphase-promoting complex. *Cell Cycle* 10, 52-56.
- Soucy, T.A., Smith, P.G., Milhollen, M.A., Berger, A.J., Gavin, J.M., Adhikari, S., Brownell, J.E., Burke, K.E., Cardin, D.P., Critchley, S., *et al.* (2009). An inhibitor of NEDD8-activating enzyme as a new approach to treat cancer. *Nature* 458, 732-736.
- Srinivasula, S.M., and Ashwell, J.D. (2011). A20: more than one way to skin a cat. *Mol Cell* 44, 511-512.
- Staudt, L.M. (2010). Oncogenic activation of NF-kappaB. *Cold Spring Harb Perspect Biol* 2, a000109.
- Staudt, L.M., and Dave, S. (2005). The biology of human lymphoid malignancies revealed by gene expression profiling. *Adv Immunol* 87, 163-208.
- Stogios, P.J., Downs, G.S., Jauhal, J.J., Nandra, S.K., and Prive, G.G. (2005). Sequence and structural analysis of BTB domain proteins. *Genome Biol* 6, R82.
- Szalmas, A., Tomaic, V., Basukala, O., Massimi, P., Mittal, S., Konya, J., and Banks, L. (2017). The PTPN14 Tumor Suppressor Is a Degradation Target of Human Papillomavirus E7. *J Virol* 91.
- Tabb, D.L., McDonald, W.H., and Yates, J.R., 3rd (2002). DTASelect and Contrast: tools for assembling and comparing protein identifications from shotgun proteomics. *J Proteome Res* 1, 21-26.
- Tan, D., Zhou, M., Kiledjian, M., and Tong, L. (2014). The ROQ domain of Roquin recognizes mRNA constitutive-decay element and double-stranded RNA. *Nat Struct Mol Biol* 21, 679-685.
- Tang, X., Orlicky, S., Lin, Z., Willems, A., Neculai, D., Ceccarelli, D., Mercurio, F., Shilton, B.H., Sicheri, F., and Tyers, M. (2007). Suprafacial orientation of the SCFCdc4 dimer accommodates multiple geometries for substrate ubiquitination. *Cell* 129, 1165-1176.

- Tian, B., Nowak, D.E., Jamaluddin, M., Wang, S., and Brasier, A.R. (2005). Identification of direct genomic targets downstream of the nuclear factor-kappaB transcription factor mediating tumor necrosis factor signaling. *J Biol Chem* 280, 17435-17448.
- Turer, E.E., Tavares, R.M., Mortier, E., Hitotsumatsu, O., Advincula, R., Lee, B., Shifrin, N., Malynn, B.A., and Ma, A. (2008). Homeostatic MyD88-dependent signals cause lethal inflammation in the absence of A20. *J Exp Med* 205, 451-464.
- Vinitzky, A., Cardozo, C., Sepp-Lorenzino, L., Michaud, C., and Orłowski, M. (1994). Inhibition of the proteolytic activity of the multicatalytic proteinase complex (proteasome) by substrate-related peptidyl aldehydes. *J Biol Chem* 269, 29860-29866.
- Vinitzky, A., Michaud, C., Powers, J.C., and Orłowski, M. (1992). Inhibition of the chymotrypsin-like activity of the pituitary multicatalytic proteinase complex. *Biochemistry* 31, 9421-9428.
- Vinuesa, C.G., Cook, M.C., Angelucci, C., Athanasopoulos, V., Rui, L., Hill, K.M., Yu, D., Domaschenz, H., Whittle, B., Lambe, T., *et al.* (2005). A RING-type ubiquitin ligase family member required to repress follicular helper T cells and autoimmunity. *Nature* 435, 452-458.
- Visco, C., Li, Y., Xu-Monette, Z.Y., Miranda, R.N., Green, T.M., Li, Y., Tzankov, A., Wen, W., Liu, W.M., Kahl, B.S., *et al.* (2012). Comprehensive gene expression profiling and immunohistochemical studies support application of immunophenotypic algorithm for molecular subtype classification in diffuse large B-cell lymphoma: a report from the International DLBCL Rituximab-CHOP Consortium Program Study. *Leukemia* 26, 2103-2113.
- Vogel, K.U., Edelmann, S.L., Jeltsch, K.M., Bertossi, A., Heger, K., Heinz, G.A., Zoller, J., Warth, S.C., Hoefig, K.P., Lohs, C., *et al.* (2013). Roquin paralogs 1 and 2 redundantly repress the Icos and Ox40 costimulator mRNAs and control follicular helper T cell differentiation. *Immunity* 38, 655-668.
- Wadham, C., Gamble, J.R., Vadas, M.A., and Khew-Goodall, Y. (2000). Translocation of protein tyrosine phosphatase Pez/PTPD2/PTP36 to the nucleus is associated with induction of cell proliferation. *J Cell Sci* 113 (Pt 17), 3117-3123.
- Wadham, C., Gamble, J.R., Vadas, M.A., and Khew-Goodall, Y. (2003). The protein tyrosine phosphatase Pez is a major phosphatase of adherens junctions and dephosphorylates beta-catenin. *Mol Biol Cell* 14, 2520-2529.
- Wang, C.Y., Cusack, J.C., Jr., Liu, R., and Baldwin, A.S., Jr. (1999). Control of inducible chemoresistance: enhanced anti-tumor therapy through increased apoptosis by inhibition of NF-kappaB. *Nat Med* 5, 412-417.
- Wang, C.Y., Mayo, M.W., and Baldwin, A.S., Jr. (1996). TNF- and cancer therapy-induced apoptosis: potentiation by inhibition of NF-kappaB. *Science* 274, 784-787.
- Wang, L., Feng, Z., Wang, X., Wang, X., and Zhang, X. (2010). DEGseq: an R package for identifying differentially expressed genes from RNA-seq data. *Bioinformatics* 26, 136-138.
- Wang, R., An, J., Ji, F., Jiao, H., Sun, H., and Zhou, D. (2008). Hypermethylation of the Keap1 gene in human lung cancer cell lines and lung cancer tissues. *Biochem Biophys Res Commun* 373, 151-154.

- Wang, W., Huang, J., Wang, X., Yuan, J., Li, X., Feng, L., Park, J.I., and Chen, J. (2012). PTPN14 is required for the density-dependent control of YAP1. *Genes Dev* 26, 1959-1971.
- Wang, Z., Shen, D., Parsons, D.W., Bardelli, A., Sager, J., Szabo, S., Ptak, J., Silliman, N., Peters, B.A., van der Heijden, M.S., *et al.* (2004). Mutational analysis of the tyrosine phosphatome in colorectal cancers. *Science* 304, 1164-1166.
- Warner, J.R. (1999). The economics of ribosome biosynthesis in yeast. *Trends Biochem Sci* 24, 437-440.
- Washburn, M.P., Wolters, D., and Yates, J.R., 3rd (2001). Large-scale analysis of the yeast proteome by multidimensional protein identification technology. *Nat Biotechnol* 19, 242-247.
- Wertz, I.E., O'Rourke, K.M., Zhou, H., Eby, M., Aravind, L., Seshagiri, S., Wu, P., Wiesmann, C., Baker, R., Boone, D.L., *et al.* (2004). De-ubiquitination and ubiquitin ligase domains of A20 downregulate NF-kappaB signalling. *Nature* 430, 694-699.
- Wilson, W.H., Young, R.M., Schmitz, R., Yang, Y., Pittaluga, S., Wright, G., Lih, C.J., Williams, P.M., Shaffer, A.L., Gerecitano, J., *et al.* (2015). Targeting B cell receptor signaling with ibrutinib in diffuse large B cell lymphoma. *Nat Med* 21, 922-926.
- Wright, G., Tan, B., Rosenwald, A., Hurt, E.H., Wiestner, A., and Staudt, L.M. (2003). A gene expression-based method to diagnose clinically distinct subgroups of diffuse large B cell lymphoma. *Proc Natl Acad Sci U S A* 100, 9991-9996.
- Wu, J.T., Lin, H.C., Hu, Y.C., and Chien, C.T. (2005). Neddylation and deneddylation regulate Cull1 and Cul3 protein accumulation. *Nat Cell Biol* 7, 1014-1020.
- Yang, Y., Kelly, P., Shaffer, A.L., 3rd, Schmitz, R., Yoo, H.M., Liu, X., Huang, D.W., Webster, D., Young, R.M., Nakagawa, M., *et al.* (2016). Targeting Non-proteolytic Protein Ubiquitination for the Treatment of Diffuse Large B Cell Lymphoma. *Cancer Cell* 29, 494-507.
- Yang, Y., Schmitz, R., Mitala, J., Whiting, A., Xiao, W., Ceribelli, M., Wright, G.W., Zhao, H., Yang, Y., Xu, W., *et al.* (2014). Essential role of the linear ubiquitin chain assembly complex in lymphoma revealed by rare germline polymorphisms. *Cancer Discov* 4, 480-493.
- Yang, Y., Shaffer, A.L., 3rd, Emre, N.C., Ceribelli, M., Zhang, M., Wright, G., Xiao, W., Powell, J., Platig, J., Kohlhammer, H., *et al.* (2012). Exploiting synthetic lethality for the therapy of ABC diffuse large B cell lymphoma. *Cancer Cell* 21, 723-737.
- Yang, Y., and Staudt, L.M. (2015). Protein ubiquitination in lymphoid malignancies. *Immunol Rev* 263, 240-256.
- Ying, J., Li, H., Cui, Y., Wong, A.H., Langford, C., and Tao, Q. (2006). Epigenetic disruption of two proapoptotic genes MAPK10/JNK3 and PTPN13/FAP-1 in multiple lymphomas and carcinomas through hypermethylation of a common bidirectional promoter. *Leukemia* 20, 1173-1175.
- Yoo, N.J., Kim, H.R., Kim, Y.R., An, C.H., and Lee, S.H. (2012). Somatic mutations of the KEAP1 gene in common solid cancers. *Histopathology* 60, 943-952.
- Young, R.M., Shaffer, A.L., 3rd, Phelan, J.D., and Staudt, L.M. (2015). B-cell receptor signaling in diffuse large B-cell lymphoma. *Semin Hematol* 52, 77-85.

- Yu, D., Tan, A.H., Hu, X., Athanasopoulos, V., Simpson, N., Silva, D.G., Hutloff, A., Giles, K.M., Leedman, P.J., Lam, K.P., *et al.* (2007). Roquin represses autoimmunity by limiting inducible T-cell co-stimulator messenger RNA. *Nature* 450, 299-303.
- Yuan, W.C., Lee, Y.R., Huang, S.F., Lin, Y.M., Chen, T.Y., Chung, H.C., Tsai, C.H., Chen, H.Y., Chiang, C.T., Lai, C.K., *et al.* (2011). A Cullin3-KLHL20 Ubiquitin ligase-dependent pathway targets PML to potentiate HIF-1 signaling and prostate cancer progression. *Cancer Cell* 20, 214-228.
- Zhang, C., Liu, J., Huang, G., Zhao, Y., Yue, X., Wu, H., Li, J., Zhu, J., Shen, Z., Haffty, B.G., *et al.* (2016). Cullin3-KLHL25 ubiquitin ligase targets ACLY for degradation to inhibit lipid synthesis and tumor progression. *Genes Dev* 30, 1956-1970.
- Zhang, P., Guo, A., Possemato, A., Wang, C., Beard, L., Carlin, C., Markowitz, S.D., Polakiewicz, R.D., and Wang, Z. (2013). Identification and functional characterization of p130Cas as a substrate of protein tyrosine phosphatase nonreceptor 14. *Oncogene* 32, 2087-2095.
- Zhang, Q., Shi, Q., Chen, Y., Yue, T., Li, S., Wang, B., and Jiang, J. (2009). Multiple Ser/Thr-rich degrons mediate the degradation of Ci/Gli by the Cul3-HIB/SPOP E3 ubiquitin ligase. *Proc Natl Acad Sci U S A* 106, 21191-21196.
- Zhao, B., Barrera, L.A., Ersing, I., Willox, B., Schmidt, S.C.S., Greenfield, H., Zhou, H., Mollo, S.B., Shi, T.T., Takasaki, K., *et al.* (2014). The NF-kappa B Genomic Landscape in Lymphoblastoid B Cells. *Cell Reports* 8, 1595-1606.
- Zhou, A., Scoggin, S., Gaynor, R.B., and Williams, N.S. (2003). Identification of NF-kappa B-regulated genes induced by TNFalpha utilizing expression profiling and RNA interference. *Oncogene* 22, 2054-2064.
- Zhuang, M., Calabrese, M.F., Liu, J., Waddell, M.B., Nourse, A., Hammel, M., Miller, D.J., Walden, H., Duda, D.M., Seyedin, S.N., *et al.* (2009). Structures of SPOP-substrate complexes: insights into molecular architectures of BTB-Cul3 ubiquitin ligases. *Mol Cell* 36, 39-50.
- Zybailov, B., Mosley, A.L., Sardi, M.E., Coleman, M.K., Florens, L., and Washburn, M.P. (2006). Statistical analysis of membrane proteome expression changes in *Saccharomyces cerevisiae*. *J Proteome Res* 5, 2339-2347.